THE EFFECTS OF HIGH ELECTRIC FIELDS ON AN EPOXY RESIN

Thesis submitted for the degree of
Doctor of Philosophy
at the University of Leicester

By

Virginie Griseri

Department of Engineering
University of Leicester

October 2000

THE EFFECTS OF HIGH ELECTRIC FIELDS ON AN EPOXY RESIN

By

Virginie Griseri

Declaration of originality

This thesis is submitted in fulfilment of the requirements for the degree of Doctor of Philosophy in the Department of Engineering, University of Leicester, UK. All work recorded in this thesis is original unless otherwise acknowledged in the text or by reference. No part of it has been submitted for any degree, either to the University of Leicester or to any other University.

Virginie Griseri

October 2000

The effects of high electric fields on an Epoxy resin

Virginie Griseri

The aim of this work was to determine some of the effects caused by the application of a high electric field on a filler-free epoxy resin material.

Two types of sample geometry were moulded. Films (55 to 300μm) were prepared to work under uniform field configurations. A frame of parallel wires (5 to 25μm radius) was introduced into the bulk to work under divergent fields.

Three non-destructive complementary methods of investigation were used. In all cases the first measurements were performed before the application of thermal-electric stress to define the properties of the material itself. Measurements were repeated after a controlled period of stress. Dielectric spectroscopy measurements were used to determine the main relaxation processes. To evaluate the impact of charge injection and localise the build up of space charge, the pulsed-electro acoustic method was chosen. Luminescence experiments were carried out to investigate the luminescence excitation parameters and pathway of radiative relaxation that are found to be directly linked with the charge injection and extraction phenomena. In addition spectral analysis was performed to complete the investigation. Light emission is associated with relaxations dependent on the chromophores that are present and that are likely to be affected by an external stress.

After thermal-electric stress one relaxation processes was detected by dielectric spectroscopy that was dependent on the stress. This was associated with a change in the local arrangement of the chemical network, which is altered by the field. A mechanism of trapping and de-trapping of charge was determined by the analysis of the PEA response, light emission analysis coupled with external current. The studies were completed by a computer simulation of the effect of injected charge on the electric field.

The three techniques were found to be useful complementary tools to determine the effects of stress on this insulation material.

Remerciements

Je tiens à souligner que c'est afin de trouver des mots plus personnels que cette page à été rédigée en Français dans la forme et dans le texte. J'espère que nul ne s'en sentira offensé.

Je remercie *Monsieur L.A. Dissado*, professeur à l'université de Leicester, de m'avoir accueillie dans le laboratoire de recherche au sein de l'équipe Power Research du département Engineering, et d'avoir supervisé ce tavail. Je voudrais également remercier *Monsieur J.C. Fothergill*, professeur à l'université de Leicester, pour ses conseils techniques et l'intérêt qu'il a porté en examinant, en tant que membre du jury, cette thèse.

J'exprime mes sincères remerciements à *Monsieur C. Mayoux*, directeur de recherche au CNRS, qui a accepté de juger ce travail en tant qu'examinateur externe.

Je tiens à remercier tout particulièrement *Monsieur C. Laurent*, directeur de recherche au CNRS, pour l'établissement d'un travail de collaboration, pour ses conseils lors des nombreuses discussions qui ont eu lieu et ses encouragements. Merci de m'avoir accueillie à plusieurs reprises dans son laboratoire dans lequel j'ai eu grand plaisirs à travailler dans une ambience si sympathique. Je ne me permettrais pas d'oublier *Messieurs G. Teyssèdre* et *D. Mary* pour leur aide et leur accueil toujours chaleureux incluant les pauses café. Je dois en particulier souligner la patience de *Gilbert* pour m'avoir laissée utiliser si souvent son ordinateur.

Mes remerciements chargés de toute ma sympathie vont à *Madame K. Fukunaga*, chercheur au laboratoire de recherche en communications de Tokyo. Je la remercie non seulement pour sa contribution au niveau technologique et son enthousiasme pour ce domaine de recherche mais aussi pour son support moral, sa patience et sa bonne humeur. Je pourrais souligner tout particulièrement le temps qu'elle m'a accordé et la construction d'une amitié qui ne s'est pas achevée après la fin de son séjour à Leicester.

J'exprime ma profonde gratitude à *Messieurs J.V. Champion* et *S.J. Dodd* respectivememnt professeur et docteur à l'université Guildhall de Londres. Je les remercie pour leurs nombreux et précieux conseils et tout le temps qu'ils m'ont consacré sans oublier le partage de quelques "secrets de fabrication" pour les échantillons.

Je remercie *Monsieur T. Forryan* pour son support technique d'une part mais surtout pour sa bonne humeur qui semble inépuisable. Un clin d'oeil à *Jean-Louis, Caro* et tout ceux qui étaient présents côté Français en tant que support moral. Merci aussi à *l'équipe du "lunchtime"* qui a su apaiser certaines périodes de haute tension.

Pour finir je voudrais citer *mes parents et ma soeur Chrystelle* à qui ce travail est dédié à juste titre. Comment leur exprimer un immense merci pour leur confiance, et leur présence à mes cotés à chaque instant. Je leur adresse mes plus profonds sentiments d'affection pour leurs encouragements pendant ce périple et cela, en dépit de la distance physique.

Summary

Chapter I - Electrical processes in polymeric insulation

Chapter II - Material description and sample preparation

Chapter III - Dielectric spectroscopy

Chapter IV - Space charge profile using PEA measurements

Chapter V - Electroluminescence

Chapter VI – Conclusions

Chapter I

Electrical processes in polymeric insulation

I- Introduction

I.1- Insulation materials in use

Electrical equipment is used to generate and carry electrical energy at different voltage levels from the power station to customers. Electrical insulation is, therefore necessary along the chain of production and transportation. Nowadays, it is usually made using a diverse range of *thermoplastic* materials such as Polyethylene (PE) and *thermoset* materials, for example epoxy resins.

I.1.1- Thermoplastic polymers

Thermoplastics are repeatedly remouldable under heat and pressure and this makes their conversion into finished products rapid and economical [1]. These materials gained popularity less on their excellence in performance than on their convenience as substitutes for other materials.

PE is a non-polar polymer, which has a simple chemical structure composed of a carbon chain (CH_2-CH_2) type. It enters into the categories of semi-crystalline polymers. Its structure has been described in many publications investigating polymers [2]. It is formed of crystalline lamella areas separated by an amorphous zone that confers on it its particular properties. This complex structure called a spherulite is an organization of ribbon-like lamellae radiating from a central nucleus. These lamellae twist periodically about the radial direction. Spherulites have a spherical shape during the initial stage of crystallization. However during crystalline growth, when two of them meet the spherical boundaries are lost. This arrangement has been observed for PE, which has been widely used as a cable insulator and has been the subject of much investigation because of both its practical and fundamental interest.

The PE group of materials includes Low and High density PE (LDPE, HDPE) that are distinguished by their preparation mode that results in variations, particularly in their crystallinity. Therefore, most of their properties, as for instance their melting point, are significantly different.

Cross-linked PE (XLPE) is another variation. Morphology studies on XLPE reveal that it crystallizes by forming spherulites [3] even if in this case some chemical

bonds are added between chains that increase its rigidity. This makes it geometrically closer to the tri-dimensional polymer network formed by epoxy resins that constitute the subject of interest of this work. Ideally, all molecules in XLPE should be part of a network but in reality some by-products like initiators, water or low molecular weight molecules are localized at the boundaries of the observed spherulites. This can lead to weak points for electrical conduction.

I.1.2- Thermosetting polymers

Epoxy resins have been selected for the present study since they are commonly used in various equipment and their electrical ageing is still the subject of research. They are often utilized as composite insulators in which the resin acts as matrices containing glass fibers, carbon, etc. Their high performance is usually linked to their high mechanical strength, high modulus and low density. These composite materials are usually moulded and have been seen as new products for the replacement of porcelain and glass insulators. This is because they are lighter and more flexible in shape. These polymers are commonly found in the electrical transmission network, for instance to insulate the overhead cables from the pylon where they have substituted the original glass or porcelain.

Epoxy resins have also been introduced into electrical insulation of transformers. They are especially used in terminals like bushings constructed to take HV through earthed barriers such as walls, floor, etc. Once again there is a large variety of bushing as reviewed by Barker [4]. Their design is the subject of much research especially from the electrical point of view, since their properties need to be improved for better reliability.

I.2- Industrial concerns

Insulation materials vary from one piece of equipment to the next one since the required properties are different. For instance, insulation in generators of electrical energy must provide, in addition to electrical insulation properties, robust mechanical properties. Moreover, since production prices of polymer materials increased after 1975, research activities have been initiated to characterize their properties and improve their quality for use.

Industries have great interest in estimating how long the electrical equipment can be used. That is why many studies are based on the determination of factors responsible for irreversible degradation. Usually insulating materials can be exposed simultaneously to electric fields, mechanical, thermal stresses that are difficult to separate and affect their chemical and physical properties dramatically. This is known as multifactor ageing. As reported [5] the ageing rate cannot be considered as a simple sum of individual processes even if it seems easier for their characterization to separate them.

Research on the electrical source of irreversible changes has been extensively developed especially on dielectric cables [6, 7]. Actually electrical failure in cables was found to depend mainly on the presence of impurities, which can be seen as sources of charges or traps. In addition, the presence of microvoids is at the origin of partial discharge damaging effects. It has been pointed out that improvement in the manufacturing processes leading to extra-clean materials are still subject to a limited lifetime. In this case the cause of ageing should be approached in the microstructure domain where the SC play a determining role [8].

II- Charge injection, charge transport and space charge

II.1- Charge Injection

At high electric field, charge can be injected into the insulator from the electrode and may move through the bulk. These mechanisms depend not only on the voltage applied but also on others factors such as temperature, the type of polymer and electrode. For instance, it has been noticed by Ieda [9] that the metal-polymer interface can be at the origin of various phenomena (table I-1).

Metal-Polymer interface phenomena
1. Electron (hole) injection
2. Surface states
3. Ohmic currents and Space Charge limitation
4. Electrochemical reaction
5. Ions neutralization/ ionization

Table I-1: Electrode-Polymer interface effects

The nature of the metal electrode has also been shown to be of significant importance [10]. The energy band diagram remains complicated because of the imperfect contact between the insulator and the metallic conductor, the presence of chemical impurities and moisture etc. However, two main mechanisms of electron injection are important and will be described here. They are based on the simplified energy-band diagram shown in figure I-1.

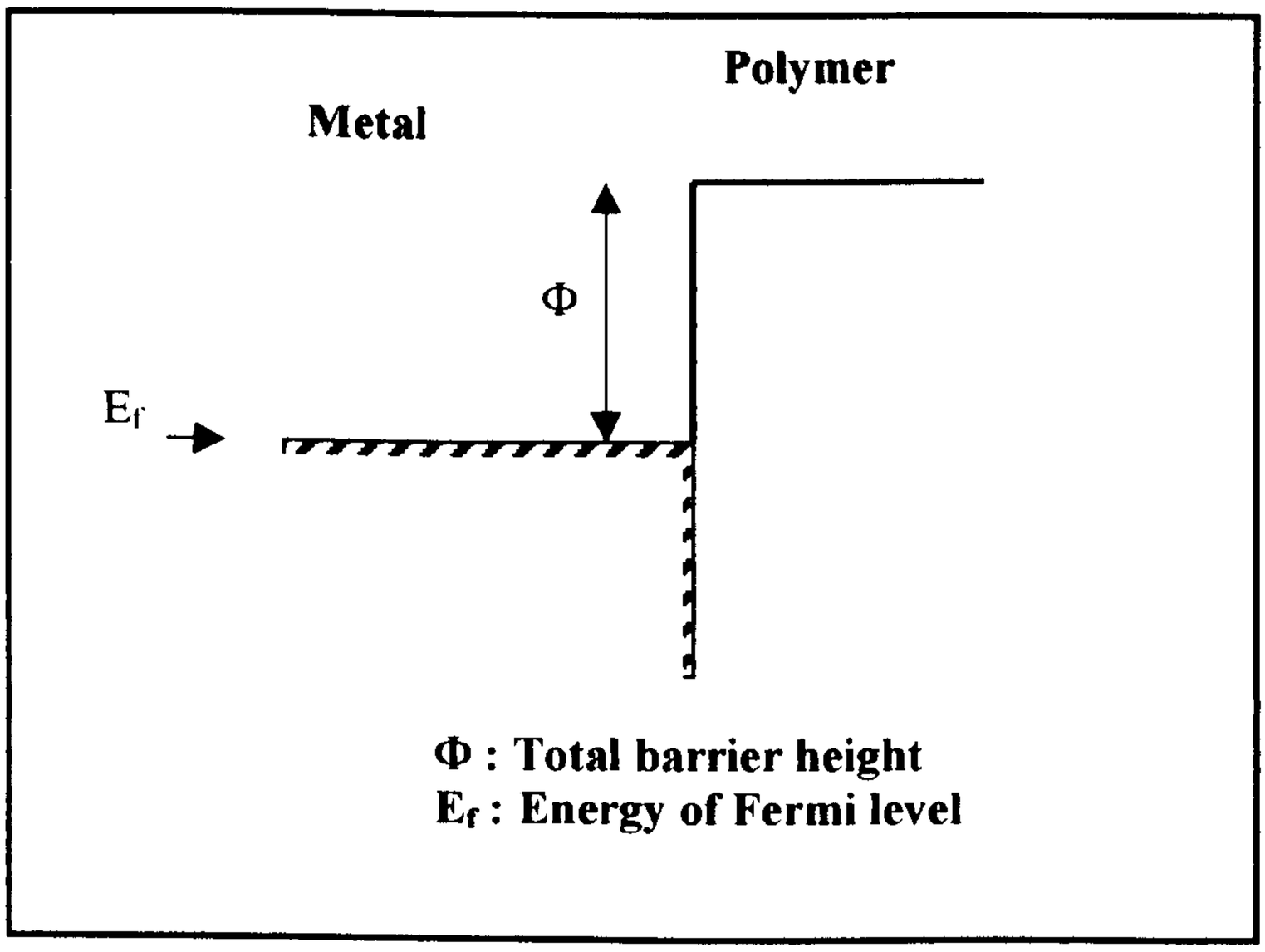

Figure I-1: Total potential barrier at a metal-polymer interface

The major problem for electron injection is to overcome the physical potential barrier that exists between the metal and the insulator. The use of high field can reduce the height Φ and width of this barrier. In figure I-2.c, the total barrier shape is represented. It is a combination of the coulombic image force and the potential energy due to the applied electric field detailed in figure I-2.a and I-2.b respectively. These modifications in the barrier are described in the sections on the Schottky and Fowler-Nordheim injection mechanisms.

Theories were first of all developed to describe the injection of electrons from a metal to a vacuum in which the barrier height was equal to the work function of the metal. In the present case, many simplifications have been made allowing the barrier to depend only on the metal-insulator work function difference and electrical polarization.

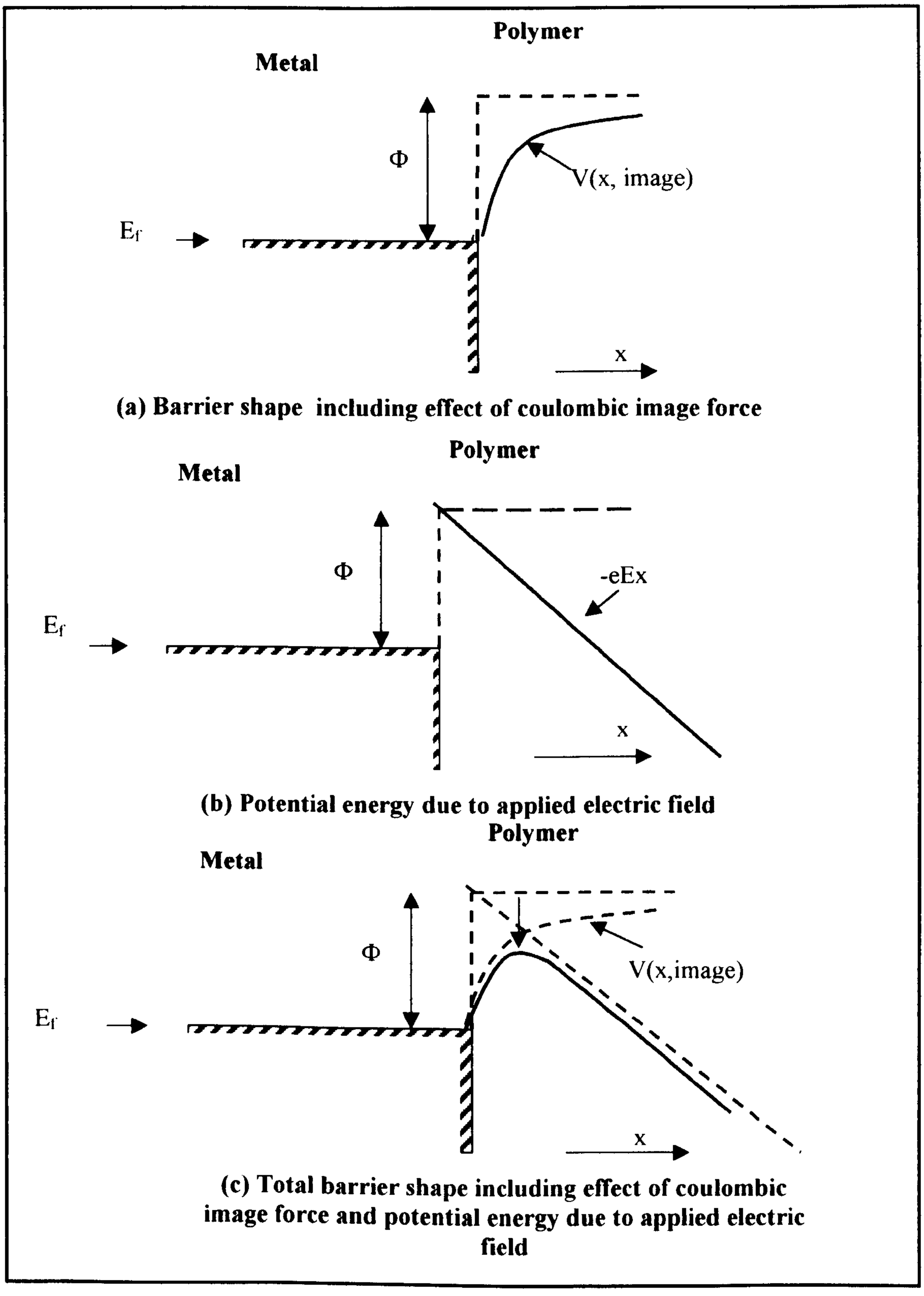

Figure I-2: Potential barrier at a metal-polymer interface

(a) With effect of coulombic image force **(b)** Potential energy **(c)** Resultant barrier

II.1.1- Schottky

If the height of the barrier is lowered enough, electrons with sufficient energy can overcome it [11]. In the present case an electrostatic attraction is used to explain a change in the barrier due to the potential energy of the electron. It is supposed that the metal is positively charged after the injection of the electron into the insulator. The image charge theorem is used to calculate the attraction between a point charge, i.e. the electron and an infinite conducting flat sheet, i.e. the metal. By assuming that the electron is at the distance x from the interface, the distance between the electron and its image becomes 2x. The force of attraction F(x) is calculated by Coulomb's Law.

$$F(x) = \frac{-e^2}{4\pi\varepsilon(2x)^2} \tag{I.1}$$

Where $\varepsilon=\varepsilon_0\varepsilon_r$ the permittivity, that is the product of the permittivity of free space ($\varepsilon_0=8.854\text{x}10^{-12}\text{F.m}^{-1}$) and the relative permittivity.

The potential energy V(x) is obtained by integration of electric field between the position x and infinity. When a voltage is applied, if we use E as the amplitude of the electric field and suppose it constant at the interface, the potential energy is modified by the value –eEx at position x. The total barrier shape is represented in figure I-2.c and the potential energy can be written:

$$V(x) = \frac{-e}{16\pi\varepsilon x} - eEx \tag{I.2}$$

The current density is given by the equation [6]:

$$J = \frac{4\pi e m k_B^2 T^2}{h^3}\left[\exp\left(\frac{-\Phi + \frac{e}{2}\sqrt{\frac{eE}{\pi\varepsilon}}}{k_B T}\right)\right] \tag{I.3}$$

k_B is the Bolztmann constant

This type of injection can be verified by the representation $\log_e(J/T^2)$ versus $E^{1/2}$ that leads to a straight line in the case where equation (I.3) applies.

II.1.2- Fowler-Nordheim

The Fowler-Nordheim injection mechanism occurs when a large applied voltage reduces the width of the potential barrier. In this case electrons that do not have enough energy to pass above the barrier pass through it by a quantum tunneling effect. This phenomenon is a pure quantum mechanical effect that is made easier as the amplitude of the electric field is increased.

The phenomenon is described using a triangular potential barrier. The effect due to the coulombic image force is neglected in this case. This phenomenon occurs in insulators at very-high fields in the range 10^8-10^9 V/m. The potential energy V(x) (figure I-2.b) is calculated depending on its position compared to the metal-insulation interface at x= 0. In that situation:

$$\begin{cases} V(x) = 0 - when : x < 0 \\ V(x) = \Phi - eEx - when : x \geq 0 \end{cases} \tag{I.4}$$

where Φ is the potential barrier at the interface, e the electronic charge and E is the applied electric field.

Because electrons can exhibit a particle-wave duality the relationship of De Broglie can be applied. By using the one-dimensional form of the Schrödinger equation and some approximations, the current density can be calculated to be [6]:

$$J = A(T,\Phi)E^2 \exp\left[\frac{B(\Phi)}{E}\right] \tag{I.5}$$

The functions $A(T,\Phi)$, $B(\Phi)$ depend on the height of the barrier and also, to a certain extent on the temperature since in the calculation one accepted approximation has been to assume a temperature of absolute zero.

Under high values of electric field ($E>10^8$ V/m), this injection can lead to catastrophic breakdown in thin films.

II.1.3- Charge injection in the "real world"

Charge injection and ejection across metal-insulation interface is a phenomenon of great importance in microelectronics technology. Generally the injection phenomena are dependent on various parameters and not only the value of the applied electric field, the electrode insulator work function and temperature.

Many factors that influence charge injection phenomena have been reported by Damamme et al. [12]. For instance, it has been observed that for Polyvinylidene fluoride PVDF the injection is controlled by the direction of the voltage applied to the material. In this case, it is the morphology variation due to processing that is held responsible for the effect. In such a situation, the anisotropy of charging must be taken into account.

Measurements on PE, after different periods of annealing, revealed that residual strain could affect the charging phenomena [12]. It has also been found that the state of surface oxidation can change the sign of the injected charge.

The presence of absorbed water as in polyamides, polyimides or epoxies can lead to electrochemical dissociation of the absorbed water under electric field application. This reaction creates mobile species, which can determine the nature and energy levels of traps.

The density of traps and their energy distribution is also important and depends on impurities, and defects concentration. It has also been reported [12] that under low injection conditions, charge injection depends on the sample size. Actually trapping may be seen as a process, which is able to preserve the material from degradation due to reduction of the local field, but in fact the energy associated with the trapping-de-trapping phenomena is large enough to give local damage [8]. These modifications can be responsible for changes in the behaviour of the material under voltage application.

II.2- Charge transport

As shown by Das-Gupta and Doughty. [13], on studies on Polyetheretherketone PEEK, several mechanisms of conduction can usually be relevant to explain the conduction current recorded in the external circuit. These mechanisms depend not only on the amplitude of the external electric field but also on the nature of the charge carriers.

II.2.1- Low field

Under low field conditions the voltage-current characteristic can be described by Ohm's law. In this situation a field-independent concentration of charge carriers i.e. electrons, holes or ions acquire a velocity proportional to the field. This

conduction is usually said to be "Ohmic". This concept was originally proposed to describe the movement of electrons in a crystal lattice. In such a material the current density J follows a linear relation with respect to the electric field E.

$$J = ne\mu E \qquad \textit{with the conductivity} \quad \sigma = n\mu e \tag{I.6}$$

However, polymers are different to the simple covalent or ionically bonded crystal of conventional solid-state physics. For most of the time electrons and holes are unlikely to be free to move and the ones that have sufficient energy to be in the conduction band are likely to be scattered and fall into traps located in the band gap. This is known as trap-limited mobility. This model has been verified on PE [14] and seems to be generally applicable to amorphous solids.

Trapping in polymers is often interpreted [15, 16] in terms of a modified band model (figure I-3). In this model, traps are localized states belonging to particular molecules or molecular groups. The polymer energy levels are affected by the environment and will usually differ from one region to another. The trap depths are distributed and activation from the local state requires thermal energy.

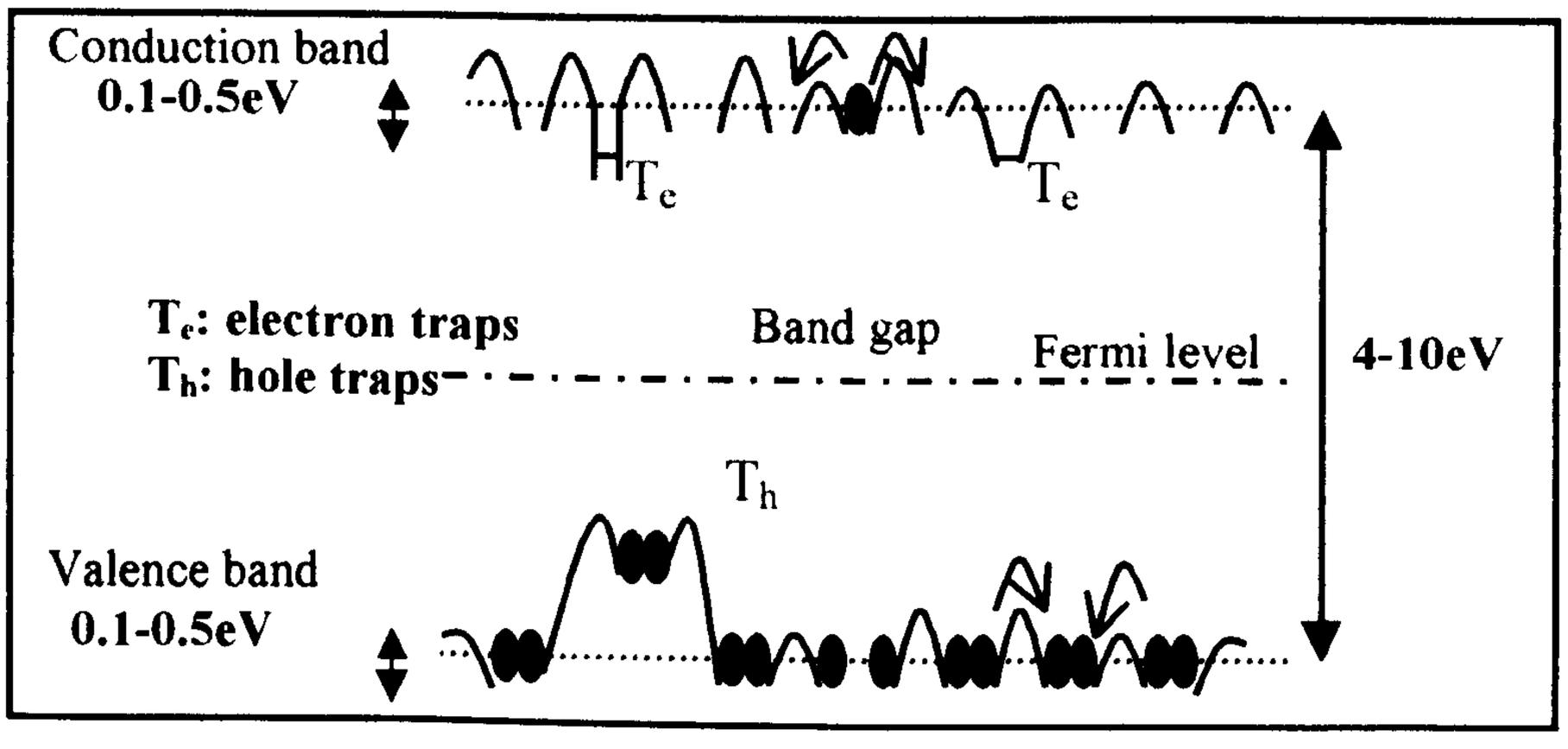

Figure I-3: Energy diagram in polymers

The carrier mobility at low field has been shown to follow the Arrhenius law:

$$\mu = \mu_0 \exp\left(\frac{-E_a}{kT}\right) \tag{I.7}$$

This expression originates from an ionic conduction mechanism and has been found to be applicable to polymers. In actual fact, the value of the activation energy, E_a, has been found to be stable over a large range of temperature. Methods to determine the nature of the carrier, which are summarized table I-2 have been used to prove the existence of ionic conductivity in polymeric materials.

Event	**Ionic conduction**	**Electronic conduction**
Mass transfer	Yes	No
Pressure	Decrease	Increase
Glass transition $T > T_g$	Increase	
Melting point $T > T_m$	Increase	Decrease
Electrochemical reaction	Yes	No
Ionic impurity	Increase	

Table I-2: Property variations involved in ionic and electronic conduction

If, instead, we consider that electrons are the charge carriers, the conduction in a single crystal and amorphous material will be different (figure I-4.a, b). In a single crystal, charges are moving in the conduction band and become trapped. They can be de-trapped and trapped again depending on the external stress. Whereas in an amorphous material charge displacement by Brownian motion, tunnel-hopping in localized states, and thermally activated hopping can occur.

Furthermore, in polymers there are a large number of chains and electrons can move through the bulk by conduction along the chain and by hopping to a neighbouring chain [9]. It is supposed that they are located in wells, and their mobility is thermally activated and can be represented by intermolecular hopping (figure I-4.c). Under field application the potential barrier is reduced in the field direction, which allows the charge carrier to move between wells with a net flow in the direction of the field.

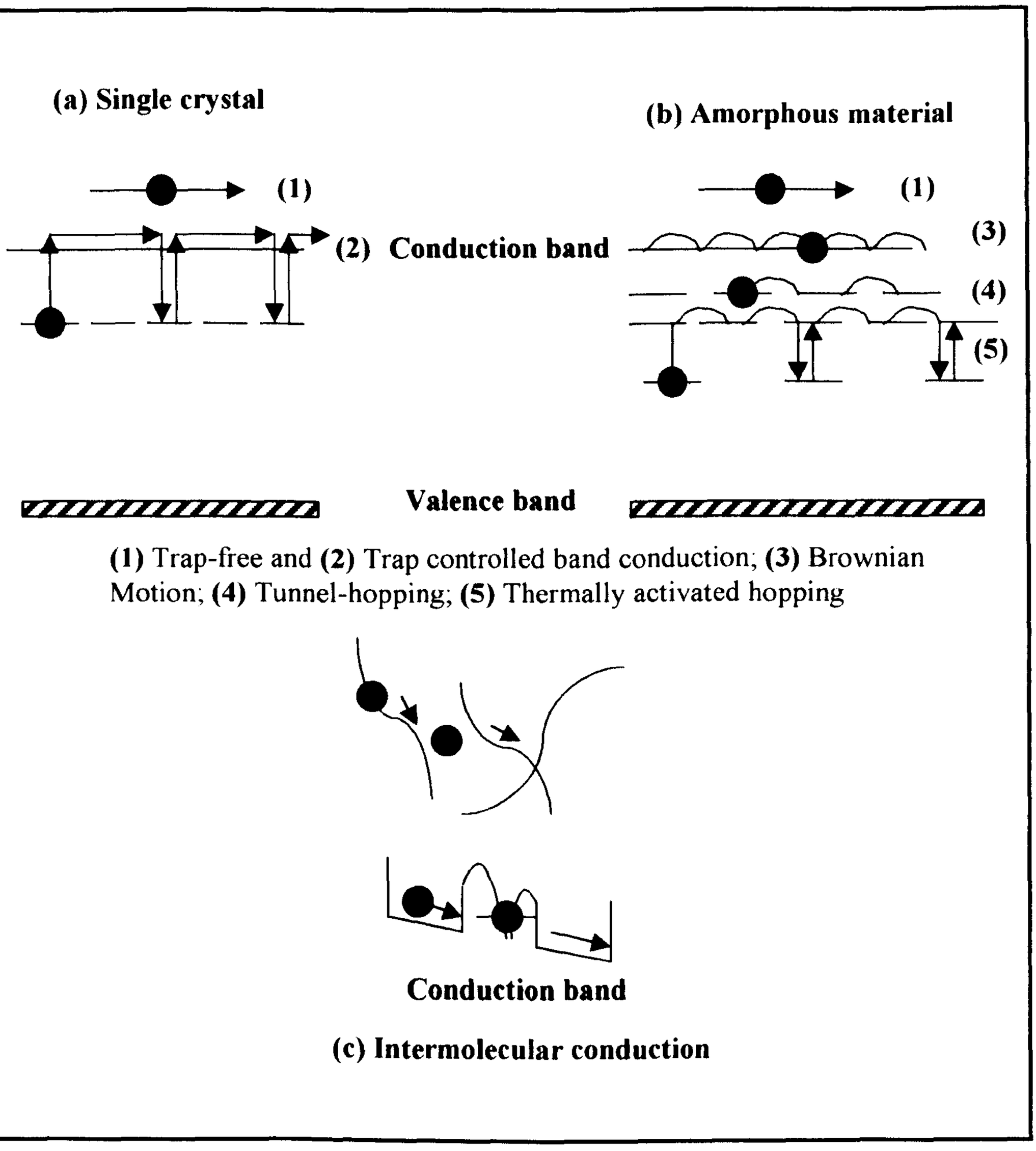

(1) Trap-free and **(2)** Trap controlled band conduction; **(3)** Brownian Motion; **(4)** Tunnel-hopping; **(5)** Thermally activated hopping

Figure I-4: Carrier transport in **(a)** Single crystal **(b)** Amorphous material **(c)** Hopping to neighboring molecules

II.2.2- High field

The current deviates from Ohm's law and rises super-linearly with field. Several mechanisms have been proposed to explain this form of conduction. Here it is assumed that bulk mechanisms are the rate limiting stage and it is these that are described.

II 2.2.1- Space charge limited current

Space charge limited current (SCLC) is generally observed in thin films. It has been suggested that if the electrode-dielectric contact is good, more free charge may be injected than extracted. If we consider that only electrons are injected, it is possible to show that a SC region is built up. Above a transition voltage V_{trans}, the SC field will limit the current. This effect will dominate the ohmic component of the current.

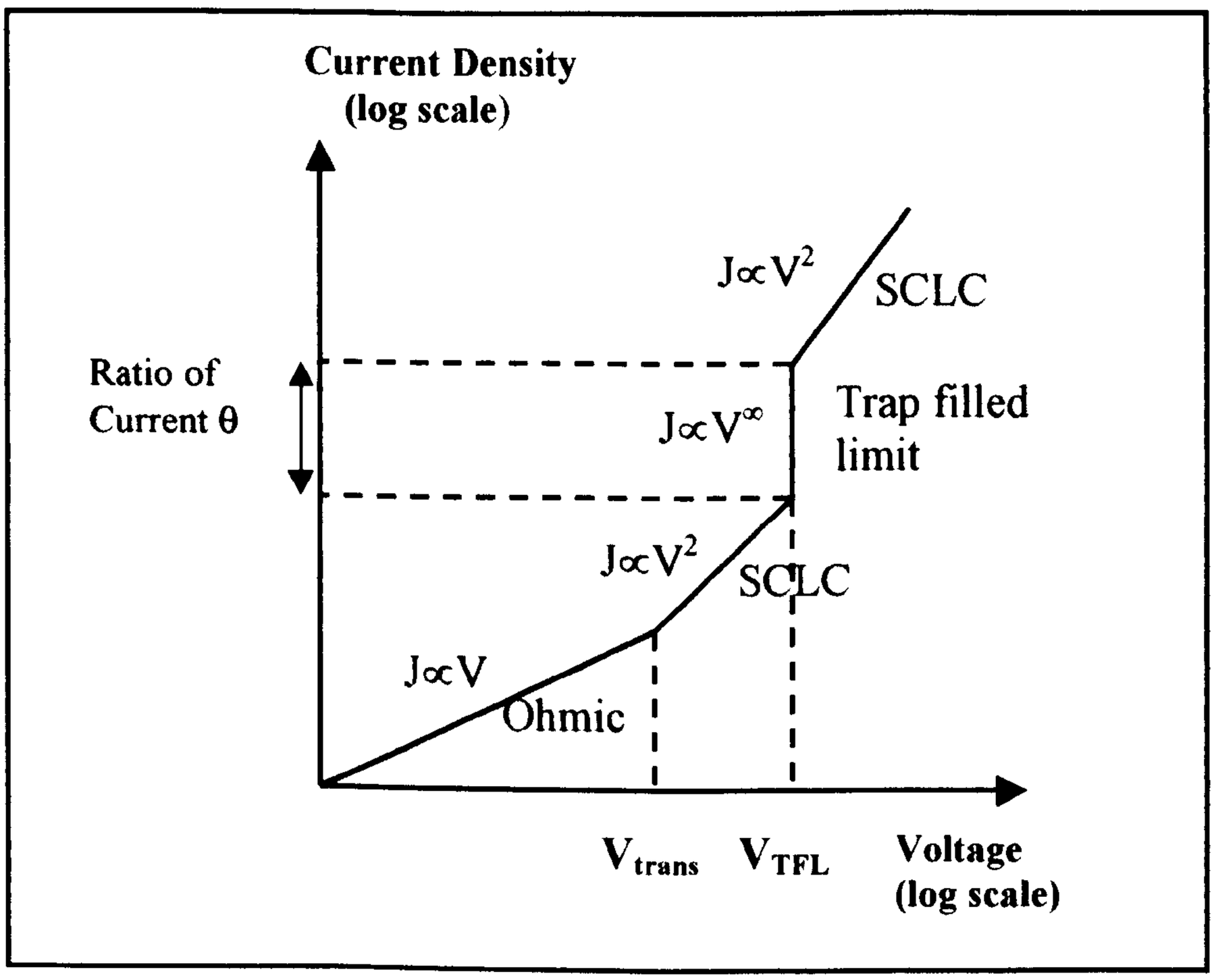

Figure I-5: Current density vs. voltage in an ideal case of Space Charge Limited Current (SCLC) phenomena

As the voltage increases the number of injected charges increase and the Fermi level moves above the trap energy level creating a sudden increases in the current density. Then, in ideal cases, as the voltage increases, a new region of SC limited current is created (figure I-5) [11].

II.2.2.2- Hopping conduction

There exists delocalised states situated in the band gap close to the conduction band and valence band separated from localized states by the "mobility edge" where the mobility is reduced [15]. In insulators with a large band gap, states that are likely to be filled are situated around the Fermi level. Because of the large number of unoccupied states in the region of the Fermi level, it is possible that the electrons situated in an occupied state close to the Fermi level acquires sufficient energy to move to an unoccupied state of similar energy. This move can be described by thermal excitation above the potential barrier, tunneling or a combination resulting in a quantum mechanical hopping process introduced by Mott [16]. The current density is given by the equations in table I-3, in the case of a single contributing process.

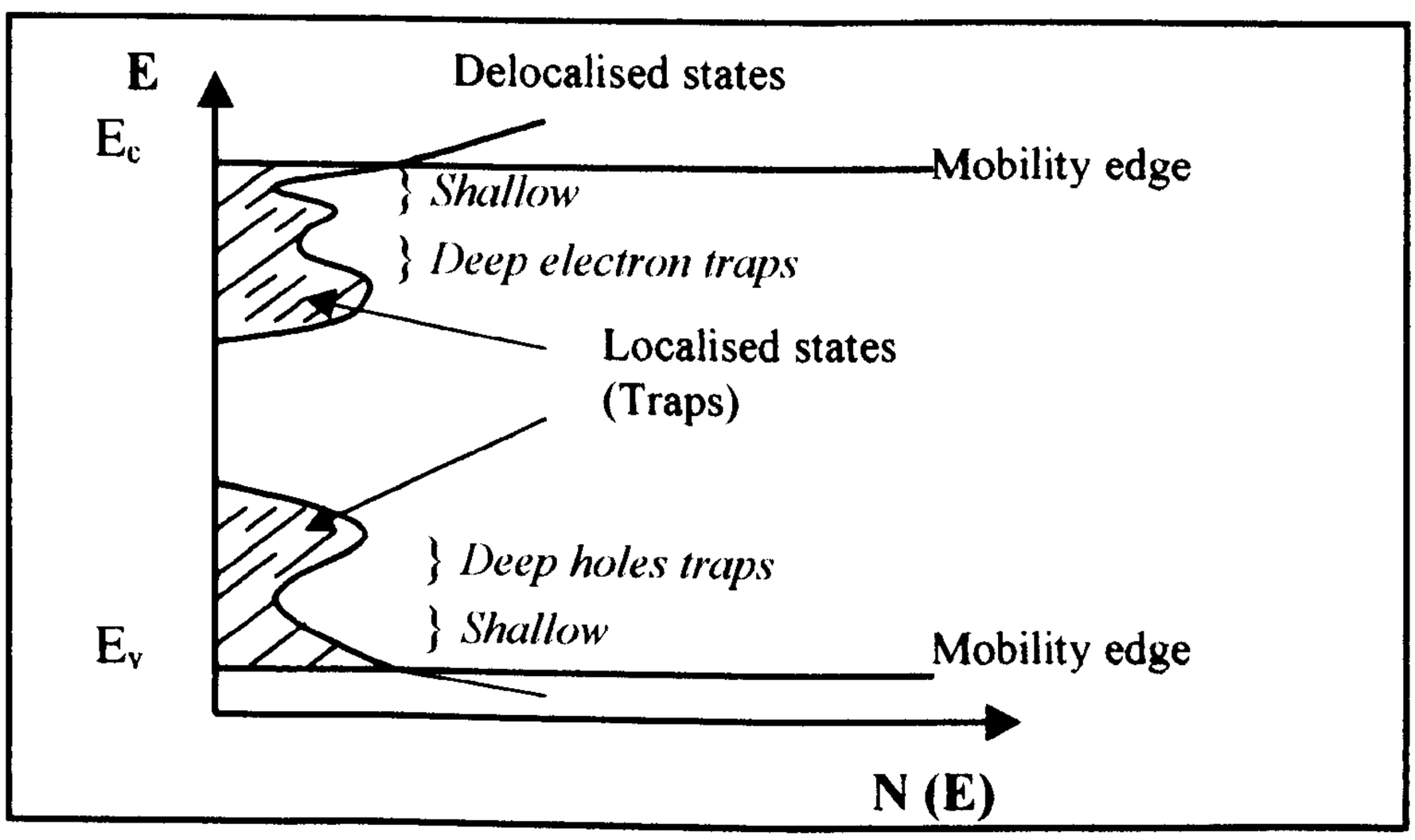

Figure I-6: Density of states N (E) in polymers (Sessler, 1980)

II.2.2.3- Poole-Frenkel Mechanism

The Poole-Frenkel mechanism is a bulk effect similar to the Schottky effect occurring at the interface. The dielectric must contain donors or acceptors. These levels do not give electrons to the conduction band nor accept electrons from the valence band at room temperature. The electric field lowers the barriers where carriers are localized allowing them to move out from the localized level. The general form of the mobility is given table I-3.

Mechanism of bulk limited conduction	**Mobility (μ) or current density (σ) relations**
Space Charge Limited Current (SCLC)	$J = \frac{9\varepsilon\mu V^2}{8d^3}$ V potential; d thickness
Hopping	$J = J_0 \sinh\left[\frac{eF\lambda}{2kT}\right]$ F Coulombic Field
Poole-Frenkel	$\sigma = \sigma_0 \exp\left[\frac{\beta_{PF}\sqrt{F}}{2kT}\right]$ β_{PF} constant

Table I-3: Résumé of bulk conduction and related formulae

II.2.2.4- Field limiting space-charge model

Injected SC near to the electrode forms a cloud that reduces the electric field in the region where they are localized. Zeller and Schneider [17] introduce a critical field above which the carriers are mobile (E_{mc}).

If this critical field does not exist and $\mathbf{E>E_{inj}}$, then SC is injected and diffuses into the insulator until equilibrium is reached at $\mathbf{E=E_{inj}}$.

In the other case if $\mathbf{E_{inj}>E>E_{mc}}$, SC present in the material will move and leave a SC free region behind. The SC will progress into the bulk, over time, as long as the field at the boundary is higher than E_{mc} and therefore equilibrium is expected after a reasonable amount of time.

Finally, if $\mathbf{E>E_{mc}>E_{inj}}$, injected SC will rapidly move from the electrode, reducing the field in the region behind them as previously. The situation is described in figure I-7.

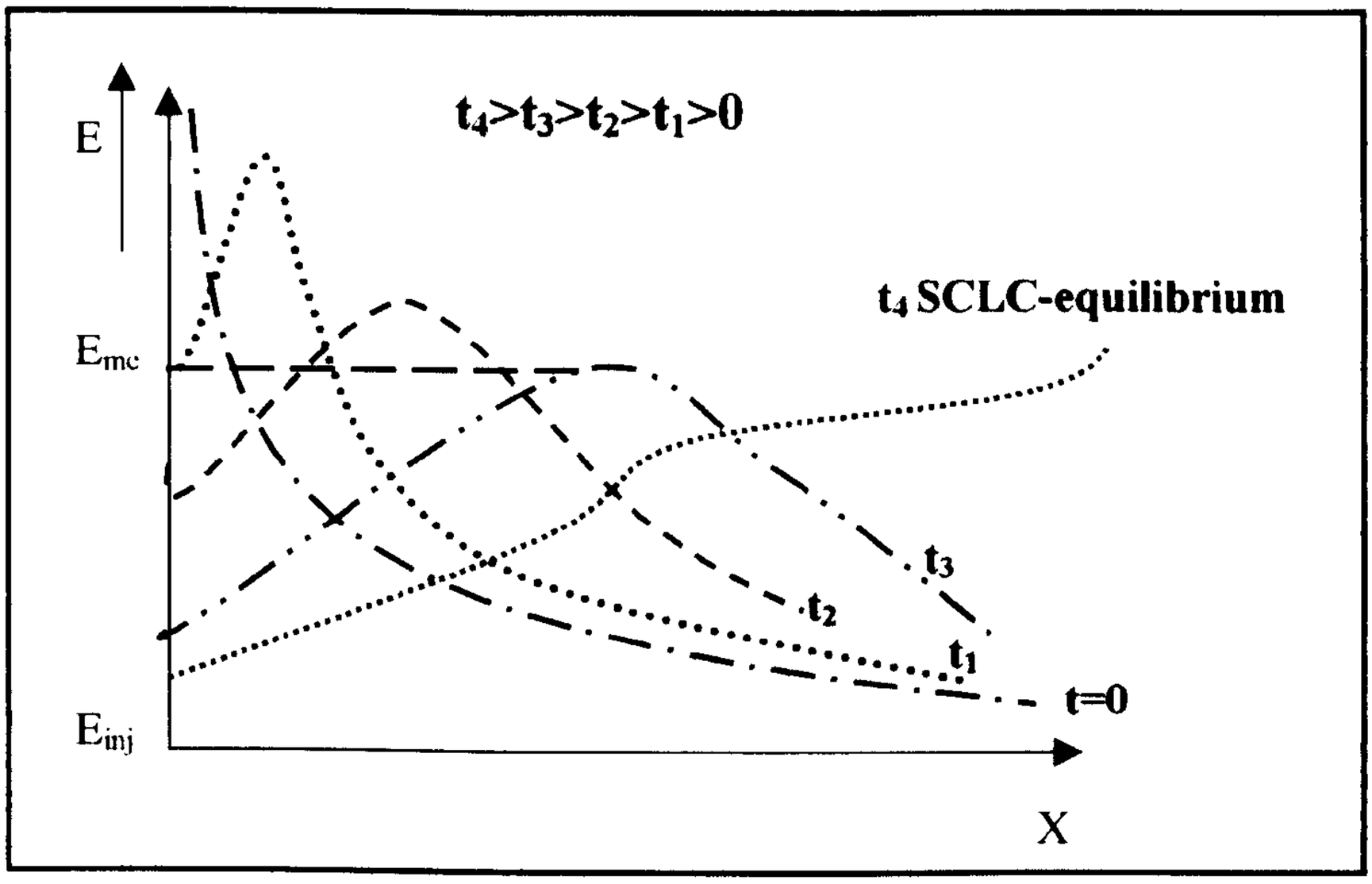

Figure I-7: Electric field vs. distance from the electrode at different periods of time

II.3- Space charge and its measurement

The measurement technologies of space charge distribution, i.e. density, polarity and location, in solid dielectric materials were developed especially after the seventies. Most of these techniques give information on dipolar relaxation, charge injection and de-trapping. These processes are directly connected to the variation of the internal electric field and then to voltage and external current variations. The notion of trapped SC has received much interest and several techniques of detection are reported in the literature [18].

II.3.1- Techniques without spatial resolution

In the Thermally Stimulated Discharge Current (TSDC) [19] general method the sample is polarized under a given voltage and temperature, the sample relaxed until the external current is constant and, then the external current is recorded as the temperature is increased at a constant rate. When the temperature of the sample is increased the thermal release of trapped charge carriers gives a maximum in the values of the detected current. In the Thermally Stimulated Current (TSC) [20] method the difference come from the cooling of the sample at the end of the application of the voltage in order to freeze the polarization. In both cases, the same kind of general information is obtained about SC presence without the determination

of their position. However, a mean depth can be estimated from the injection electrode as presented by Hino [20].

The thermoluminescence technique of investigation has been coupled to TSC [21] measurements and was proposed as a reliable technique to get information on release and recombination of trapped charge carriers.

II.3.2- Techniques with spatial resolution

The interest of this second group of techniques consists in the measurement of the average of the net charge in the volume and their spatial location.

II.3.2.1- Thermal methods

The thermal step method uses a step-change of temperature applied on one side of the sample situated between two sets of electrodes in short-circuit. The thermal step expands or contracts the material causing a movement of the space charge. As a result the "image charge" on the electrodes are re-distributed to balance the effect, causing a current in the external circuit that can be recorded. The method has been developed and shown to be valid especially for thick samples [22, 23]. This is convenient for the investigation of industrial products since the geometry and the range of material that can be used is extended to polymers, ceramics and glasses of diverse shape. But, if compared with acoustic methods, despite the absence of reflection at interfaces, the time resolution is lower due to the lower speed of thermal pulse propagation.

II.3.2.2- Acoustic methods

Pulse Electro-Acoustic (PEA) [24, 25] and Pressure Wave Propagation (PWP) [26] or Laser Induced Pressure Pulse (LIPP) [27] methods are particularly adapted to detect fast changes in the charge distribution that happens in the bulk of the sample. Whatever the nature of the pulse, i.e. electrical or laser, applied on one electrode, the space charges are submitted to a stress that displaces them creating a signal that is detected at the second electrode. This signal is directly proportional to the variation of the internal electric field that is related to the space charge profile. In one case (PEA) the probe stress is electrical and it is the mechanical (acoustic) signal that travels to the detector, in the other case (LIPP) the inverse effect is used, i.e. a traveling mechanical probe creates a charge displacement which is instantaneously detected.

Coupling these methods with the record of total external current during polarization and discharge is expected to bring complementary information on injection, conduction, and polarization phenomena.

III- Ageing and breakdown

Once in use, these insulators are subjected to multiple sources of stress that may induce ageing and shorten their working life dramatically. As mentioned the stresses most frequently encountered by electrical systems are voltage, temperature, mechanical and environmental. It is rarely possible to separate the different effects. Even if they do not occur simultaneously, at least temperature and voltage are very often coupled. Obviously, any weak link can lead to catastrophic failure. The understanding of the mechanism involved in the breakdown then becomes a priority.

III.1- Breakdown

The electrical breakdowns that are irreversible processes, are divided into three main categories: electronic, thermal, and mechanical [15]. These phenomena have been analyzed in detail by Dissado and Fothergill. [11] and are summarized in table I-4.

Ieda et al. [28] described the relationship between breakdown and properties inherent to polymers such as the morphology and chemical structure that influence the electric strength in PE and copolymers. In PE, for instance it has been shown that in a spherulite structure the ac breakdown is preferably found to propagate in the amorphous part or crystalline boundary where usually defects and impurities are rather concentrated. It was also noticed that the dielectric breakdown differs between the amorphous part in the sperulite boundary region and that in the inter-lamella region inside the spherulite [29, 30].

Electronic Breakdown Theories
Intrinsic breakdown (electronic thermal breakdown (Fröhlich)) Electron avalanche breakdown Field emission breakdown Free volume breakdown
Thermal Breakdown Theories
Steady state thermal breakdown Impulse thermal breakdown
Mechanical Breakdown Theory
Electromechanical breakdown
Secondary Effect
Space charge, Local heating, Maxwell stress etc.

Table I-4: Electrical breakdown processes of solids

III.2- Ageing

Tanaka et al. [31] give an overview of life expectation and the principal cause of ageing of the most common insulation systems in use. They present, in particular, XLPE cables and composite materials. They consider the extensive research carried out on XLPE related to electrical treeing, from the initiation to the final stage. Treeing has been found to be the degradation process for almost all ageing mechanisms. In particular, bulk morphology and interfaces (insulation/electrode) have been identified as weak areas where the critical ageing processes occur. They have been broadly brought under control in cable industry research, but understanding is still not complete.

It has been shown that most of the time, defects are due to conductive contaminants in the resin or protrusions on the metal insertion. Two types of interface exist in composite materials that could be held responsible for initiating the degradation processes. These weak points where the electrical strength is reduced, are the external interface (composite/air or oil) and the internal interface (polymer/fillers).

Because embedded fillers can enhance the electrical ageing phenomena special specimens have been prepared to study their effects. For that purpose, several investigations have been made using the following type of configuration that reproduces the shape of the fillers:

- Needle inserted in insulating material [32]
- Resin shell with glass-resin interface
- Flat specimens with metal foil inserted

Parpal et al. [33] proposed a model to explain the ageing of dielectric cables. They introduce the notion of sub-micro cavities that will grow into cavities. When submitted to a critical value of voltage, Partial Discharges (PD) in the voids would then originate electrical trees. This PD is reported to be the first step for a tree like deterioration in many cases. Voids may remain in the bulk during the casting process and are likely to be present in epoxy resin specimens.

In a model proposed by Bahder et al. [34] the scission of molecular chains, caused by the movement of electric charge, is suggested to be one of the most detrimental effects of partial discharges. It is also pointed out that below a threshold field, bond breaking may be matched by repair. However at higher field, the ageing time for dielectric materials might be associated to the time necessary to reach a critical fraction of broken bonds. Above this critical time, crack propagation leads to rapid failure [35].

As described by Bernstein and Brancato [36], the mechanical, thermal and electrical stress varies for each class of equipment used in the distribution grid of electrical energy. The observation of the electrical stress itself shows a large diversity in the values of operational voltage stress employed from one piece of equipment to another (table I-5). It has been shown that the mechanism of ageing and life reduction involves partial discharges and this seems to be the main cause of failure in rotating machinery. However, in cables it has been observed that non-partial discharge induced phenomena can occur prior to failure. The dielectric strength related to the age of the insulating material has often been associated with trapped space charge in cable insulation. It is believed that field distortion due to secondary effects like SC accumulated in solid polymers strongly affects high field conduction and electrical breakdown. Mizutani [37] has reviewed his studies on PE and SC distribution. He points out the influence of additives and impurities as well as electrode material and interface in SC formation.

Equipment	Electric Field Operating Stress (kV/mm)
Generators	2.5 (ac)
Cables	7-8 (ac)
Transformers	10 (ac)
Capacitors	200 (dc)

Table I-5: typical values of electrical field in various piece of equipment

Recently, the notion of SC influences has been raised and it has been proposed that SC detection in cable insulation could be one of the methods to detect insulation degradation [31]. Also some theoretical models have been elaborated to associate ageing due to thermal-electrical stress with SC [38, 39]. That is the reason why SC forms an important part of this investigation.

IV- Definition of the objectives of the work

IV.1- Previous investigations on epoxy

IV.1.1- Breakdown related studies

Epoxy resins have been much investigated with the aim of estimating relative service life and electrical tree growth [40]. Tree inception and growth have been linked to the enlargement of micro-voids or micro-cracks in which PD enhances the propagation of damage. Two kinds of studies have been performed:

IV.1.1.1- Constant stress

Measurement of the time interval between the tree initiation and failure at constant values of ac voltage has been carried out using a pin-plane geometry. Champion and Dodd [41] show reproducible results on tree growth as a function of voltage and time of electrical ageing provided that a sample of the same age has been used. To be reproducible it is also necessary to eliminate the effect of the initiation time that fluctuates greatly from one sample to another. This is done by pre-initiating the sample under the same conditions. It has been shown that the inception depends, in particular on the electric field at the pin/point. On the other hand propagation depends on the electric field in the tree due to PD in addition to the pin/plane distance

and the applied voltage parameters i.e. propagation depends on the local fields at the tree tips.

It appears that for an epoxy resin in the glass state structural relaxation of the network is the most important long-term contribution to ageing under ac electrical stress [41]. This conclusion is implied by changes in residual mechanical stress and hence refractive index, glass transition temperature and dielectric loss. Such physical ageing could explain the large variation in tree growth behaviour in various materials. First of all, it has been shown that an increase in the compressive stress leads to suppression of tree initiation, whereas an increase in the tensile stress enhances the processes. In addition, a region of zero stress has been observed to act as a passivation barrier for tree growth [42]. Recently, the application of additional mechanical stress has been found not to change electrical tree growth whereas the absorption of water seems to act as a tree growth inhibitor [43].

IV.1.1.2- Step ramp stress

The step ramp process is a method by which progressive voltage step-stress is applied until failure occurs. This study is rather complicated since the electrical ageing depends on step ramp stressing rate [44]. Three kind of light emission have been detected as the RMS value of the ac applied voltage is increased. The light detected is linked to the mechanisms that occur in the tree initiation and growth.

IV.1.2- Ageing related studies

IV.1.2.1- Space charge in divergent field

Detection of SC in epoxies has attracted attention with the development of modern methods of investigation such as PEA methods and LIPP. Studies under high divergent electric field in a wire lattice/plane geometry have been studied by Naz et al. [45, 46]. Using 2mm thick samples they show that charges can be transferred from the wires to the neighboring polymer when a positive or negative short voltage pulse is applied. Using the LIPP method they measured the charge density and observed an increase in the broadening of the charge distribution, which stabilizes about 1s after the beginning of the voltage application. They investigated the mechanism of charge trapping and described a model in which charges that are trapped fill deep levels first. The charge density increases with time and increased amplitude of applied voltage

[47]. In this model the charges are supposed to be injected around the wires creating a cylinder of SC. The injection mechanism was found to follow a FLSC model at the beginning of the application of the voltage. Subsequently the charges were supposed to have a low mobility so that only a small increase in the broadening of the SC area was detected. It was also noticed that the deepest level of traps was constant whatever the voltage, duration and temperature applied whereas the shallowest level of traps moved closer to the conduction band as the voltage amplitude is increased.

IV.1.2.2- Field properties

Luminescence experiments associated with charge injection/extraction under constant stress in pin-plane configuration [48] also show different regimes of emission. At first, the light is associated with charge injection, then micro discharge activities are added and micro-channels are supposed to be formed. Finally, PD occurs within channels leading to breakdown. The light is observed close to the pin electrode and spreads along the cone rather than in the bulk. It has been suggested that high-energy charge carriers cause bond breaking in the polymer.

According to Tanaka and Greenwood. [49], charges in PE are expected to move back and forth when an ac voltage is applied. They assume that this movement will create a narrow channel of material degradation leading to a first step of tree initiation. It has also been suggested that UV-induced bond scission may occur if the energy involved is greater than 4-5eV [50]. It is suggested that a critical field is required for light emission and the light-inception field could be the threshold field at which the deterioration starts. This statement is assumed to be true in the absence of impurities that could locally enhance the electric field and which allow local charge injection without detectable light emission.

A model of charge recombination to explain the light emission in a uniform or divergent field configuration was proposed by Alison et al. [51]. Injection and field limiting injection current behaviour are presented as the key feature to explain the phase profile of light emission. Further details will be given in the chapter relating to electro-luminescence measurements on our samples.

IV.1.2.3- Additional ageing effects

Physical ageing has been investigated by Li and Unsworth [52]. They show that the thermal histories of materials can have an important effect upon their properties. Their observations have been based on dielectric measurements and determination of the glass transition temperature (T_g) by Differential Scanning Calorimeter (DSC) studies. They show that the dielectric loss, and moisture content decrease with physical annealing whereas T_g increases due to reorganization in the bulk that can occur even below the glass transition temperature.

On the other hand the effect of absorbed water on electrical trees reveal that moisture influences the fractal dimensions of branch trees [53]. It has been shown that after polymerization reactions are considered to be completed, i.e. after 20-30days following the preparation, when the moisture content increases, the time to failure increases since the tree fractal dimension increases. In fact, it is the relative humidity and not the absolute magnitude of water uptake that controls the fractal dimension. It has also been pointed out that the saturated value of moisture absorbed depends on the resin system and the temperature.

IV.2- Overview of current investigation

In the present work it is proposed to study, by different methods, the ageing effect due to charge injection in epoxy resin film samples. Both uniform and divergent field configurations will be used to identify the effect due to voltage application. The effect of temperature and especially the effect of the glass transition will be studied.

IV.2.1- Dielectric spectroscopy

Dielectric spectroscopy will be used especially to determine the conduction phenomena at low frequency and the effect of voltage application and temperature on the polarization phenomena. These studies will be carry on in the range 10^{-4} and 10^{5}Hz This technique can also be a tool to identify the effect of the electric fields on the structure of the epoxy and on the degree of liberty of the dipoles.

Conductivity values associated with the dc limit can be obtained at low frequency and are a useful tool to check the reliability of the data obtained from external current measurements made during polarization. Here a dc current is assumed

when a steady state current is reached, but it is often difficult to identify its value because of noise fluctuations.

IV.2.2- Space charge distribution

PEA measurements, sometimes in combination with the external current, will be used to determine the charge carrier distribution in the bulk and determine their lifetime as a function of the temperature and the applied stress voltage. This study is especially based on charge injection and transportation but it is combined with the polarization of the sample material from which it is difficult to separate.

This non-destructive method is particularly adapted to work with thin films in the range 100-300μm thick. The analysis will require more attention to be paid to the wired sample since this signal is much more complicated than that of the homogenous films. The investigations on pure epoxy resin films is intended to give a base for understanding of the behaviour of the material under electrical stress.

IV.2.3- Electroluminescence analysis

Luminescence emission is used in order to identify the mechanism of charge injection and subsequent energy release processes by the quantification of the light energy released. This work will be followed by a study of the charge relaxation after the removal of the voltage. It will be carried out in order to estimate the energetic level of traps in which charges are likely to be trapped during voltage application.

Spectral studies will also be carried out in order to identify the molecular groups involved in the light emission phenomena. These spectra are rather complex due to the variety of chemicals included in the epoxy resin materials. This study is intended to determine which molecules or molecular groups are involved in the structure of the network and which remain as independent entities in the system.

Each technique and the results will be detailed in the following chapters. During the analysis of the data obtained, the origin of the features will be identified and the results from different techniques compared. As electrical ageing is expected to occur by creating irreversible damage, the various techniques of investigation will be also used as tools to determine the variation in the properties as the material is stressed.

Chapter II

Material description and sample preparation

I- Epoxy resin

I.1- Chemical description

From the commercial point of view, epoxy polymer resins are the most important of the non-vinyl polymers [1]. In the present work the Araldite CY1301 and the hardener HY1300 have been selected because they are non-toxic products. Besides, they are convenient to handle because they can be cured at room temperature giving a glassy final product.

- The Araldite is described by the manufacturers Ciba-Geigy as a Bisphenol-A epoxy resin containing reactive solvent. It appears as a clear straw coloured liquid. The viscosity at 25°C is estimated to be between 800 and 1500mPas [2].

- The hardener is a clear yellow liquid. The viscosity is lower and situated between 170 and 210mPas at 25°C [2].

The manufacturers do not supply details of their products for commercial reasons. However, it has been found [3] that the base resin is a mixture of Diglycidyl Ether-Bisphenol A (DGEBA) and Iso-Octyl Glycidyl Ether (IOGE). The Chemical formulae are given figure II-1.a.

The composition of the hardener [3] reveals the presence of three main components represented by the most likely formulae figure II-1.b:

- Polyoxypropylene (mayor percent by weight) that may act as a diluent if the end groups do not contain reactive moieties such as for instance amine groups.

- Triethylene Tetra Amine (TETA) containing the main reactive amine groups

- Salicylic Acid (a few percent by weight) that may operate as an accelerator

DGEBA

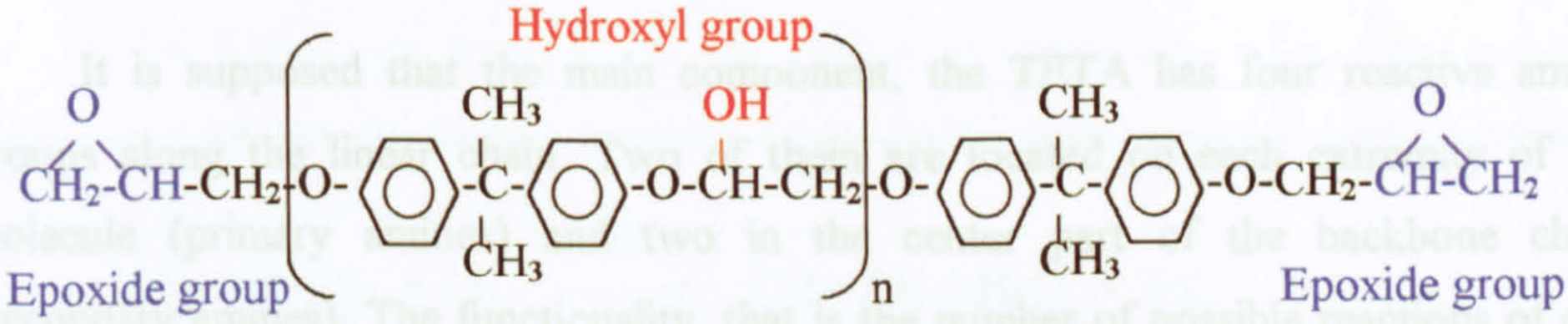

n number of repeat groups: 0 for prepolymers

IOGE

Example of isomer of octane:
2 2 2 Trimethylpentane

Isomer of
Octane

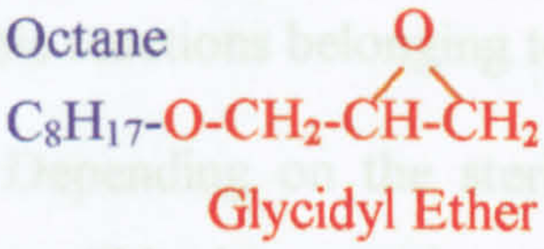

Glycidyl Ether Group

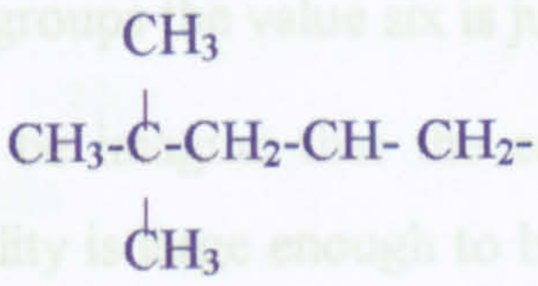

(a) Diglycidyl Ether-Bisphenol A (DGEBA), Iso-Octyl Glycidyl Ether (IOGE)

TETA

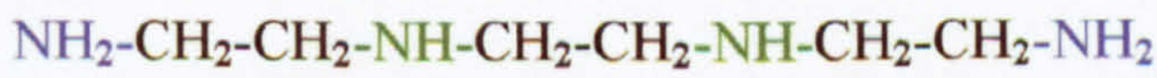

Primary Amine — Secondary Amine — Primary Amine

Polyoxypropylene

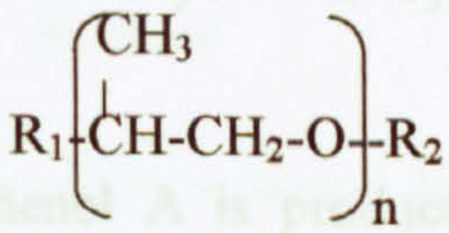

n: number of repeat unit (unknown)
R_1, R_2 alkyl groups (unknown)

Salicylic Acid

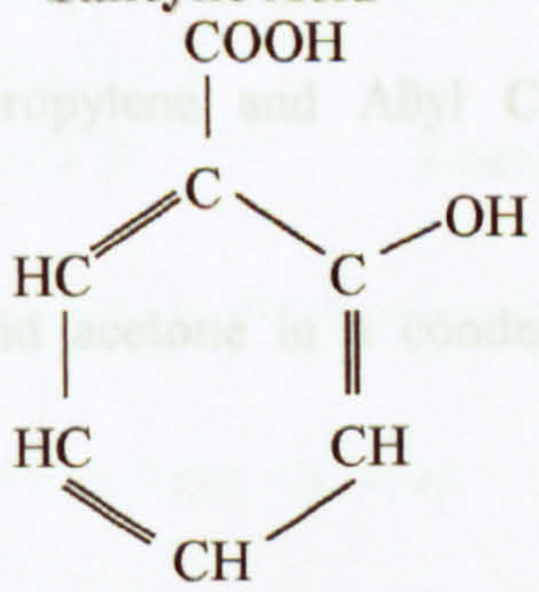

(b) Triethylene Tetra Amine (TETA), Polyoxypropylene, Salicylic Acid

Figure II-1: **(a)** Components of the base resin

(b) Hardener components

It is supposed that the main component, the TETA has four reactive amine groups along the linear chain. Two of them are located on each extremity of the molecule (primary amines) and two in the center part of the backbone chain (secondary amines). The functionality, that is the number of possible reactions of one type is then supposed to be equal to six when related to the amine groups. Theoretically, from a primary amine two reactions can be completed and from a secondary amine only one chemical reaction can occur. By adding the number of possible reactions belonging to all the four amines groups the value six is justified.

Depending on the steric dimensions it can be imagine that the central amine groups will be less reactive. Anyway the functionality is large enough to build a three-dimensional polymer network after reaction with epoxide groups. In order to create a network the functionality of the reactive molecule must be higher or equal to three otherwise only linear chains can be grown.

I.2- Product synthesis

Epoxies have a complex molecular network and are usually formed in a two-stage process. First of all the pre-polymer DGEBA is prepared by a base catalyzed step-growth reaction of a dihydroxy compound such as bisphenol-A with an epoxide like Epichlorohydrin [4].

- The Epochlorohydrin is synthesized from propylene and Allyl Chloride (Figure II-2) [5].

- The Bisphenol A is produced with phenol and acetone in a condensation reaction producing water (figure II-3) [5, 6].

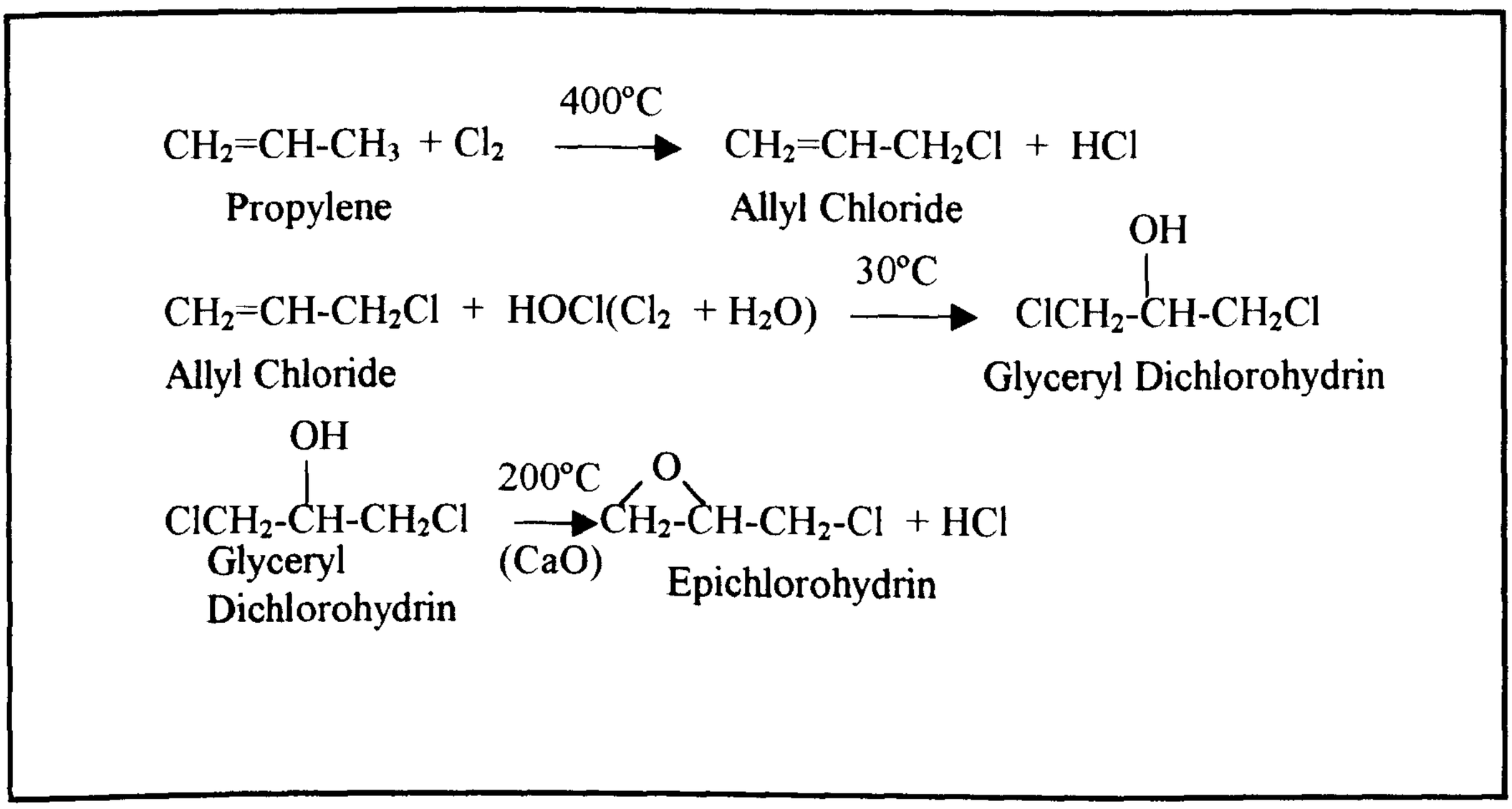

Figure II-2: Preparation of Epichlorohydrin from Propylene and Allyl Chloride

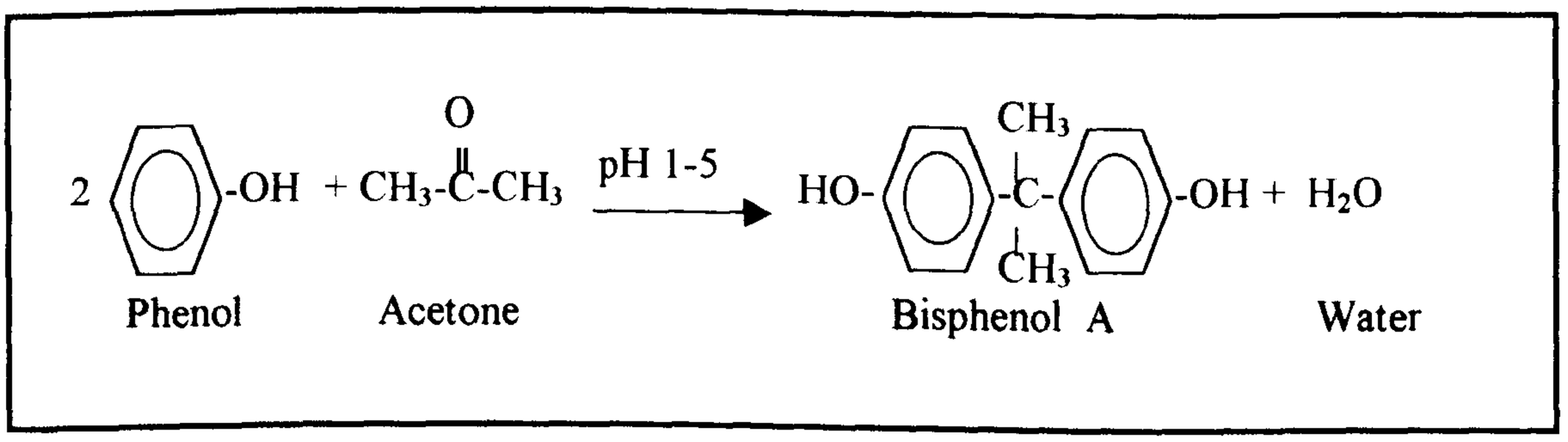

Figure II-3: Preparation of Bisphenol A from Phenol and Acetone

To prepare the DGEBA, two steps are necessary (figure II-4) [5, 6]:

- The initial epoxy group of the Epichlorohydrin reacts with the phenolic hydroxyl groups of the Bisphenol A. This reaction is catalysed by NaOH and gives a chlorohydrin intermediate component.

- The hydrogen and chlorine are then removed from the chlorohydrin intermediate, by reaction with NaOH, to produce new epoxy groups.

The molecular weight of the resulting resin depends on the ratio of Epichlorohydrin to Bisphenol A employed. In general high molecular weights are not desirable because of the handing difficulties. In theory the monomeric DGEBA (n= 0) is obtained by mixing two moles of Epichlorohydrin with one mole of Bisphenol A. In practice the ratio of Epichlorohydrin required must be tripled otherwise higher molecular weight products predominate. An excess of Epichlorohydrin is therefore necessary [4].

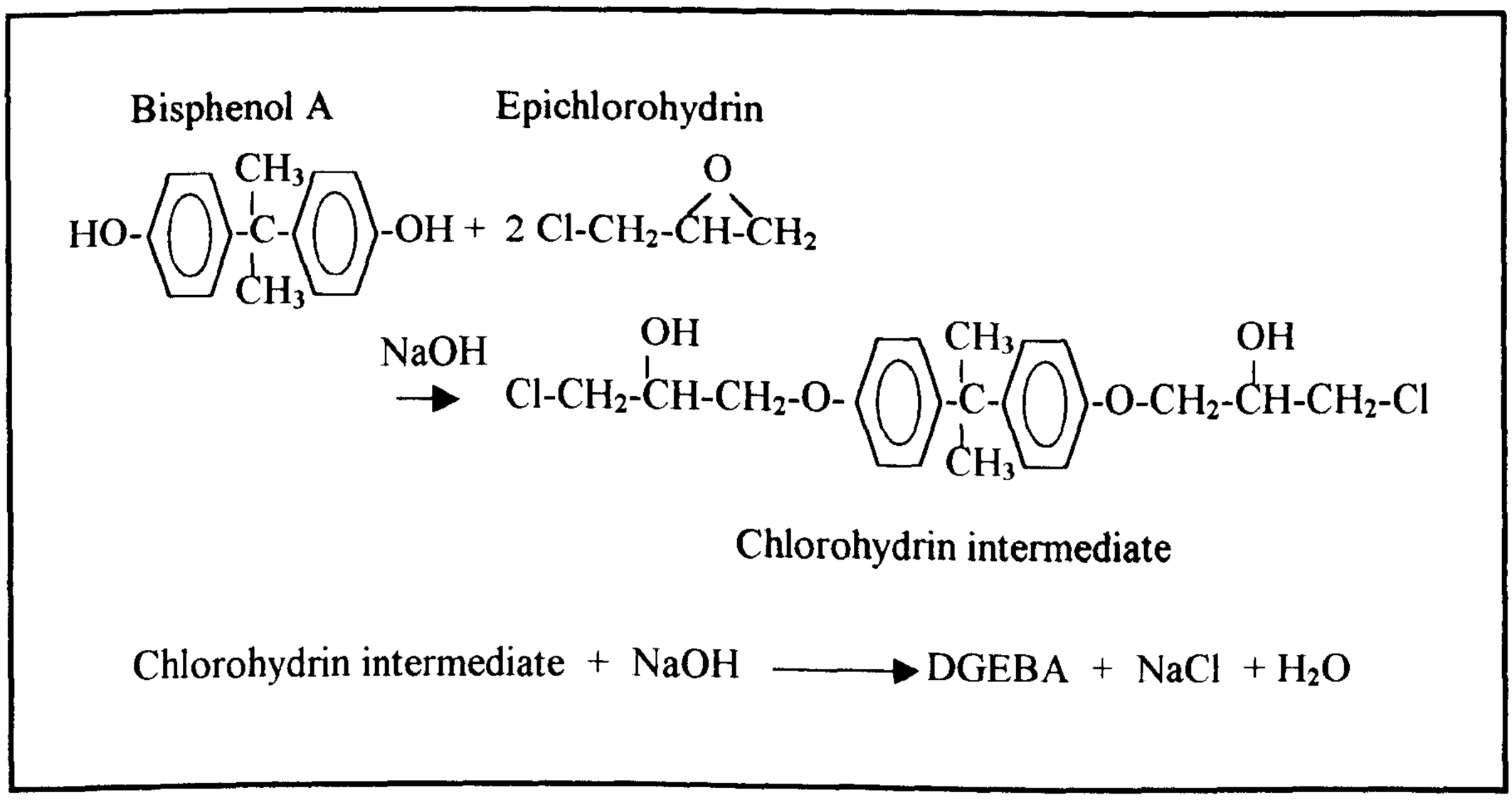

Figure II-4: Synthesis reactions of DGEBA

I.3- Polymerisation mechanism

The final curing of the epoxy resin involves a reaction with a hardening agent such as a diamine with the terminal epoxide group thus forming a cross-linked polymer structure.

In the present case the epoxy resin base is mixed with the hardener containing primary and secondary amine active groups. The pre-polymer molecular weight is increased and the network is formed during a separate cure step. The bridging oxygen in the epoxide group is opened up in a nucleophilic poly-addition reaction. The reaction between an amine and an epoxide group is shown figure II-5. At first, the primary amine reacts with the epoxide group to give a secondary amine and a hydroxyl group. Secondly, the secondary amine reacts with another epoxide group to give a tertiary amine [7].

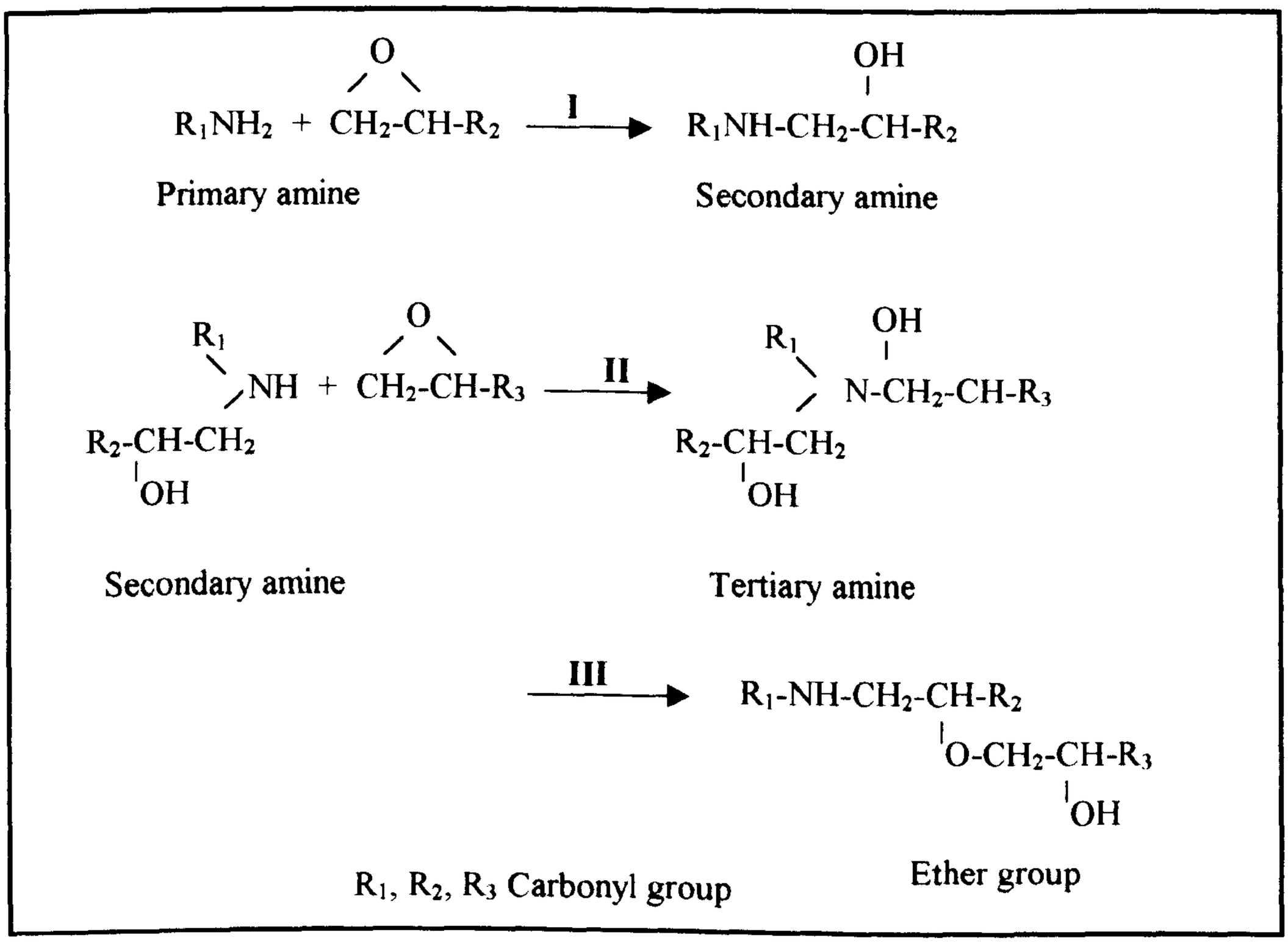

Figure II-5: Polymerisation reaction between molecules with amine group and epoxide group. **(I)** Primary amine to secondary amine reaction. **(II)** Secondary amine to tertiary amine reaction. **(III)** Secondary amine to ether reaction

On the other hand, if the concentration of hydroxyl group is high, etherification becomes highly possible. This other reaction takes place between –OH groups along the chain and epoxide rings forming ether groups [7]. This latter reaction does not affect the hydroxyl group concentration but consumes epoxide sites limiting the use of amine groups. It has been shown that this reaction is emphasized if the chemical reaction is carried out in contact with air. It is common in room temperature cured epoxy resins and it can affect the mechanical properties. A post-cure at higher temperature has been shown to make this reaction reversible and can therefore be used to reduce its contribution to the final product. The presence of this undesirable reaction is easily identified since it produces noticeable white marks on the surface of a sample that is expected to be transparent and clear. Another way to limit this reaction is to reduce the hydroxyl group concentration, that is why the DGEBA pre-polymer with the number of repeat unit $n \cong 0$ is initially chosen. But in fact each amine-epoxy reaction site will produce an additional OH group and might make it impossible to prevent the etherification reactions from occurring once the polymerization process has been initiated.

In addition, it is noticeable that the presence and development of hydroxyl groups will influence the rate of reaction. The reaction can be accelerated in the presence of proton donors (e.g. salicylic acid) as shown in figure II-6. It is supposed that in the presence of amine groups, the salicylic acid can react giving a mono-anion. The acid group may open the epoxide ring. It is also possible that a fraction of the salicylic acid exists in the mixture as a mono-anion or as the di-anion if an additional proton donation takes place. The concentration of both species will depend on the equilibrium conditions. This hypothetical reaction would justify the role of salicylic acid in the system.

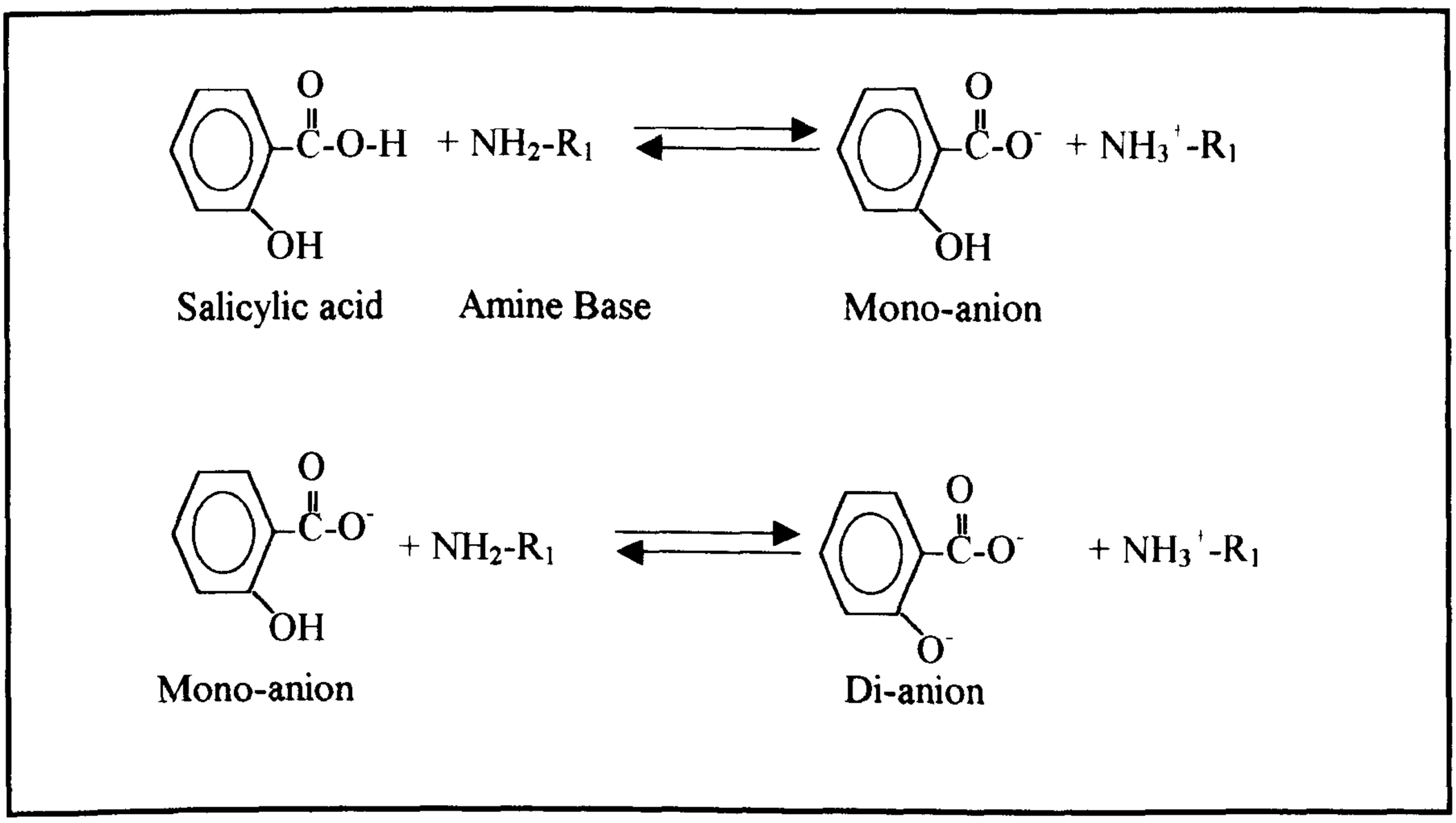

Figure II-6: Reaction between salicylic acid and amine group leading to an equilibrium

Finally, a condensation reaction involving salicylic acid and the hydroxyl groups may take place, especially later on during the process when the hydroxyl group concentration increases (figure II-7).

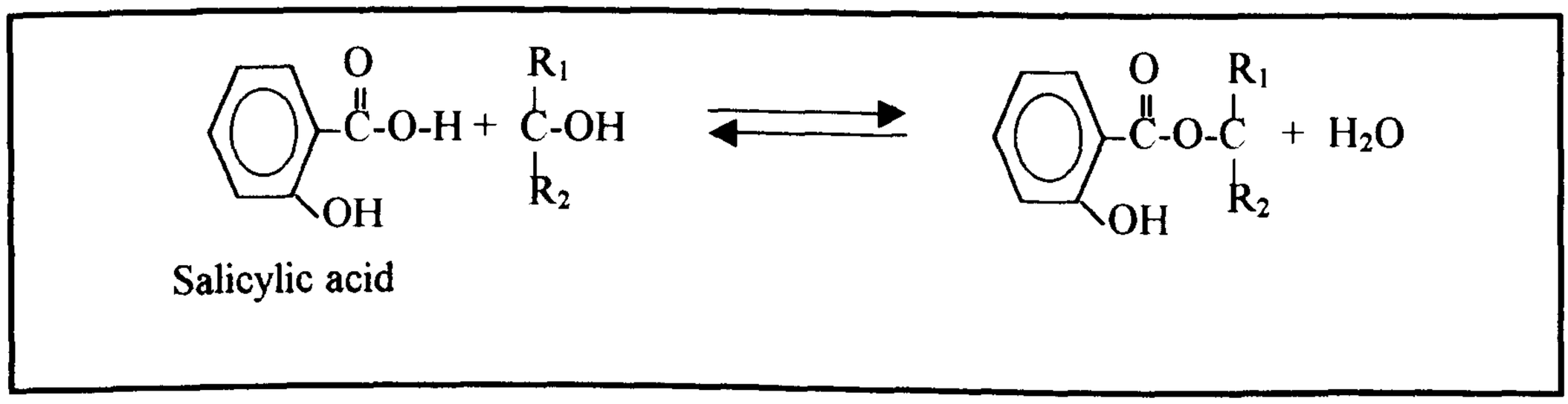

Figure II-7: Reaction between salicylic acid and hydroxyl groups

To conclude, the role of salicylic acid may be quite complex. It may help the polymerization to be initiated by the generation of hydroxyl groups and then subsequently limit it by their use in a reversible reaction

I.4- Network structure

A huge increase in the molecular weight of the polymer occurs during the hardening reaction. This is a consequence of the formation of a three-dimensional polymer network. In the ideal situation of a fully cured system the epoxy is comprised of a single giant molecule.

In general the cross-linking density is defined as the number of effective cross-links per unit volume [6]. In DGEBA (n= 0), if the aromatic groups are counted as one unit, the epoxide groups are then separated by seven units. It is considered to be this short spacing that gives a rigid final product [6]. The flexible properties of the molecular system and the system functionality are strongly dependent on the number of joins and also on the curing agent. That is why the presence of diluents and reactions that prevent links between amine groups and epoxide groups may help to create a glassy system [8]. These secondary reactions prevent the system from evolving with time because they may have consumed all the reactive sites. But it is also possible that some small molecules like salicylic acid for instance remain in the system acting as a plasticizer.

The final structure, shown in figure II-8 as a two-dimensional representation, gives an idea of the complexity of the system. The unreacted groups (A*) are supposed to be able to give further reaction. The number of such active groups increases as the size of the structure increases. The growth of the network will stop at some stage when the mobility of the molecules is limited by the increase of the viscosity [9].

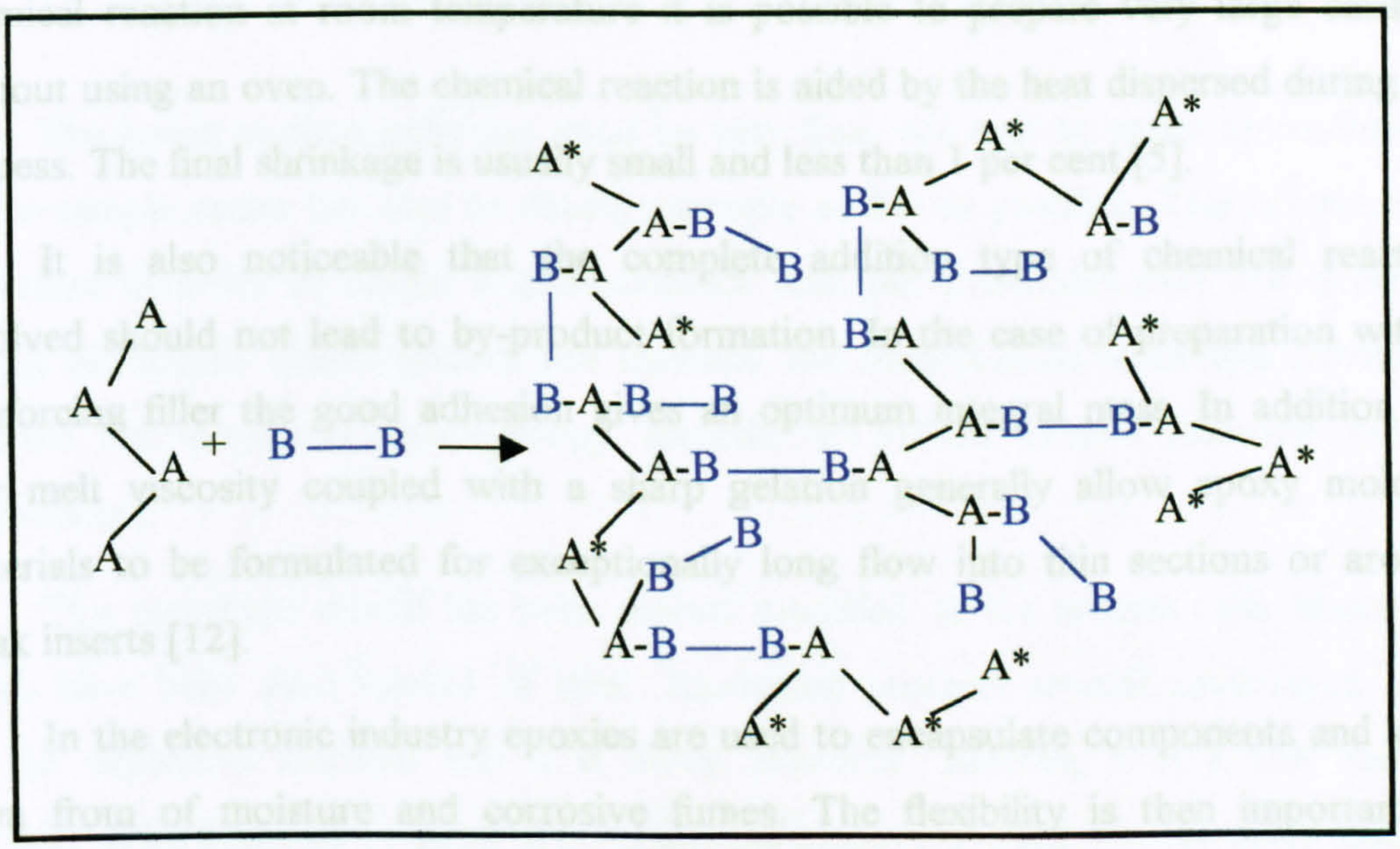

Figure II-8: Two-dimensional structure of a network build by polymerisation

I.5- Properties of the cured resin

The initial uncured epoxy base resin is classified as a *thermoplastic* because it can be liquefied by an increase in the temperature and the liquefaction can be reversed on cooling. After reaction with the hardener the material obtained is not "plastic" any more, and belongs to the *thermoset* group of polymers. The principal difference between thermosets and thermoplastic materials is the formation of a network structure upon fabrication. This network may be formed by covalent or physical links that connect individual molecules. Thermosets materials are considered to have a high density of cross-links that make them infusible, insoluble and dimensionally stable [10]. Once formed, these cross-linked networks are expected to resist heat softening, creep, and solvent attack. This makes these materials suitable for composite, coating and adhesive applications.

In the present case, no volatile products escape during the hardening reaction and the contraction of the solid-state compared to the liquid is minimal. This is useful in a moulding process where the material is required to retain the shape of the mould without retraction [11]. One of the properties appreciated by manufacturers is the fact that to initiate the polymerization reaction no pressure need be applied to the

base/hardener mixture. Because the amine groups of the hardener can initiate the chemical reaction at room temperature it is possible to prepare very large castings without using an oven. The chemical reaction is aided by the heat dispersed during the process. The final shrinkage is usually small and less than 1 per cent [5].

It is also noticeable that the complete addition type of chemical reaction involved should not lead to by-product formation. In the case of preparation with a reinforcing filler the good adhesion gives an optimum integral mass. In addition the low melt viscosity coupled with a sharp gelation generally allow epoxy molding materials to be formulated for exceptionally long flow into thin sections or around weak inserts [12].

In the electronic industry epoxies are used to encapsulate components and keep them from of moisture and corrosive fumes. The flexibility is then important to maintain a good adhesion while the embedded components expand or contract due to temperature variations.

Electrical and physical properties for the present resin have been quoted [2] for samples a week after preparation at room temperature and reported in appendix 1.

It has been found that a post-cure of 1h at 100°C can modify some of the properties. For instance the electric strength was found to rise to about 13-14MV/m after post cure, whereas the loss tangent decreased to 0.005-0.007.

II- Moulding process

II.1- Mould design

II.1.1- Prototype from Guildhall university

In order to prepare some epoxy resin films from originally unmixed Araldite and hardener products, a mould is a necessity. The first mould used the design of J. Champion from London Guildhall University. This elementary mould is composed by two rectangular metal plates of the same dimension. The dimensions of the plates are 60x90mm with a thickness of 7mm.

The inside surface polishing must be very fine, not only to make the collection of the sample easier but also to obtain a sample as flat as possible. This is extremely important in order to obtain a good contact with the electrodes used for electrical ageing or analysis measurements. For instance, the contact must be as near perfect as possible for dielectric spectroscopy records or Pulsed Electro-Acoustic (PEA) experiments.

This prototype mould has been slightly modified. In the present case, aluminum plates have been used instead of steel. Aluminum presents several advantages. It is not an expensive material and it is easily procured. Besides, it is a soft enough material to be polished by hand in a reasonable amount of time. On the other hand, it is easy to scratch the surface. For this reason, it is necessary to handle the plates carefully after preparation.

The plates have been cut in a sheet 1cm thick and then polished on one surface. In this case, the plates have surface dimensions of 78mmx7.7mm (figure II-9). The polishing has been carried out by using several kinds of emery papers. The plates have been polished first on a flat surface with a 2/0 emery cloth and then on a grinder polisher with waterproof silicon carbide papers number 220, 1000 and at last 4000grit. Each step can take between 5 and 10 minutes depending on the quality of the aluminum.

If the original metal contains a lot of impurities, then the impurities are removed during polishing creating some little cavities on the surface. Extra polishing time is then required to remove the cavity. After these operations the plates are polished with liquid metal polish using a paper tissue leading finally to a mirror finish. The liquid metal allows cleaning the surface of the plate. A soft paper tissue is used to spread it on the surface without scratching it.

Both plates have four holes, one in each corner where the screws are positioned to close the mould. The top plate (figure II-9.a, b) also contains two pouring slots parallel to the width of the plates and four more holes than the bottom plate. A distance of 55mm separates the slots. This distance represents the useful length of the sample (figure II-9.a). The slots are 7mm wide and possess an inclination of two degrees between the external and polished internal side of the plate so as to make the collection of the sample easier. These slots have three main uses. First one slot is used to fill the mould, secondly the opposite slot is used to check that the resin has crossed the whole length before becoming hard. Thirdly, they can be used to aid the release of the sample from the mould. For this reason the walls of the slots must be properly polished.

To help the resin to pass through the mould the slot must be deep enough to contain more resin than needed to prepare the thin film. It is for this reason that a thick plate is used. In fact, the viscous mixture epoxy resin/hardener is pushed inside the mould by means of its weight. The four extra threaded holes on the top plate are used to open the mould. Four screws are used simultaneously to separate the two plates with the same pressure on the four corners.

To control the thickness of the sample between the plates some spacers are positioned (figure II-9.c). They are held in place by the screws used to close the mould. Obviously, the thickness of the sample can be varied by changing the spacer or using more than one at the same time. Transparent sheets, such as OHP sheets, are convenient to use as spacers because they are easy to cut with a scalpel and can be replaced each time. This prevents any difficult cleaning since the resin can be hard to remove after hardening. The thickness of the spacers used in the present case varies from 60 to 110 microns. It is important to notice that the thickness can limit the size of the sample. The mixture epoxy resin/ hardener polymerizes while filling the mould. It is known that 50ml of resin once mixed has a lifetime of about two hours and a half at 25°C. After that time it no longer flows. The viscosity increases with time and if the thickness is small the resin might not reach the second slot before becoming too hard to flow.

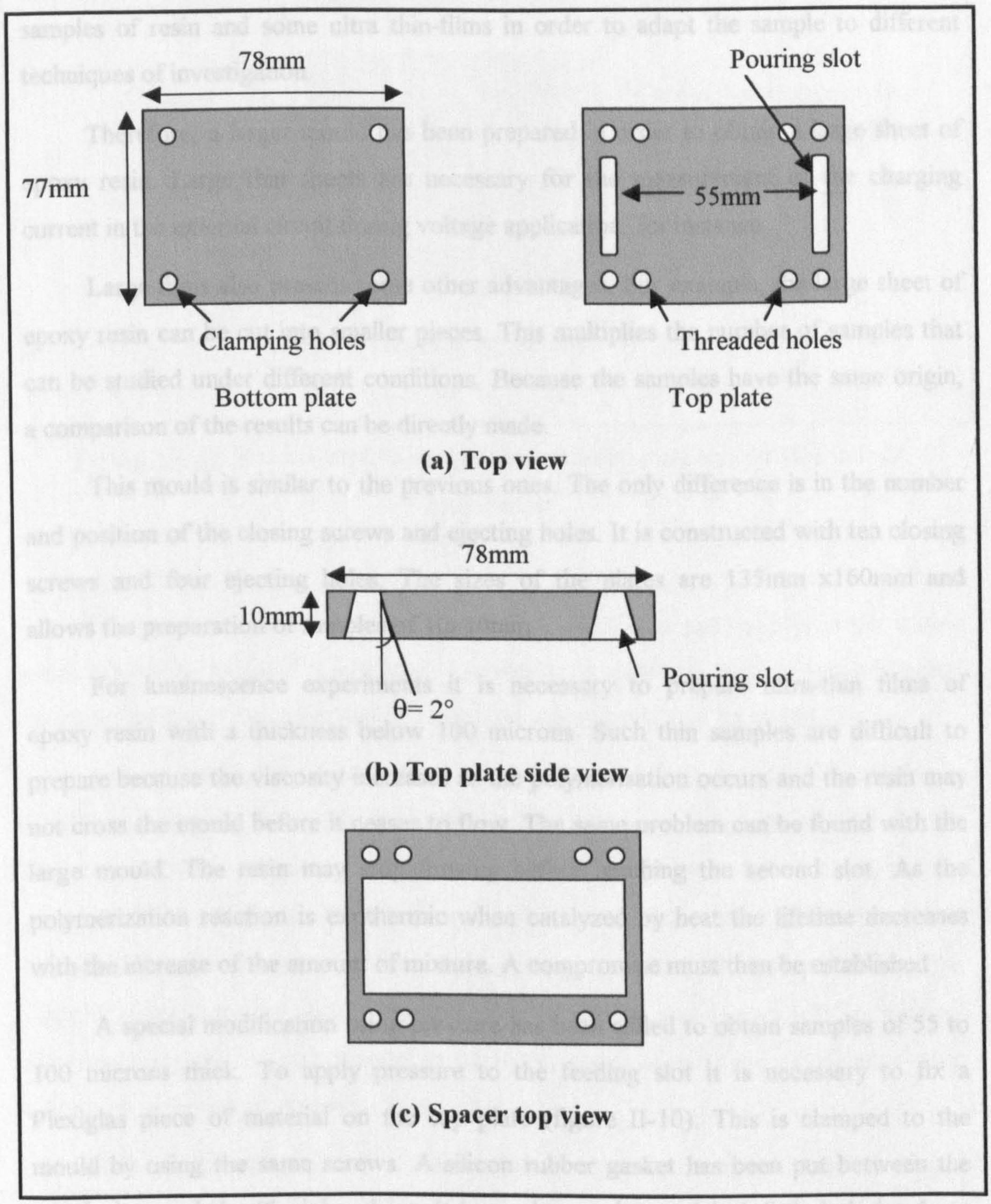

Figure II-9: **(a)** Top view of top and bottom plates of the mould.
(b) Side view of top plate **(c)** Top view of a spacer

II.1.2- Modifications for large sheets and ultra thin samples

Two other objectives have been set. It has been decided to prepare some large samples of resin and some ultra thin-films in order to adapt the sample to different techniques of investigation.

Therefore, a larger mould has been prepared in order to obtain a large sheet of epoxy resin. Large thin sheets are necessary for the measurement of the charging current in the external circuit during voltage application, for instance.

Large films also present some other advantages. For example, the large sheet of epoxy resin can be cut into smaller pieces. This multiplies the number of samples that can be studied under different conditions. Because the samples have the same origin, a comparison of the results can be directly made.

This mould is similar to the previous ones. The only difference is in the number and position of the closing screws and ejecting holes. It is constructed with ten closing screws and four ejecting holes. The sizes of the plates are 135mm x160mm and allows the preparation of samples of 10x10mm.

For luminescence experiments it is necessary to prepare ultra-thin films of epoxy resin with a thickness below 100 microns. Such thin samples are difficult to prepare because the viscosity increases as the polymerisation occurs and the resin may not cross the mould before it ceases to flow. The same problem can be found with the large mould. The resin may stop flowing before reaching the second slot. As the polymerization reaction is exothermic when catalyzed by heat the lifetime decreases with the increase of the amount of mixture. A compromise must then be established

A special modification using pressure has been added to obtain samples of 55 to 100 microns thick. To apply pressure to the feeding slot it is necessary to fix a Plexiglas piece of material on the top plate (figure II-10). This is clamped to the mould by using the same screws. A silicon rubber gasket has been put between the metal plate and the Plexiglas sheet. It is used as seal material. A little hole has been drilled in the Plexiglas in order to be above the mould's slot. From this hole a pipe is connected to a compressor or a pressurised gas bottle. The pressure is applied to the epoxy resin mixture that fills the slot, until it reaches the other extremity of the mould.

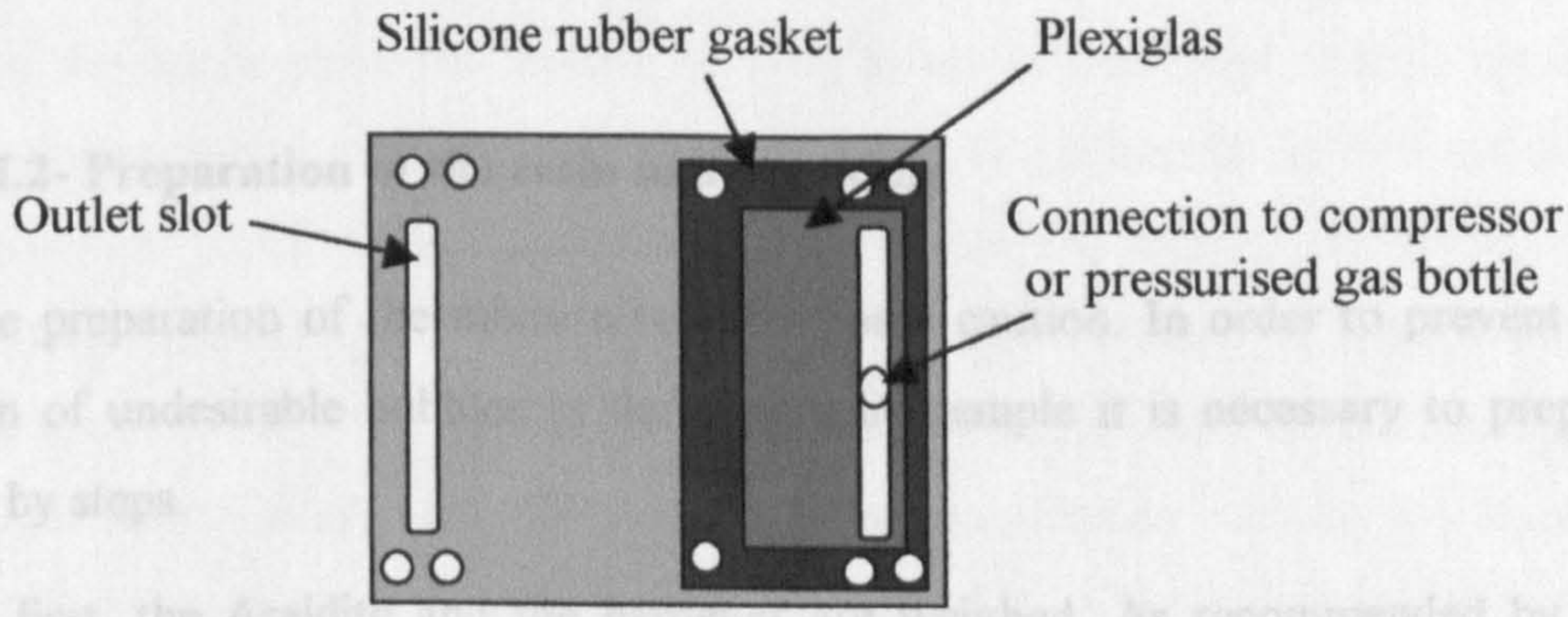

Top view of top plate

Figure II-10: Systems used to apply pressure on pouring slot for thin sample preparation

The pressure must not be so large that it introduces gas bubbles in the epoxy resin. 1/3 bar of pressure is sufficient. Obviously the pressure must be stopped when the resin appears at the other end of the mould otherwise it may be emptied.

After polishing the metal plates must be treated further before the different moulds can be used. They must first be cleaned with a solvent such as acetone and then covered with a thin layer of silicone grease. The plates are then placed in the oven at 150°C and heated for 10hours. When removed and cooled down, the plates are cleaned again with paper to remove the extra grease. They are then polished with a piece of chamois leather cloth. This operation of cleaning and heating will be repeated after the preparation of ten samples, in order to remove all extra pieces of epoxy resin that could remain stuck to the surface.

Before every utilisation it is also necessary to spread some silicone oil release agent on the surface. It is important remove the excess with a piece of cloth. This oil will prevent the sample sticking to the plate without affecting the properties of the epoxy resin.

II.2- Preparation of the resin and moulding

The preparation of the mixture requires some caution. In order to prevent the formation of undesirable bubbles in the final solid sample it is necessary to prepare the resin by steps.

At first, the Araldite and the hardener are weighed. As recommended by the manufacturer the ratio used is 100:33 base epoxy resin to hardener by weight. The two components are put into two different plastic beakers. The use of polypropylene beakers is recommended [2] since the products are very sticky and beakers are difficult to clean with a small amount of solvent after use. Both beakers are put under a bell jar connected to a vacuum pump (figure II-11). The whole system is heated by using a hot plate. The hot plate is placed under the metal sheet on which the bell jar is settled. The aim is to gently heat the metal sheet and the beakers under vacuum. Some silicone grease is used to assure a good contact between the bell jar and the metal sheet and improve the vacuum.

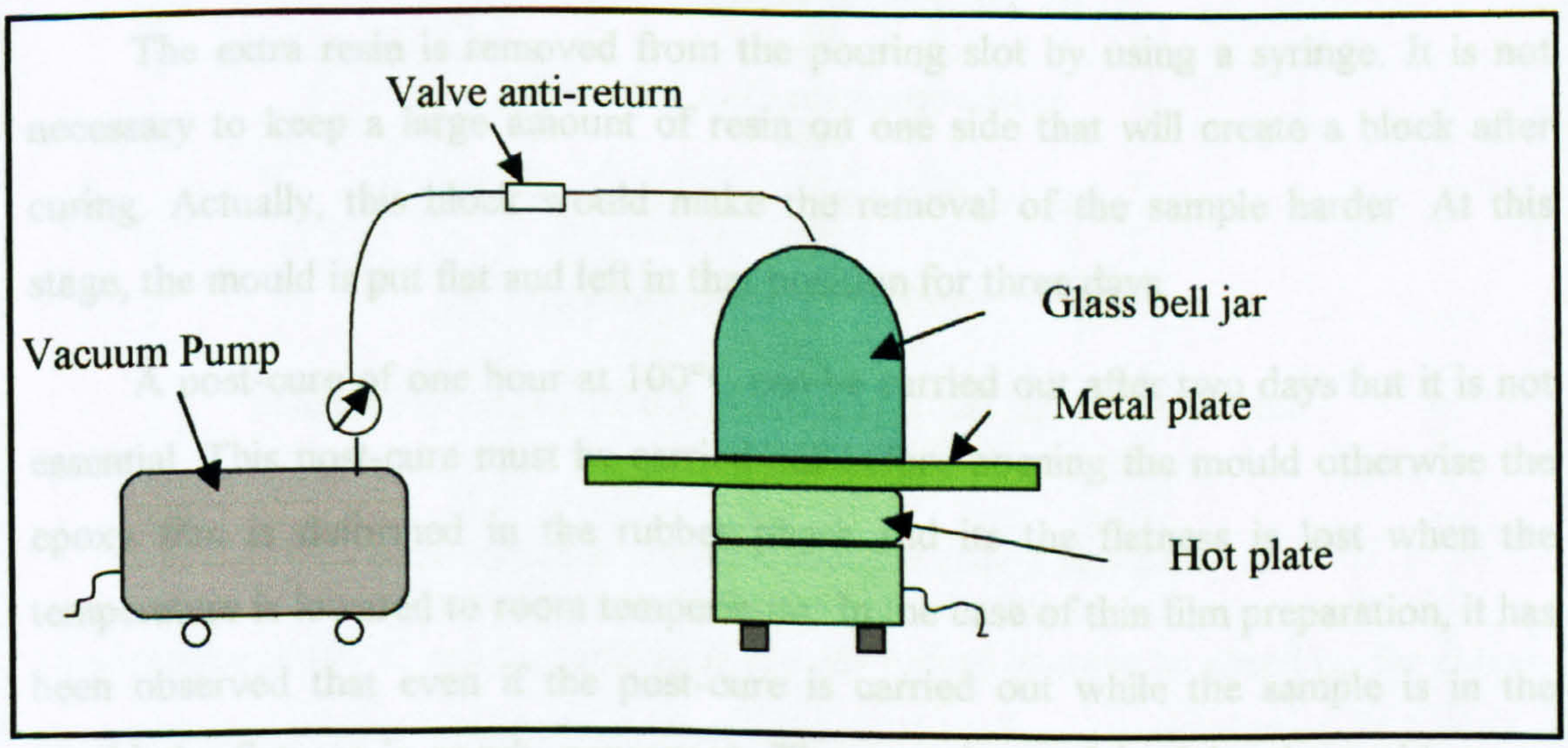

Figure II-11: Equipment used to degas the resin

The temperature is set at 35°C to make the degassing process easier. By increasing the temperature the viscosity of the products decreases and the included gases can be extracted in a shorter amount of time. The products are left two hours under vacuum at about 1mbar. After that period of time, the Araldite and hardener are collected and mixed at room temperature using a magnetic stirrer. It is necessary to use a low speed to mix the components in order not to introduce a lot of bubbles in the preparation. This mixture is carried out at room temperature because the chemical reaction of polymerisation is exothermic and therefore it is not necessary to heat further since we do not want to accelerate the process before the mould is filled. The mixture is carried out for a few minutes and supposed acceptable when there are no cloudy parts, visible in the beaker.

This sequence is followed by a new period of vacuum for about 15min. This is sufficient to remove the large bubbles introduced during mixture. At this stage the resin is still fluid enough to flow across the mould. It is poured immediately into one slot of the mould. To facilitate the filling process and to avoid trapped air, the mould is tilted. The resin usually crosses the mould and reaches the second slot in less than one hour, though the exact time depends upon the thickness of the spacers and the temperature of the room.

The extra resin is removed from the pouring slot by using a syringe. It is not necessary to keep a large amount of resin on one side that will create a block after curing. Actually, this block would make the removal of the sample harder. At this stage, the mould is put flat and left in that position for three days.

A post-cure of one hour at 100°C can be carried out after two days but it is not essential. This post-cure must be carried out before opening the mould otherwise the epoxy film is deformed in the rubber phase and its the flatness is lost when the temperature is lowered to room temperature. In the case of thin film preparation, it has been observed that even if the post-cure is carried out while the sample is in the mould the flatness is poorly conserved. That may be explained by the rapid cross-linking reaction that occurs with the increase of the temperature that tightens the system which then tends to relax to a less constraining shape after the mould has been opened.

This is the reason why most of the samples have not been high temperature post-cured during this study. In these cases, it was considered that the chemical reaction of cross-linking is completed after one week at room temperature, i.e. a 'so-called' room temperature post-cure. It will be shown later in the chapter by Differential Scanning Calorimetry (DSC) measurements that the glass transition temperature (Tg) of the samples is influenced by the post-curing procedure. Actually, if no post-cure is carried out at high temperature the material might not be fully cured even after several months. In order to obtain flat and cured samples, a compromise should be applied as for instance the reduction of the post-curing temperature to below 100°C or the length of post-curing time.

A résumé of the procedure used to prepare the resin is given figure II-12.

Vapourise silicone oil on the surface of the mould before closing

↓

Weigh Araldite/ hardener in a ratio 33/100 in polypropylene beakers

↓

Put under **vacuum** at **35°C** for **2h**

↓

Mix at RT with magnetic stirrer

↓

Put under **vacuum** for **15min** at **RT**

↓

Pour the mould and tilt it

↓

Remove extra resin from pouring slot and lay the mould flat

↓

Open mould and **collect sample** after a few days
Sample is considered fully cured after 1week
1h post cure at 100°C can be performed the day before opening to speed up the curing

Figure II-12: Experimental protocol for the preparation of epoxy resin samples

III- Configuration for sample with wires

III.1- Modifications to the mould

In order to work with divergent electric fields it has been decided to embed some thin wires into the resin. The idea is to put several of them in the middle of the sample. It is important to control their position and keep them flat. To achieve this it is necessary to have a good tension on the wires. A sample with wires is presented figure II-13.

A frame to support the wires is essential. At first the wires were wrapped around the bottom plate. Then it was decided to use both sides of the bottom plate to prepare wired samples. In this case there is no waste of wire. The bottom plate has been modified to become a duplication of the top plate. Finally a new central plate was prepared (figure II-14). The length of this has been increased compared to the other two plates. This has been done in order that the wires extend far enough on each side of the mould of the sample so as to be able to be connected together later on. Both sides have been carefully polished. In the middle of the long side a screw has been fixed which will be used as a plate holder for the wiring step.

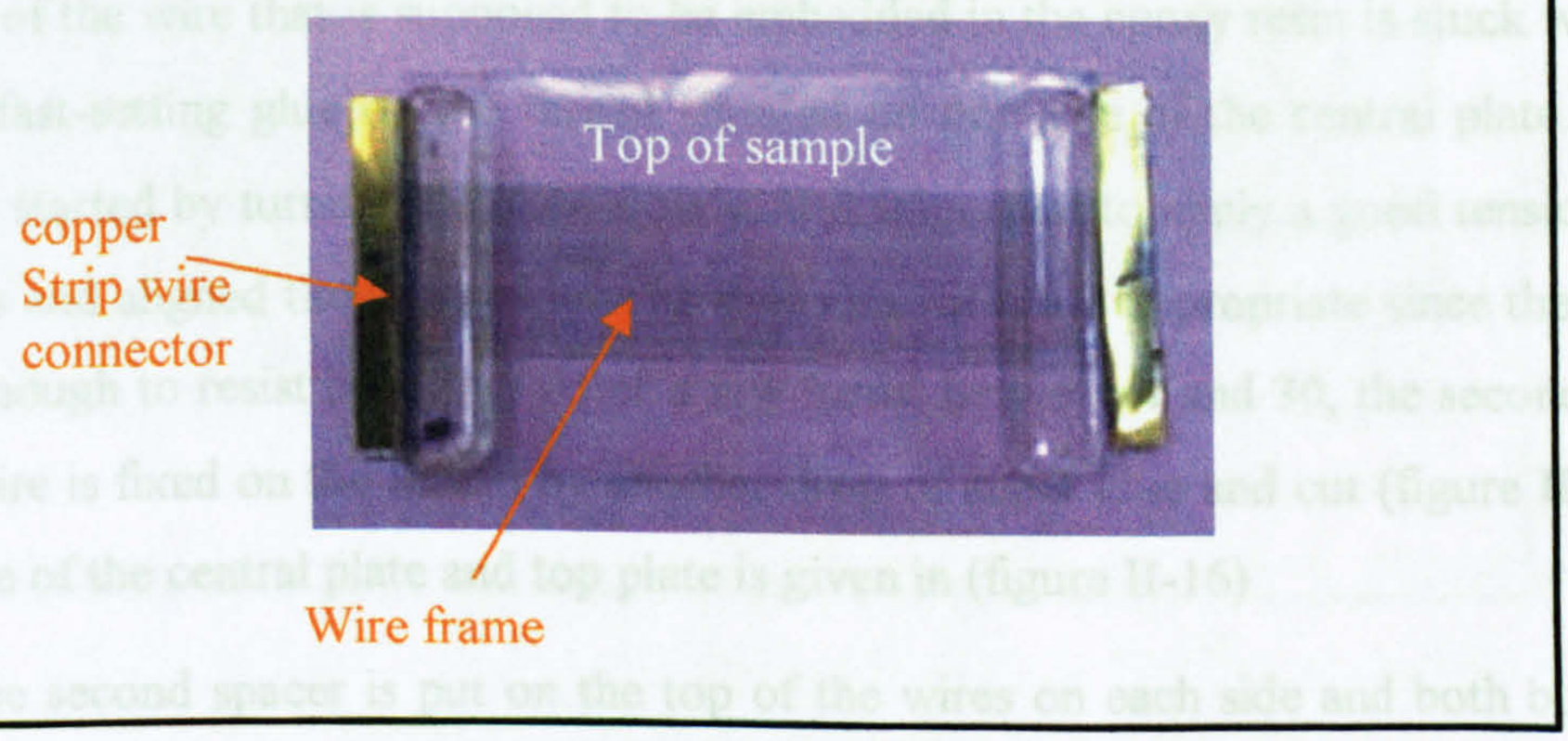

Figure II-13: Sample with wires observed from the top

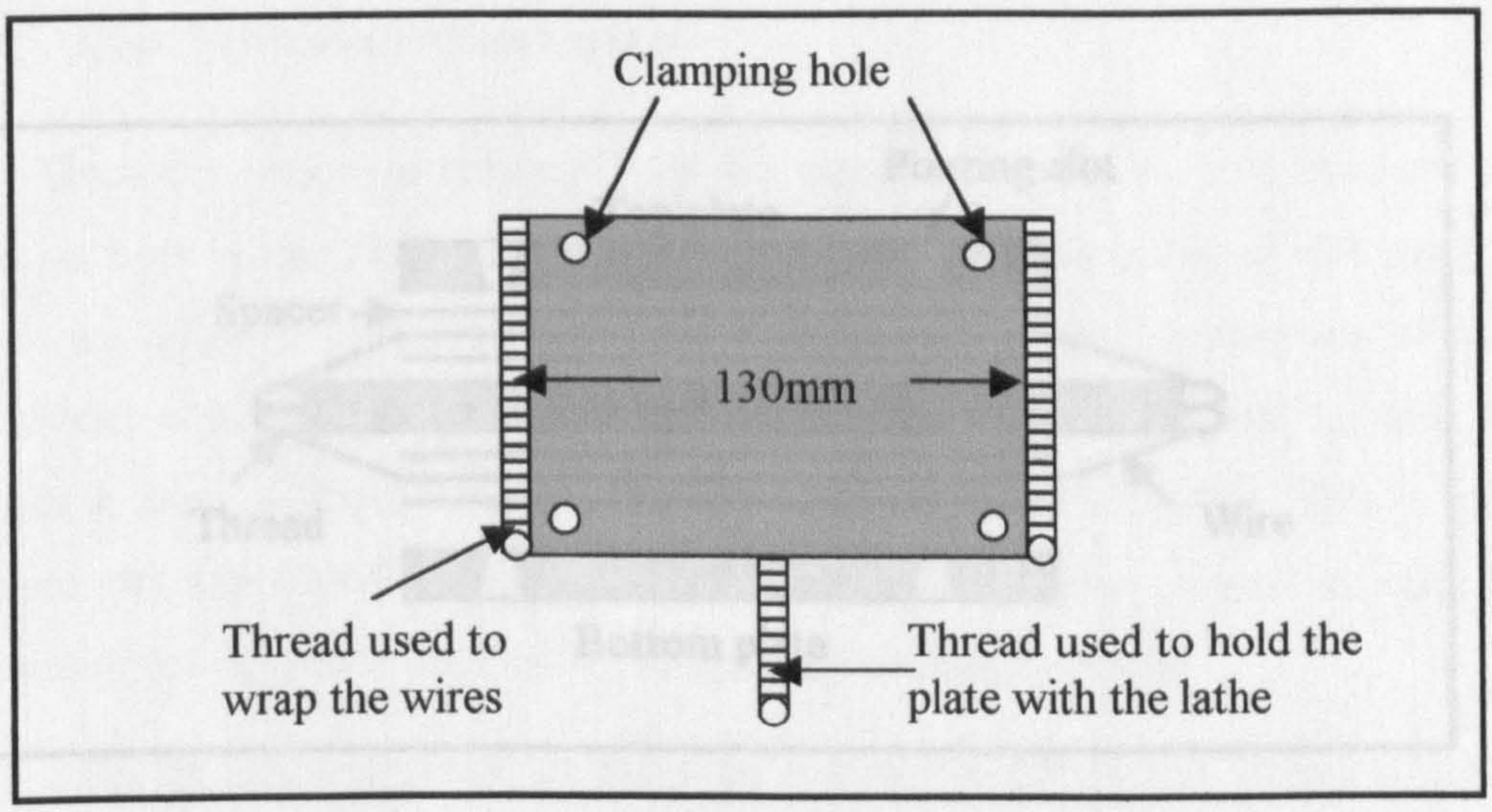

Figure II-14: Top view of central plate designed to prepare samples with wires

Two spacers must be prepared for each side in order to position the wires in the middle of the thickness of the sample. Finally the whole system can be clamped together as previously. In this case, the screws have been replaced by cross threads locked by nuts on both side of the mould.

III.2- Technique for moulding samples with embedded wires

The central plate and one spacer on each side are clamped. The plate is held by the metal side thread and positioned on the lathe. The lathe will be operated manually. The end of the wire that is supposed to be embedded in the epoxy resin is stuck with a drop of fast-setting glue on the thread situated on one side of the central plate. The wiring is started by turning the plate slowly. It is important to apply a good tension on the wires and aligned them properly. The tungsten wires are appropriate since they are strong enough to resist breaking. After a few turns, between 4 and 30, the second end of the wire is fixed on the thread by another drop of super glue and cut (figure II-15). A picture of the central plate and top plate is given in (figure II-16)

The second spacer is put on the top of the wires on each side and both bottom and top plates are clamped on to the central plate. Because it is not possible to fill both sides of the mould at the same time the two samples are prepared with a 24h-time difference.

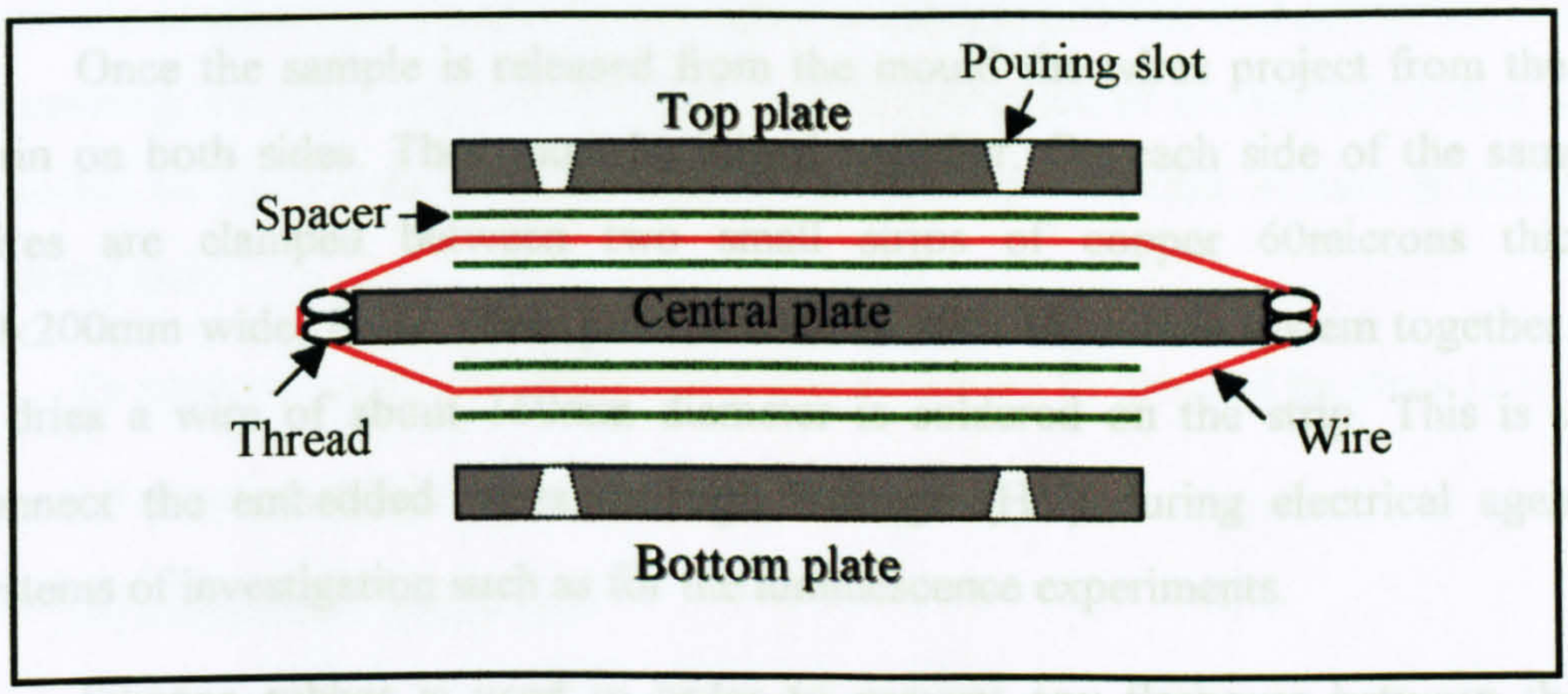

Figure II-15: Side view of the mould designed for wire sample preparation

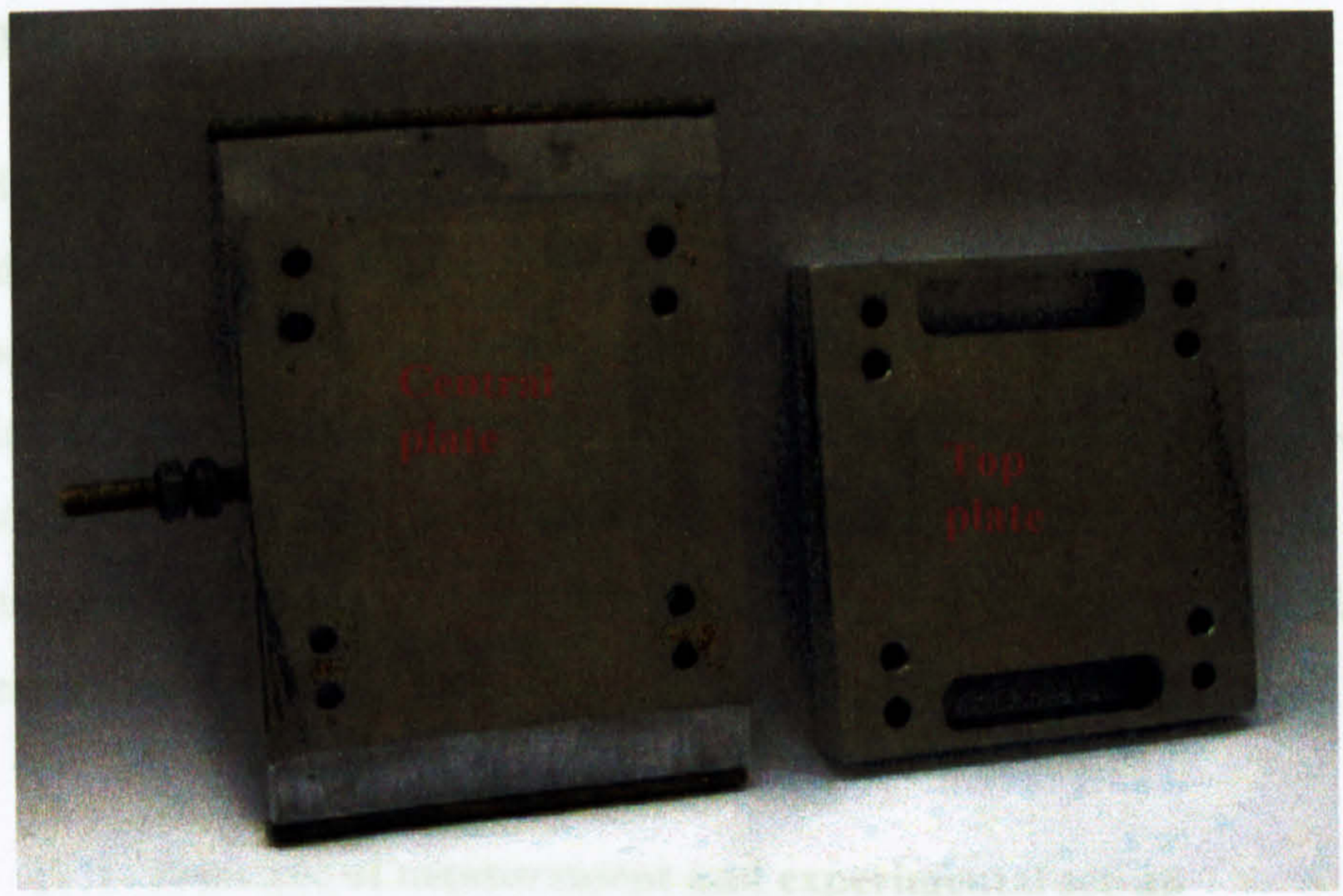

Figure II-16: Central plate and top plate

III.3- Wire connection system

Once the sample is released from the mould the wires project from the epoxy resin on both sides. They must be joined together. On each side of the sample the wires are clamped between two small strips of copper 60microns thick and 50x200mm wide. Some silver paint is used to stick the whole system together. When it dries a wire of about 150mm diameter is soldered on the strip. This is used to connect the embedded wires to High Voltage (HV) during electrical ageing and systems of investigation such as for the luminescence experiments.

Silicone rubber is used in order to prevent any flashover between the earth electrodes on both surfaces of the sample and the wires linked to HV during electrical ageing. It covers and insulates both strips where the wires are connected. The silicone rubber is a white component prepared by Rhône-Poulenc. This component becomes hard after several hours exposure to air. It acts as a barrier and is considered to be a good insulator.

IV- DSC measurement of the glass transition temperature

Usually the properties of polymers change by several orders of magnitude around the temperature associated with the glass transition phenomena. That is why, it is important to estimate this value in any study of the characteristics of polymeric material. One of the most common methods to determine this transition temperature consists in using the Differential Scanning Calorimetry (DSC) technique. Unfortunately, the value cannot be obtained directly because of kinetic effects due to the measurement system. As a result T_g depends significantly on the heating rate.

IV.1- Principle of measurement and experimental set-up

Properties such as specific heat capacity C_p of polymers show a step-increase at the glass transition temperature T_g that belong to the second order of transitions. It is known that the DSC signal is proportional to C_p. This value is obtained from conversion of the heat flow measured by a calorimeter, between two temperatures bracketing T_g.

The DSC system [10] is composed by two aluminum pans, one is empty and the other one contains the sample that is under investigation. The measurements consist in determining the difference of heat that must be provided to the sample during a phase transition to keep both pans in thermal equilibrium while the system is heated at a constant rate.

To perform reliable measurements it is necessary to proceed by steps [13]:

(a) measure the weighed sample (about 10mg)

(b) measure an empty pan

(c) measure a weighed reference, i.e. a sapphire in most of the cases with known characteristics

In each case a curve representing the heat flow toward the sample is drawn as shown figure II-17 and 18. The treatment of data is presented in the following section. Each step is carried out by following a particular protocol described in appendix 2. The repetition of the measurements, i.e two ramps in temperature, on the sample is carried out to provide more accurate results.

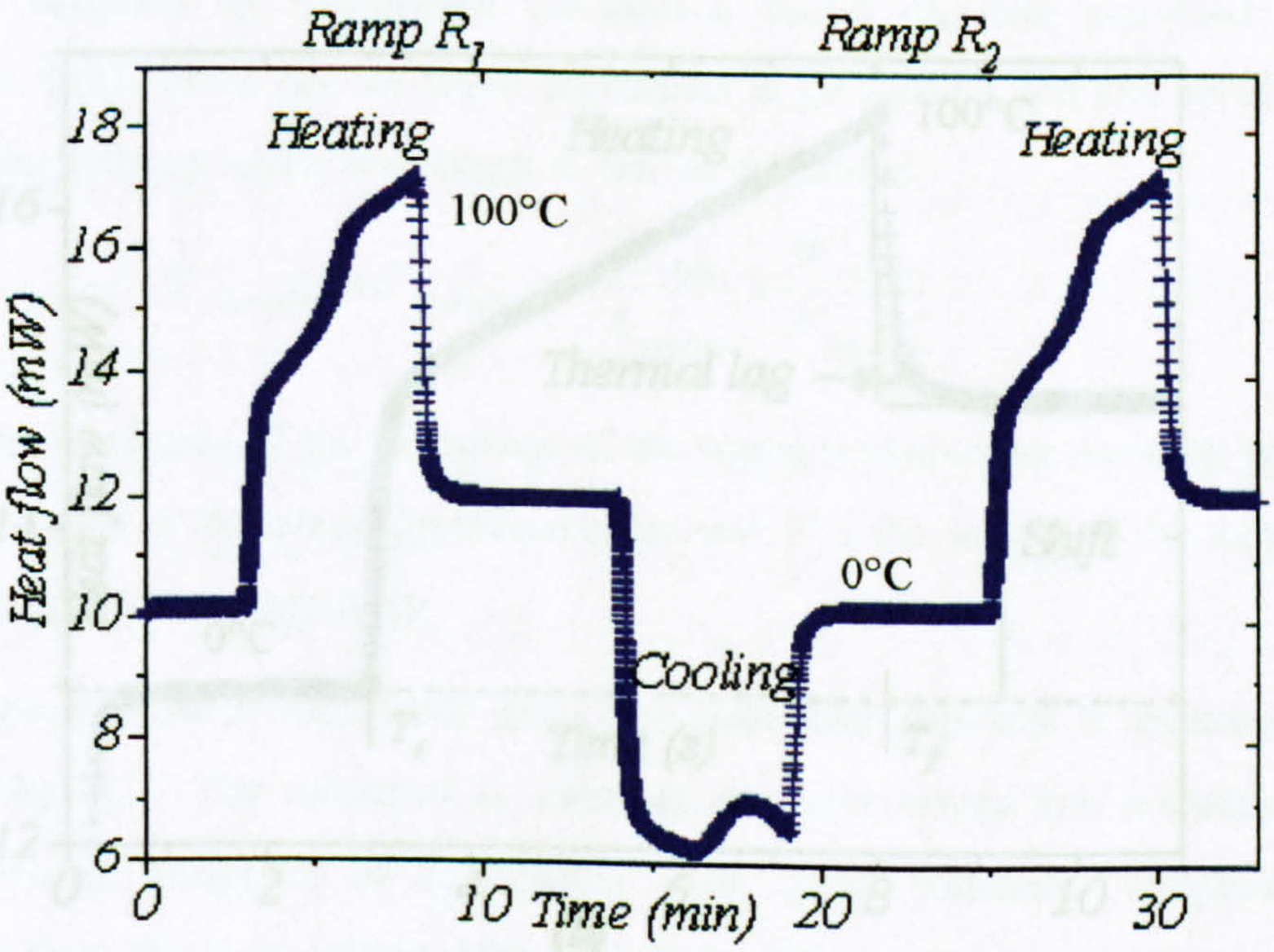

Figure II-17: Recorded heat flow of epoxy resin sample

It is important to use a piece of resin that comes from the bulk to avoid problems created by impurities that are expected to be more numerous at the surface such as absorbed water. Before each measurement of the sample the temperature is raised to 100°C then lowered to 0°C in order to remove residual low molecular weight impurities. The measurement is initiated after stabilization of the heat flow.

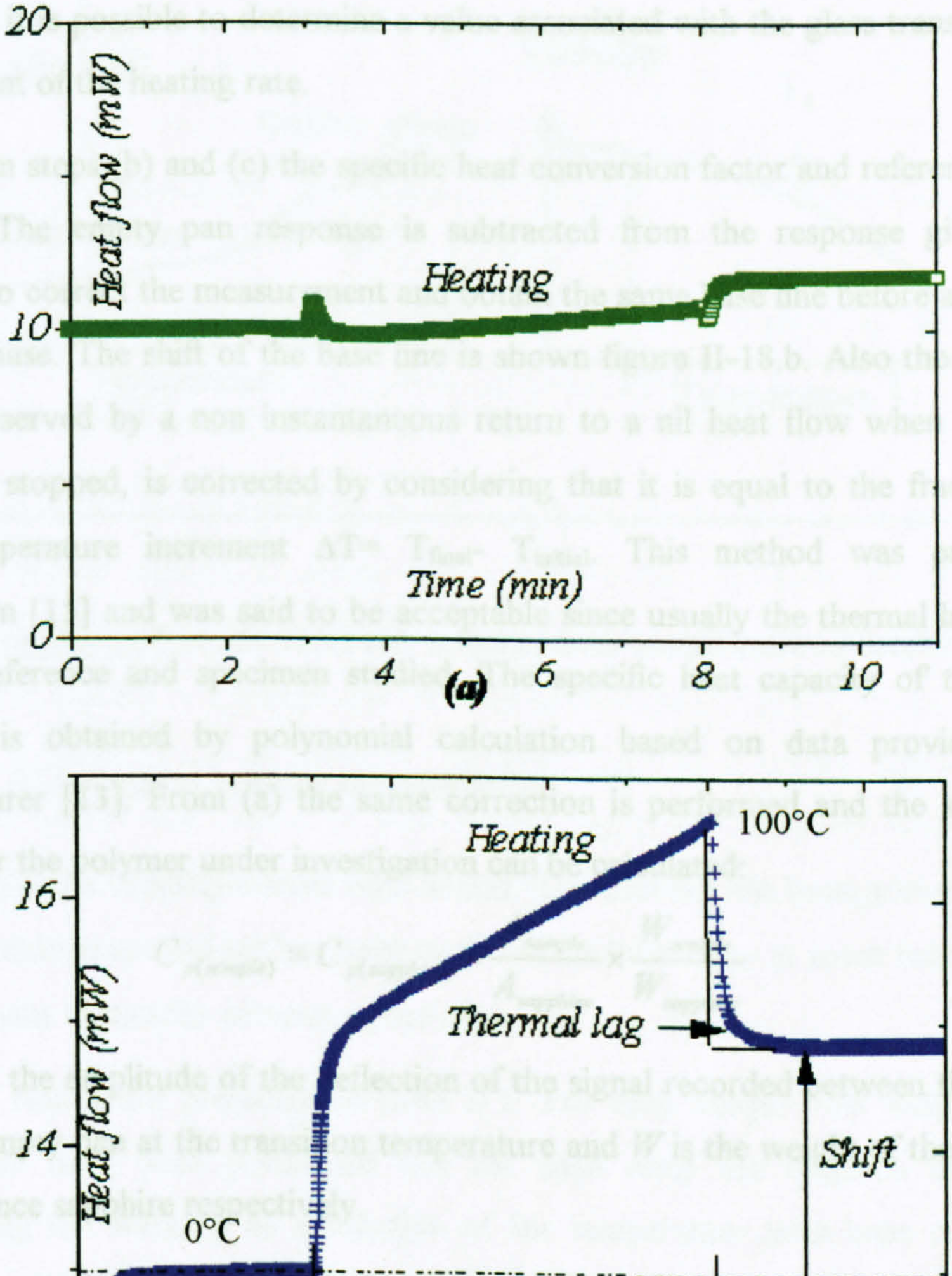

Figure II-18: Heat flow recorded over time **(a)** Empty pan;
(b) Sapphire standard

IV.2- Accurate determination of T_g

The main problem in finding a value related to the glass transition phenomena by means of different techniques comes from the fact that the methods are based on dynamic measurements. They give dynamic T_g values that can only be used to compare samples amongst themselves. By using the method presented by Richardson et al. [14] it is possible to determine a value associated with the glass transition that is independent of the heating rate.

From steps (b) and (c) the specific heat conversion factor and reference data are reached. The empty pan response is subtracted from the response given by the sapphire to correct the measurement and obtain the same base line before and after the heating phase. The shift of the base line is shown figure II-18.b. Also the thermal lag that is observed by a non instantaneous return to a nil heat flow when the heating system is stopped, is corrected by considering that it is equal to the fraction of the total temperature increment $\Delta T = T_{final} - T_{initial}$. This method was proposed by Richardson [15] and was said to be acceptable since usually the thermal lag is similar for the reference and specimen studied. The specific heat capacity of the sapphire standard is obtained by polynomial calculation based on data provided by the manufacturer [13]. From (a) the same correction is performed and the specific heat change for the polymer under investigation can be calculated:

$$C_{p(sample)} = C_{p(sapphire)} \times \frac{A_{sample}}{A_{sapphire}} \times \frac{W_{sample}}{W_{sapphire}} \qquad (II.1)$$

A is the amplitude of the deflection of the signal recorded between the specimen and the empty pan at the transition temperature and W is the weight of the sample and the reference sapphire respectively.

For epoxy resin in the glassy state, the heat flow capacity is expected to be around 1.5 $J.g^{-1}°C^{-1}$. The values of C_p obtained are transformed into enthalpy values by a computing program of calculation. The glass transition temperature is extrapolated from the inter-section of the tangents of the enthalpy curve that are taken in the glassy and rubber region. The accuracy is much better if the tangents are taken as far as possible from the transition region (figure II-19).

Comparison between the first and second ramp of measurements should give values of T_g of the same order since this technique is gives results with an error of +/- 2°C.

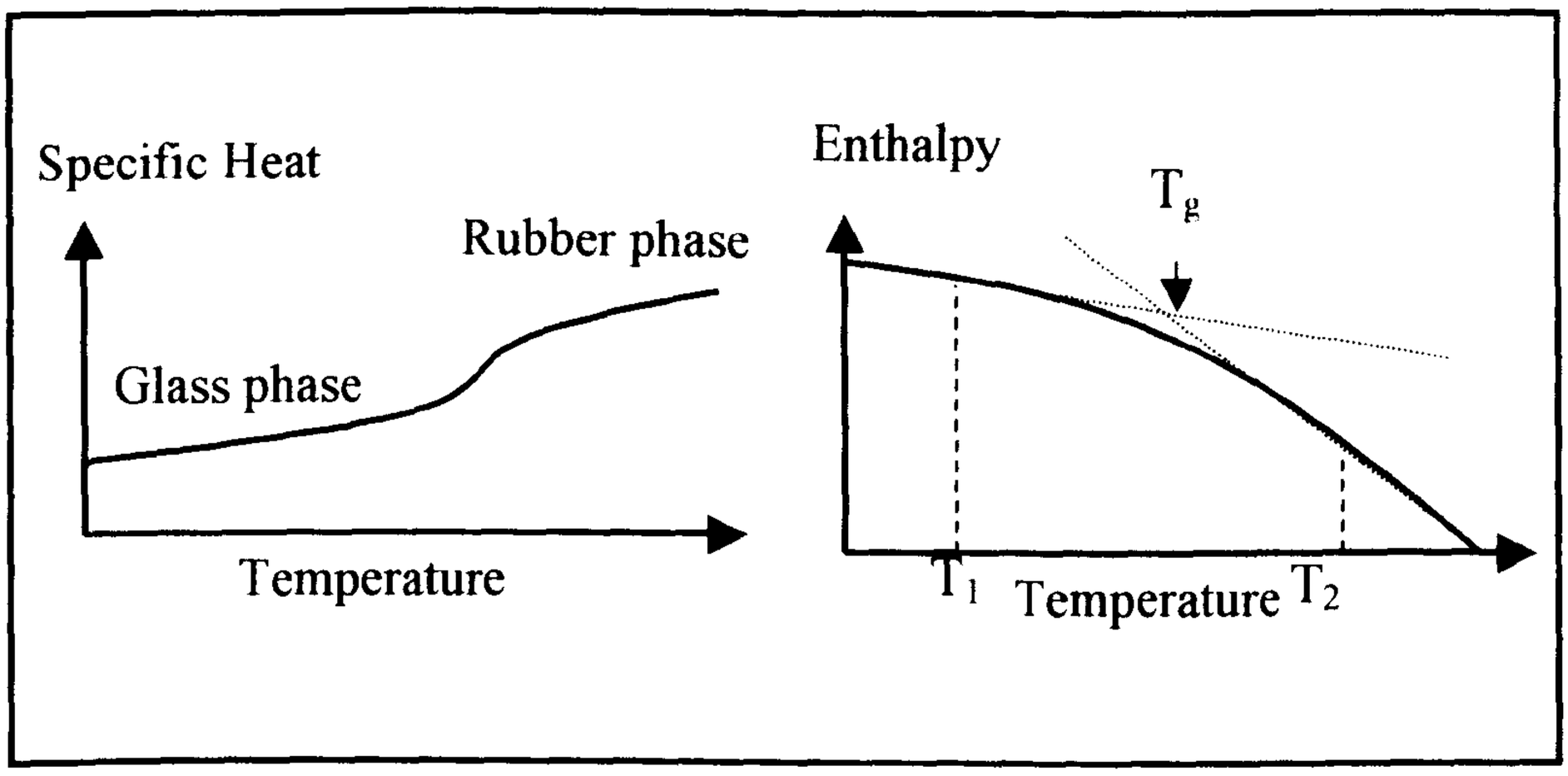

Figure III-19: Specific Heat and enthalpy over temperature to determine T_g

IV.3- Results of present investigations

Two kinds of sample have been tested. The first set has been post-cured for 1h at 100°C and the second set has been stored in the laboratory at room temperature for several weeks to months without a post-cure.

The results are presented in table II.1. For each sample two ramps R_1, R_2 of temperature have been performed and for each ramp the tangents of the curve representing the enthalpy as a function of the temperature have been calculated by using two temperatures T_1, T_2 in the glass and rubber state. T_g was extrapolated from these tangents.

	Test R_1		Test R_2	
Non post-cured sample	T_1= 20°C T_2= 80°C	T_1= 15°C T_2= 85°C	T_1= 20°C T_2= 80°C	T_1= 15°C T_2= 85°C
	T_g= 40.4°C	T_g= 39.9°C	T_g= 42.9°C	T_g= 43.75°C
	Tg= 42+/-2°C			
Post-cured Sample	T_1= 20°C T_2= 80°	T_1= 15°C T_2= 85°C	T_1= 20°C T_2= 80°C	T_1= 15°C T_2= 85°C
	T_g= 44.9°C	T_g= 46.4°C	T_g= 45.2°C	T_g= 46.8°C
	T_g= 46+/-2°C			

Table II-1: Résumé of the glass transition temperatures obtained by DSC on the unpost-cured sample and post-cured sample

From these measurements it seems that when the sample is not post-cured but stored for several months at room temperature in the laboratory the cross-linking reaction is not completed. On the first temperature ramp further cross-linking might be performed leading to a significant increase in the value of the T_g obtained. For the post-cured sample the values obtained are stable and remain similar between the first and second ramp. The effect of post-curing might be important concerning the physical ageing of the system. This needs to be kept in mind when analysing the results of other investigations presented in this work.

Chapter III

Dielectric spectroscopy

Dielectric materials have been investigated for more than a century [1]. The variety of studies is broad but the present chapter will be limited to dielectric relaxation.

Dielectric spectroscopy is based on the polarization/relaxation phenomena that are induced in dielectric materials during and after the application of an external stress. Relaxation is associated with the recovery of strain and occurs for all kind of stress relief, as for instance electrical, or mechanical stresses. In the present case, an electric field constitutes the source of stress.

Following a step-change in the electric field the dielectric polarization will relax in time to a new equilibrium value. As long as the polarization is linearly dependent upon the change in field, a Fourier transformation of the relaxation rate will give the polarization response to an ac driving field.

The first measurement of the dielectric relaxation of materials was performed on dilute solutions. The first theory proposed for a dilute dipolar solution or gases in which there are no interactions was that of Debye. It has been reported since that the Debye theory is not applicable to the case of a condensed solid medium and modifications have been sought to describe the behaviour of the various systems [2, 3].

The properties of solid dielectrics are related to the morphology as well as their chemical structure. After Debye established the basic theory of dipolar relaxation, dielectric spectroscopy has been broadly used for studying the conformation and dynamics of amorphous polymers. This technique has also been used to follow the polymerisation reaction [4].

In the present case, the analysis of the epoxy resin is expected to reveal its dielectric characteristics in the frequency domain of the material under study. The main parameter that will be changed will be the temperature. Measurements will be performed before and after a session of high electric field stress so as to identify the origin of any changes brought about. High field charge and discharge currents measured to help characterise the processes associated with the detected relaxation phenomena.

I- Origin of the polarization

The dielectric properties of a material are associated with the response of the system to an applied electric field at microscopic and macroscopic levels. In the case of an ac driving field, these phenomena are expressed by the *polarization* and *dielectric loss* as a function of frequency [5]. The frequency dependent (ac) permittivity is defined through the linear relationship between the polarization and the ac driving field [6].

The polarization is a vector quantity defined as the magnitude and direction of the electric moment per unit volume induced in the material under an applied electric field. It can be written as:

$$P(\omega) = P(0) + \varepsilon_0 \chi^{(1)}(\omega) E(\omega) + \chi^{(2)}(\omega) E^2(\omega) + \ldots \qquad \text{(III.1)}$$

Where P(0) is the permanent polarization which is usually zero except for materials without a centre of symmetry. The material in use in the present investigation has P(0)=0. Some materials, such as ferro-electrics, possess a permanent polarization. In this case the resultant polarization is the addition of the polarization in the presence of the field and the permanent polarization.

ε_0 is the permittivity of free space and is equal to $8.854x10^{-12}F.m^{-1}$, $\chi(\omega)$ the susceptibility and, $E(\omega)$ the electric field strength are dependent on the frequency.

The non-linear terms only take effect at high fields such as is found in lasers and give rise to non-linear optical effects. These non-linear terms are $\chi^{(2)}E^2+\ldots$etc. We will concentrate on the linear term since the investigation is carried out under low fields. In this case the polarization can be defined by:

$$P(\omega) = \varepsilon_0 \chi^{(1)}(\omega) E(\omega) = \varepsilon_0 (\varepsilon' - 1) E(\omega) \qquad \text{(III.2)}$$

Where ε' is the real part of the complex relative permittivity.

I.1- Electronic, atomic polarization

In the absence of an external electric field, the positively charged nucleus and the negative cloud of electrons in an atom are symmetrically disposed, i.e. it has no dipole moment. When an electric field is applied a slight displacement, D, of the electrons with respect to the positive nucleus position occurs. D can also be defined as an electrical flux density by analogy with Maxwell's equations. D is given by equation III.3

$$D = \varepsilon' \varepsilon_0 E \qquad \text{(III.3)}$$

The permittivity is a quantity that varies slowly with variables such as temperature or pressure. It is usually an intrinsic property of the material. It can be determined by the ratio of the capacitance measured between two parallel plates in the presence of the material and the capacitance measured between the same parallel plates in vacuum. In this geometry the capacitance is given by the expression $C = (\varepsilon' \varepsilon_0 A)/d$ (A the area of the plates, and d the distance between electrodes).

Such a displacement of electric charges makes the atom acquire a dipole moment and is called the *electronic or induced polarization* (figure III-1.a). It undergoes quantum vibrations at very high frequencies, i.e. above 10^{14}Hz. These correspond to electric fields in the optical, Ultra-Violet (UV) and higher domain of frequencies.

The application of an electric field on polar systems tends to stretch the bonds and change the dipole moment of the molecule. This molecular distortion is called *atomic or ionic polarization* (figure III-1.b). This phenomenon can be observed between 10^{12}Hz and 10^{14}Hz and is associated with modes of atomic motion, which change the permanent dipole. This range is situated in the Infra-red (IR) and micro-wave frequency domains. When the molecule concerned is polyatomic, this kind of polarization can occur even when it does not initially possess a permanent dipole moment. All that is required is for atomic displacements to generate a dipole moment.

I.2- Orientational and interfacial polarization

In molecules composed of atoms with different electro-negativities a permanent dipole moment can exist due to the position of the individual atoms. If no field is applied to the material the permanent dipoles of the molecules are usually oriented randomly leading to an absence of net polarization.

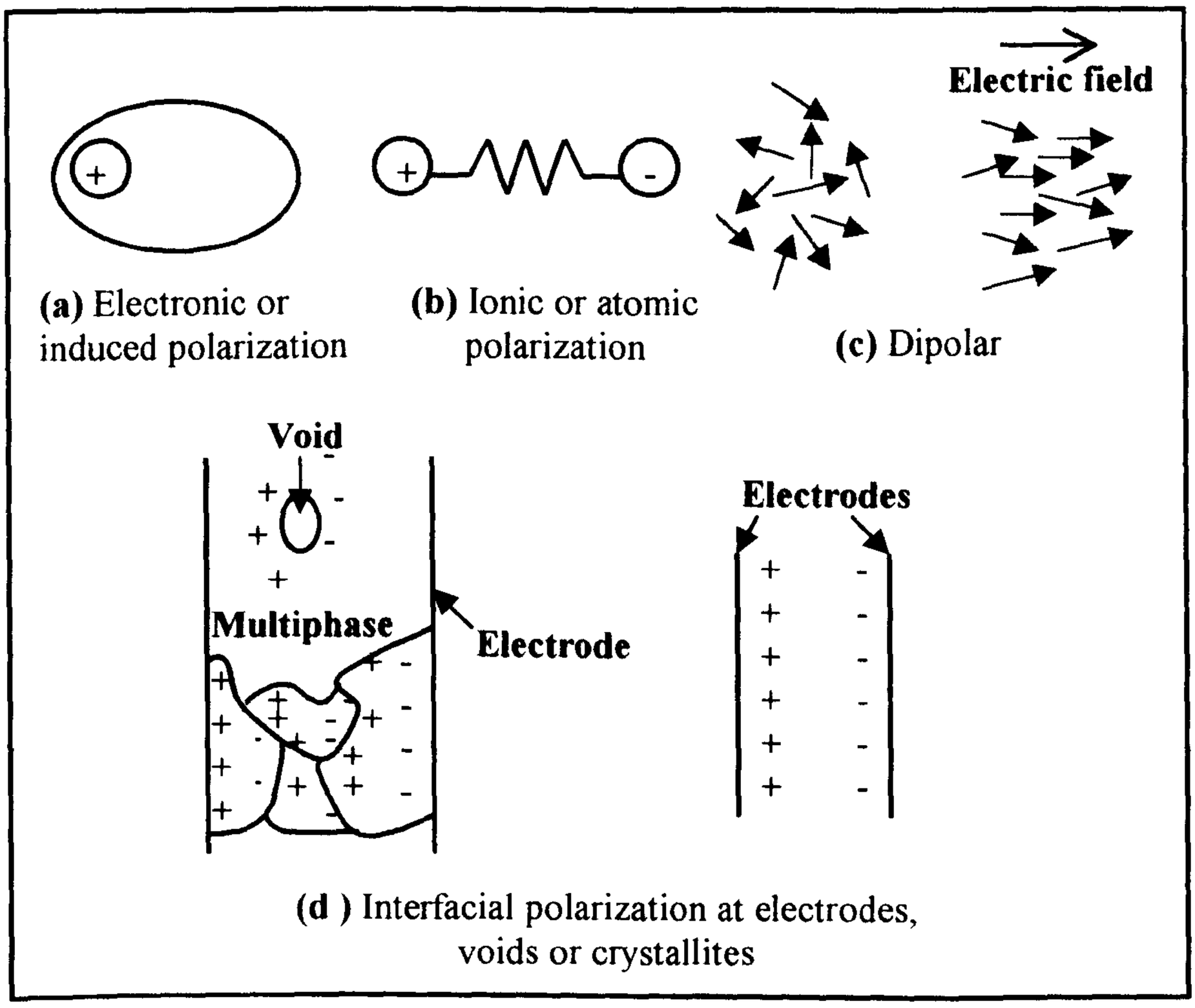

Figure III-1: Representation of the various forms of electrical polarization

The third type of microscopic polarization occurs when the electrical stress causes permanent dipoles to align with the applied field giving a net polarization in that direction. This phenomenon depends particularly on the variety of the molecular and inter-molecular interactions in the system and can be spread over a large range of frequency. It can be observed at all frequencies below 10^{12}Hz. This is the domain of dielectric spectroscopy and includes the radio and audio frequency range. The process is called *orientational polarization* and is represented in figure III-1.c.

Orientation polarization is strongest in polar liquids or gases because the energy barriers opposing dipole alignment are weak or non-existent. The rate of orientation is essentially governed by the viscosity of the medium and is very high, therefore the dipoles will respond at frequencies toward the top end of the range, i.e. 10^{9}-10^{12}Hz. In solids the molecular and lattice structure produces energy barriers to the re-orientation of dipoles. The dipoles will only re-orient slowly. Their response will therefore occur at frequencies below 10^{9}Hz. Many dipoles may be unable to respond at all, since they may become locked into orientations, which require changes in a large part of the solid structure before they can move.

Orientation polarization in solids is therefore usually low in magnitude and frequency. Their response frequency will however usually increase with temperature as thermal promotion over the barrier increases. The magnitude may also increase with temperature if this increase frees more dipole to respond, but this is not always the case and such an effect is strongly dependent upon morphology.

Finally, the *interfacial polarization* (figure III-1.d) is the result of a build up of space charge at boundary regions as found for instance in semi-crystalline materials or more generally in non-homogenous materials. Such non-uniformity can also be due to the presence of impurities, cracks or voids. This form of polarization is named the Maxwell-Wagner-Sillars (MWS) effect and its characteristic timescale is governed by the transport process of the charge. It will appear at the electrodes in conducting homogeneous materials if the electrodes are not ideally Ohmic.

Thus in the case of bulk conductivity and imperfect electrode contact, accumulation of charges at the interface leading to polarization becomes prominent. This accumulation of charges at the electrode/material interfaces is characterised at low frequency by a large increase of the capacitance and consequently of the apparent permittivity.

All the polarization effects are reported in table III-1.

Type of polarization	**Specie involved**	**Type of dielectric response**
Electronic	Atomic charge clouds	Resonance from vibration motion
Ionic – atomic	Atomic nuclei	Resonance from vibration motion
Dipolar orientation	Permanent dipoles	Relaxation motion
Interfacial	Space charge at the boundaries	Motion driven by charge transport

Table III-1: Origin of the polarization

In figure III-2, the variation of the real part and imaginary part of the permittivity over a large range of frequency has been represented. The complex relative permittivity is defined by:

$$\varepsilon_0 \varepsilon^* = (\varepsilon' - i\varepsilon'')\varepsilon_0 \qquad \text{(III.4)}$$

The frequency of the maximum in ε", the imaginary part of the relative permittivity, varies strongly with temperature, pressure and other variables and most of the time it is considered as an intrinsic property of the material. In the case of polymers the displacement of the peak can be weak and this may make the analysis difficult.

The main interest in the dielectric response is due to the fact that the value of the dielectric permittivity varies with frequency and that at particular frequencies the energy can be dissipated into the material. This dissipation is at the origin of loss at low frequencies and even dispersion of light at higher frequencies. The energy dissipated is of importance in insulating material, as it may be used to damage the material. In this work the value of the characteristic frequency and the magnitude of the response are of importance for the information they yield about the material morphology and chemical nature.

Each region of response corresponds to a specific type of polarization, i.e. electronic, ionic dipolar or interfacial. The energy absorbed by the polarising species is maximum at a characteristic frequency where the permittivity of the material is enhanced. The response of this particular species is not possible at higher frequencies because they cannot move quickly enough to respond to the external stress [6]. The polarization mechanism can no longer keep in step with the applied field at frequencies above the characteristic "peak" frequency.

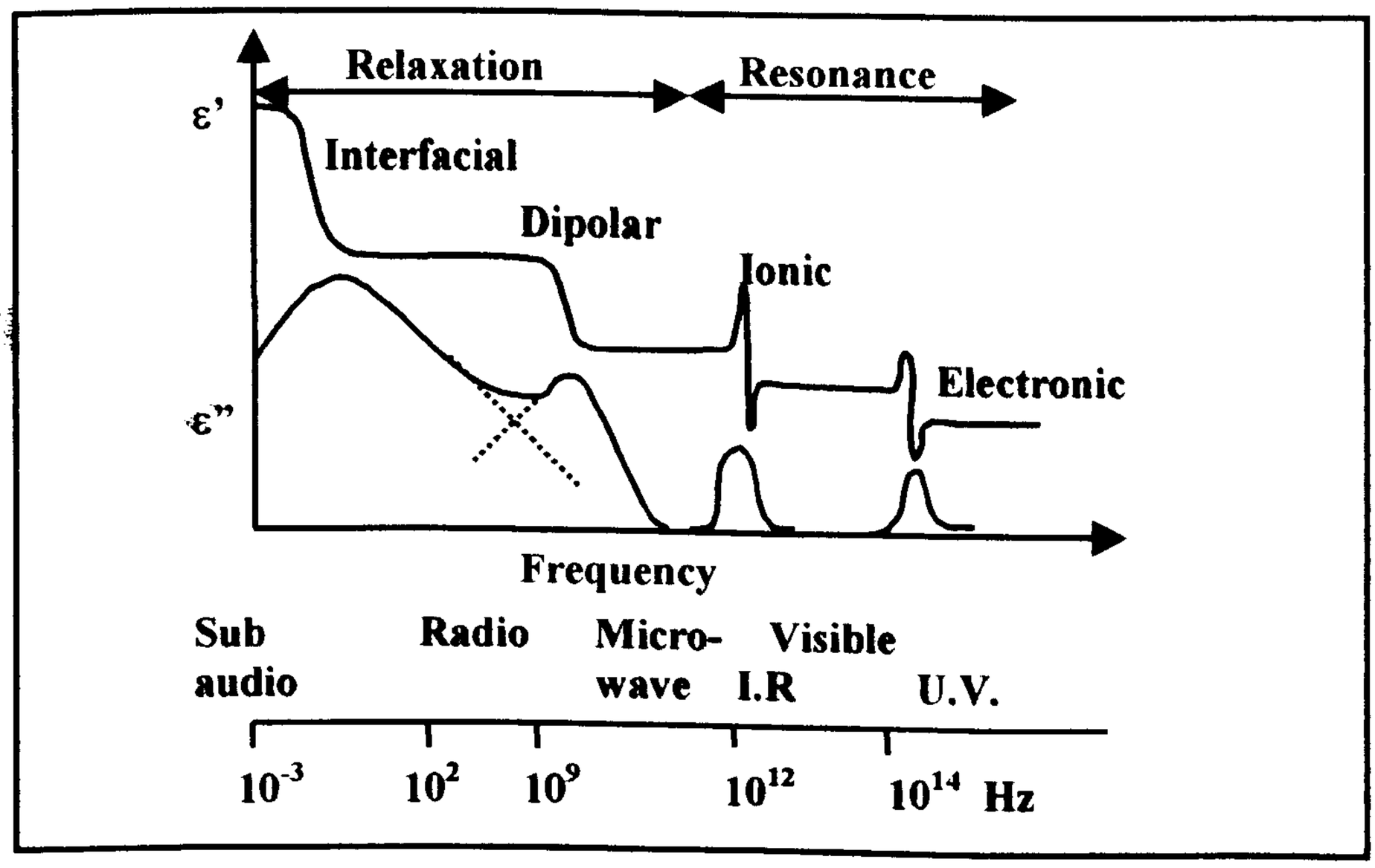

Figure III-2: Variation of the real and imaginary part of the permittivity over the frequency domain

I.3- Total polarization and internal electric field

The total polarization of a multiphase material containing permanent dipoles will be the result of the contribution of the electronic, ionic, orientational and interfacial polarization.

$$P = P_e + P_i + P_o + P_s \qquad \text{(III.5)}$$

On a molecular level the polarization is defined as a product of the number of molecules per unit volume N_0 that have the polarisability α multiplied by the local electric field E_l

$$P = N_0 \alpha E_l \qquad \text{(III.6)}$$

The internal local field depends upon the interaction of the dipoles, which are induced on the molecules by the external stress. This field is the summation of the field due to the charges on the electrodes and the other dipoles.

II- Frequency domain response

The general form of the induced displacement field D, equal to electrostatic flux density, can be written:

$$D = \varepsilon^* E \qquad \text{(III.7)}$$

As shown figure III-2, the real part of the permittivity increases as the frequency tends to zero. In other words the largest displacement corresponds to the long time scale.

When an alternating electric field E is applied, the polarization, which alternates in direction to follow the field, will be out of phase with the applied stress. This phase-lag is defined by the phase angle δ and it is usually represented by the equation $tan\delta = \varepsilon''/\varepsilon'$ that also represents the ratio of the energy dissipated per cycle to the energy stored.

The time lag can be determined by the measurement of the current that flows in the external circuit. The graph figure III-3 represents the complex plane characteristic of recorded out-of phase and in-phase current. The loss tangent (Tan δ) is equal to the ratio of the in-phase current to the out-of-phase current. In order to determine the dielectric response in the very low frequencies domain it has been found convenient to analyse the transient displacement current, which flows after the application and removal of a step voltage. This method has been used [8] to separate the loss due to

relaxation from the dc conductivity. This technique has been used to determine the imaginary part of the permittivity in the frequency domain by using the Hamon approximation [9].

$$\varepsilon_0 \varepsilon''(\omega) = i(t)/\omega \qquad \text{(III.8)}$$

It is then possible to calculate the dielectric constant increment ($\varepsilon'(0)-\varepsilon'_\infty$) by the integral:

$$\varepsilon'(0) - \varepsilon'_\infty = \frac{2}{\pi}\int_{-\infty}^{\infty} \varepsilon'' d(\ln \omega) \qquad \text{(III.9)}$$

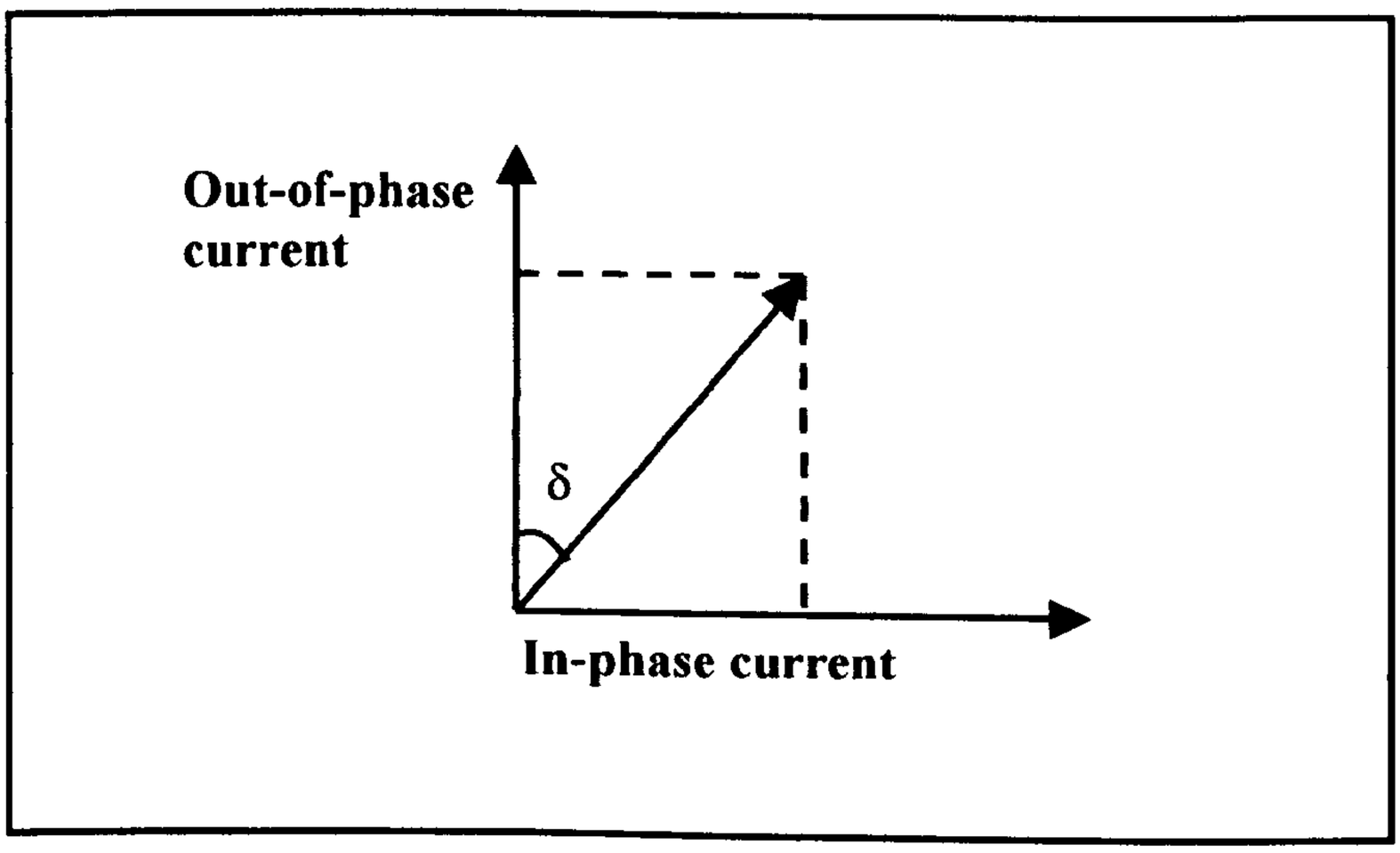

Figure III-3: Diagram current-voltage leading to the phase lag δ

The interest in working in the frequency domain is multiple. Most of the application of dielectric materials involves response to harmonic signals of definite frequencies. Besides, measurements in the frequency domain lead to accurate results since signals can be obtained in very narrow range of frequencies thus limiting the noise level recorded.

The polarization is defined by the equation:

$$P(\omega) = \varepsilon_0 \chi(\omega) E(\omega) \qquad \text{(III.10)}$$

The frequency-dependent susceptibility is defined:

$$\chi^*(\omega) = \chi'(\omega) - i\chi''(\omega) \qquad \text{(III.11)}$$

Where the real and imaginary parts are given by:

$$\chi'(\omega) = \int_0^\infty f(t)\cos(\omega t)dt \qquad \text{(III.12)}$$

$$\chi''(\omega) = \int_0^\infty f(t)\sin(\omega t)dt \qquad \text{(III.13)}$$

$\omega = 2\pi f$ (where ω is the circular frequency and f the frequency in Hertz)

f(t) is a real function of time that is equal to the discharge current subsequent to a step-down field.

$\chi'(\omega)$ and $\chi''(\omega)$ components vary in phase and in quadrature respectively compared to the harmonic signal applied. From this data other characteristics are accessible such as the impedance, Z, and the capacitance, C, that are useful for the interpretation of the data. The following relations link them:

$$\chi^*(\omega) \propto C^*(\omega) - C_\infty \text{ with } C_\infty \text{ the high frequency capacitance} \qquad \text{(III.14)}$$

$$Z^*(\omega) = 1/(i\omega C^*(\omega)) \qquad \text{(III.15)}$$

In parallel plate geometry the capacitance is given by:

$$C^*(\omega) = \varepsilon_0(\chi^*(\omega) + \varepsilon_\infty)A/d \qquad \text{(III.16)}$$

III- Measurement system

III.1- The high frequency response

The frequency range over which dielectric measurements can be performed has been increased by the use of the Frequency Response Analyser (FRA) apparatus. Classical bridge techniques are used for measurements down to 10Hz or even 1Hz, whereas the development of FRA allows us to record data down to 10^{-4}Hz [9]. The actual range of measurements available in the present investigation goes from 10^6 to 10^{-4}Hz.

The FRA in used is a Solatron instruments 1255 H.F FRA [10, 11]. The principle of the measurement consists of recording the current response of the material to an ac driving electric field.

In the present case, an harmonic function denoted sin(ωt) is used, with ω the radian frequency. It is delivered digitally by a generator and the frequency available can go from 10μHz to 20MHz. The amplitude of the probe voltage can be changed from 0 to 3V rms on the system in use. The analyser correlates the input V_1 and the output V_2 at the generator output frequency to obtain the frequency response of the system under test (figure III-4). In other words the system consist of two mains parts:
- a *generator* producing the sine wave of different frequencies
- a *correlator* measuring the in-phase and quadrature components of any input signal with reference to the output of the generator.

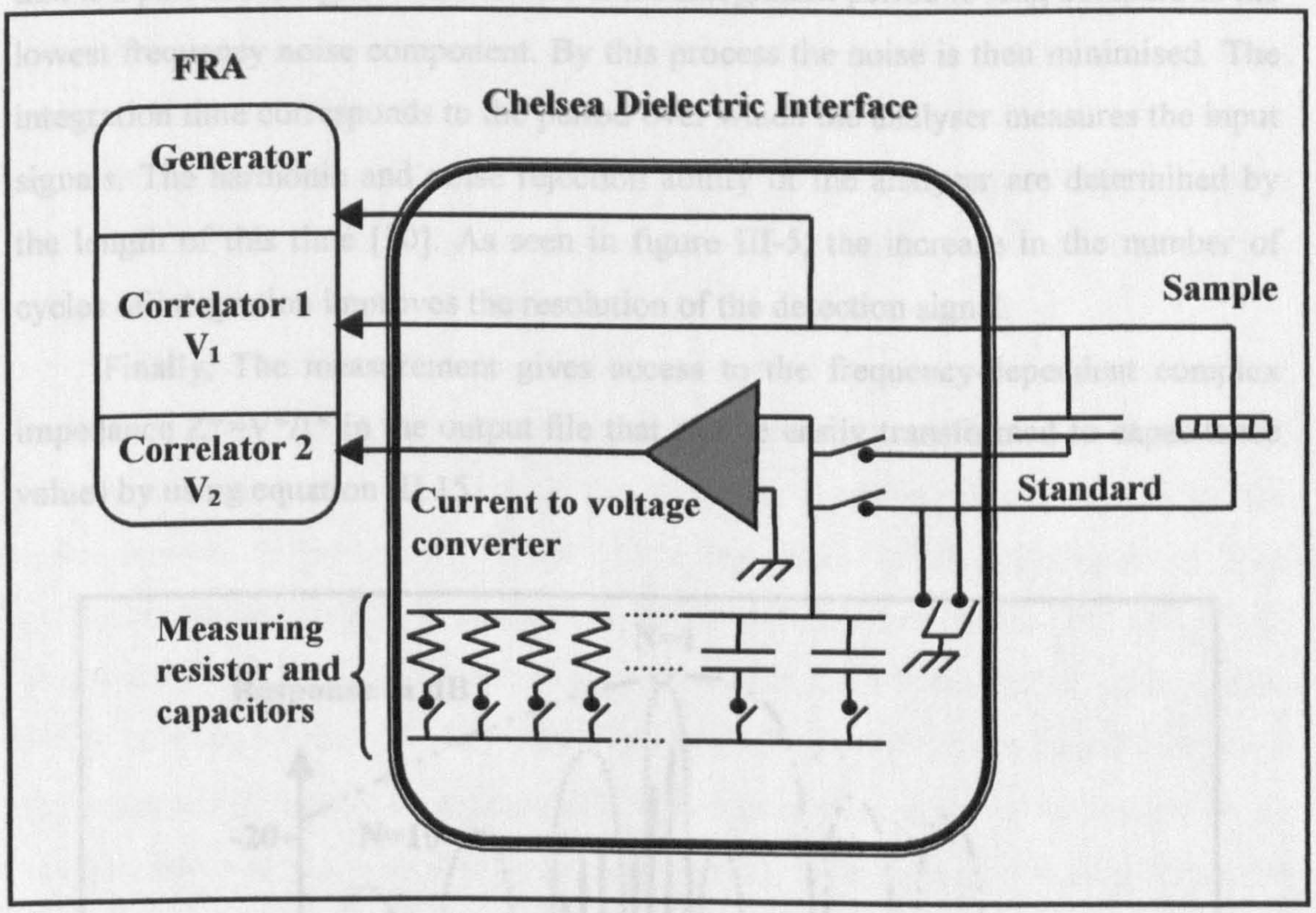

Figure III-4: Frequency Response Analyser system of measurements

The FRA is based on the measurement of the ratio of the alternating current, *I*, and the alternating voltage, *V*, in a capacitive element under the action of a sinusoidal varying voltage signal. The signal produced by a generator is applied to the sample by the means of two plane electrodes. The resulting current I(t) is measured by a current operational amplifier. A small current range must be detected and so the spectrometer must be of very high input impedance and the sensitivity must cover a broad frequency range. The amplifier with these characteristics is then linked to the

correlator of the FRA where the signal is integrated with the input signal and its quadrature waveform.

Therefore, the parallel and quadrature integrals following are obtained:

$$j_p = \int_0^{2\pi N/\omega} i(t)\sin(\omega t)dt \qquad \text{(III.17)}$$

$$j_q = \int_0^{2\pi N/\omega} i(t)\cos(\omega t)dt \qquad \text{(III.18)}$$

The integration is run over N determined cycles. The current I(t) is phase shifted by an angle ϕ compared to the applied voltage at the frequency ω. The noise that is a part of the signal tends to zero if the integration period is long compare to the lowest frequency noise component. By this process the noise is then minimised. The integration time corresponds to the period over which the analyser measures the input signals. The harmonic and noise rejection ability of the analyser are determined by the length of this time [10]. As seen in figure III-5, the increase in the number of cycles of integration improves the resolution of the detection signal.

Finally, The measurement gives access to the frequency-dependent complex impedance $Z^*=V^*/I^*$ in the output file that can be easily transformed to capacitance values by using equation III.15.

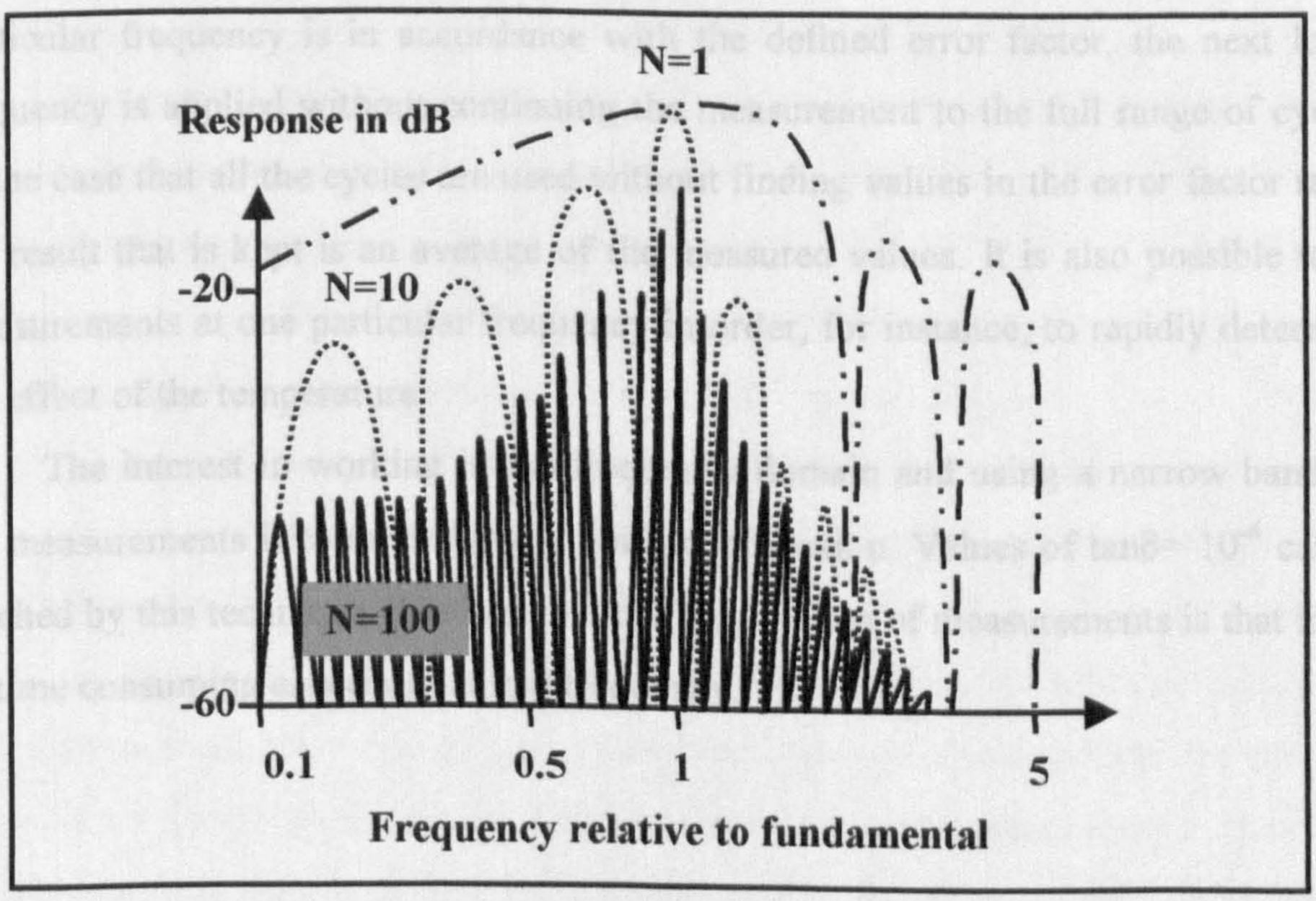

Figure III-5: Rejection curves for N cycles of integration [10]

III.2- Interface unit system

The role of the interface unit is to switch the measuring resistors and capacitors used in the system of measurement to balance the varying magnitude of sample impedance in the frequency domain. In fact, the impedance of a typical capacitor can change by several magnitudes over the frequency range used that is why the variety of resistors and capacitors in the system must be wide.

The FRA has a low impedance of about $10^6\Omega$ compared with a typical low-frequency impedance of some $10^{13}\Omega$, whereas the interface between the FRA and the sample must have a very flat amplifier characteristic in order not to introduce a large error in the phase shift.

When the measurement is performed it is common to start at high frequency and reduce it step-wise. The usual way is to fix a certain amount of measuring frequencies per decade.

When an isothermal measurement is performed, a series of results are taken at each frequency. Typically, a number of cycles is chosen for which the measurements are repeated and compared. While the program is running a comparison of the measurements is performed. When the convergence of the measurement at a particular frequency is in accordance with the defined error factor, the next lower frequency is applied without continuing the measurement to the full range of cycles. In the case that all the cycles are used without finding values in the error factor range the result that is kept is an average of the measured values. It is also possible to do measurements at one particular frequency in order, for instance, to rapidly determine the effect of the temperature.

The interest in working in the frequency domain and using a narrow band for the measurements is to minimise the noise contribution. Values of $\tan\delta = 10^{-4}$ can be reached by this technique. The drawback of this system of measurements is that it can be time consuming especially at low frequency.

III.3- Reference system

There are some limitations in the use of a standard technique that consists of a direct measurement on the sample due to the various phase lags, which are expected to occur in the system of measurement independently of the material. In addition, the measuring resistor or capacitor used has been calibrated only at spot frequencies throughout the frequency range and dispersion in their values can occur especially when they are used at values far from the initial frequency of calibration.

A reference technique is therefore used to limit the dispersions in the results. The first technique was to choose a reference standard capacitor, which matches the dielectric sample capacitance. This reference capacitor is connected to the input of the interface in parallel with the sample. When the measurement is performed the system measures the sample and then the reference alternatively so as to compensate the external effects due to the system of measurement. In order to limit the effect of the phase shift due to various pieces of equipment in the system, a calibration should be done at every frequency by using the method of substitution. This can be carried out by means of a high quality solid capacitor or air capacitor with known characteristics. While the measurement is done on the reference sample a loss value is recorded, the interface then sets a resistance and capacitance in order to adjust the result to the ideal value. This calibration is then used during the measurement on the sample under investigation reducing by a large amount the error due to the apparatus.

The lower value of conductance that can be measured is determined by the leakage conductance of the elements in the interface in addition to the limiting current in the operational amplifier. The value is usually limited to 10^{-13}S. The lowest value of tanδ depends on the ability to measure a very small value against a large one. In general the upper and lower limits are 10^{3} and 10^{-4} respectively.

The capacitance window resolution, from which the tan delta window can be deducted, is given figure III-6.a [11]. These limits are valid in the case of the use of the Chelsea Dielectric Interface with the Solatron 1255 FRA, when the generator output is 1V rms and 0V dc. The upper threshold is due to a bound where the generator is loaded to 66% of the preset output level. Above 10^{6} Hz the problem comes more from high frequency limitations and connection interferences. The lower threshold corresponds to the low sample reactance of about $5x10^{-13}$mΩ, above 10^{-1}Hz the limit is due to the low sample capacitance of 0.5pF.

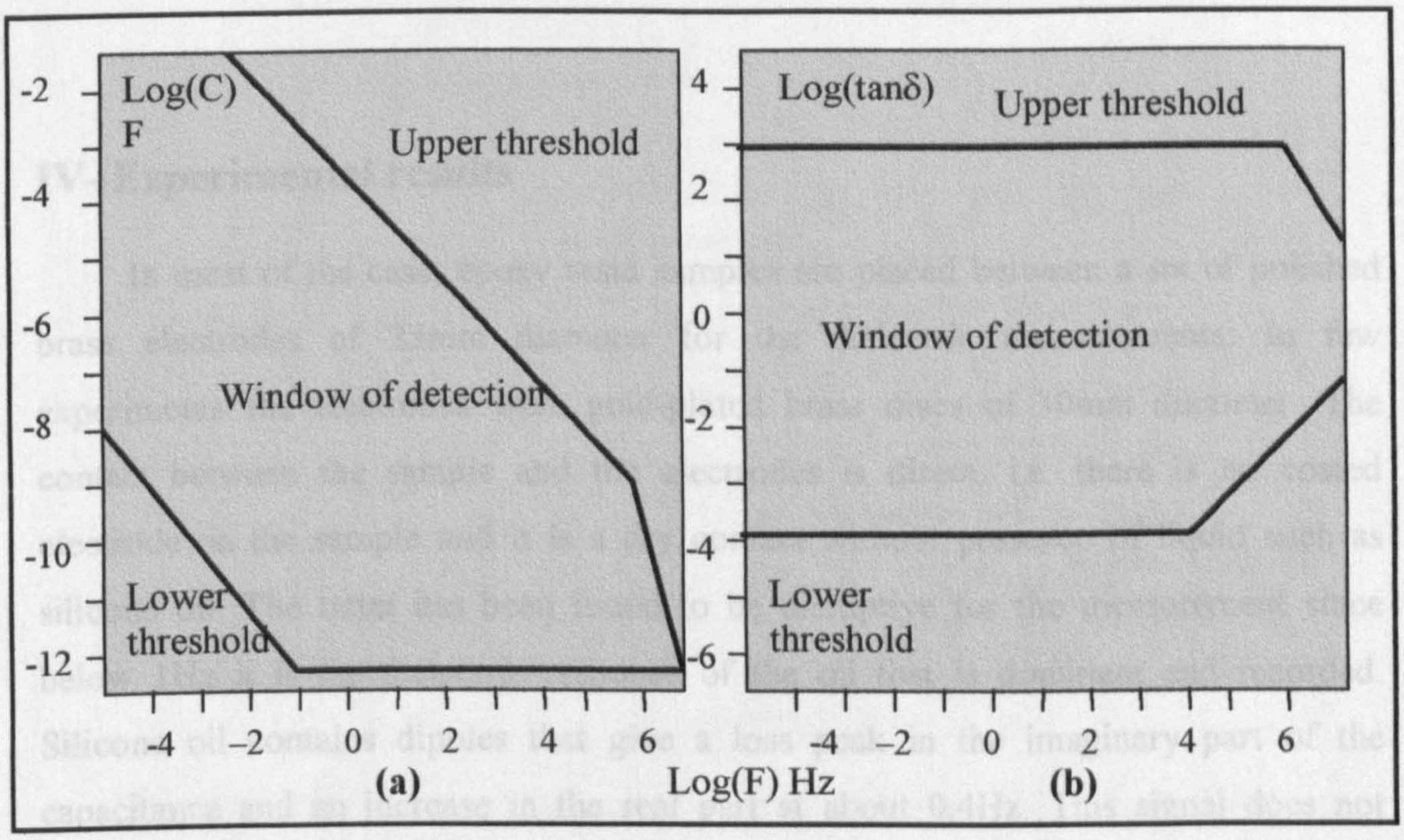

Figure III-6: Window of detection limits **(a)** Capacitance, **(b)** tanδ

For Solatron 1255 FRA-Chelsea Dielectric Interface, generator output 1V rms, 0V dc

[12]

The upper limit of measurement in the case of the tanδ is due to the error in the discrimination of the sample capacitance whereas the lower limit comes from the error in the discrimination of the sample conductance (figure III-6.b).

When the measurement is taken over a large range of frequency it becomes necessary to use several reference capacitors. It is then convenient to use the internal reference method that lets the system of measurement choose the best reference as the measurements are performed. The changes in the reference capacitor values limit the error that would be introduced by the use of a unique capacitor reference. This last internal method seems suitable since it is usually difficult to choose a reference at first sight because the value of the capacitance of the sample under investigation is unknown before the measurement is performed. The internal method seems to be really helpful and more accurate. Besides, this method seems appropriate because it presents a large choice of capacitor values that are following the small changes that are occurring in the sample over the domain of frequencies studied.

IV- Experimental results

In most of the case, epoxy resin samples are placed between a set of polished brass electrodes of 23mm diameter for the dielectric measurements. In few experiments the electrodes were gold-plated brass discs of 30mm diameter. The contact between the sample and the electrodes is direct, i.e. there is no coated electrode on the sample and it is a dry contact without presence of liquid such as silicone oil. The latter has been found to be disruptive for the measurement since below 1Hz it is the dielectric response of the oil that is dominant and recorded. Silicone oil contains dipoles that give a loss peak in the imaginary part of the capacitance and an increase in the real part at about 0.4Hz. This signal does not appear on similar measurements carried out by dry contact. Therefore, direct contact electrode/sample is found to be the solution to avoid such a problem.

In all cases, the internal reference was used, and the driving ac voltage was chose to be 1V ac.

IV.1- Dielectric response of virgin sample

IV.1.1- Shape of dielectric response

A non post-cured epoxy film of 290µm has been measured over the full range of frequency available, i.e. 10^{6}-10^{-4}Hz. The measured system is placed in an oven that allowed working at controlled temperature with an error of +/-0.1°C. For such measurements an integration period of 200s was chosen. The number of points per decade was set at 4. At high temperature a clearer signal was found showing the main characteristics of the dielectric response (figure III-7).

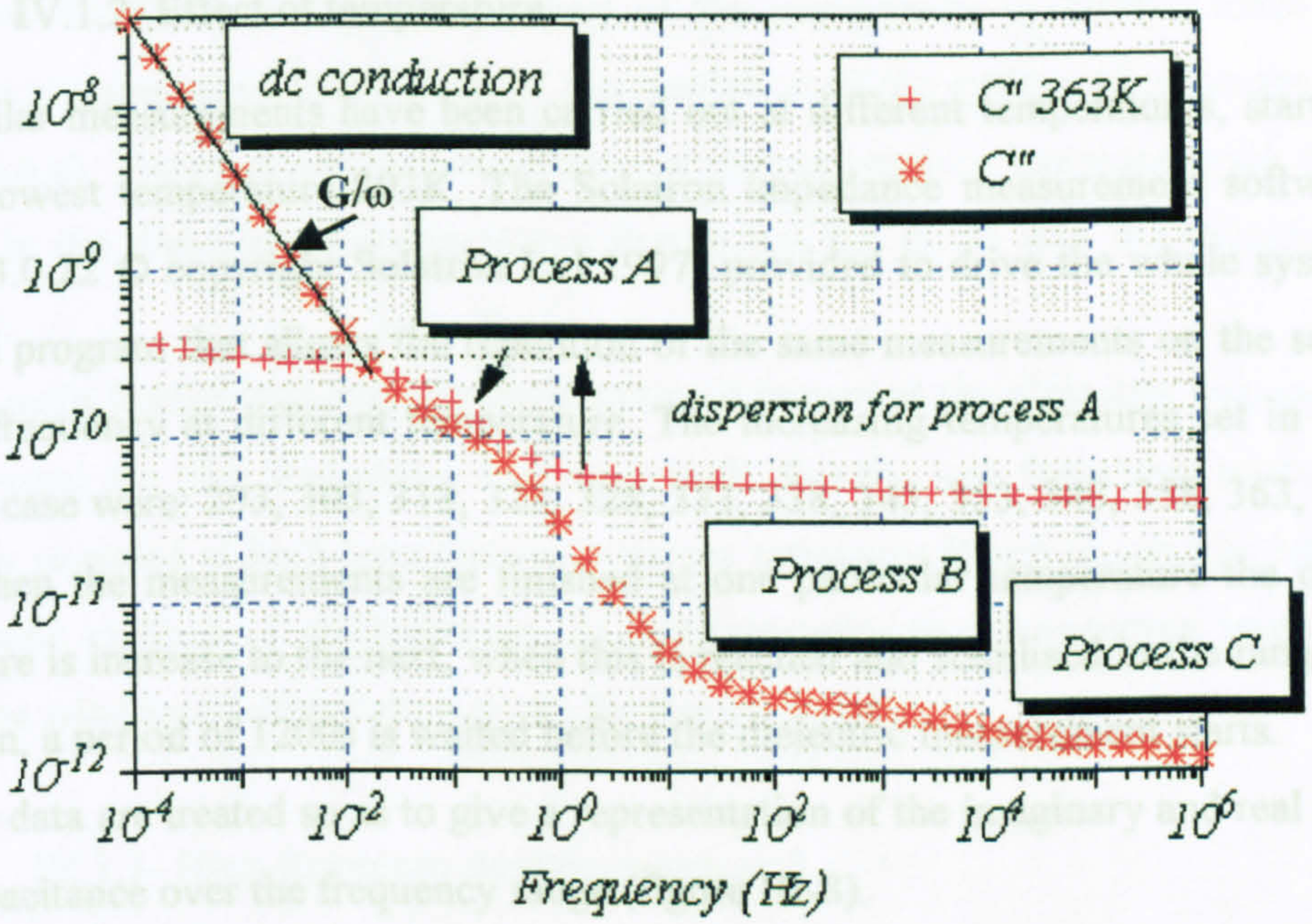

Figure III-7: Dielectric response of an epoxy resin sample, 290μm, 363K, range 10^{-4}-10^{6}Hz, internal reference, integration 200s

The signal can be described by the following processes:

- A *dc conductance* response at low frequencies where the real part of the capacitance crosses the imaginary part. The response of the imaginary part of the capacitance is characterised by a rapid increase as the frequency is going down with a slope of gradient –n. The value $1 \geq n > 0.99$ was estimated from $\cos(n\pi/2) = \varepsilon'/\varepsilon''$.

- A *low frequency loss peak* in the imaginary part of the capacitance noted A with a dispersion in the real part of the capacitance from $6\text{x}10^{-11}$ to $3\text{x}10^{-10}$.

- An *intermediate process* noted B weakly pronounced in the imaginary and real part of the capacitance.

- A *high frequency loss peak* in the real part of the capacitance noted C associated with a very weak dispersion in the real part. The maximum of the peak might be situated around $2\text{-}4\text{x}10^{5}$Hz but it remains difficult to identify since it is situated at the upper limit of measurement of the system in use.

IV.1.2- Effect of temperature

Similar measurements have been carried out at different temperatures, starting with the lowest temperature 293K. The Solatron impedance measurement software (Version 3.0.22 © copyright Solatron Ltd 1997) provided to drive the whole system includes a program that allows the repetition of the same measurements on the same range of frequency at different temperature. The increasing temperatures set in this particular case were: 293, 303, 313, 323, 328, 333, 338, 343, 353, 348, 358, 363, and 368K. When the measurements are finished at one particular temperature the oven temperature is increase to the next, when this is reached and stabilised in the range of error given, a period of 1200s is waited before the dielectric measurement starts.

The data are treated so as to give a representation of the imaginary and real part of the capacitance over the frequency range (figure III-8).

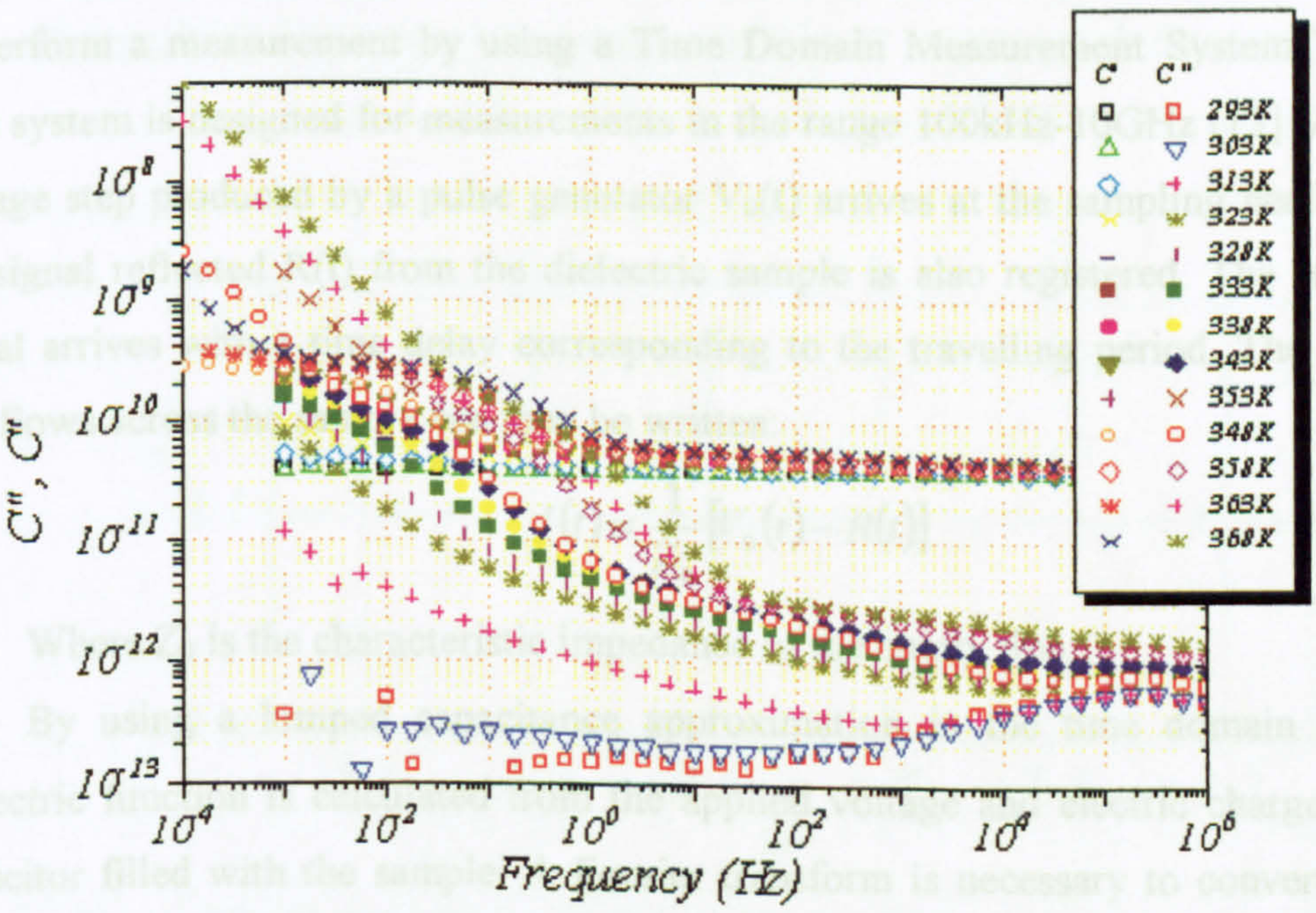

Figure III-8: Real and imaginary part of the capacitance over frequency, and over a range of temperature going from 293K to 368K, internal reference, integration 100s

Below 313K the low frequency part of the capacitance is "noisy" since the response is situated close to the limit of the resolution of the system of measurement (figure III-6.a). The response become clearer as the temperature increases since there is a shift in the dielectric response curve that brings the curve into the window of resolution.

The main feature is that as the temperature is increased the dielectric response is shifted toward the high frequency. It is noticeable that the low frequency processes are mainly revealed at high temperature, whereas processes B and C seem to have a much slower kinetics of displacement. In fact, changing the temperature results in moving the window of observation in the frequency domain.

IV.1.3- High frequency domain response

In order to check the dielectric response at high frequency it has been decided to perform a measurement by using a Time Domain Measurement System TDMS. This system is designed for measurements in the range 100kHz-10GHz [13]. A sharp voltage step produced by a pulse generator $V_0(t)$ arrives at the sampling head where the signal reflected R(t) from the dielectric sample is also registered. The reflected signal arrives with a time delay corresponding to the travelling period. The current that flows across the sample can then be written:

$$I(t) = \frac{1}{Z_0}[V_0(t) - R(t)] \qquad \text{(III.19)}$$

Where Z_0 is the characteristic impedance of the empty line.

By using a lumped capacitance approximation in the time domain [13], a dielectric function is calculated from the applied voltage and electric charge of the capacitor filled with the sample. A Fourier transform is necessary to convert to the frequency domain. The complex permittivity values are obtained by integration of the dielectric response function. The present experiment has been performed at room temperature, i.e. 298K.

In the present case two representations of the data are given in figure III-9 and 10. The first one represents the imaginary part of the permittivity over the frequency range $4x10^3$-$6x10^8$Hz and the second a Cole-Cole plot. Two peaks are distinguished one at $9x10^5$Hz and a second at 10^8Hz.

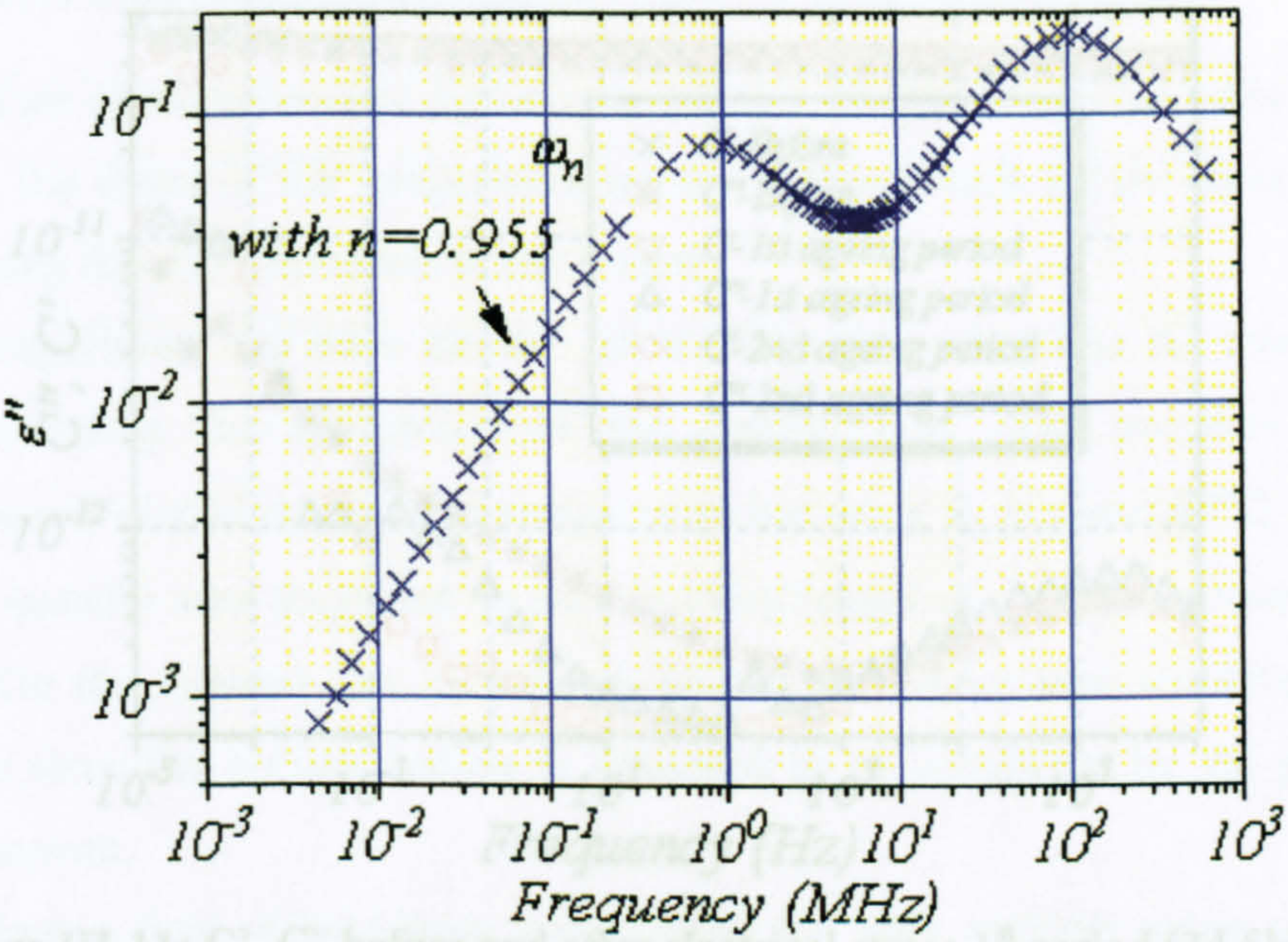

Figure III-9: Dielectric losses represented by ε" over the high frequency range $4x10^{-3}$-$6x10^{3}$MHz available in TDMS

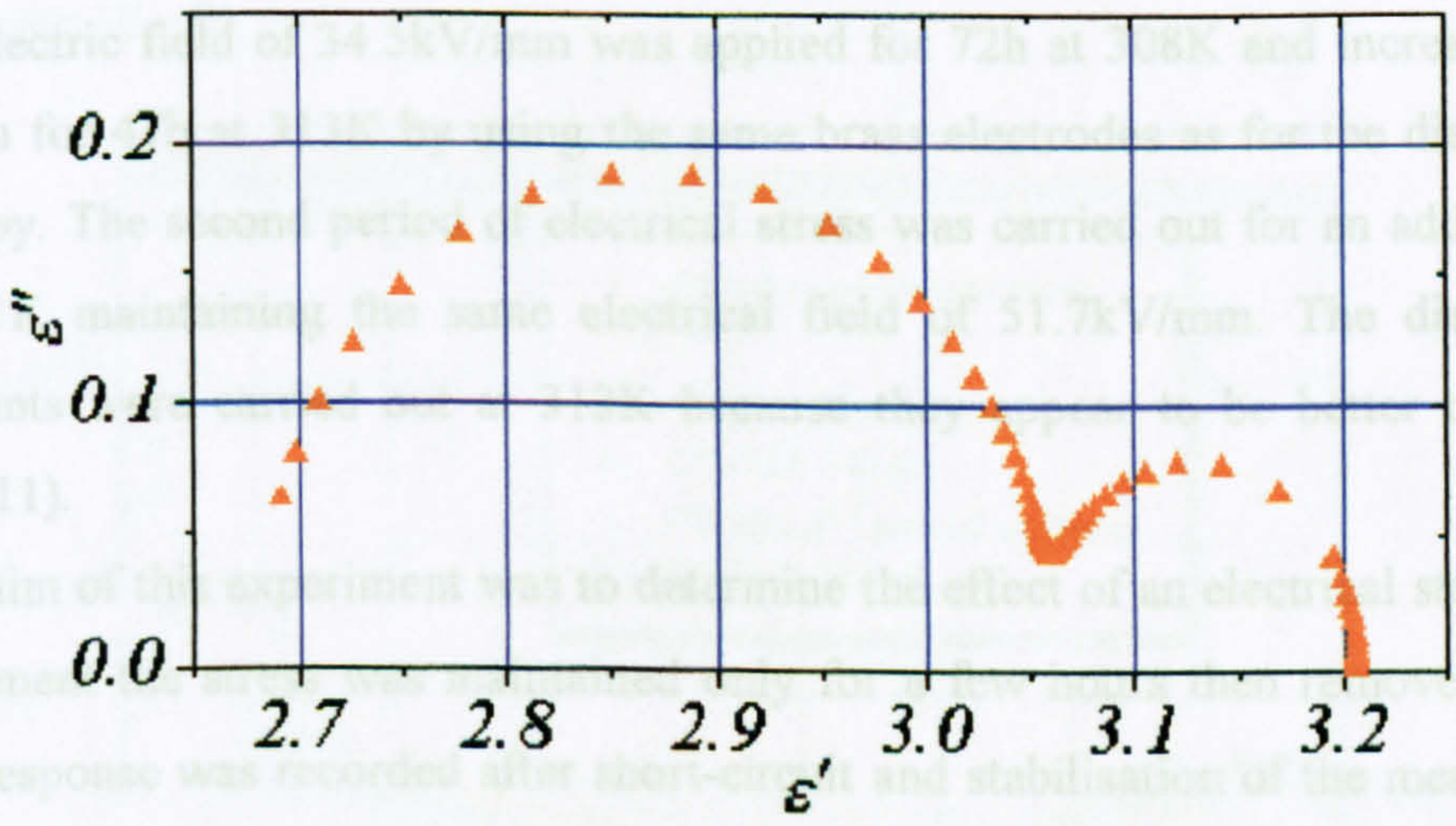

Figure III-10: Cole-Cole plot from high frequency domain response $4x10^{3}$-$6x10^{8}$Hz at 298K

IV.1.4- Analysis after voltage application

Similar measurements have been carried out on an epoxy sample before and after different periods under high electrical stress. The dielectric response was measured before electrical stress, then after the first and second period of stress. The dc voltage was supplied by a Glassman H.V., series F.C. amplifier.

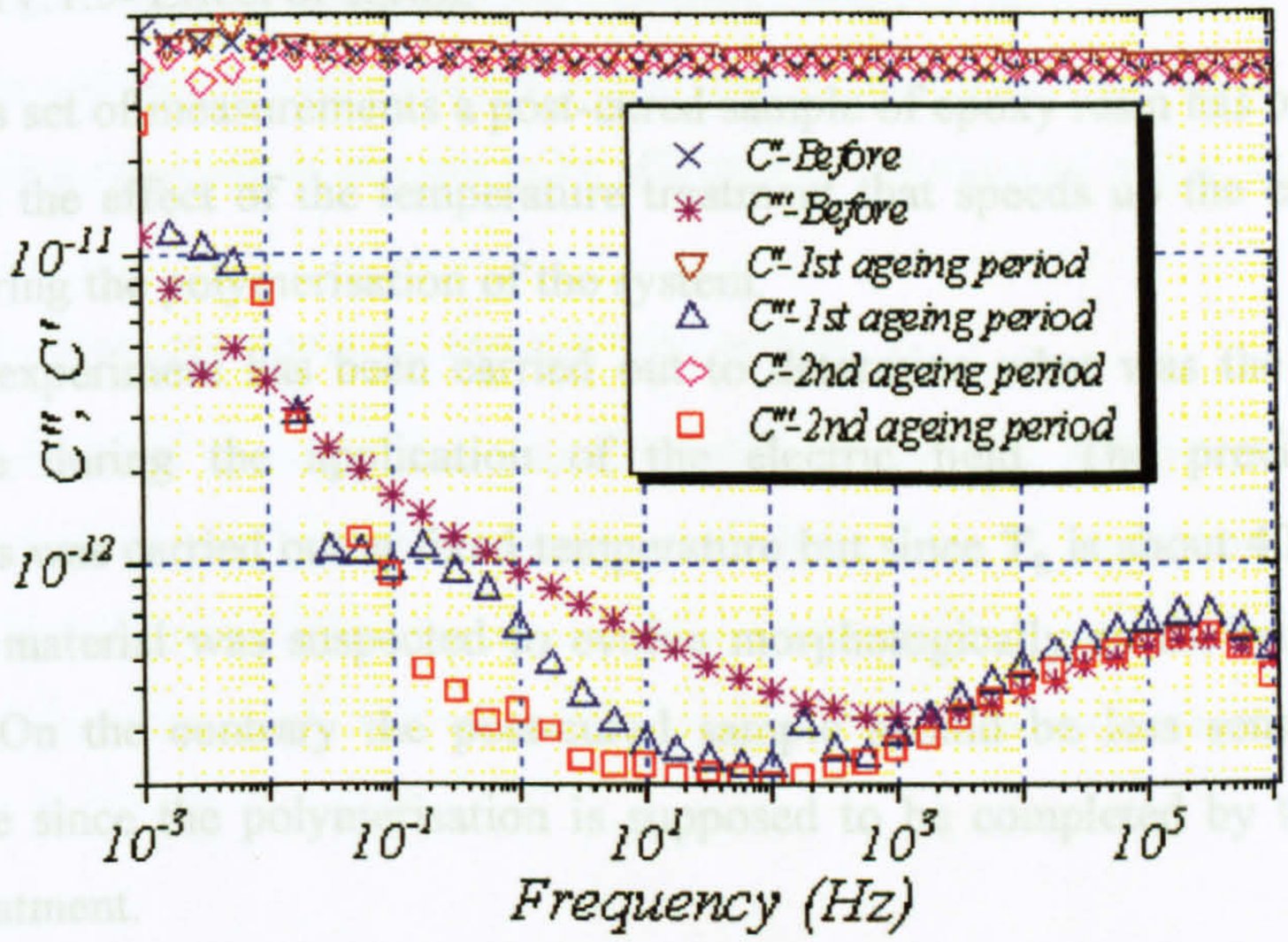

Figure III-11: C', C" before and after electrical stress 1st period (34.5kV/mm, 72h, 308K + 51.7kV/mm, 47h, 313K), 2nd period (51.7kV/mm, 47h, 313K), 1V ac, internal reference, integration 100s, 313K

An electric field of 34.5kV/mm was applied for 72h at 308K and increased to 51.7kV/mm for 47h at 313K by using the same brass electrodes as for the dielectric spectroscopy. The second period of electrical stress was carried out for an additional 47h at 313K maintaining the same electrical field of 51.7kV/mm. The dielectric measurements were carried out at 313K because they appear to be better defined (figure III-11).

The aim of this experiment was to determine the effect of an electrical stress. In this experiment the stress was maintained only for a few hours then removed. The dielectric response was recorded after short-circuit and stabilisation of the measuring temperature. From figure III-11, it is possible to see that the main change is observed at low frequency, and only in the imaginary part of the capacitance. In fact, the real part remains essentially the same whereas the imaginary part decreases in amplitude below 10Hz as the electrical stress period increases. It seems that the electrical stress affects mainly the process B, effectively removing it from the response and hence revealing the high frequency tail of process A more clearly. Process A hardly seems to be affected at all, and the dc conductivity cannot be observed at this temperature.

IV.1.5- Effect of curing

In this set of measurements a post-cured sample of epoxy resin has been used so as to check the effect of the temperature treatment that speeds up the cross-linking reaction during the polymerisation of the system.

This experiment has been carried out to determine what was the role of the temperature during the application of the electric field. The previous set of experiments was carried out at fixed temperature but since T_g is about 40°C, the non post-cured material was suspected to evolve morphologically as the temperature is increased. On the contrary the post-cured sample should be less sensitive to the temperature since the polymerisation is supposed to be completed by the previous thermal treatment.

An electric field of 35kV/mm was applied for 170h at 303K using the same brass electrodes as for the dielectric spectroscopy. The second period of electrical stress was carried out for 121h at 313K maintaining the same electrical field. The dielectric measurements were carried out at 313K because they appear to be better defined (figure III-12).

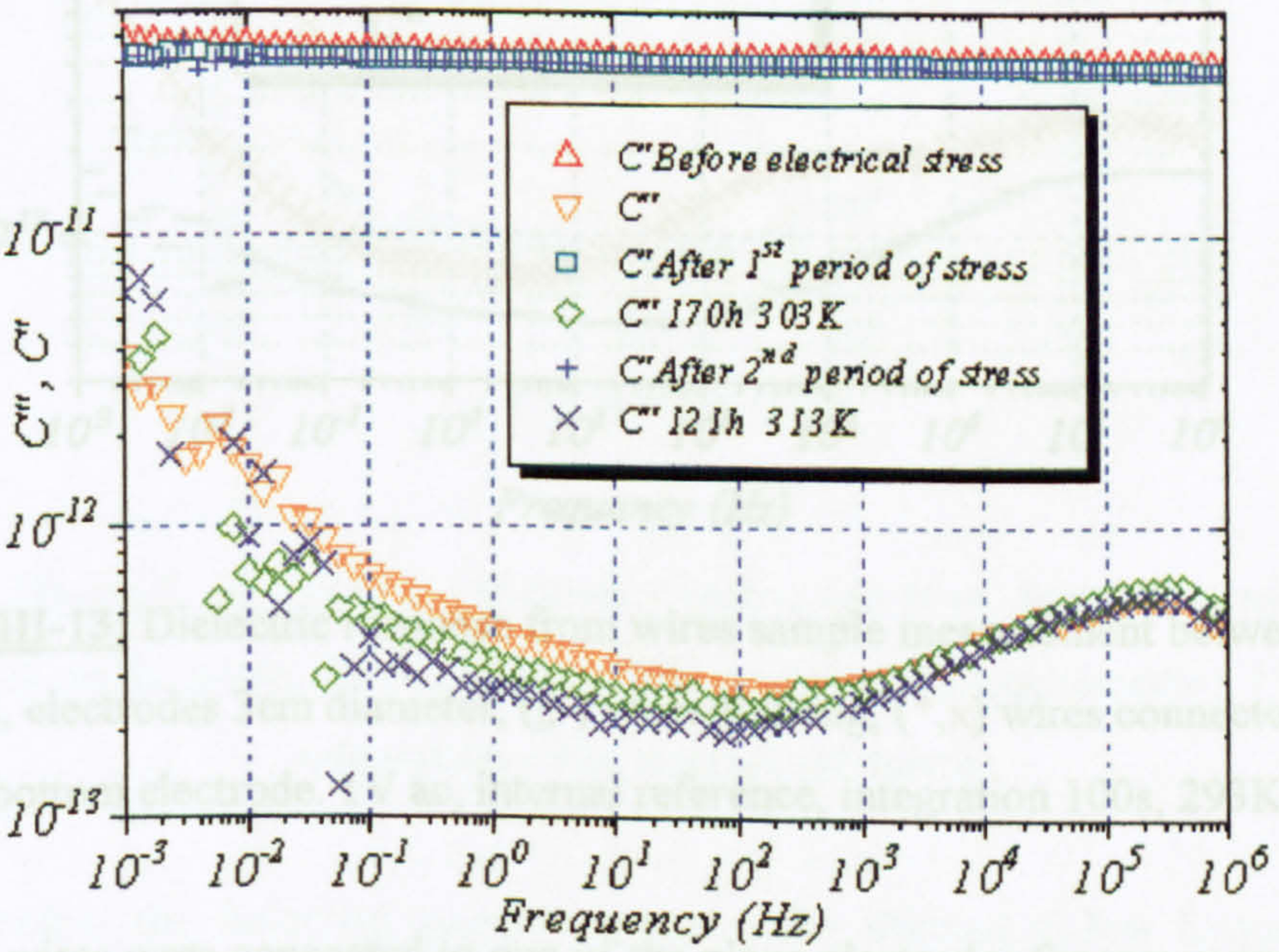

Figure III-12: C', C" before and after electrical stress (35kV/mm), 170h 303K then 121h 313K, 1V ac, internal reference, integration 100s, 313K

Here again the main change after electrical stress is observed in process which is reduced in amplitude. Any changes in process A are lost in the scatter of the data. High frequency response seems not to be affected by the external stress applied.

IV.2- Measurements on sample with wires

Measurements on wires samples were also performed. In this case, the wires were connected to the bottom electrode or left floating at an unknown potential during the measurement. For these sets of experiment two polished electrodes of 30mm diameter were used on both surfaces. The measurements are reported figure III-13.

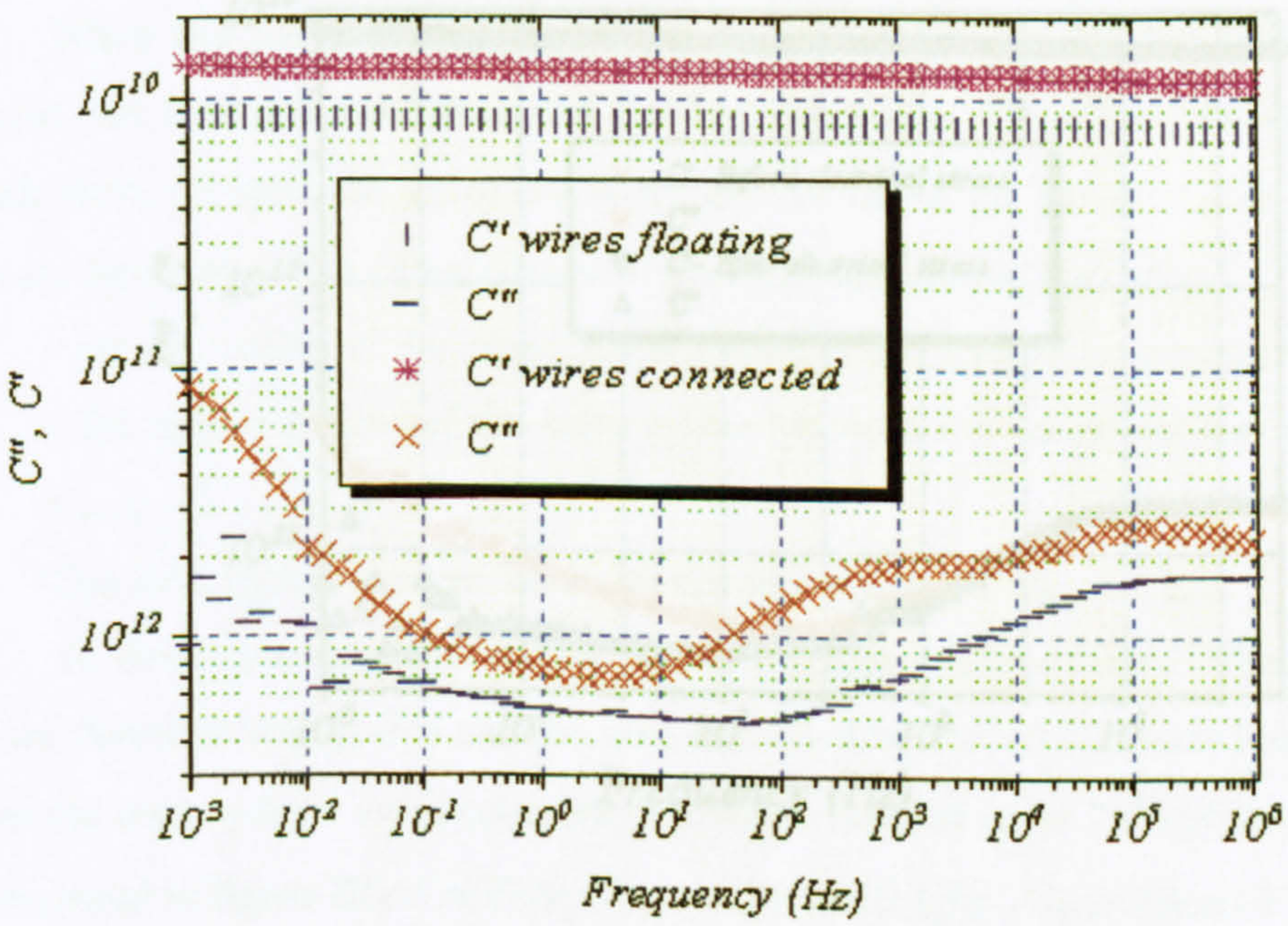

Figure III-13: Dielectric response from wires sample measurement between both surfaces, electrodes 3cm diameter, (|,-) wires floating, (*,x) wires connected to the bottom electrode. 1V ac, internal reference, integration 100s, 293K

The wires were connected to one of the plane electrodes for two reasons. In the first place when the wires are left floating unwanted capacitive coupling may occur. In the second place the measurement between wires and plane takes advantage of the higher local field and reduced dielectric thickness to give a more accurate response.

It is possible to observe a change in the amplitude of the response when the wires are connected to the bottom electrode. The response is shifted from 7.99x10^{-}11 to 1.24x10^{-10}F at 100Hz. Because of the increase in amplitude the response recorded is clearer since it is brought more into the window of resolution of the detection system. The shape of the response remains overall the same.

Other measurements have been carried out after a period of electrical stress separately the wires and each surface. No difference was observed between the two cases. Results presented in figure III-14 correspond to measurements before electrical stress and after 7days (168h) of voltage application (-2kV) applied to the tungsten wires of 50μm diameter.

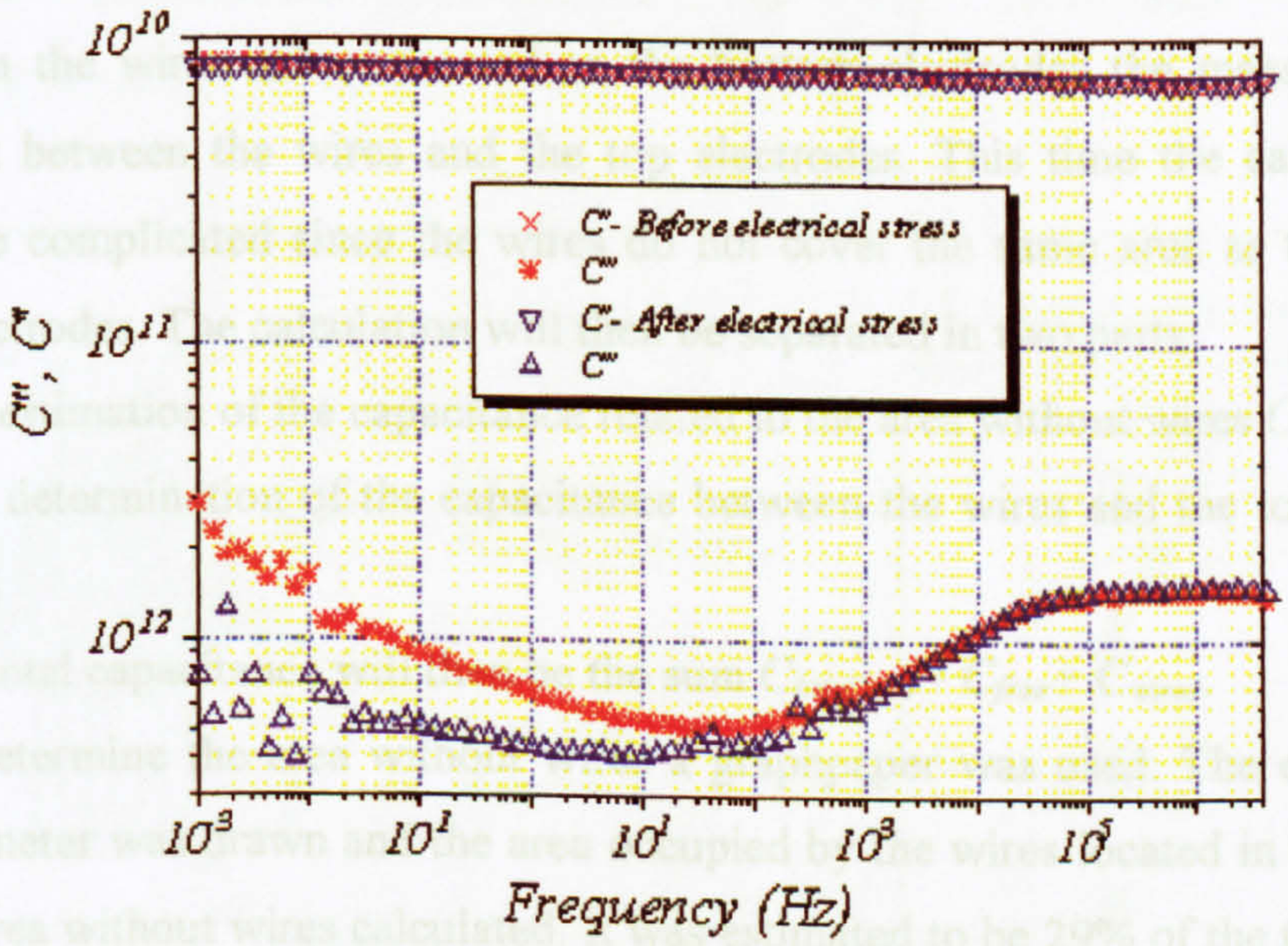

Figure III-14: C', C'' over the frequency before and after electrical stress –2kV applied on the wires, 7days (168h), 293K (stress and measurements), 1V ac, integration 100s, internal reference

As before the dielectric response seems to be affected at low frequency. The imaginary part of the capacitance is reduced indicating a decrease in magnitude of process B and also some change to process A below 10^2Hz.

IV.3- Dielectric response from sample with wires

First of all it is observed that the presence of wires in the bulk do not disturb the dielectric response of the material. Dielectric responses with the same shape were detected with the sample free of wires. This remark can be validated by the calculation of the expected value of capacitance. It is possible to calculate the value of the capacitance while the measurement is carried out between both surfaces by using $C = \varepsilon_0 \varepsilon' A/d$. With $\varepsilon' = 3.8$, $A = \pi (1.5 \times 10^{-3})^2$ and $d = 280\mu m$, the estimated capacitance is then $C_{cal} = 8.49 \times 10^{-11} F$ that matches the experimental results for which $C_{exp} = 7.99 \times 10^{-11} F$ at 100Hz.

When the wires are connected to the bottom electrodes the measurement is carried out between the wires and the top electrodes. This time the calculation is much more complicated since the wires do not cover the same area as the top and bottom electrodes. The calculation will then be separated in two parts:

- the estimation of the capacitance related to the area without wires C_{free}
- the determination of the capacitance between the wires and the top electrode C_{wires}

The total capacitance will then be the sum $C_{total,\,cal} = C_{free} + C_{wires}$.

To determine the area without wires a graphpaper was used. The electrode of 30mm diameter was drawn and the area occupied by the wires located in the middle. Then the area without wires calculated. It was estimated to be 29% of the total area as represented in figure III-15.a Then $C_{free} = \varepsilon_0 \varepsilon' (0.29A)/d$, $C_{free} = 2.46 \times 10^{-11} F$

To determine C_{wires}, it is first more convenient to work on a single wire. It is assumed that the wires form lines of charges when a potential difference is applied between them and a plate electrode. For each wire Q will be the charge per unit length of wire. The system is represented in figure III-15.b.

The potential at a point (x,y) is called $\Phi(x,y)$ and is determined by the equation III.20.

$$\Phi(x,y) = \frac{Q}{4\pi\varepsilon_0\varepsilon'} \sum_{n=-m}^{n=+m} \ln\left[\frac{A(y,n) + \sin^2\left[\frac{\pi(x+D)}{2h}\right]}{A(y,n) + \sin^2\left[\frac{\pi(x-D)}{2h}\right]}\right] \quad \text{(III.20)}$$

$$\text{with } A(y,n) = \sinh^2\left[\frac{\pi(y-nl)}{2h}\right] \quad \text{(III.21)}$$

Where x, y are the position of the wire for which the calculation is carried out, m=33 the number of wires, D the distance between the wire and the plane electrode ($140x10^{-6}$m), h the thickness of the sample ($280x10^{-6}$m), l the distance between two neighbouring wires ($1x10^{-3}$m) $\Phi(x=0)$ and $\Phi(x=h)$ are zero.

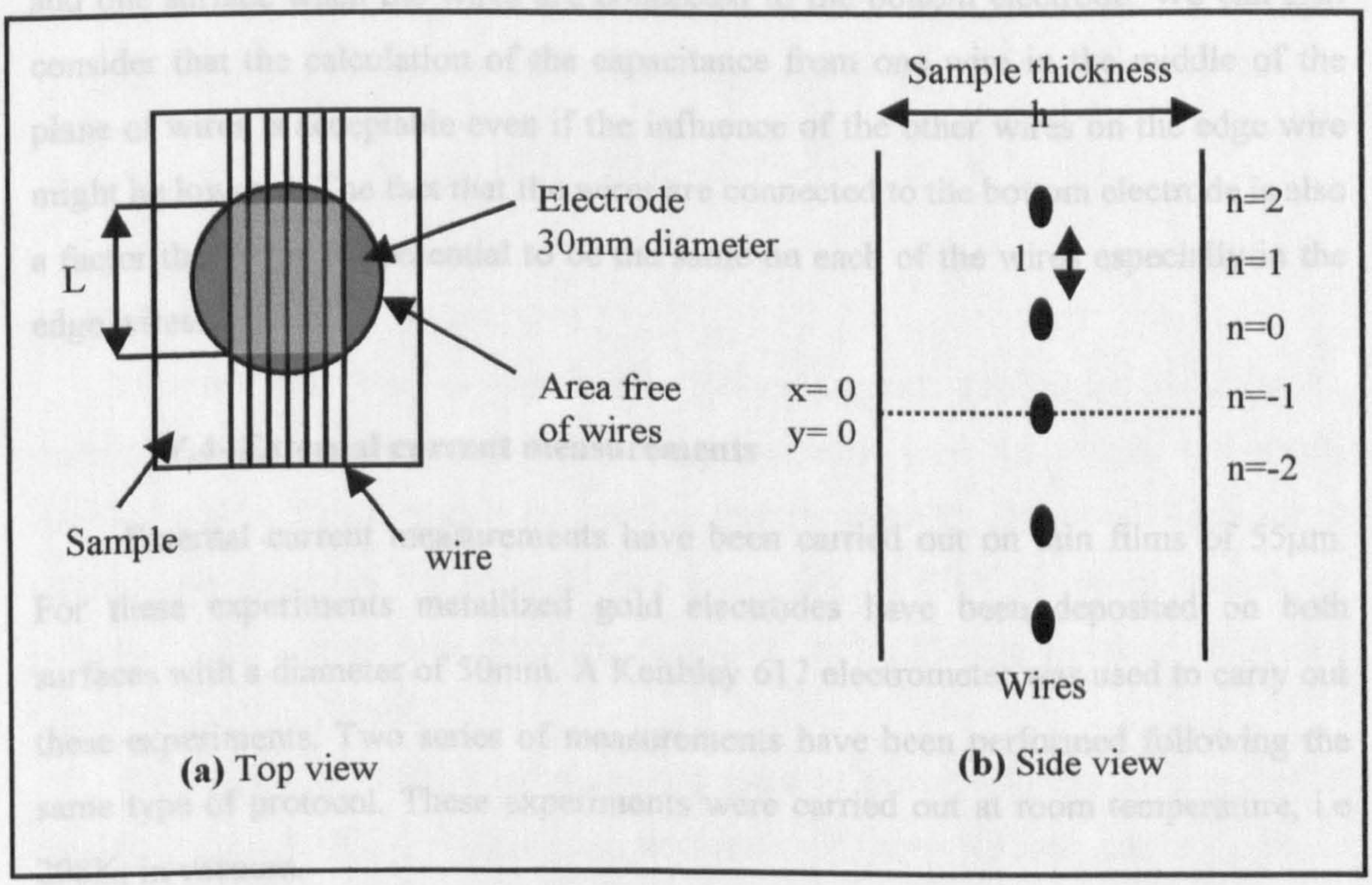

Figure III-15: Sample with wire characteristics used for the capacitance calculation

The calculation is carried out with the wires assumed to lie in a plane in the middle of the sample. $\Phi(x,y)$ is calculated for x=D-a where a is the radius of the wire ($25x10^{-6}$m), and y=0. Since the voltage is applied between the wires and the plane electrodes the capacitance per unit length of wire is $Q/\Phi(x=D-a)$ by definition.

The value of the capacitance per metre for a single wire in these conditions is estimated to be $C_w = 1.08X10^{-10}F.m^{-1}$. Then for the total amount of wires $C_{wires} = C_w mL$ where L is the length of the wires. L is approximated to be $2.8x10^{-2}$m leading to an effective length of wire as if they were a rectangular plane in the sample. Then $C_{wires}=9.98x10^{-11}F$

Finally, the total capacitance can be determined $C_{total,\ cal} = 1.24x10^{-10}F$. The experimental value taken at 100Hz is $C_{total,\ exp} = 1.24x10^{-10}F$. There is then a good accordance between the calculation and the experimental results.

This result is valid when the measurements are carried out between the wires and one surface when the wires are connected to the bottom electrode. We can also consider that the calculation of the capacitance from one wire in the middle of the plane of wires is acceptable even if the influence of the other wires on the edge wire might be lowered. The fact that the wires are connected to the bottom electrode is also a factor that helps the potential to be the same on each of the wires especially in the edge wires.

IV.4- External current measurements

External current measurements have been carried out on thin films of 55µm. For these experiments metallized gold electrodes have been deposited on both surfaces with a diameter of 50mm. A Keithley 617 electrometer was used to carry out these experiments. Two series of measurements have been performed following the same type of protocol. These experiments were carried out at room temperature, i.e 298K, in vacuum.

-The first series was carried out using a step ramp technique. The dwell time was 300s on the ascending ramp and 150s on the descending ramp. The current was averaged after the first 50s. The results are reported figure III-16 by the triangle fitted by two powers laws. The crosses represent an exponential fitting curve that matches especially at high field.

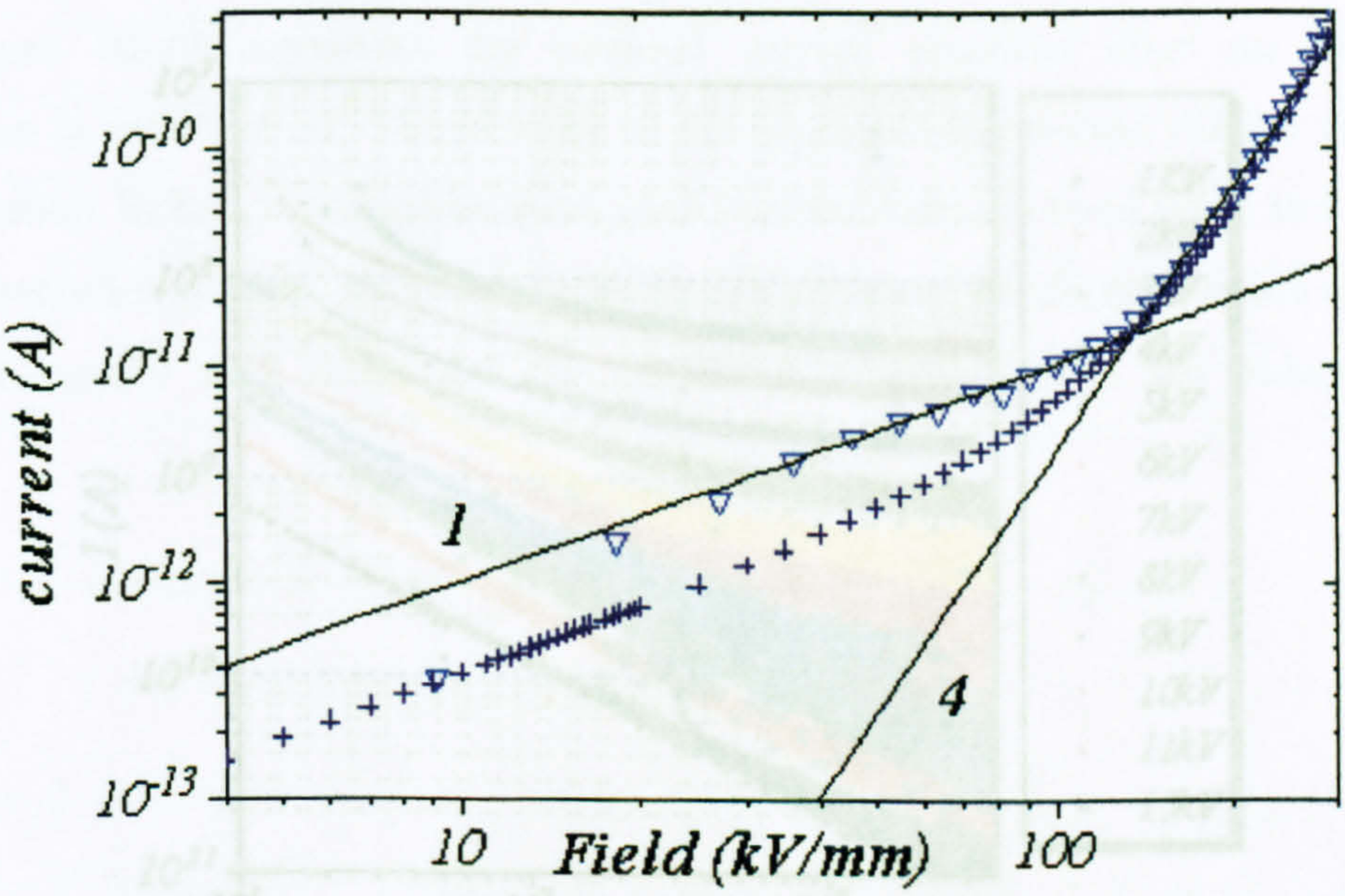

Figure III-16: I-E plot for the polarization ramp with two powers laws fit and

$$(+)\ \mathrm{I} \propto \exp\left[ae^{E}/_{k_B T}\right] - \exp\left[ae^{E}/_{k_B T}\right]$$

-For the second set of experiments the voltage was applied for 1h while the external current was recorded. After this polarization time the sample was short-circuited and the depolarization current was then recorded for 1h as well. The applied voltage was increased by steps of 1kV from 1kV to 13kV at which breakdown occurred. The current was therefore measured for to electric fields in the range 18KV/mm to 236kV/mm.

As the applied voltage increases, the detected external current is increased in amplitude (figure III-17). This current decreases with time without reaching a stable level at the lower voltages, i.e. 1kV to 5kV. Above this value the current that flows in the external circuit seems to become constant beyond 1000s. In this case the current beyond 2500s was averaged and plotted as a function of the applied electric field in figure III-18. From this representation it is possible to note a change in the slope that can correspond to the change in the regime from a transient to a conduction process.

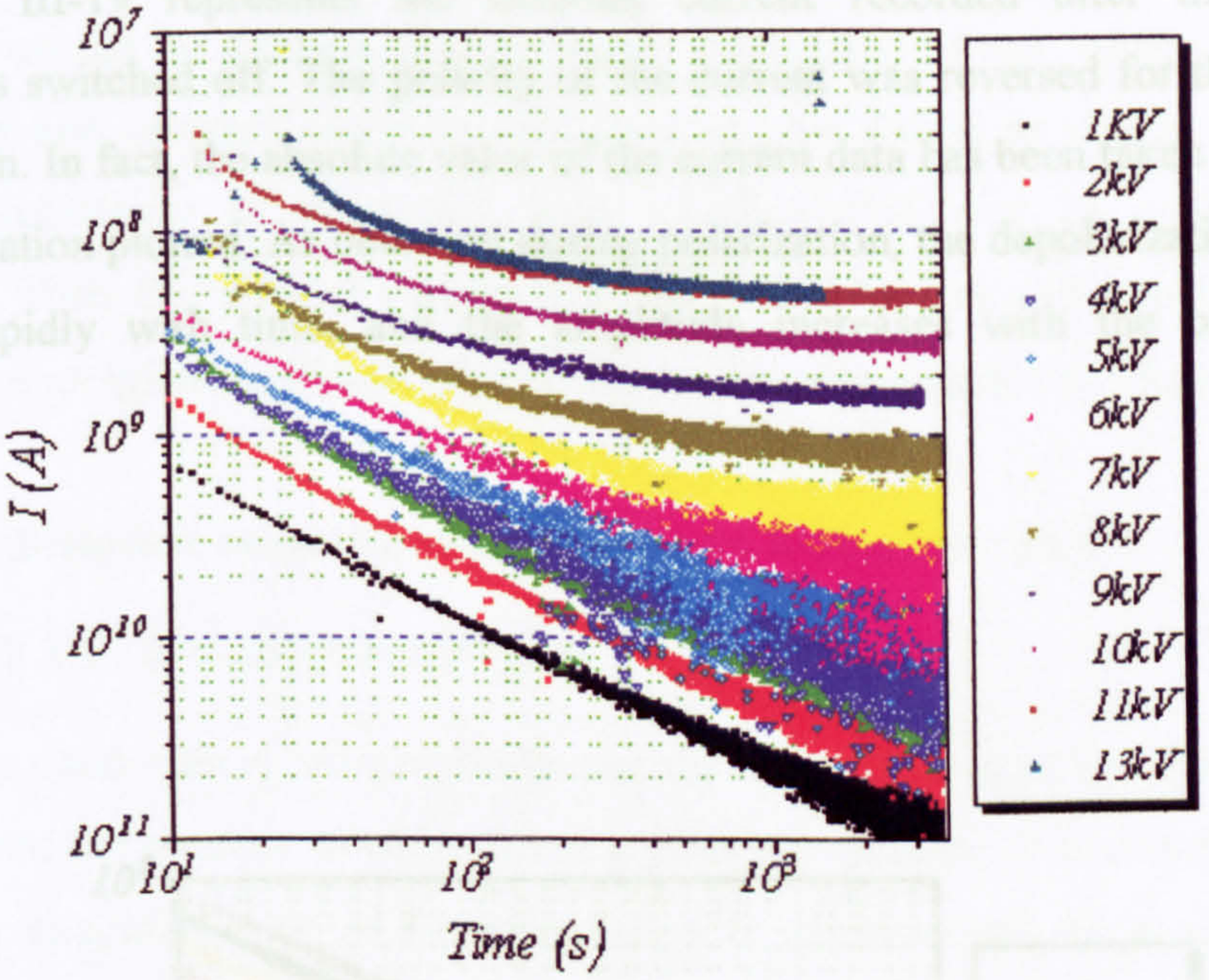

Figure III-17: External current recorded during polarization. dc voltage from 1kV to breakdown. Epoxy 55µm, metallized on both sides, 298K

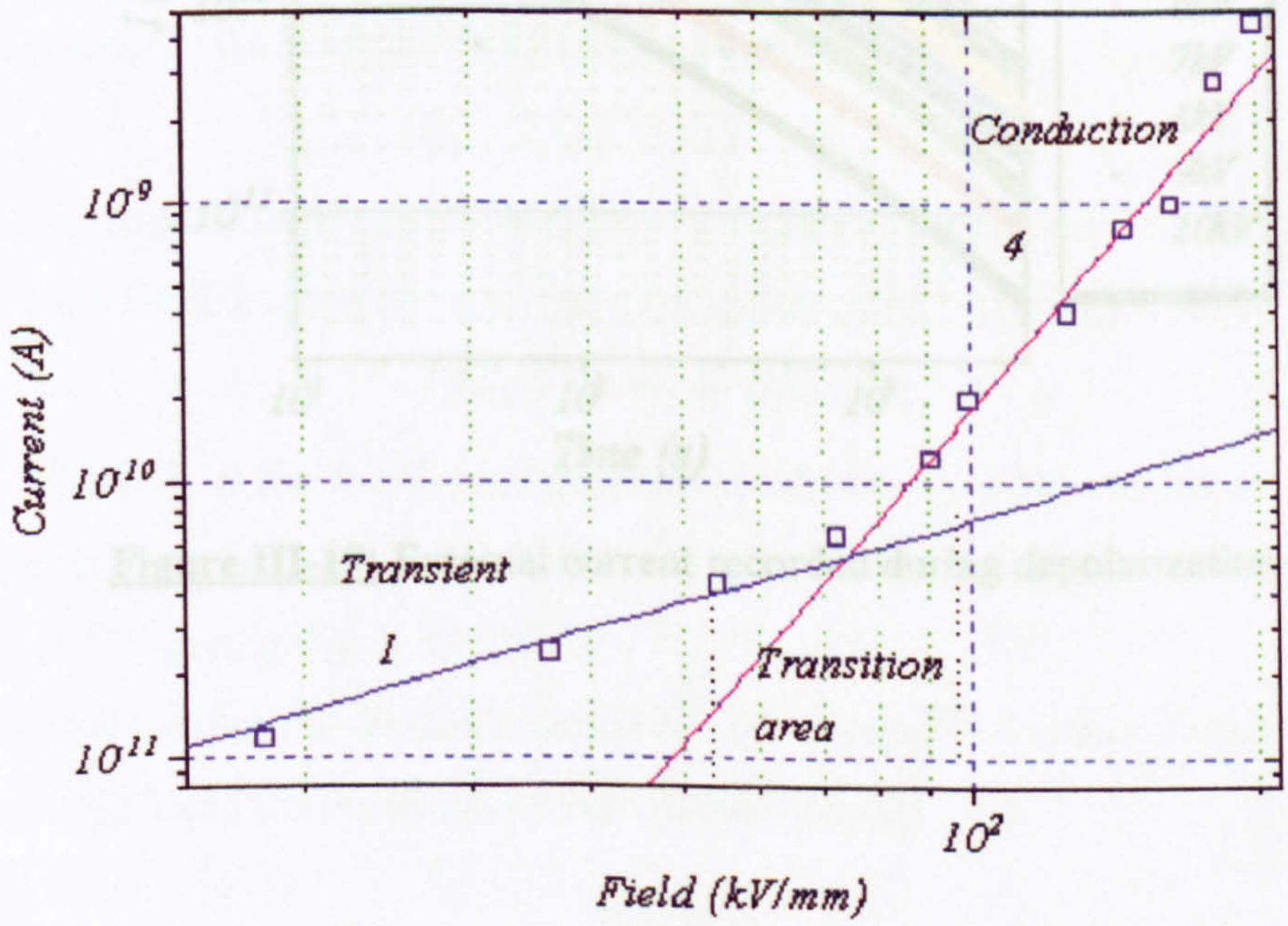

Figure III-18: I-E plot for the polarization ramp, 1h, average current above 2500s

Figure III-19 represents the external current recorded after the voltage application is switched off. The polarity of the current was reversed for the graphic representation. In fact, the absolute value of the current data has been taken and a log-log representation plotted. As observed during polarization, the depolarization current decreases rapidly with time, and the amplitude increases with the polarization voltage.

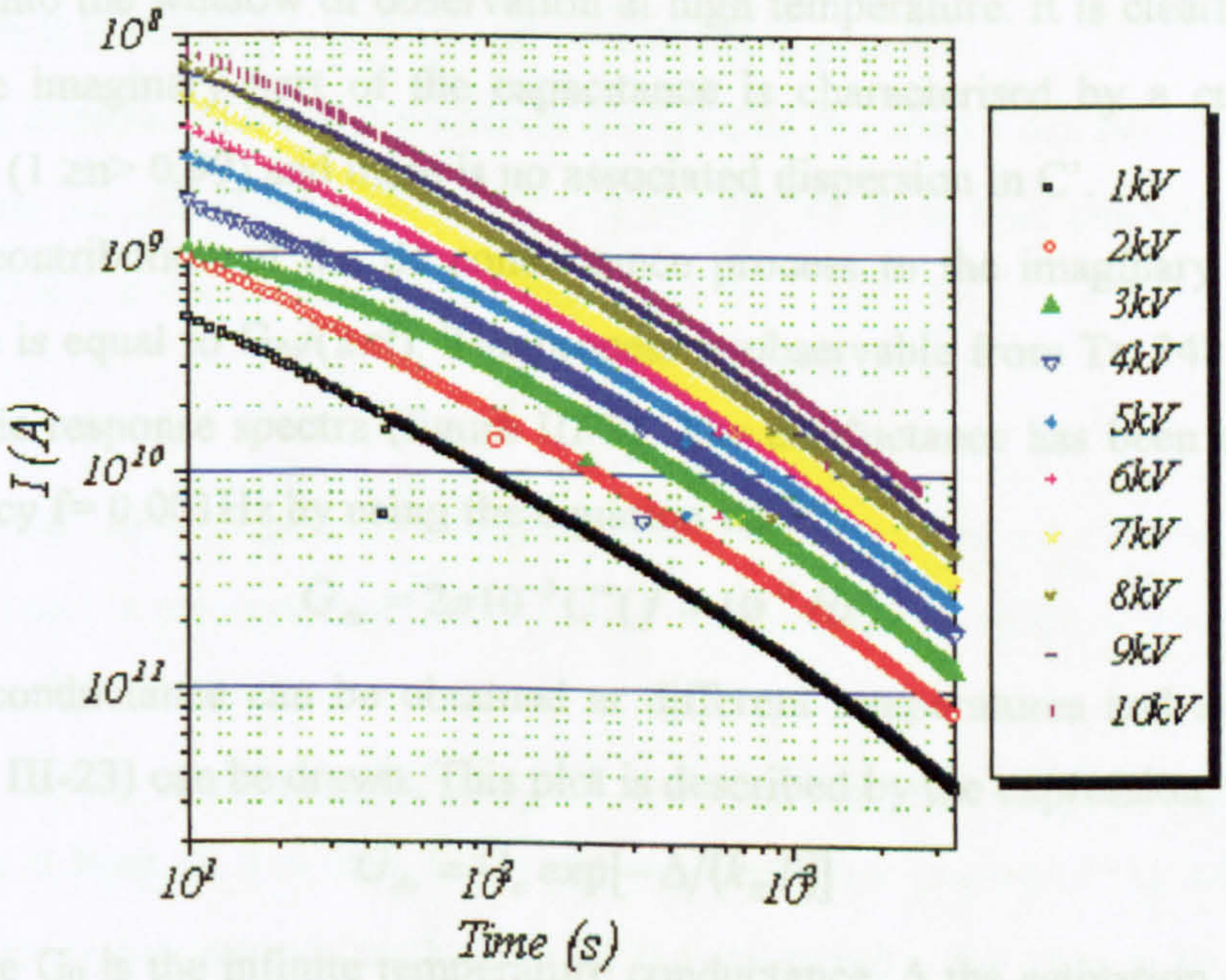

Figure III-19: External current recorded during depolarization

V- Discussion

The discussion will start by the analysis of the response shape of the different processes observed on a virgin sample before application of any voltage. Dielectric spectroscopy and external current measurements give access to similar parameters such as conductivity or relaxation peak position that will be compared and commented. Then the effect of voltage application will be analysed together with the post-curing consequences. Finally, the results on the wire samples will be analysed.

V.1- Dielectric response analysis over the frequency range

V.1.1- dc conductance process

The dc conductance process dominates the dielectric loss at low frequency and is brought into the window of observation at high temperature. It is clearly identified because the imaginary part of the capacitance is characterised by a curve with a gradient $-n$ ($1 \geq n > 0.99$) and there is no associated dispersion in C'.

The contribution of the dc conductance process to the imaginary part of the capacitance is equal to $G_{dc}/(2\pi f)$. The process is observable from T= 348 to 368K in the dielectric response spectra (figure III-8). The conductance has been estimated at the frequency f= 0.001Hz by using the equation III-22.

$$G_{dc} = 2\pi 10^{-3} C''(f = 10^{-3} Hz) \qquad \text{(III.22)}$$

The conductance can be obtained at different temperatures and an Arrhenius plot (figure III-23) can be drawn. This plot is described by the expression:

$$G_{dc} = G_o \exp[-\Delta/(k_B T)] \qquad \text{(III.23)}$$

Where G_0 is the infinite temperature conductance, Δ the activation energy, and k_B Boltzmann constant ($k_B = 1.38 \times 20^{-23} J.K^{-1}$). It is found that Δ= 1.6eV (1eV= 1.602×10^{-19}J) giving $G_0 = 3.63 \times 10^{11}$S.

From the plot the dc conductance can be extrapolated to lower temperature (i.e. around 293K) and the conductivity calculated by using:

$$\sigma = G\frac{L}{A} \qquad \text{(III.24)}$$

where the area of the electrode $A = \pi (23 \times 10^{-3}/2)^2 = 4.15 \times 10^{-4} m^2$, and the thickness of the sample L= 290μm.

The results are given table III-2:

Temperature (K)	**Conductance G (S)**	**Conductivity σ ($S.m^{-1}$)**
293	$1.6x10^{-16}$	$1.1x10^{-16}$
297	$3.2x10^{-16}$	$2.2x10^{-16}$
368	$4.65x10^{-11}$	$3.25x10^{-11}$

Table III-2: Conductance and conductivity extrapolated from the Arrhenius plot

The conductivity can also be estimated from external current measurements. From the I-E plot (figure III-11) it is possible to determine two regions described by different processes. The linear region observed at low fields is crosses over to a power law (I proportional to E^4) at the field E= 120kV/mm. This is identified as the transition field between a transient and a conduction process.

In the external current experiment the area of the electrodes have a diameter of 50mm giving an area $A= \pi x(25x10^{-3})^2 = 1.96x10^{-3}m^2$. It is then possible to estimate the conductivity in the linear region by using:

$$\sigma = \frac{I}{AE} \qquad \text{(III.25)}$$

From the linear region, by using E= 30kV/mm from the first set of experiments (figure III-16) I is estimated to be $I= 3x10^{-12}A$, this gives a value of conductivity $\sigma= 5.1x10^{-17}S.m^{-1}$ at T= 298K.

The current in figure III-16 will include transient currents up to around 120kV/mm at least. If it is then supposed that the linear region of the I-E curve (i.e. E< 120kV/mm) corresponds to the low field conductivity, the values for σ estimated from the two different techniques should be the same. These values ($2.2x10^{-16}$ and $5.1x10^{-17}S.m^{-1}$) are close in magnitude and their difference could be caused by inaccuracies in determining sample thickness, electrode and in the extrapolation of the dielectric results to low temperature. However, the second set of polarization current measurements indicate that a stable dc-current is not reached by 500s until the field reaches ~ 126kV/mm (see figure III-16, V= 7kV). It therefore seems clear that the linear I-E characteristic relates to a transient current which should be observable in the dielectric response at frequencies between 10^{-1}Hz and 10^{-3}Hz. The dc conductivity at T= 298K should have a magnitude less than $5.1x10^{-17}S.m^{-1}$, which

indicates that the temperature extrapolation of the conductance from the dielectric data is not valid. This could be the case if the dc conductance is affected by the glass transition which lies between room temperature and the temperature of the dielectric measurements in which it is observed.

An interpretation of the linear region of the I-E characteristics as a transient polarization current in this region to be much less than the observed value of I. This would be consistent with an extrapolation of the high-field dc conduction as a field assisted hopping between neutral traps $I = I_0[\exp(ae E/(k_B T)) - \exp(-ae E/(k_B T))]$, where a= 0.52nm is the average distance between traps. The low-field region of the behaviour gives $I = I_0(2ae E/(k_B T))$ which as figure III-16 shows is much smaller than the transient current. A trap-to trap hopping mechanism would be consistent with a thermally activated process with a high activation energy. The dielectric results indicate that the trap depth is Δ= 1.6eV, at T> 248K and possibly higher values below the glass transition. By using the dielectric result $G_0 = 3.63\times10^{-11}$S= σ_0A/L an estimate of the infinite temperature conductivity, $\sigma_0 = en\mu_0$, $n\mu_0$ is found to be $n\mu_0 = 1.58\times10^{9}V^{-1}m^{-1}S^{-1}$. Although the infinite temperature mobility μ_0 ($\mu = \mu_0 \exp(-\Delta/k_B T)$) cannot be determined, this value indicates a very low carrier concentration. Recent calculations [14, 15] indicate that trap depths of this magnitude are associated with chemical moieties and the small trap separations suggest that they form part of the monomer units of the epoxy. A possible candidate would be the bridging oxygen atoms.

An alternative description in terms of intrinsic charge promotion is unlikely unless carrier injection also occurs to neutralise the traps. In this case the high-field current would obey a Poole-Frenkel law. This cannot be ruled out but in this case it is unlikely that the source of carriers are oxygen traps, rather in this case we should look to the amine groups. It is also notable that the number density of carriers is very low. If a mobility of $\mu_0 = 10^{-3}m^2V^{-1}S^{-1}$ (appropriate to band conduction) is assumed the $n \approx 2\times10^{12}m^{-3}$ which is about $3\times10^{-7}C.m^{-7}$. This would not be detected by any existing space charge technique. Nevertheless SC is found at the higher fields (E≥ 20kV/mm) and this may be responsible for modifying the I-E law towards a $I \propto E^4$ form. At the fields below E≈ 90-120kV/mm we can expect only a small fraction of the injected charge to carry the current while the rest forms a layer of SC trapped close to the

electrodes. The SC results report in the later chapter will allow the discussion of SC effects to be carried further.

V.1.2- Low frequency process

To be able to characterise process A and estimate the position of the peak, it would be necessary to subtract the contribution of the dc conductance process. Subtraction of the contributions of processes B and C would be required to completely isolate process A, but this is not necessary to obtain the main part of the loss peak thus $C''(f) - G_{dc}/(2\pi f)$ should be plotted. This calculation is expected to reveal the process A as ideally represented figure III-20. The gradient of the higher frequency part of the lost peak can be measured from experimental results, whereas the gradient of the lowest part cannot be determined without the subtraction. n-1 was found equal to –0.68 leading to n= 0.32.

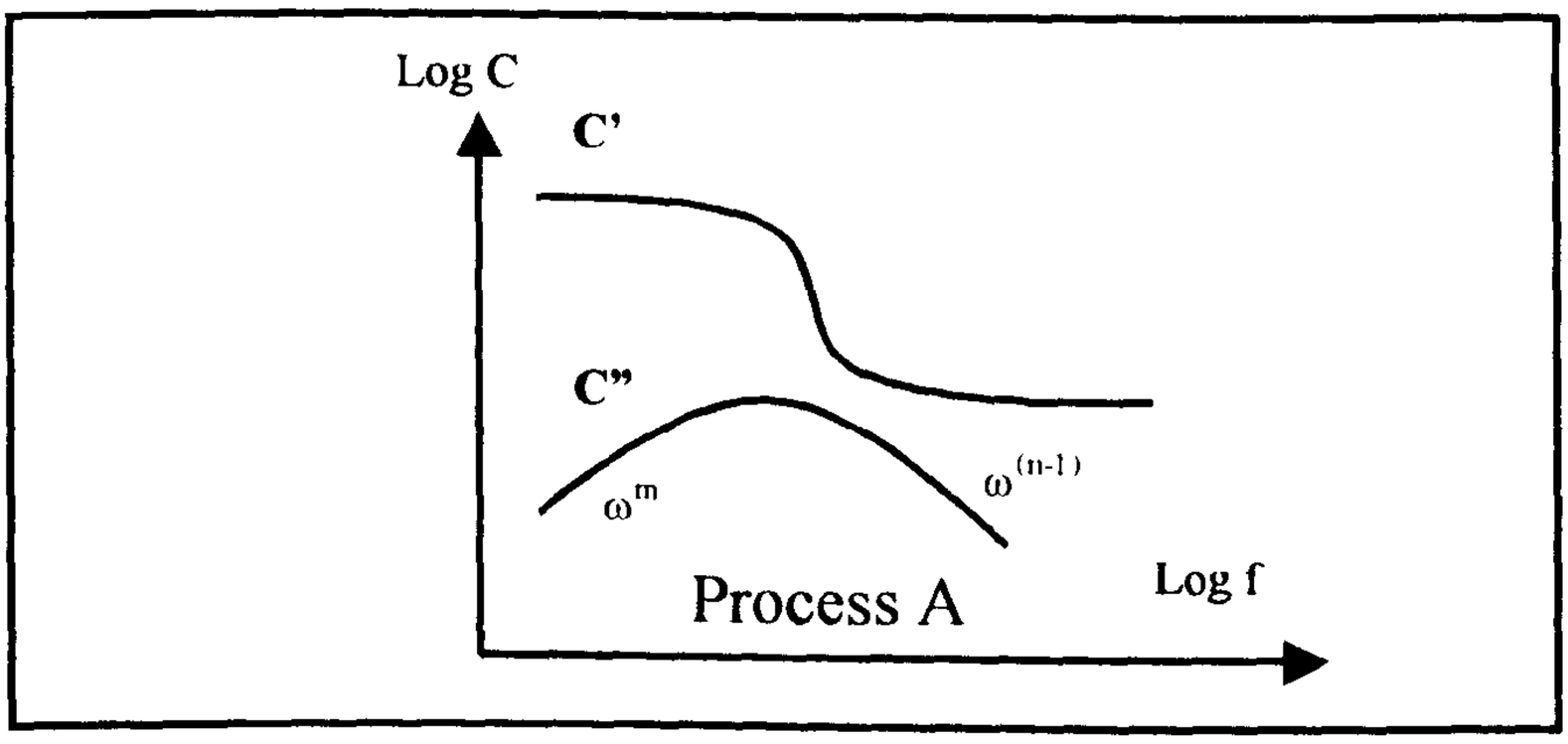

Figure III-20: Schematic representation of the expected shape of the process A after subtraction of the dc conductivity

Another solution to obtain the characteristics of the process A consists of drawing a master curve by fixing one set of results obtained at one particular temperature and bringing the others into coincidence. The displacement of each curve is taken into account so as to determine the relative positions of the peaks associated with the process under investigation. Finally, an Arrhenius plot can be drawn and by using equation III.26, it is possible to determine the activation energy associated with the process.

$$f_{peak,T} = f_{peak,ref} \exp\left(\frac{-E_a}{k_B T}\right) \qquad \text{(III.26)}$$

This procedure has been applied to the low frequency response region by choosing the curve at 353K as reference. A rough estimation of the peak associated with the process A has been performed, and the position of the peak has been set at 0.056Hz.

The curves obtained in the range 313-353K are shifted toward the high frequency to come into coincidence with the curve at 353K. The curves in the range 353-368K are shifted toward to low frequency for the same purpose. Table III-3 gives the values of displacement determined for each temperatures. The master curve is represented in figure III-21 and the corresponding Arrhenius plot in figure III-22.

Temperature (K)	f_{peak} (Hz)	$f_{peak}/f_{peak,353K}$
293	3.62E-6	0.00006
303	7.62E-6	0.00014
313	0.00178	0.03167
323	0.00316	0.05623
328	0.00562	0.1
333	0.009	0.16014
348	0.01	0.17794
353	0.0562	1
358	0.0582	1.03559
363	0.1	1.77936
368	0.17783	3.16423

Table III-3: Estimation of f_{peak} for each temperature.

Reference temperature 353K

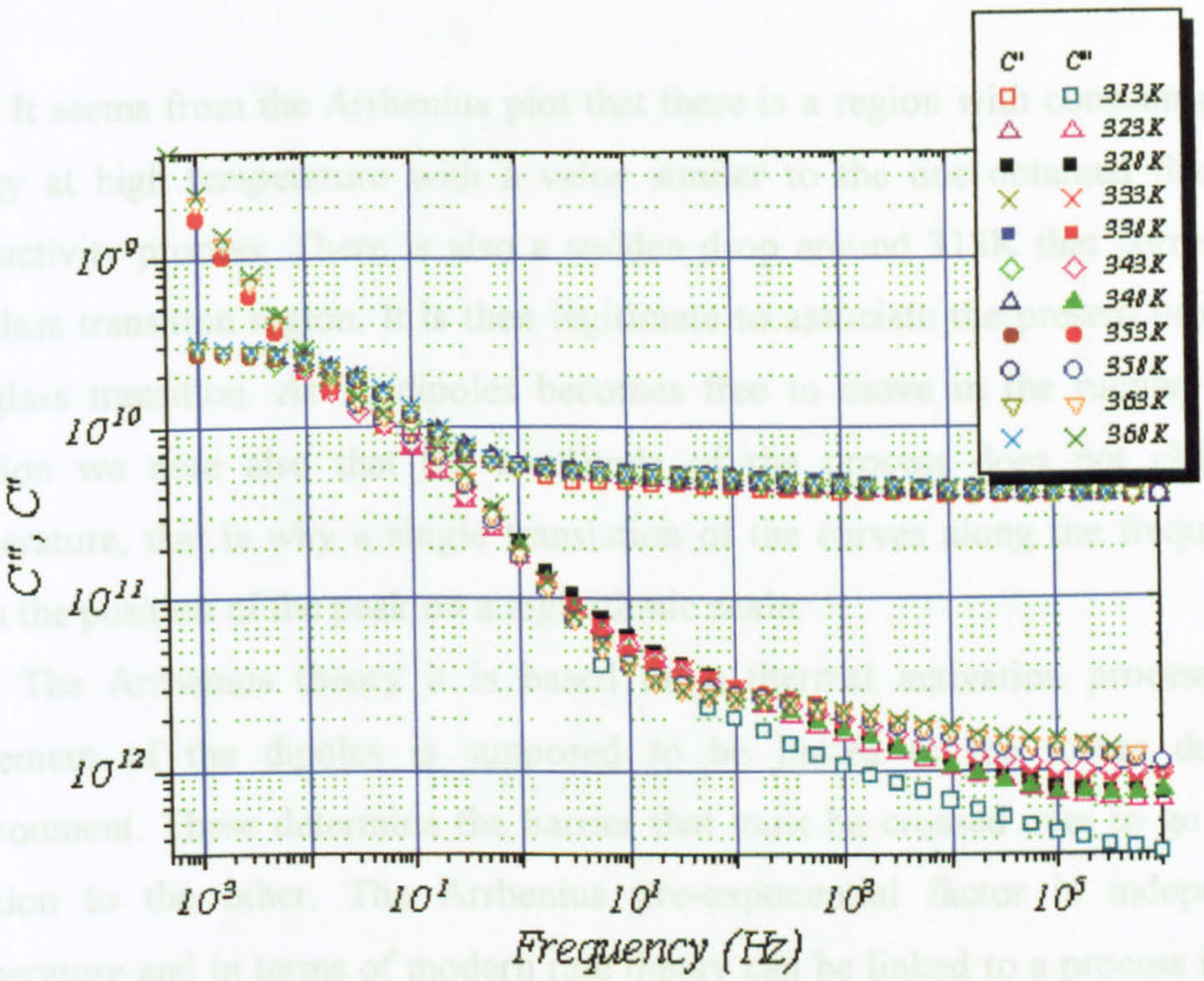

Figure III-21: Master curves at 353K, process A

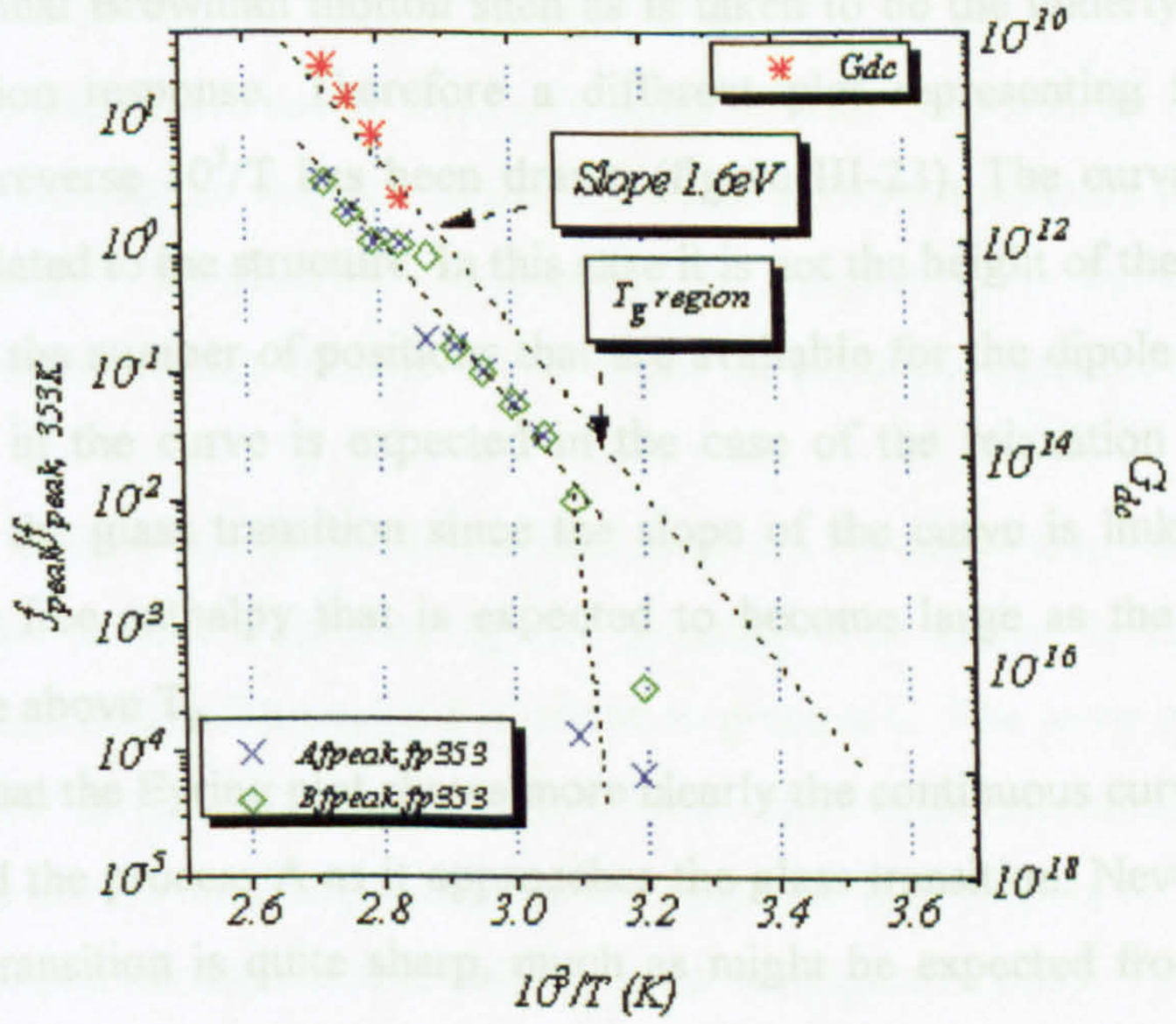

Figure III-22: Arrhenius plot. Left scale $f_{peak}/f_{peak,\ 353K}$ process A (diamond) and B (cross), right scale dc conductance versus $10^{3}/T$ (asterisk)

It seems from the Arrhenius plot that there is a region with constant activation energy at high temperature with a value similar to the one obtained from the dc conductivity process. There is also a sudden drop around 313K that corresponds to the glass transition region. It is then legitimate to associate the present process with the glass transition. At T_g dipoles becomes free to move in the rubbery state. In addition we note also that the amplitude of the process does not change with temperature, that is why a single translation of the curves along the frequency axis gives the position of the peak on a logarithmic scale.

The Arrhenius theory it is based on a thermal activation process and the movement of the dipoles is supposed to be linked to the forces due to the environment. These determine the barrier that must be crossed over to go from one position to the other. The Arrhenius pre-exponential factor is independent of temperature and in terms of modern rate theory can be linked to a process in which a single quantum vibration or specific set of vibrations are used to pass through the barrier. If the barrier state involves a re-organisation of the quantum vibrations Eyrings theory of chemical reaction rates should be used. In this case the pre-exponential factor is given by k_BT/h. It is usually assumed that the Eyring theory applies to rotational Brownian motion such as is taken to be the underlying process for glass-transition response. Therefore a different plot representing f_{peak}/T as a function of the reverse $10^3/T$ has been drawn (figure III-23). The curvature of the Eyring plot is related to the structure. In this case it is not the height of the barrier that is important but the number of positions that are available for the dipole considered. A sudden drop in the curve is expected in the case of the relaxation phenomena associated with the glass transition since the slope of the curve is linked with the variation of the free enthalpy that is expected to become large as the dipoles are allowed to move above T_g.

It seems that the Eyring plot shows more clearly the continuous curvature of the curve associated the process A as it approaches the glass transition. Nevertheless the onset of glass transition is quite sharp, much as might be expected from a melting crystal.

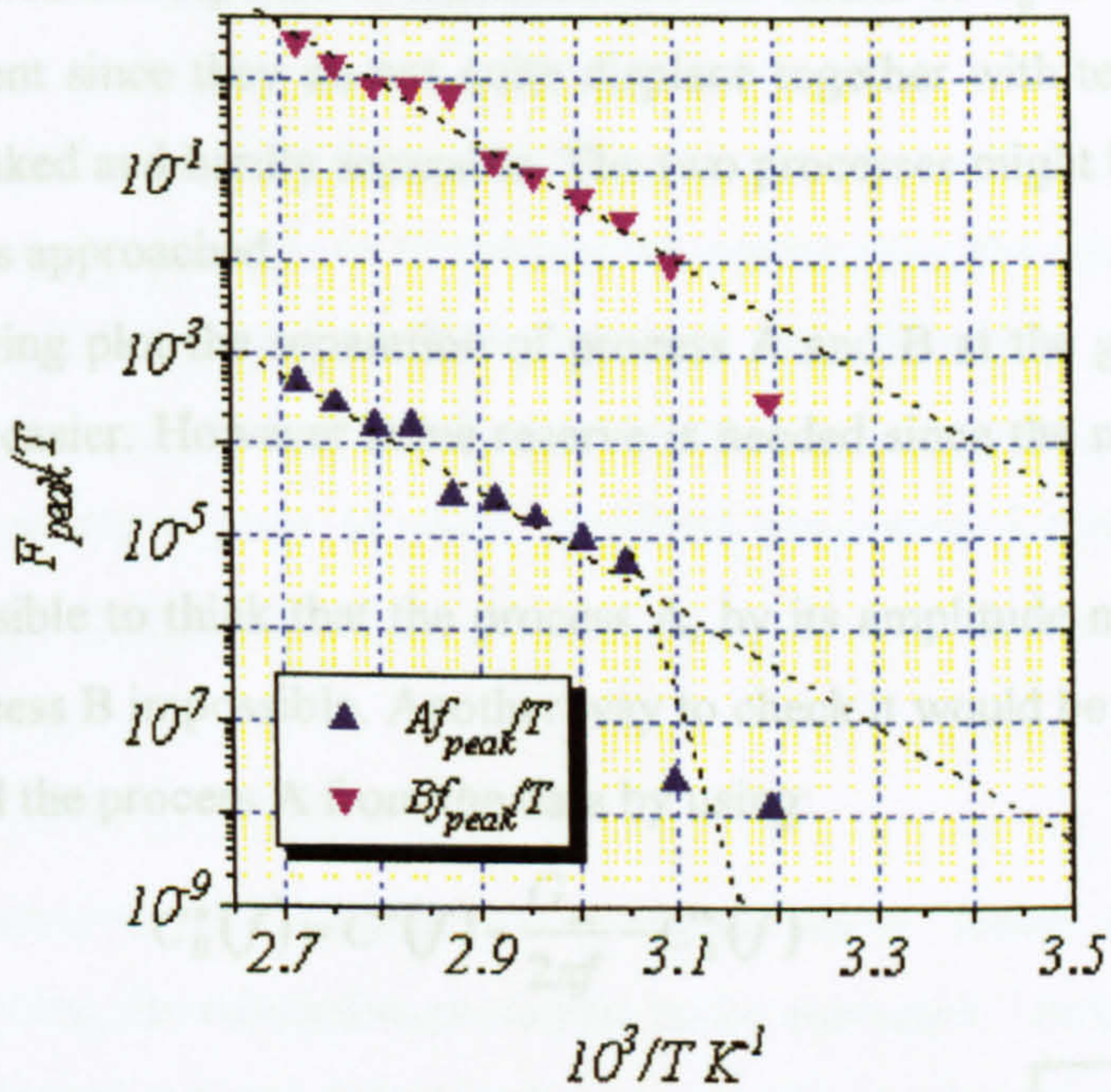

Figure III-23: Eyring plot, for process A and B, F_{peak}/T as a function of $10^3/T$ 353K reference temperature

V.1.3- Intermediate and high frequency processes

Processes B and C also suffer from a masking of their response by one another and process A, since they do displace at the same rate as the temperature is increased. They remain difficult to describe. Moreover, the process C is cut-off at high frequency because it extends outside the window of possible measurement by the FRA system.

In the case of the Process B it is difficult to give a complete analysis because it is partially hidden at low frequency by the process A or maybe is merged with process A, whereas at high frequency it is added to process C. The same procedure as the one carried out for process A can be followed. The translation along the log of frequency axis gives the relative position of the response with respect to the position at 353K that can still be used as the reference curve (figure III-24). The Arrhenius plot obtained follows almost the same behaviour as the one drawn for process A. It might be possible that for process B, the curvature is not present in this process leading to a straight line as the temperature decrease but is seems difficult to conclude

(figure III.21). Even if this process is not directly associated with the glass transition it seems that the dielectric response is dependent on the values of T_g. Process A and B are however different since they do not quite displace together with temperature but they seems to be linked and hardly separable. The two processes might becomes more independent as T_g is approached.

From the Eyring plot the separation of process A and B at the glass transition temperature seems easier. However some reserve is needed since the number of data is not large.

It is also possible to think that the process A, by its amplitude makes a proper analysis of the process B impossible. Another way to check it would be to subtract the dc conductance and the process A from the data by using:

$$C''_B(f) = C''(f) - \frac{G_{dc}}{2\pi f} - C''_A(f) \qquad \text{(III.27)}$$

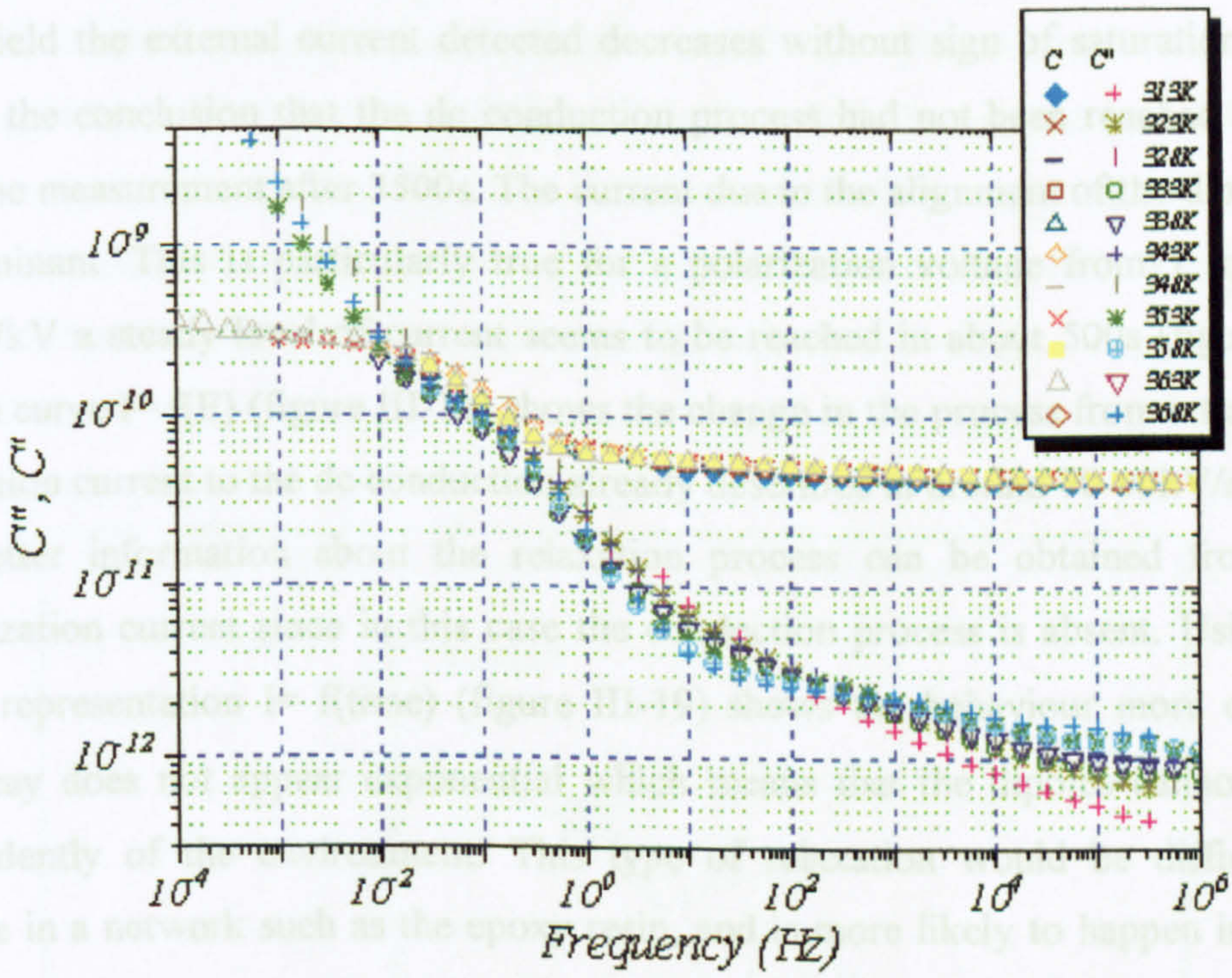

Figure III-24: Master curves at 353K, process B

After subtraction a peak surrounded by two power laws would be expected as in the case of the process A. An estimation of the slope of the high frequency side has performed without the subtraction and the parameter n was found to be n= -0.27+1= 0.71.

In the case of the process C no translation can be carried out. Amplitude displacement seems to be possible to fit the curves representing the imaginary part of the capacitance but if it doesn't work for the real part then it is not acceptable. Besides as the temperature is increased the process B seems to overlap the process C that might then become a sum of two combined processes. Little can then be extracted from this process.

V.1.4- External current analysis

The polarization and depolarization currents allow some complementary information concerning the relaxation processes to be extracted. During polarization at low field the external current detected decreases without sign of saturation. This leads to the conclusion that the dc conduction process had not been reached by the end of the measurement after 3500s. The current due to the alignment of the dipoles is still dominant. This is particularly true for a polarization voltage from 1 to 5kV. Above 7kV a steady level of current seems to be reached in about 500s (figure III-17). The curve I= f(E) (figure III-18) shows the change in the process from a transient polarization current to the dc conduction already described at around 70-90kV/mm.

Better information about the relaxation process can be obtained from the depolarization current since in this case the conduction process is absent. Using the log-log representation I= f(time) (figure III-19) shows the behaviour more clearly. The decay does not appear exponential which means that the dipoles cannot relax independently of the environment. This type of relaxation would be difficult to envisage in a network such as the epoxy resin, and is more likely to happen in polar liquids where dipoles are free to align in an external electric field. By using the change in the slope it is possible to define a relaxation time τ and identify which process the relaxation current corresponds to the dielectric spectroscopy response.

From the dielectric spectroscopy a loss peak is described by a maximum and two powers laws. The coefficients already defined from the dielectric response can be extracted from the I-t plot. Since the dielectric spectroscopy experiment is carried out at low field it is necessary to choose the curve obtained from the current detection at

the lowest applied voltage so as to be sure that we are in the linear domain response. Note, however, that the linearity is assured by reference to figure III-18. From such analysis the relaxation time was found to be τ= 278s, which is equivalent to a response frequency of $3.6x10^{-3}$Hz. This would correspond to the B process. The value of the power exponent n from the current $I(t) \propto t^{-n}$ was found to be 0.69 which agrees very well with the estimate of n= 0.73 from the frequency dependence of the B process in the dielectric response. A similar value (n= 0.78) can be obtained from the polarization current. At times $t>\tau$ the current is expected to behave at $I(t) \propto t^{-(1+m)}$. This is masked by the beginning of conduction in the polarization current, but can be seen better in the depolarization current where $m \approx 0$. This small value may be the result of an inadequate time range beyond τ, but if it is correct suggest a very flat response for process B at frequencies below its loss peak. Because it cannot be resolved by dielectric spectroscopy it is difficult to be precise.

It is interesting to note that this process in the charging current is dependent upon past history. If the ramping of the sample is cycled, then it was found that the transient current measured at the same field decreased. Over a period of 24hours, however, the current transient associated with the B process are a further indication that this process is modified by exposure to electrical stress.

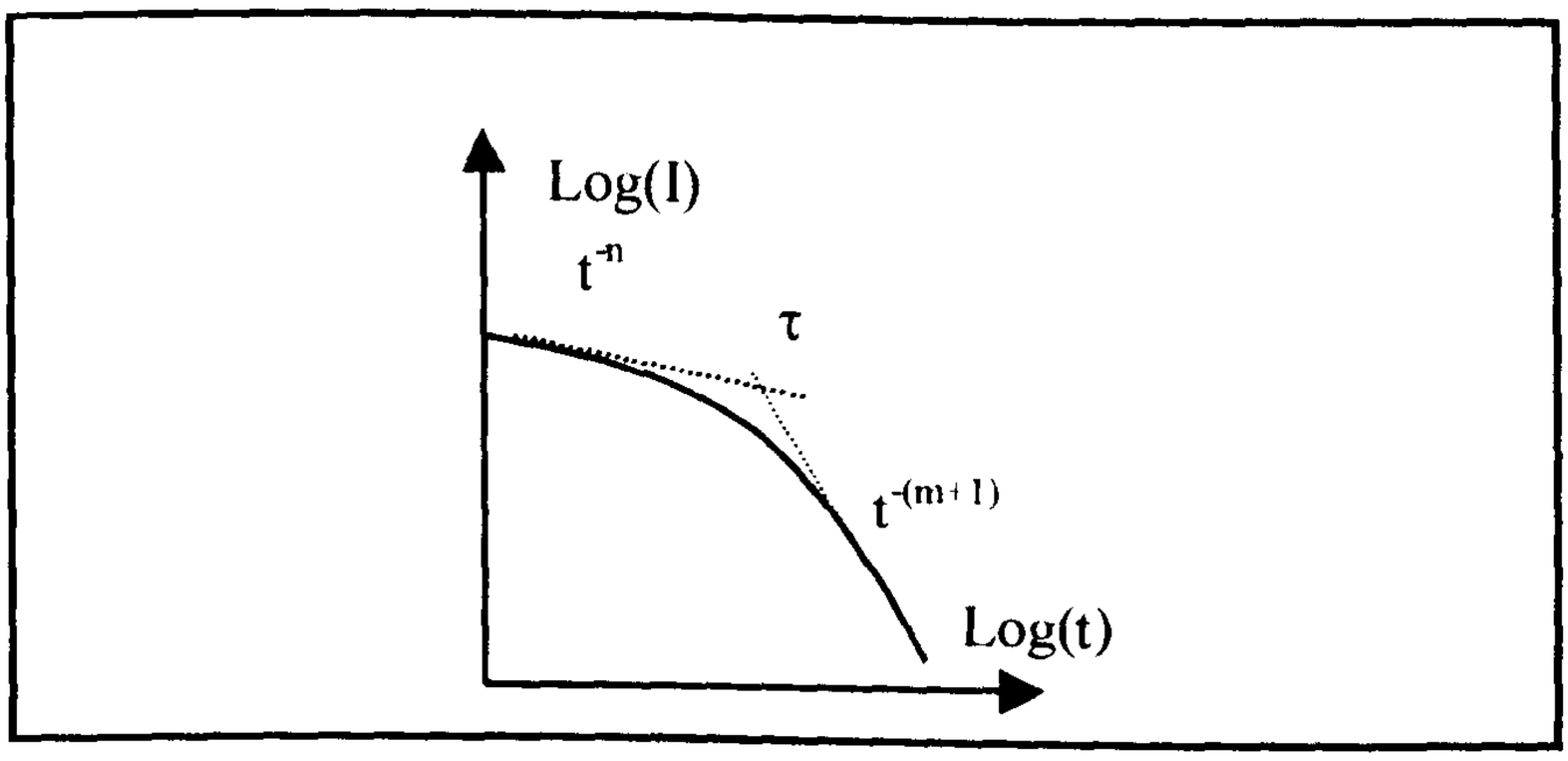

Figure III-25: Schematic representation of the expected behaviour of the time dependence of a relaxation process

V.2- Effect of post-curing

It has been observed that even after post-curing the low frequency dielectric response of the sample changes under electrical stress. However, this change appears to be smaller in comparison with results from non post-cured samples. Because the ageing was carried out in the glass transition region the system is more or less flexible depending on the curing. In addition to the effect due to the application of a voltage the temperature effect might be dominant on non post-cured sample especially at the beginning of application of the stress. Later the electrical stress might become the main factor that cause changes in the material.

It is thought that high thermal stress, i.e. 40-50°C above T_g might cause major changes in the morphology even with post-cured samples. This implies that the effect of electrical and thermal stress in the experiments cannot be separated easily.

The experiment concerning the measurements before and after electrical stress on the wired samples, however, shows the same changes. Here they can be supposed to be due more to the voltage application more the temperature since in this case the measurements and stressing were performed below the glass transition (293K). This time it is the high electric field due to the divergent field configuration that might be held responsible for the changes even if the stress become really small as the distance from the wires increases.

Chapter IV

Space charge profile using PEA measurements

The Pulse Electro-Acoustic (PEA) method of investigation was first applied to thin epoxy samples free of wires. PEA system used measured the external current simultaneously with the space charge different controlled temperatures. The aim was to first determine the characteristics of the material investigated from a simple geometry, i.e. a plane film of material.

Space charge (SC) measurements have also been carried out on wire samples. Since the sample geometry gives a divergent field it is not really adapted to the measurement system, and the analysis of the results is found to be complex. Other difficulties come from reflections of the signal from the wires. However, similar measurements have been recorded by Laser Induced Pressure Pulse (LIPP) [1] in the case of wire samples with a different type of epoxy resin. These studies will constitute a starting point for comparison with our own results. It is noticeable that both of the techniques are based on the same principle, namely that of using the propagation of an acoustic wave. As a result, measurements obtained by PEA or LIPP systems have often been compared to study the charge distribution in various dielectric materials [2].

I- Principle of PEA

The PEA method coupled with external current measurements is expected to give some information about the electrical characteristics of insulating materials by a non-destructive technique [3]. This technique was developed for the measurement of a volume SC distribution and was first built in Japan in the middle nineteen eighties [4]. The aim was to determine the density, the polarity, and the position of the charges present in solid dielectric materials.

I.1- Principle of detection

In the PEA method a voltage pulse is applied to the sample of thickness d situated between two plane electrodes. Under the effect of the pulse electric field $e_p(t)$ the surface charges $\sigma(0)$ and $\sigma(d)$ that are due to the voltage application and the SC distribution in the material noted $\rho(x)$ are displaced slightly. The displacement produces an acoustic wave that will travel across the sample and will be collected by the bottom electrode where the detector is situated. The detection of the waves by a

piezoelectric device yields the profile of the SC. The amplitude of the signal and the magnitude of the SC are related, as is the time lag between the voltage pulse and the signal leading to the position of the SC.

I.2- Spatial resolution

It is by the determination of the electric charge distribution $\rho(x)$ that the electric field $E(x)$ and the potential distribution $V(x)$ become accessible. All these values are dependent on the time, t, and on the position, x, within the sample. Calculations are based on Poisson equation [1]:

$$E(x) = \int \frac{\rho(x)dx}{\varepsilon_0 \varepsilon_r} \qquad \text{(IV.1)}$$

$$V(x) = -\int E(x)dx \qquad \text{(IV.2)}$$

The position in the depth direction is given by $x = s.t$ where s is the velocity of sound in the material. Actually the signal is recorded from a digital microscope. Each point corresponds to a quantity of charge contained in a plane normal to the wave propagation direction. The thickness of the plane, that is considered as an homogeneous charged volume, is particularly dependent on the oscilloscope sampling frequency. A Fourier transformation is then used to associate the response in the frequency domain to a response in the time domain that will be finally transformed to a charge distribution in the one dimensional spatial domain by using the time/position relationship.

The PEA method was widely developed for measurements on thick samples (1 to 10mm) [5]. The system has since been modified for the measurement of thin materials [6] and thus the technique has become suitable for the detection of SC distributions in dielectric films. Most of the time the samples under investigation have the shape of a plane parallel sheet (from 100 to 300μm thick) though coaxial cables with a conducting inner core and outer sheath and the insulator inbetween has also been studied [7]. The method has been extensively refined. For instance in recent years, the application of a very high voltage for the investigation of cables has become available. A three-dimensional measurement system is also the subject of development [8]. This latter expansion of the technique reflects the great advance of knowledge in the field.

II- Response of the PEA to various charge distributions

II.1- Uniform dipolar polarization

When a dielectric material is inserted between two plane electrodes and when a dc voltage V_0 is applied between the electrodes, the internal electric field is initially defined as $E_0 = V_0/d$ where d is the thickness of the sample.

Molecular dipoles that are oriented by the applied field do not give a field distortion as long as they are uniformly distributed in space. They do, however, induce a corresponding charge on the electrodes, with the same polarities as that which would be produced by an hereto-charge region built-up close to the electrodes. A schematic representation of the induced charges on the electrodes and expected PEA signal after voltage removal are given in figure IV-1.

Molecular dipoles can be regarded as possessing a zero net charge within the spatial limits of resolution of the PEA technique. They therefore do not contribute to the bulk signal as long as they are uniformly distributed in space. In divergent fields however the dielectric polarization is also divergent. Since $divP$ is equivalent to a charge density ρ a molecular dipole contribution to the signal would be expected in this case [9].

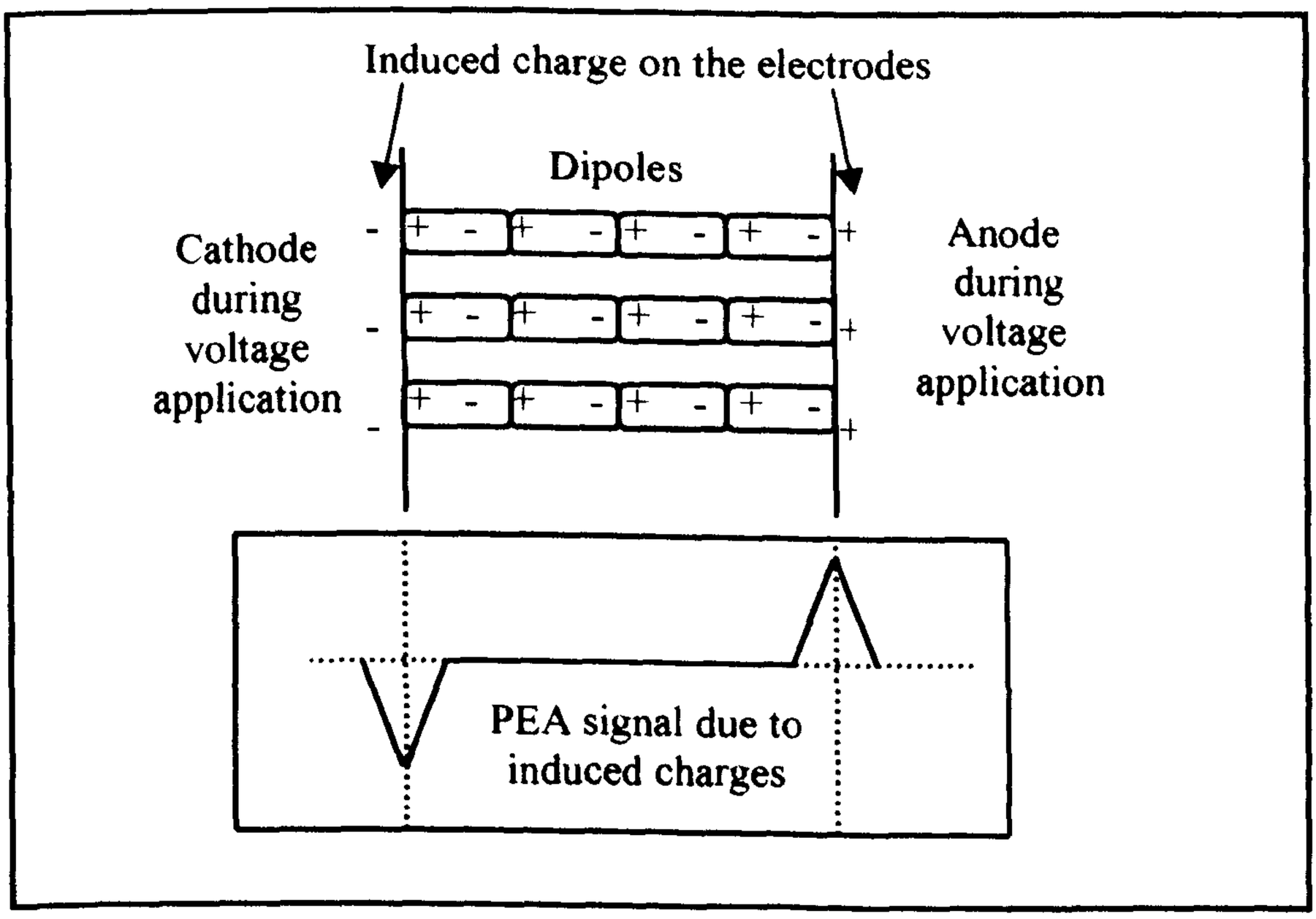

Figure IV-1: Dipolar orientation, inducing charges on the electrodes in a uniform field configuration and the expected PEA signal after voltage removal

II.2- Net internal space charge

In the presence of net internal charges, a Coulomb force affects them when the pulse voltage is applied [10] this induces a perturbation force proportional to the local net charge that is transmitted to the system instantaneously. The pressure wave propagates through the insulator as two components travelling in opposite directions. The component that reaches the lower electrode is transmitted to the detection system. The pressure, $p(t)$, of the acoustic wave thus detected is proportional to $\rho(x)$ the one dimensional charge density distribution in the material. The SC region is treated as sheet of charges or as a sequence of sheet charges, the thickness of the layer being determined by the sampling rate of the oscilloscope.

II.3- Measurements under voltage

An impulsive Maxwell stress f(x, t) appears at the material-electrode interface as soon as the HV pulse is applied due to the difference in the dielectric constant [10]. This effect appears on both side of the plane sample. In this case, the polarity and magnitude of the generated pressure wave is proportional to the electric field $E(x) = V_{dc}/d$. The signal related to the sample side in contact with the top electrode is time delayed due to the necessary propagation across the sample before it reaches the bottom electrode of the apparatus where the detector is located.

The effect of SC, that can be schematised by two extremes cases (figure IV-2), is added to the signal associated with the surface sheet charges due to voltage application. For instance, if homo-charges are injected from both electrodes a SC region is built up on both sides (figure IV-2.a). The electric field is lowered at the interface compared to the calculated uniform electric field. However, it becomes higher in the bulk. On the other hand, if charge from ionised impurities is dominant close to the electrodes an hetero SC region is built up (figure IV-2.b). The field is enhanced at the interface and lowered in the bulk compared to E_0. In both cases the internal electric field is distorted by the presence of SC. The same effect as the one produced by dipolar polarization is expected in the hetero-charge case.

A similar effect can be induced by the presence of net charges in the bulk, which create an internal field distortion. This net internal SC will induce surface sheet charges of the same sign on both electrodes but with different magnitude. The closer the space charge to a given electrode the larger the charge it induces on that electrode. As previously, the effect will be to reduce or increase the signal due to the voltage application.

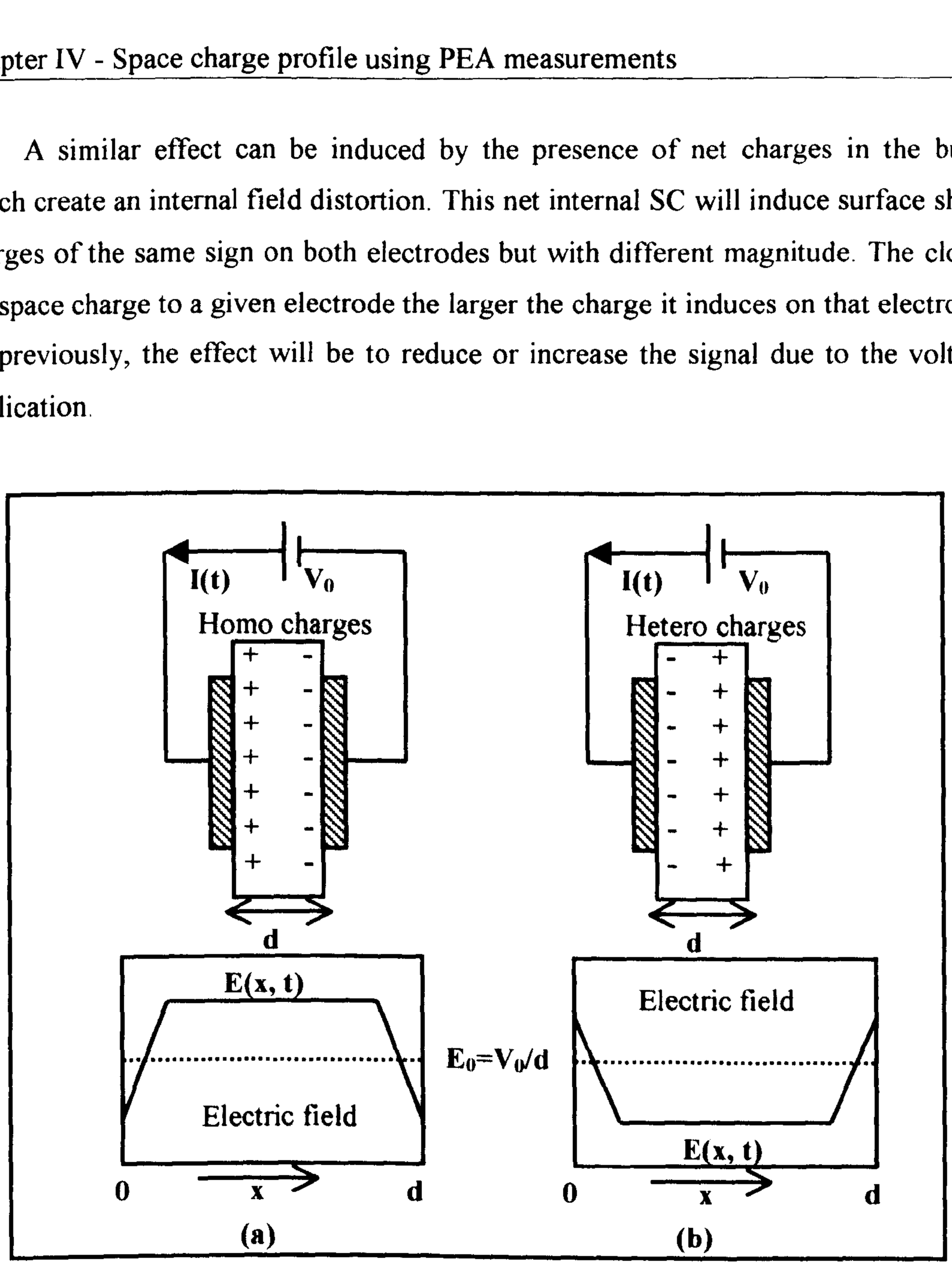

Figure IV-2: Distortion of the electric field due to the build up of a Space Charge region **(a)** Homo charge **(b)** Hetero charge region built into a dielectric material inserted between two parallel plane electrodes

The sample polarization increases the signal detected on the electrodes during voltage application since in order to keep the potential difference between the electrodes constant extra charges need to be supplied to the electrodes as the polarization increases. After the polarization is completed changes in the signal can only be due to SC effects.

III- Experimental set-up

III.1- Electric pulse characteristics

There are some requirements for the electric pulse characteristics if useful measurements are to be obtained. First of all, the width of the pulse voltage must be shorter than the transit time across the sample in order to be able to detect the SC distribution [7]. The transit time can be defined as the ratio of the distance to the speed of the acoustic wave (d/s), and is an intrinsic property of the sample.

A general feature of the measurement method is that the acoustic wave generated and detected has the same shape as the HV electric pulse applied. It is then important to apply a narrow electric pulse in order to create a narrow acoustic pulse to propagate through the bulk. In other words to improve the spatial resolution of the SC distribution it is necessary to reduce the width of the acoustic signal detected. This can be achieved by reducing the length of the applied electric pulse. Usually the resolution is measured in terms of "half width" for the signal detected from the electrodes, but because it is difficult to distinguish the charges in the "width" it seems to be reasonable to speak about resolution within a range of microns.

Finally, the acoustic impedance of the sample and the HV electrode must match in order to retain the narrow shape of the pulse that is transmitted in the bulk of the polymer under investigation. This is achieved by inserting a piece of semi-conducting impedance matching material, usually PVC, between the top electrode and the polymeric film. It is called backing material in figure IV-3. This procedure prevents any reflection and loss of the signal at the sample-electrode interface.

In the system in use that was initially constructed by Maeno et al. [5] the pulse had a duration of 5ns and a repetition rate frequency of 400Hz. The voltage applied varies with the thickness of the sample. It is usual to apply a pulse that produces an internal electric field of about 1kV/mm. The available values of voltage were 100, 200 and 400V. If only the pulse is applied to the normal plastic film, 1kV/mm is supposed harmless and no signal is detected by the system. During the dc voltage application the pulse electric field must represents only a few percent of the bias applied voltage.

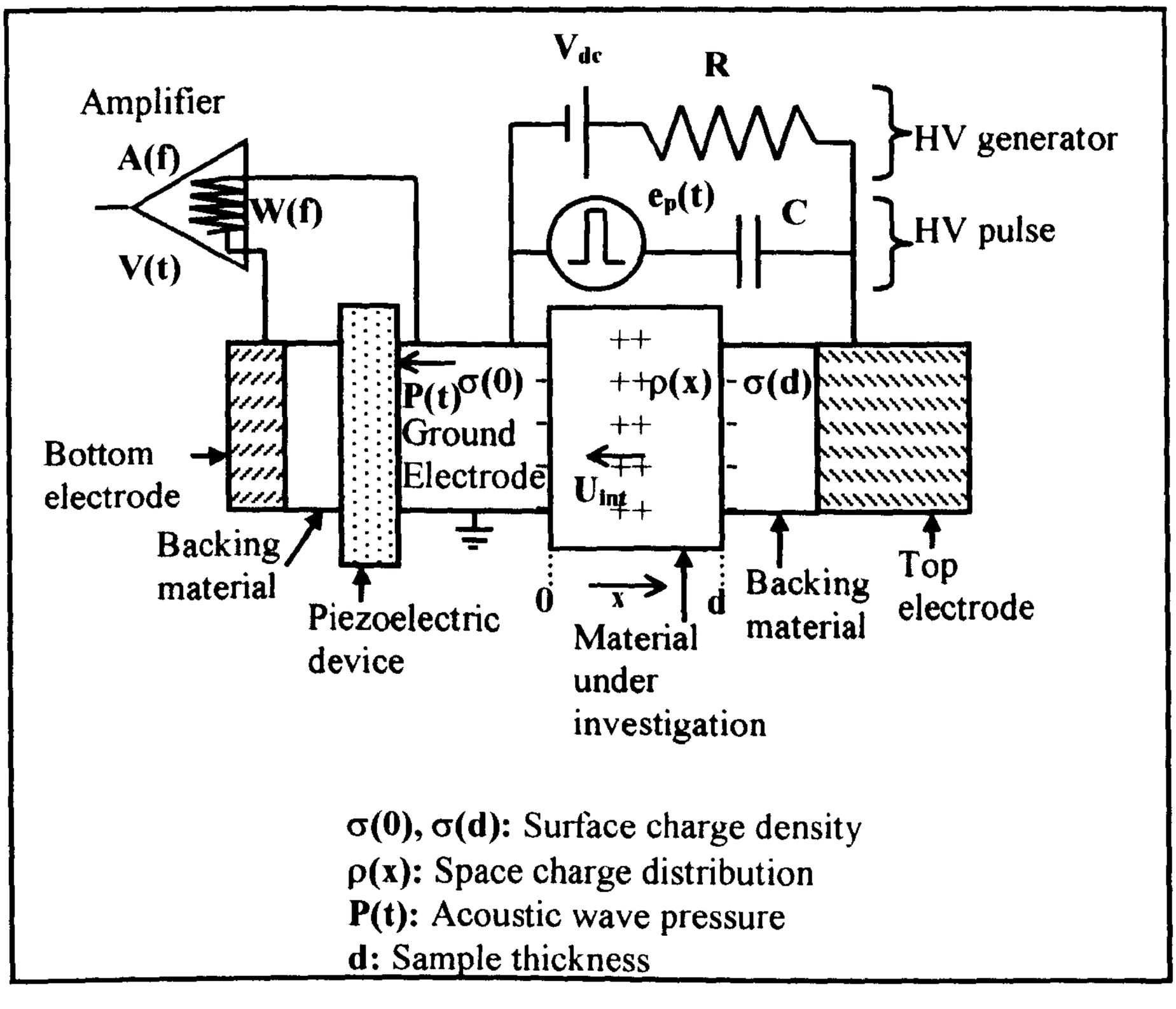

Figure IV-3: PEA set-up

III.2- High voltage supplies

HV is applied to the sample by the mean of the top electrode. The system has been built so that it is possible to apply the electrical stress at the same time as the measurements are performed by the application of the HV pulse voltage. The dc HV is supplied through a charging resistor that is of 5MΩ in the case of Maeno system (figure IV-4). The bias voltage source available runs from 0 to 10kV.

The top electrode assembly can be embedded in an epoxy block in order to screen out the electrical noise generated during the discharge of the pulse generator. It is also used as a guard ring for the HV electrode in the high-resolution system used by Maeno et al. [11]. This system was utilised for several measurements in the present work. In order to make simultaneous measurements of the external current and the space charge a system by Alison [3, 12] described was also used. Both systems are shown in the schematic figure IV-4.a, b.

In addition to a clamping system with a screw or spring, the contact between electrode and sample was improved by a drop of silicone oil added to both sides of the film sample.

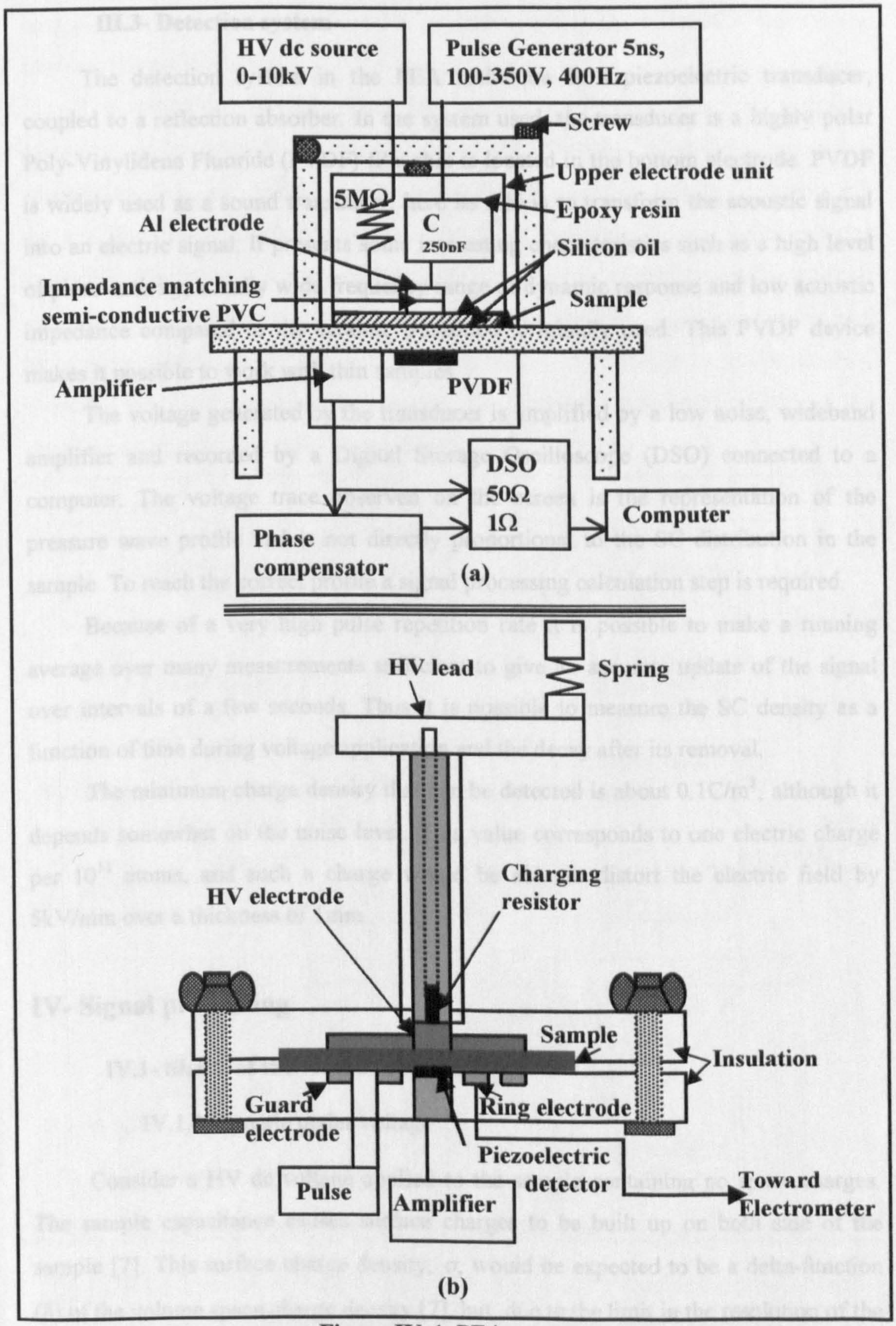

Figure IV-4: PEA systems

(a) From Maeno and Fukunaga [6] **(b)** From Alison [3, 12]

III.3- Detection system

The detection system in the PEA technique is a piezoelectric transducer, coupled to a reflection absorber. In the system used, the transducer is a highly polar Poly-Vinylidene Fluoride (PVDF) film that is located in the bottom electrode. PVDF is widely used as a sound transducer, here its role is to transform the acoustic signal into an electric signal. It presents some interesting characteristics such as a high level of piezo-activity, a really wide frequency range of dynamic response and low acoustic impedance compared to the ceramic transducer originally used. This PVDF device makes it possible to work with thin samples.

The voltage generated by the transducer is amplified by a low noise, wideband amplifier and recorded by a Digital Storage Oscilloscope (DSO) connected to a computer. The voltage trace observed on the screen is the representation of the pressure wave profile and is not directly proportional to the SC distribution in the sample. To reach the correct profile a signal processing calculation step is required.

Because of a very high pulse repetition rate it is possible to make a running average over many measurements sufficient to give an accurate update of the signal over intervals of a few seconds. Thus it is possible to measure the SC density as a function of time during voltage application and the decay after its removal.

The minimum charge density that can be detected is about $0.1 C/m^3$, although it depends somewhat on the noise level. This value corresponds to one electric charge per 10^{11} atoms, and such a charge would be able to distort the electric field by 5kV/mm over a thickness of 1mm.

IV- Signal processing

IV.1- Shape of the recorded signal

IV.1.1- Sample under voltage

Consider a HV dc voltage applied to the sample containing no space charges. The sample capacitance causes surface charges to be built up on both side of the sample [7]. This surface charge density, σ, would be expected to be a delta-function (δ) of the volume space charge density [7], but, due to the limit in the resolution of the detection apparatus and the finite width of the probe electric pulse, the induced surface charge signals appear as broadened peaks. The charge density will appear to

be a positive peak at the anode and a negative peak at the cathode in the present situation (figure IV-5.a).

The resolution can be defined by the signal to noise ratio, and was first estimated to be between 10 and 20μm in the direction of the acoustic wave propagation. Actually, due to advances in the detection system such as the sensor and the amplifier coupled with powerful oscilloscopes that allow a rapid collection and averaging calculation, the space charge, the electric field and the potential profile can be observed in real time. In order to reach a high resolution, signal processing was found to be necessary [11]. It is performed by means of a computer that introduces a measured reference to correct the response. It increases the resolution in depth of the signal detected to 12-15μm in the present system.

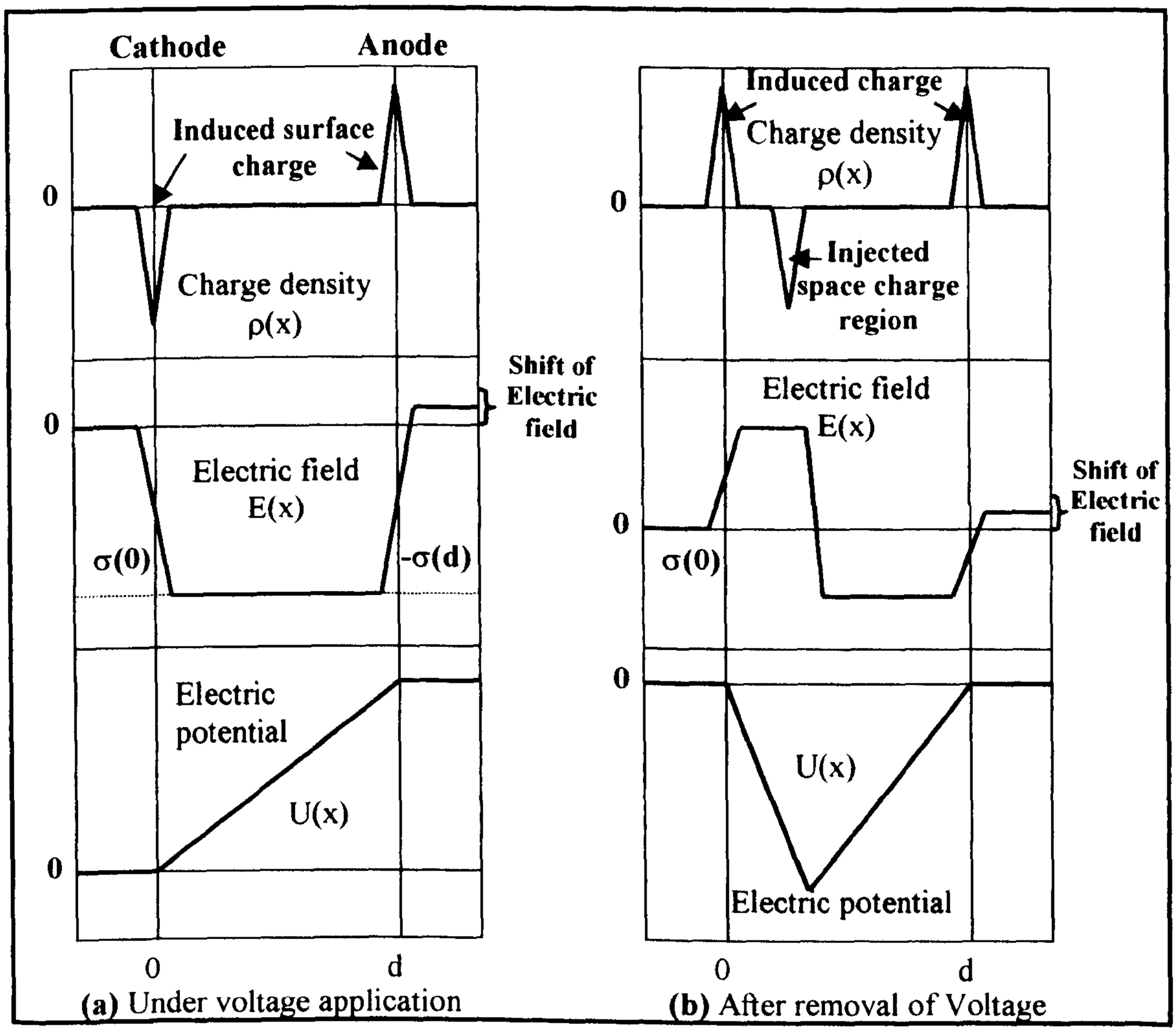

Figure IV-5: Schematic representation of charge density, electric field and electric potential recorded by the PEA method **(a)** During voltage application, **(b)** After short circuit in the case that a net space charge region has been built up

In the case of the signal originating on the top electrode the modification of the pulse during propagation of the acoustic wave through the sample should be taken into account. It was found lately [10] that the broadening effect on the signal travelling in the sample is due to scattering rather than an absorption or a dispersion of the acoustic wave. Once this is done the integration of the area below the peak usually gives correct results for the surface charge density.

The electric field $E(x)$ and the Voltage $V(x)$ are calculated by integration of the charge density, equation IV.1 and IV.2. In the absence of space charge the internal electric field is constant whereas the potential increases linearly.

The electric field should be zero on the electrodes. Experimentally it has been observed that due to a mismatch of acoustic impedance between the sample and the electrode the values of $E(x)$ can be slightly different from zero and then some corrections are necessary in the software for the calculation.

IV.1.2- Short-circuited configuration

A schematic representation of the signal obtained after short circuit, for a sample containing a negative space charge region in the bulk is shown in figure IV-5.b. This time two positive peaks are observed at the electrode/sample interface and are termed induced charges (figure IV-5.b). A negative peak is localised in the negative space charge region. The electric field changes sign and goes through zero in the region of the SC. In the same region there is a change in the slope of the potential. As expected in absence of voltage application the potential returns to zero at the electrodes. The only way to obtain an accurate charge distribution profile in the sample is by using the technique of calibration [13].

IV.2- Calibration of the system

It is not always possible to use the material under investigation to do the calibration because in several cases the signal is unstable. This may be observed when internal charges appear easily after the voltage has been applied or when the initial accumulated charge stays for a long time after the end of the excitation [10]. That is why very often the reference sample is different from the one studied. The reference signal must be recorded with caution since it is used for the calibration process.

The calibration carried out by using the reference signal obtained by the measurement from a material different from the one under investigation has been shown to give good results. The calibration consists in the determination of the interface charge due to the application of a dc voltage V_{dc} which does not produce SC. Actually the output signal recorded is likely to be independent of the material because it is caused by the electrostatic force generated at the interface (electrode/sample). The only parameters used are the sample thickness and sound velocity.

The signals associated with each electrode are similar in shape, magnitude and width as reported by Alison [13]. The dispersion in the acoustic pulse in the material is then found to be negligible.

It has been also observed that the difference in the acoustic impedance of polymers dielectrics is usually small enough to be neglected and then no correction is necessary to be carried out concerning that parameter [10].

In the present case the calibration was carried out by using a piece of PMMA. Its relative permittivity is 2.46, the sample sound velocity is taken as 2750m/s, the sample used was 1mm thick with an acoustic factor of 1 under a pulse voltage of 600V. PMMA has been adopted since it does not significantly attenuate or distort the acoustic wave during the propagation. Besides the accumulation of internal SC is not observed in the condition used for the calibration. It seems then to be an ideal material to use for the reference signal for the calibration [10]. Therefore, the calibration of the instrument response needs to be determined once and not for each sample. To do so, a voltage is applied between the electrodes in addition to the pulse voltage. The charge signals recorded are only due to surface charge on the electrodes.

This calibration can be performed only if the system gives a linear response. Several methods have been analysed. The methods in use are the naive time domain technique; the Philips and Twoney method and the fast Fourier transformed that is most of the time adopted [13].

It has been shown [5] that in order to obtain the charge distribution $\rho(x)$ it is necessary to divide $V_s(f)$ the output signal voltage of the sample by $V_{s1}(f)$. $V_{s1}(f)$ is the output signal voltage obtained from an impulse pressure generated by a sheet of charges. To obtain this signal it is necessary to apply a dc voltage on the sample having no accumulated charges such as PMMA. The sheet charge is the layer that is built at the surface of each electrode. Only one value is necessary, that is why it is

usually the signal coming from the layer of charge appearing at the bottom electrode that is used. It is the signal that originates closest to the detector and hence it is likely to suffer least from any pulse shape distortion.

Once the voltage ratio is calculated, $\rho(x)$ can be calculated by one of several integration and Fourier transformations [5]. This technique was found to be an important step to reach accurate charge distribution profiles. It will be performed here even though it has been reported that when a thin polymer transducer with an extremely wide frequency range was used together with a short electric pulse calibration could be avoided [4].

IV.3- External current measurements

In the system used it is possible to measure simultaneously the distribution of the SC in the sample and the external current. The two measurements are not obtained from the same region of the sample [12], however, it is considered that the SC distribution is the same in both regions.

The total current measured in the external circuit is converted to current density by dividing by the electrode area. The total current in the external circuit is given by the sum of the conduction current $J_c(x,t)$ and the displacement current $d[\varepsilon_0\varepsilon_r(x,t)E(x,t)]/dt$. In this form, the displacement current includes the effect of the relaxation of molecular dipoles as well as the evolution of the space charge distribution. If the contribution of the molecular dipoles can be assumed to have relaxed by the minimum time of the measurements ($\approx$ 5s) then:

$$J_{total} = J_c(x,t) + \varepsilon_0\varepsilon_r \frac{dE(x,t)}{dt} \qquad \text{(IV.3)}$$

Since J_{total} is accessible by measurement and the variation of the electric field calculated from the PEA signal, it is possible to access the values of the conduction current at a particular position. Because of current continuity $J_c(x,t)$ will vary with position and time if $E(x,t)$ does.

It should be noted that in many cases the relaxation of molecular dipoles will not be complete by 5s, in which case the more exact form for the displacement current should be used. In fact, it has been mentioned that the measurement of charging/discharging currents with a better time resolution than 5 seconds is often used to obtain the dielectric response.

V- Experimental results

V.1- Charge profile in plane sample configuration

Various parameters have been tested among them the polarity of the applied voltage in addition to the amplitude and voltage duration. Since the behaviour of the material appears different below and above its T_g the investigations and presentation of the results will be split in two parts; above and below T_g.

V.1.1- Analysis below T_g

As it is convenient to work at room temperature the first experiments to check the various effects concerning the voltage application has been carried out below the glass transition.

V.1.1.1- Shape of the signal

PEA measurements carried out on the sample by using only the pulse is expected to give a flat response since there should be no charges or dipolar orientation before the application of the external voltage. Actually, when only the pulse is applied peaks at each electrode are detected and assimilated to the surface electrostriction force. This phenomenon is a shrinking effect produced as a response of the pulse. In reality because these signals are rather small ($<0.23 C/m^{-3}$) they can be neglected.

During voltage application, the charge density signal detected depends on the polarization voltage. The first signal detected, from the left to the right, corresponds to the bottom electrode side since it is closer to the detector, whereas the second signal corresponds to the top electrode side response (figure IV-6.a). If the top electrode is the anode and the bottom electrode the cathode, then a negative peak and positive peak are respectively detected at the expected position of each electrode/material interface. There is no signal in between. This measurement is convenient to check the position of the sample and the interfaces.

After voltage removal, two peaks of opposite polarity are detected on the left side of the figure associated with the bottom electrode/sample interface. The signal from the top side of the sample seems to be less clear (on the right) and this can be explained by the dispersion of the acoustic wave in the bulk. In most of the cases the signal located close to the bottom electrode is sharper. That is why, in many cases the

sample was reversed to check the response of the sample from both sides by the analysis of the signal on the left only. At the bottom electrode (cathode during voltage application) a positive peak followed by a negative peak is detected. A positive peak only is observed on the top electrode side, without any signal in between. However, after reversal of the sample both positive and negative peaks were observed at this interface, see figure IV-7.b, that had previously been overlaid due to dispersion and the limited spatial resolution as previously discussed.

In reality, it is difficult to determine the real position of the electrode/material interface. Since the detection system is built to obtain a direct reading of the position of the space charges only one spatial dimension, the thickness of the sample is estimated and reported in each figure. The horizontal axis in the figures showing the signal actually represents time (ns). In order to convert it to a distance it is necessary to multiply the scale by the acoustic sound velocity in the material.

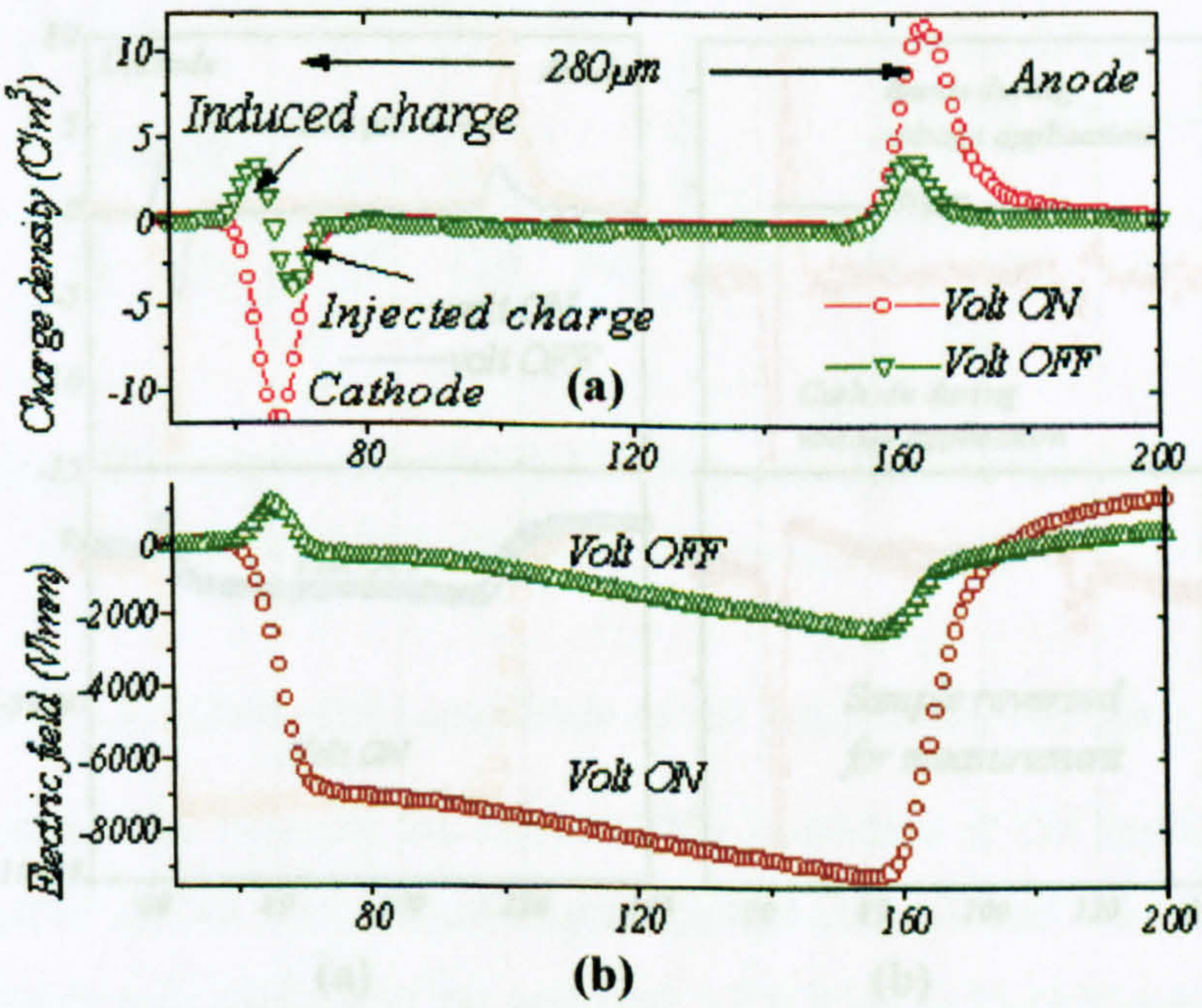

Figure IV-6: During polarization and after the removal of the polarization voltage **(a)** Charge density, **(b)** Electric field

The electric field showed strong distortions at both sample edges after voltage removal (figure IV-6.b). During voltage application, the field should be constant between the electrodes. The actual slope observed in the curve is associated with the dispersion of the detected signal in the bulk since the electric field is calculated from the charge density detected.

V.1.1.2- Effect of the polarity

It has been decided to test the effect of the polarity of the voltage. To do so, two samples of 270µm, from the same original large sheet, have been used.

On one sample a polarization voltage of +2.7kV, equivalent to a field of +10kV/mm, was applied to the top electrode for 1h at 298K. After voltage removal, the signal from the bottom electrode reveals a positive peak followed by a negative peak (figure IV-7.a). The signal coming from the top electrode appears not really well defined. To check the response coming from this side, the sample has been reversed. After having reversed the sample, the detected signal is also reversed (figure IV-7.b). This demonstrates that a symmetrical effect is produced on the sample by voltage application. In fact, after reversing the sample the signal on the right appear also better defined showing two small non-symmetrical peaks of opposite polarity.

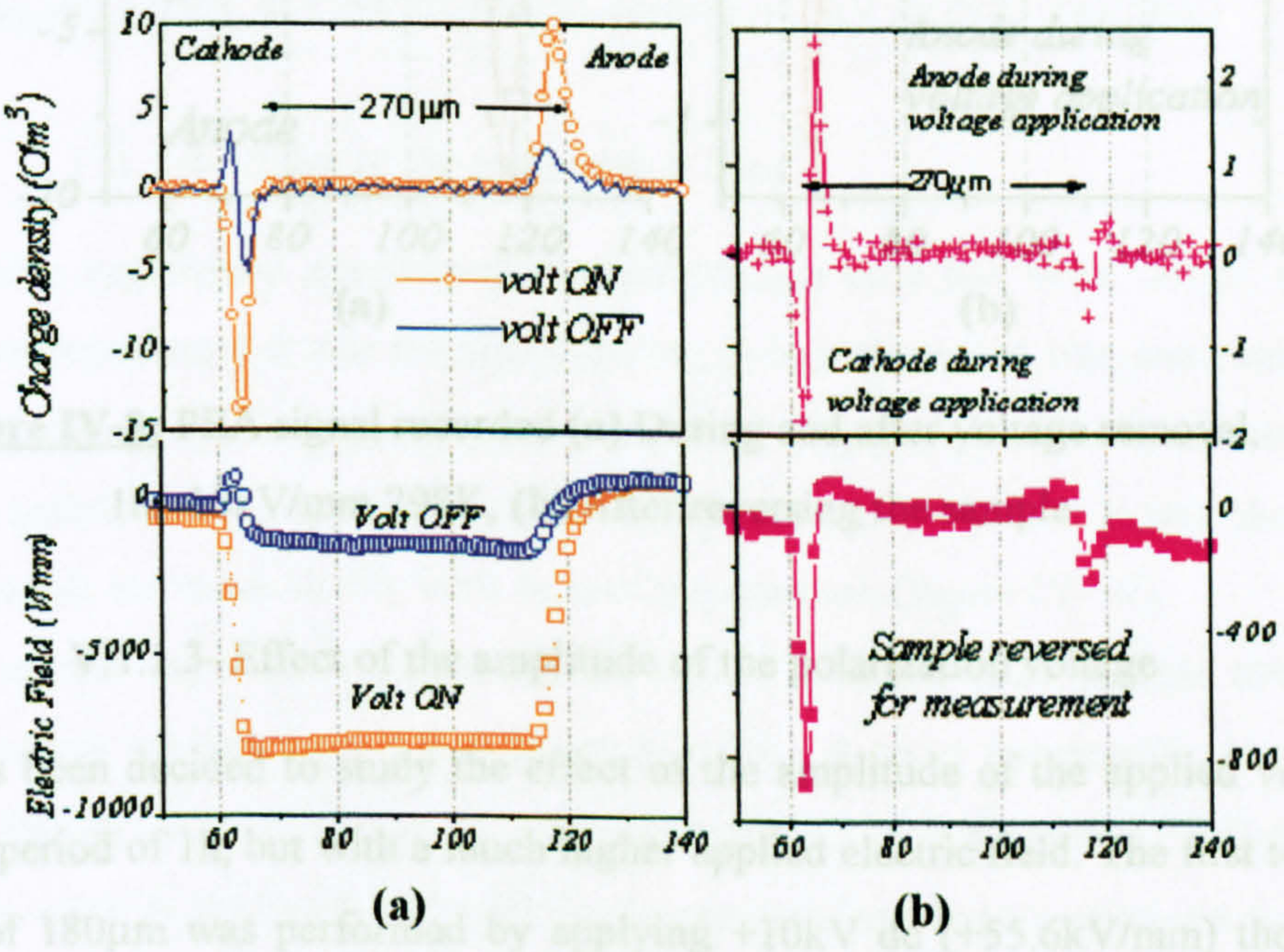

Figure IV-7: Charge density and electric field **(a)** During and after removal of the voltage 1h, +10kV/mm, **(b)** Reversed sample at 298K

The second set of experiments consisted in reversing the polarity of the voltage applied for the stress. The second sample has been polarised at the same temperature for 1h at –2.7kV (-10kV/mm). The same measurements have been carried out after the removal of the voltage. The resulting signals are inverse of figure IV-7. From the

bottom electrode side (anode during voltage application), a negative peak followed by a positive peak is recorded after voltage removal (figure IV-8.a). The complete signal from the cathode side was observed only after reversing the sample and showed a positive and a negative peak on the left hand side (figure IV-8.b).

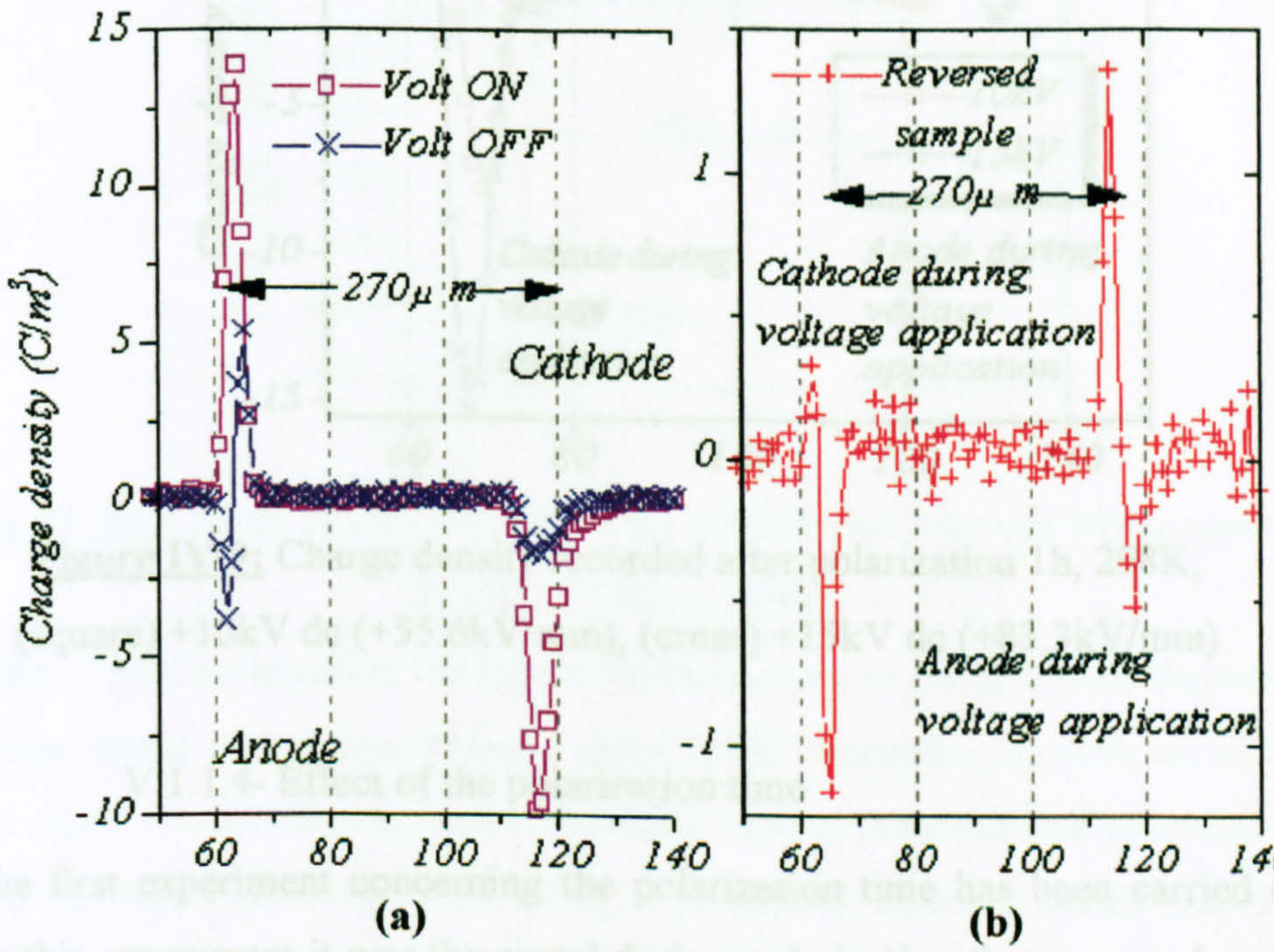

Figure IV-8: PEA signal recorded **(a)** During and after voltage removal, 1h –10kV/mm 298K, **(b)** After reversing the sample

V.1.1.3- Effect of the amplitude of the polarization voltage

It has been decided to study the effect of the amplitude of the applied voltage for a short period of 1h, but with a much higher applied electric field. The first test on a sample of 180µm was performed by applying +10kV dc (+55.6kV/mm) then the voltage was increased to +15kV dc (83.3kV/mm). The application of the voltage was carried out by using two polished brass electrodes (23mm diameter) since the PEA system was not built for such high voltage.

In both cases, the signal was recorded after removal of the voltage. As seen in figure IV-9, the effect of increasing the polarization voltage leads to a significant enhancement in the charge density detected immediately after the removal of the electrical stress.

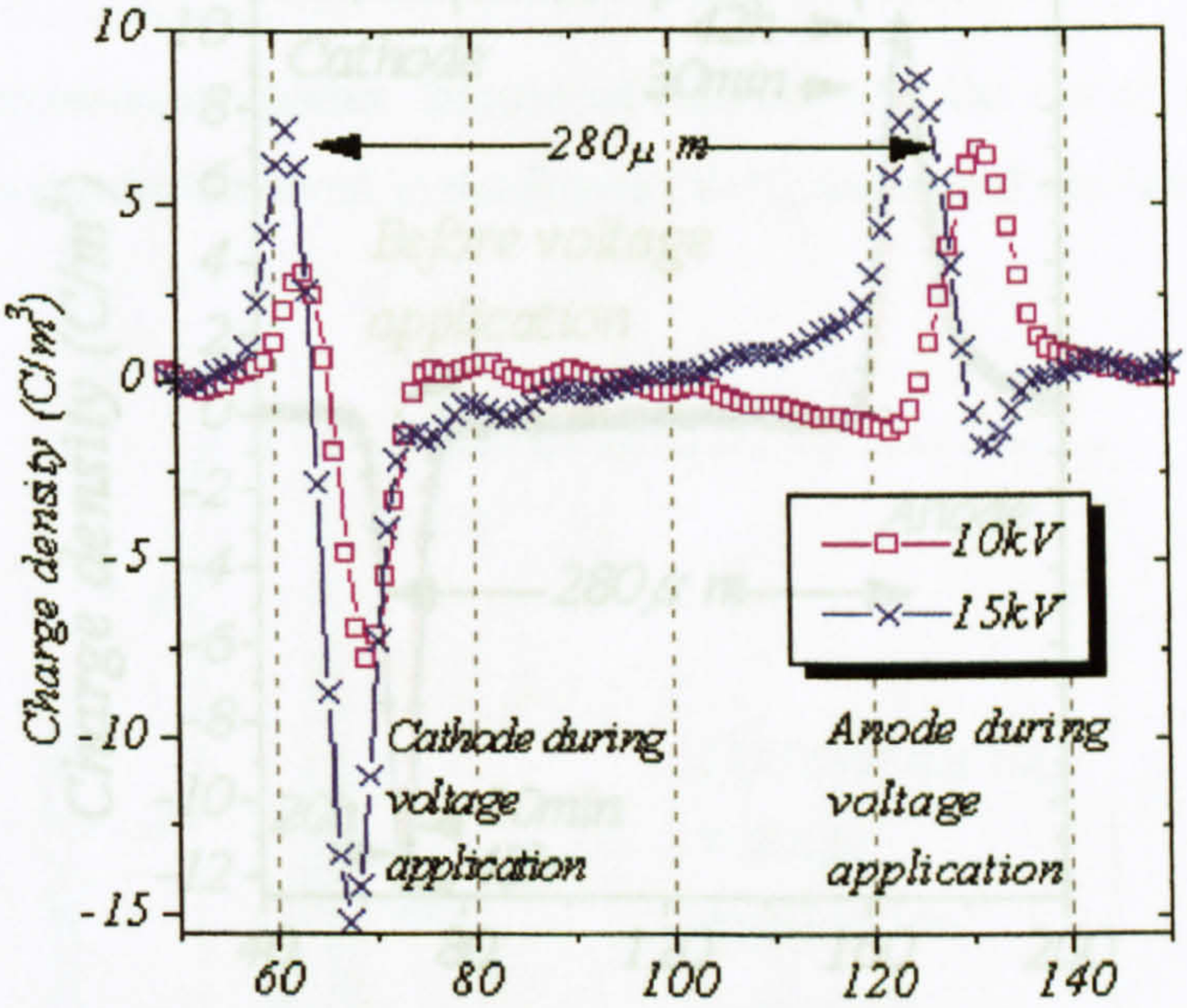

Figure IV-9: Charge density recorded after polarization 1h, 298K, (square) +10kV dc (+55.6kV/mm), (cross) +15kV dc (+83.3kV/mm)

V.1.1.4- Effect of the polarization time

The first experiment concerning the polarization time has been carried out at 308k. In this experiment it was the signal during polarization that was analysed. The voltage (+2kV) was applied for 42h on a sample of 180μm thick. The measurements were taken before voltage application then at different time intervals. It was observed that the signal is increases slowly with time of polarization (figure IV-10).

The second experiment concerned the signal recorded after voltage removal. The voltage was applied from a few hours to weeks at room temperature to a film sample of 280μm by using the set of brass electrodes (23mm diameter). The voltage applied was +2kV (+7kV/mm). Actually measurements have been carried out on three samples of the same original sheet. The first measurement was taken after 15h under stress; the second one after 1 week and the last one after 3 weeks. The polarization was performed at about 293K. All the measurements were recorded after voltage removal and compared.

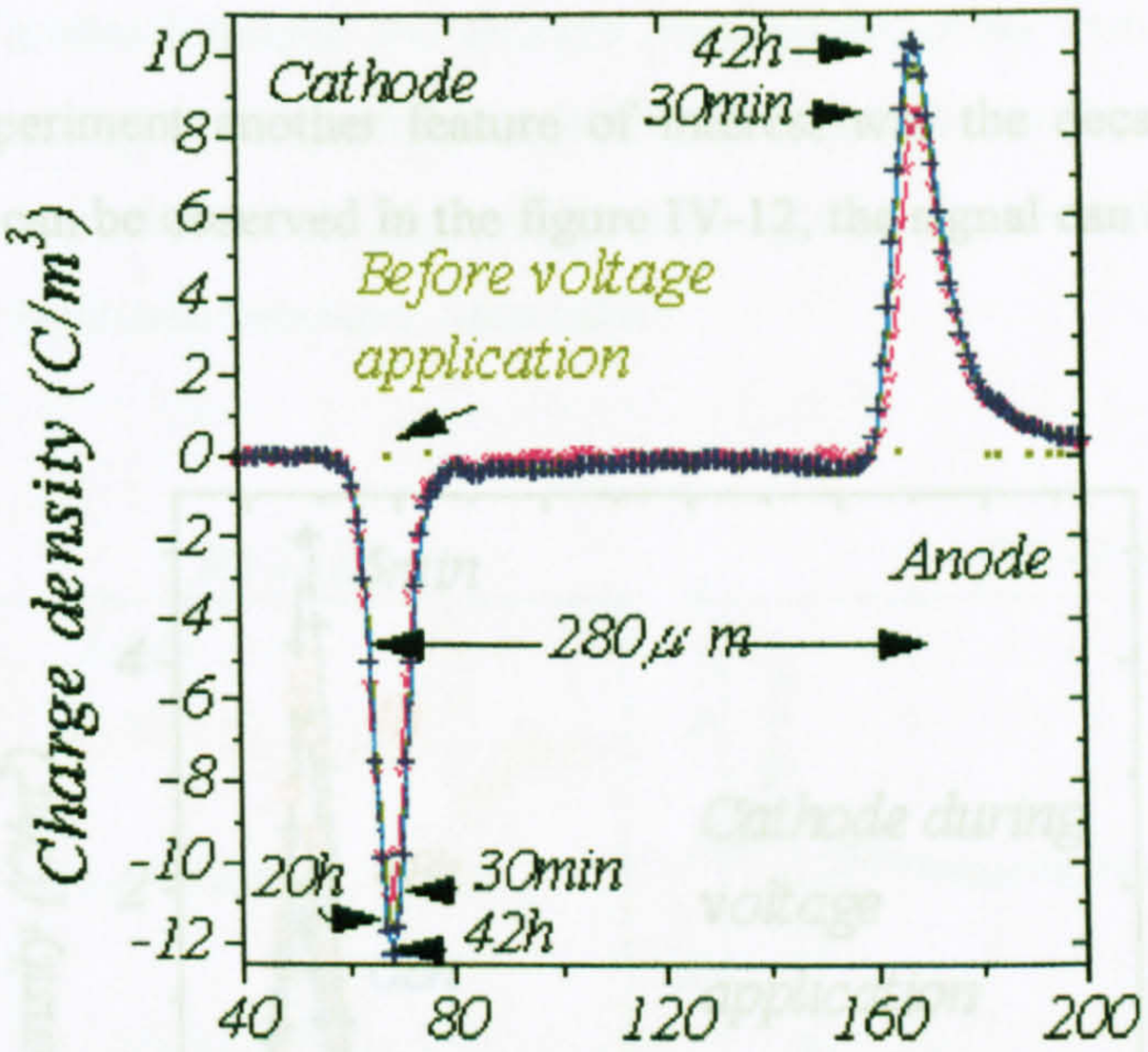

Figure IV-10: Charge density profile during polarization between 30min and 42h, 2kV (+7kV/mm), 308k

After 15h of polarization the signal recorded close to the electrode shows nearly symmetrical peaks of opposite polarity close to the electrodes on both sides (figure IV-11.a). After 1 week of polarization the same kind of response was recorded but in this case the peaks were far from being symmetrical. After 3 weeks polarization (figure IV-11.b), the amplitude of the signal recorded a few minutes after the removal of the voltage was much bigger than after 1 week of polarization.

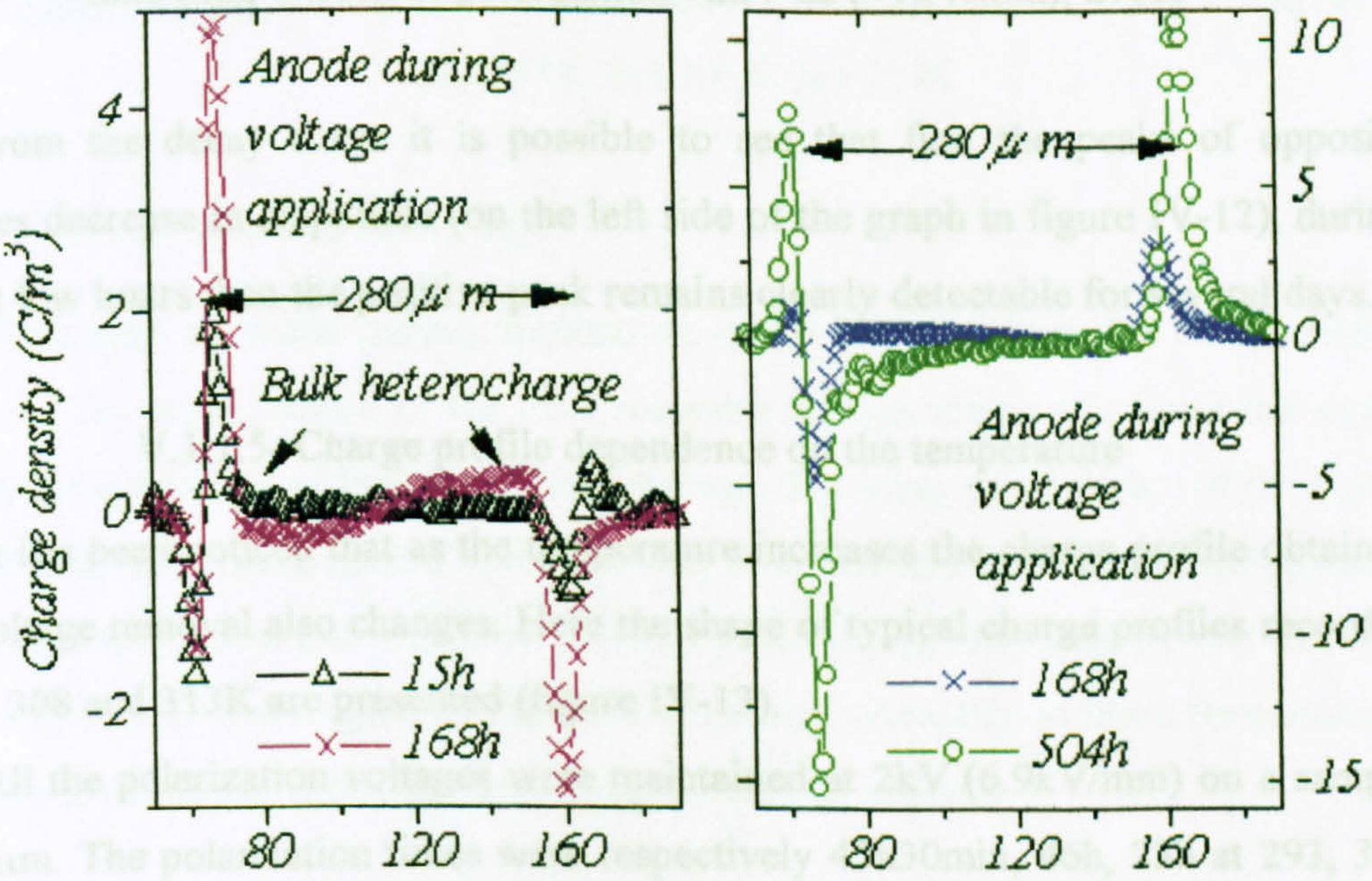

Figure IV-11: Comparison of charge density recorded at volt-off 293k

(a) 15h and 1 week, **(b)** 1 and 3 weeks of polarization,+2kV (+7kV/mm)

From this experiment another feature of interest was the decay time of the recorded signal. As can be observed in the figure IV-12, the signal can last for several hours.

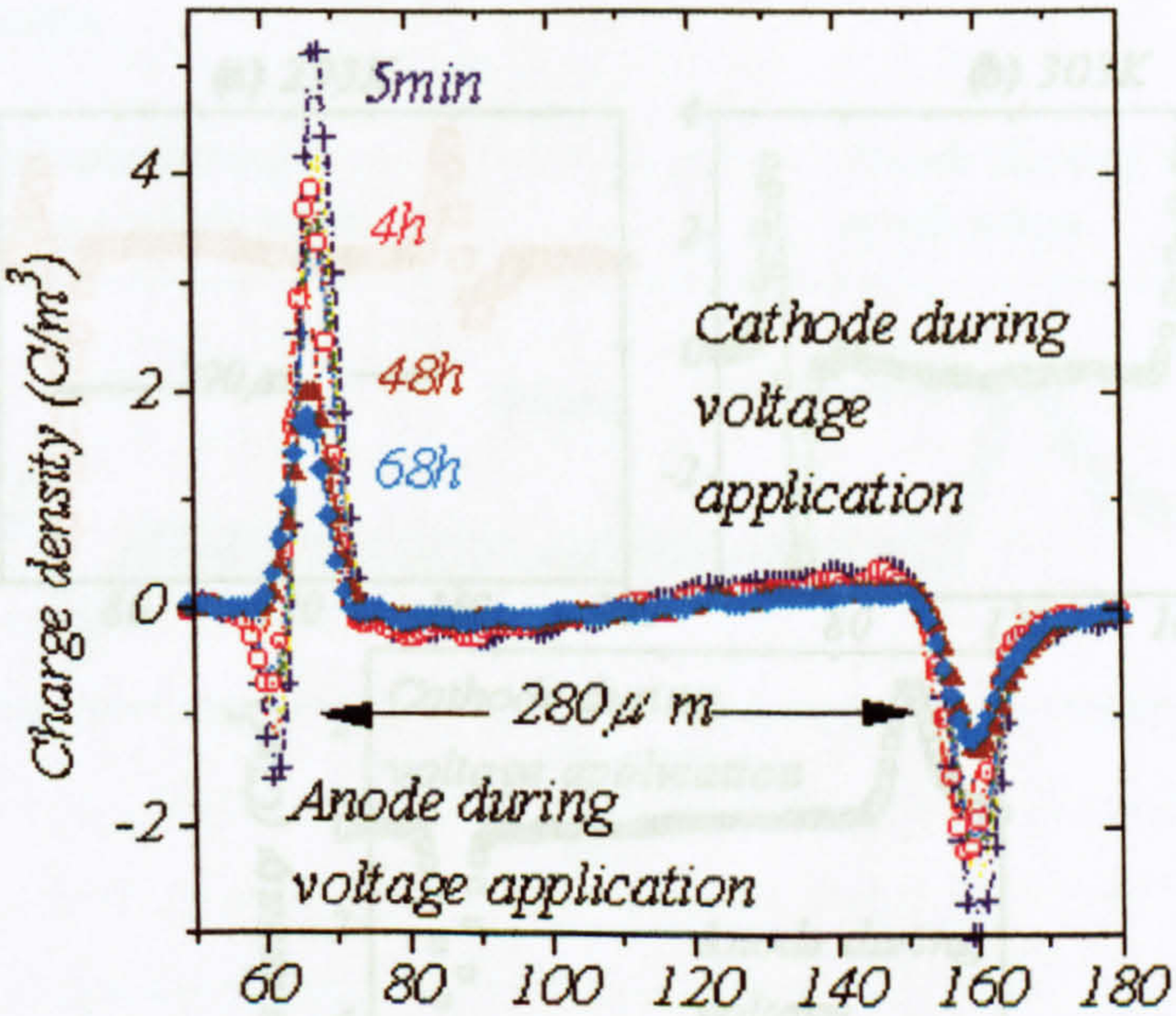

Figure IV-12: Space charge decay recorded after the removal of the voltage following 1 week of polarization +2kV dc (+7kV/mm), 293K

From the decay curve it is possible to see that first the peaks of opposite polarities decrease in amplitude (on the left side of the graph in figure IV-12), during the first few hours then the positive peak remains clearly detectable for several days.

V.1.1.5- Charge profile dependence on the temperature

It has been noticed that as the temperature increases the charge profile obtained after voltage removal also changes. Here the shape of typical charge profiles recorded at 293, 308 and 313K are presented (figure IV-13).

All the polarization voltages were maintained at 2kV (6.9kV/mm) on a sample of 290μm. The polarization times were respectively 45h30min, 46h, 23h at 293, 303 and 313K.

The main difference between the charges profiles on going from 293 to 303K comes from the symmetry in the peaks that is clearly observed on the left side of the graph as the temperature increases. However, as the glass transition is approaches a single peak on each electrode becomes detectable.

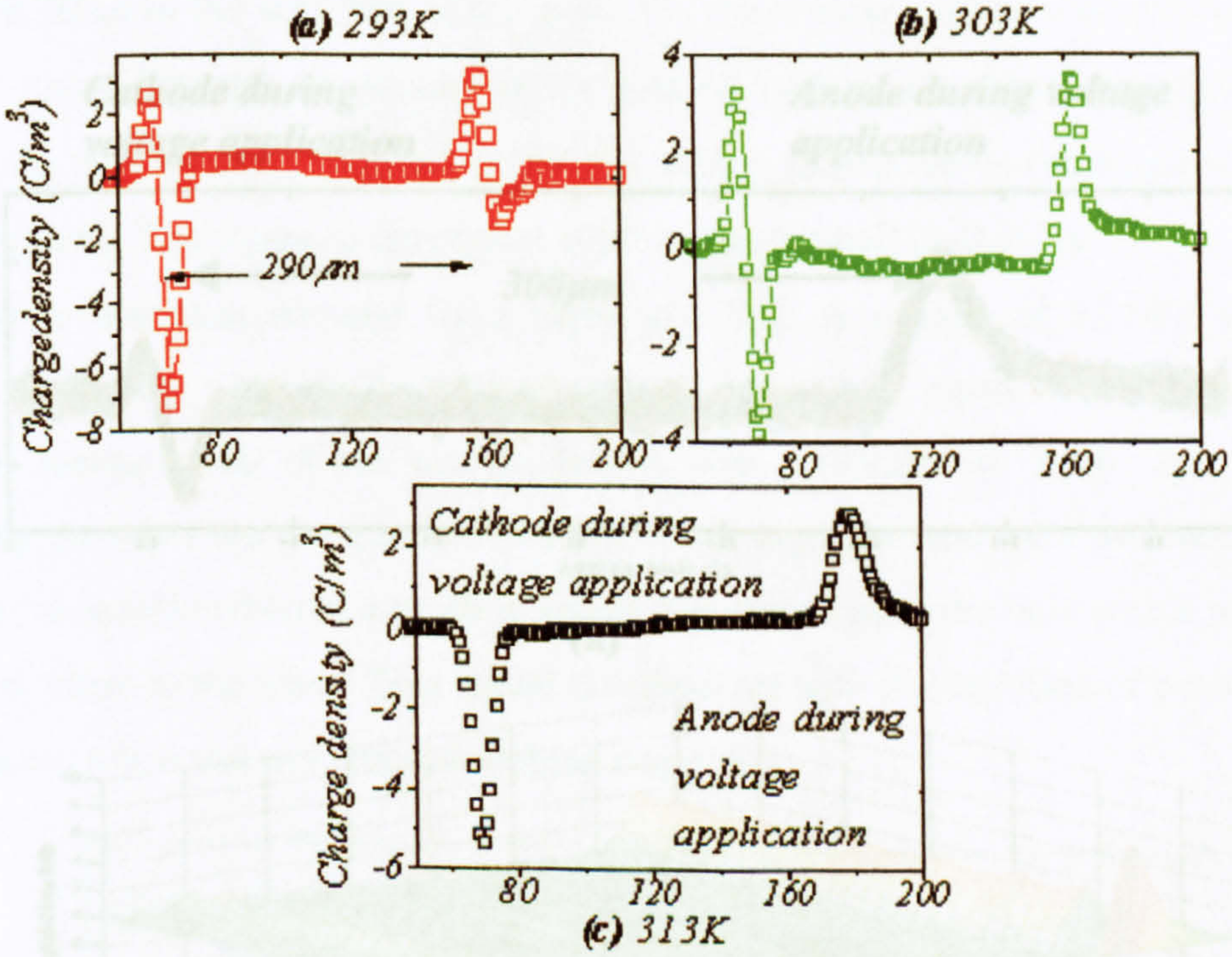

Figure IV-13: Charge profile after voltage removal (+2kV, +6.9kV/mm) at **(a)** 293K, **(b)** 303K, **(c)** 313K

V.1.2- Analysis above Tg

The signal recorded during application of the voltage does not really evolve with time. The main feature of the PEA response at high temperature was the signal recorded after removal of the polarization voltage. By using a fast record of the signal after removal of the polarization voltage it was observed that the decay of the signal is really very rapid. During the first few seconds peaks of opposite polarity are recorded on the left side then a single peak remains dominant. Actually at these temperatures the decay of the signal is occurs in the range of several seconds.

Figure IV-14 represents the measurement taken on a sample after voltage removal. The polarization +2kV was held for 42h at 323K then removed at that temperature. The decay was followed by taking a record of the data every second for 30s, then the sampling time was increased to 10s. Actually, after the first few seconds a single peak remains dominant on both side of the sample and as before it is quite stable for several hours.

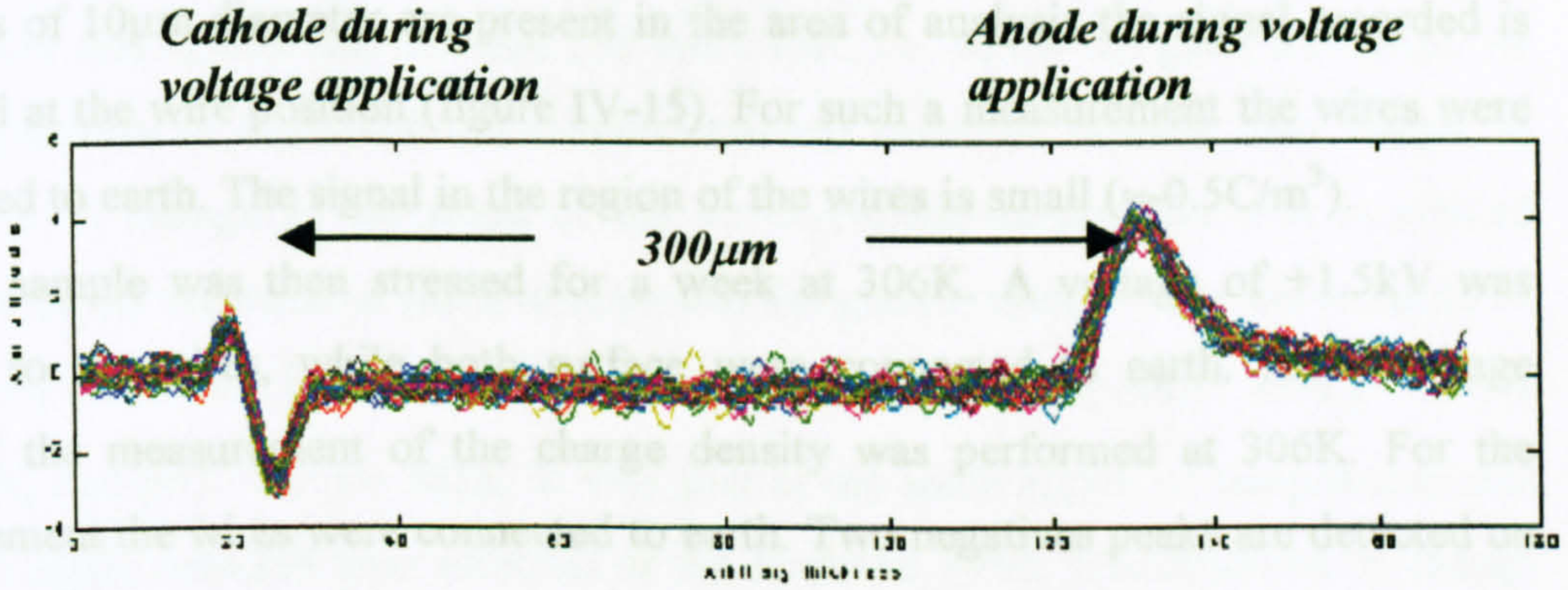

(a)

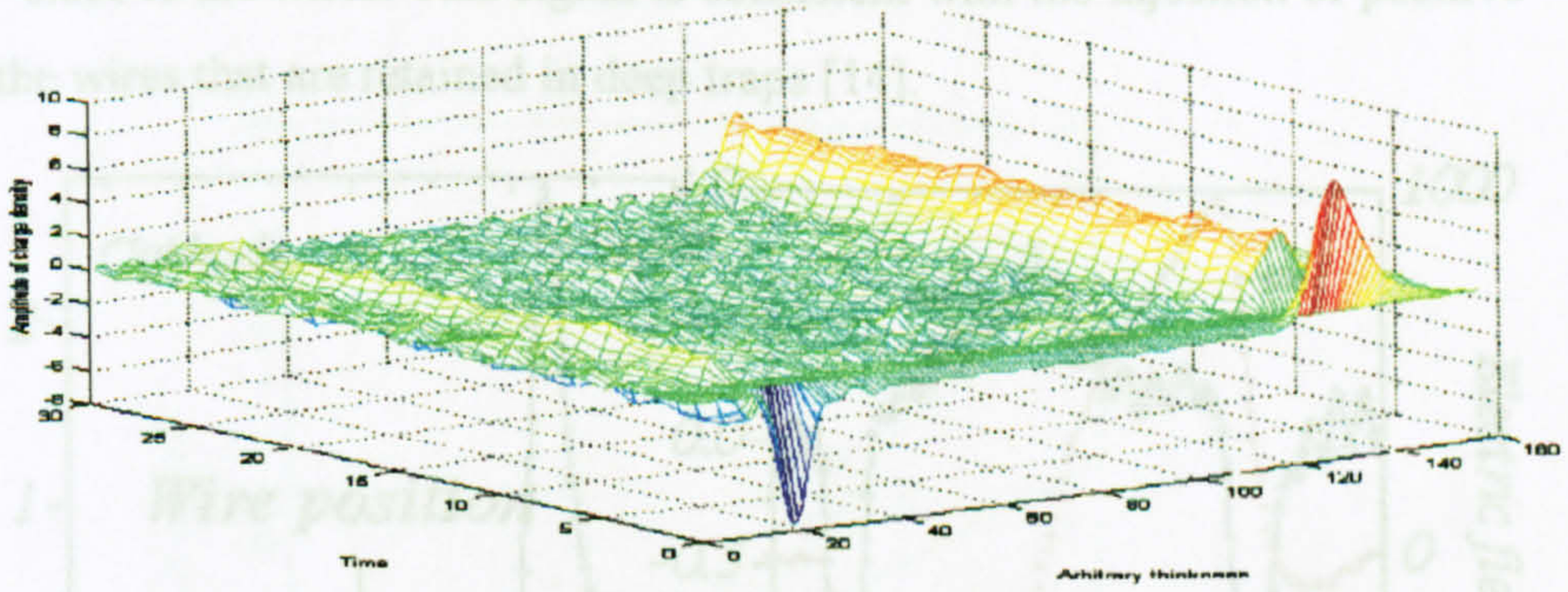

(b) Three dimensional plot

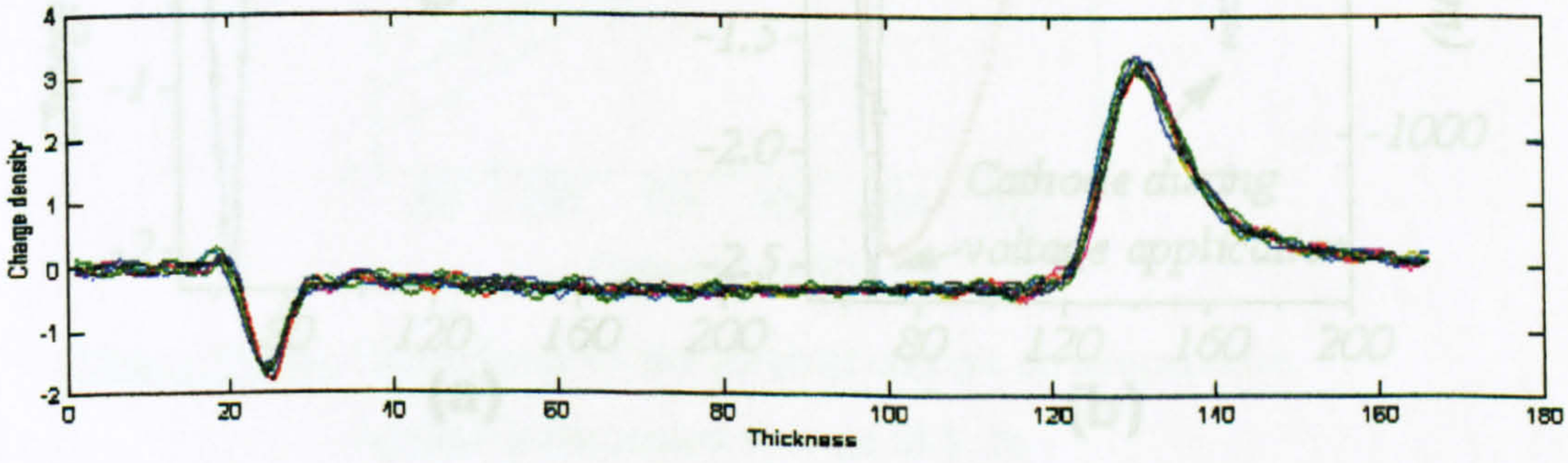

(c)

Figure IV-14: Decay after 42h under voltage +2kV dc (6.7kV/mm) 323K

(a) (b) 0-30s **(c)** 30-150s

V.2- Charge profile in divergent field configuration

Measurements have also been carried out on samples with wires. The first measurement was carried out before application of any voltage to the wires. Using a sample with a single wire of 50μm diameter and applying a voltage of +0.67kV dc across the thickness on top that of the pulse, shows no observable difference to the measurement taken in the area free of the wire. On the contrary when a sample with 13 wires of 10μm diameter are present in the area of analysis the signal recorded is distorted at the wire position (figure IV-15). For such a measurement the wires were connected to earth. The signal in the region of the wires is small ($\approx$-0.5C/m^3).

A sample was then stressed for a week at 306K. A voltage of +1.5kV was applied to the wires, while both surface were connected to earth. After voltage removal the measurement of the charge density was performed at 306K. For the measurement the wires were connected to earth. Two negatives peaks are detected on both side of the sample whereas a positive signal was observed in the bulk with a peak of $\approx$0.75C/m^3 close to the wires. This signal is consistent with the injection of positive charge from the wires that are retained in deep traps [14].

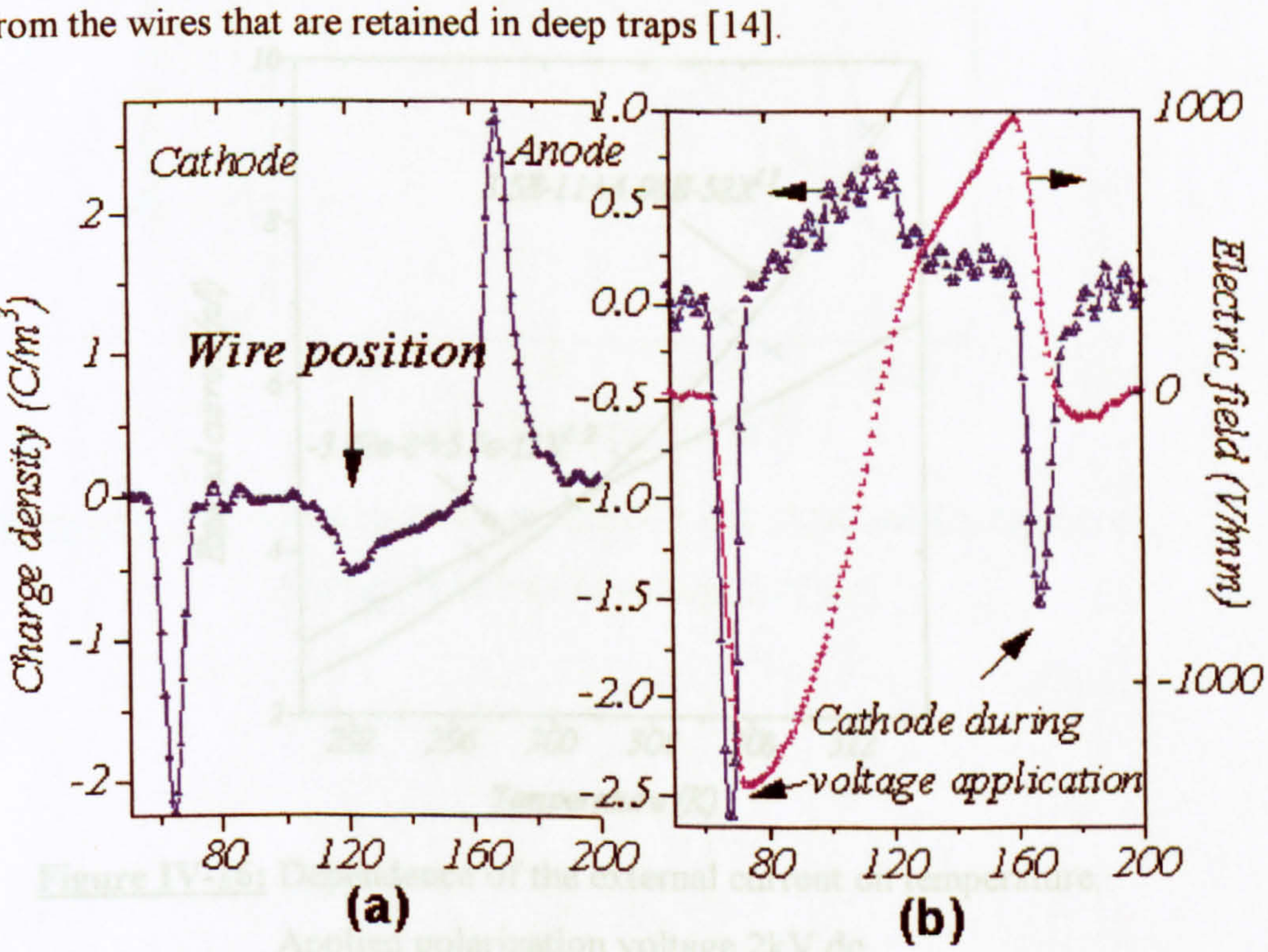

Figure IV-15: PEA response from wired sample **(a)** Pulse and +0.67kV applied between both surfaces, **(b)** Pulse only after 1 week of voltage application +2kV dc between the wires and both surfaces

V.3- External current measurements

The external current has been studied in order to collect more information about the behaviour of the charges as the temperature is increased. The sample (280μm) used was polarised by a voltage of 2kV dc (+7kV/mm). Values of external current recorded at the beginning (6s) of the application are reported figure IV-16. The experiment was carried out between 293 and 313K, i.e. below the glass transition. As the temperature is increased the external current detected become also higher in amplitude. A change in the slope of the curve current-temperature plot is noticed above 303K, as the material starts to approach the glass transition. The curve could be fitted by a cross-over between two power laws of type: $y = A + BX^p$ with p=1.2 for T< 303K, and p=17 for T> 303K. It was also in the same region of temperature that the PEA signal detected after removal of the electrical stress was observed to change in shape.

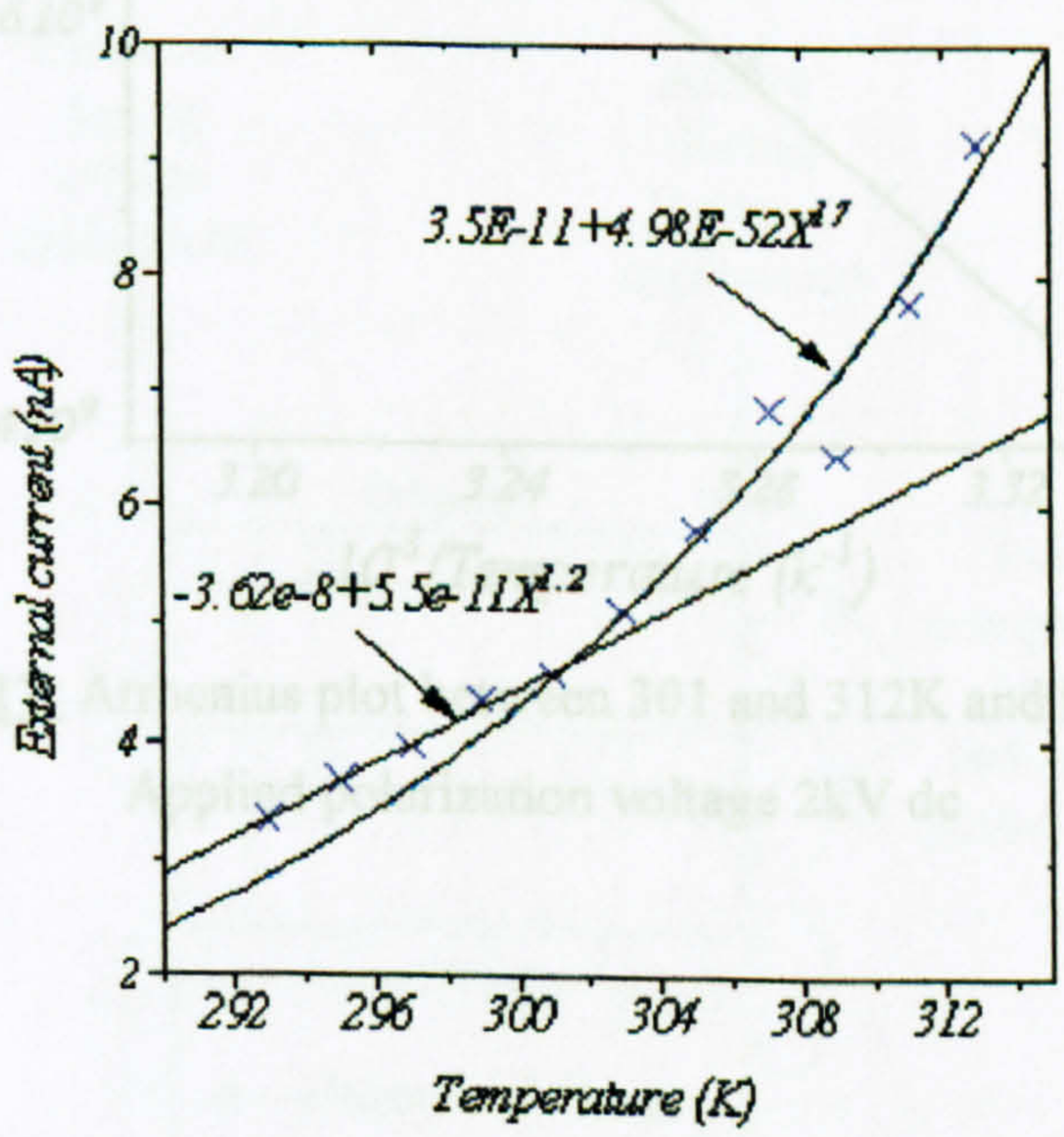

Figure IV-16: Dependence of the external current on temperature.
Applied polarization voltage 2kV dc

Above 300K the recorded current was found to increase such as a thermally activated current. The representation as an Arrhenius plot is given figure IV-17. The fitting curve is described by the equation $I = I_0 \exp(-\Delta_c / kT)$ giving access to the parameters $\Delta_c \cong 0.5$eV. This initial transient current magnitude is proportional to the sum of all the polarization contributions, i.e. to the static charge on the capacitor.

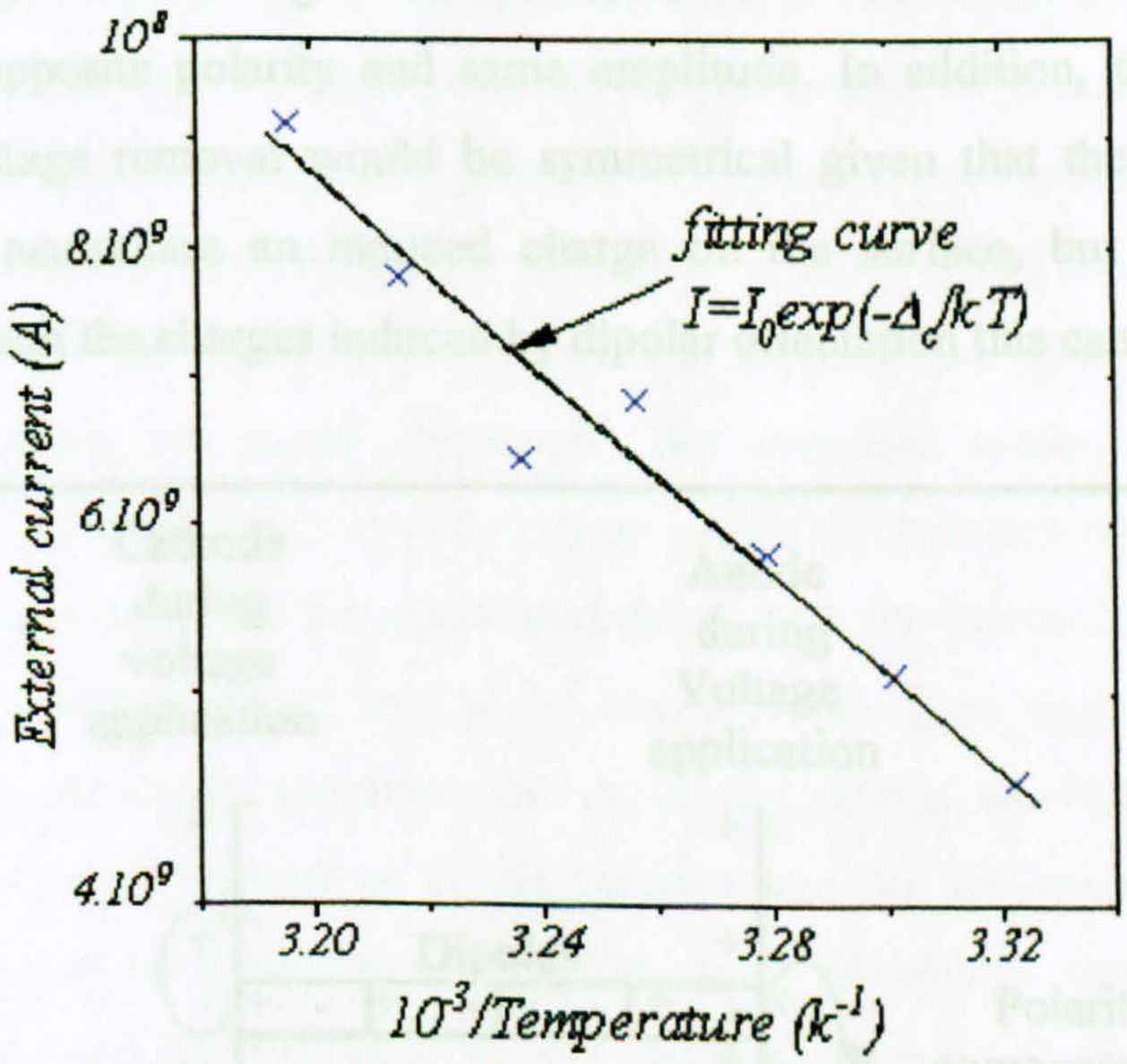

Figure IV-17: Arrhenius plot between 301 and 312K and fitting curve. Applied polarization voltage 2kV dc

VI- Discussion

VI.1- Effect of temperature

Below the glass transition, the PEA signal recorded after the removal of the voltage should be due to the addition of the polarization and the SC injection as shown in figure IV-18. The both effects can compensate because injected SC and oriented dipoles induce charges of opposite polarity on the electrodes. In fact, since the epoxy contains dipoles, it is difficult to detect the contribution of just the SC because the relaxation of the dipoles is not instantaneous after voltage removal. Actually, if only the induced charges on the electrodes due to injected SC were present then a symmetrical signal on each electrode would be detected consisting in two peaks of opposite polarity and same amplitude. In addition, the decay of the signal after voltage removal would be symmetrical given that the extraction of a charge carrier neutralises an induced charge on the surface, but because of the compensation with the charges induced by dipolar orientation this cannot be the case.

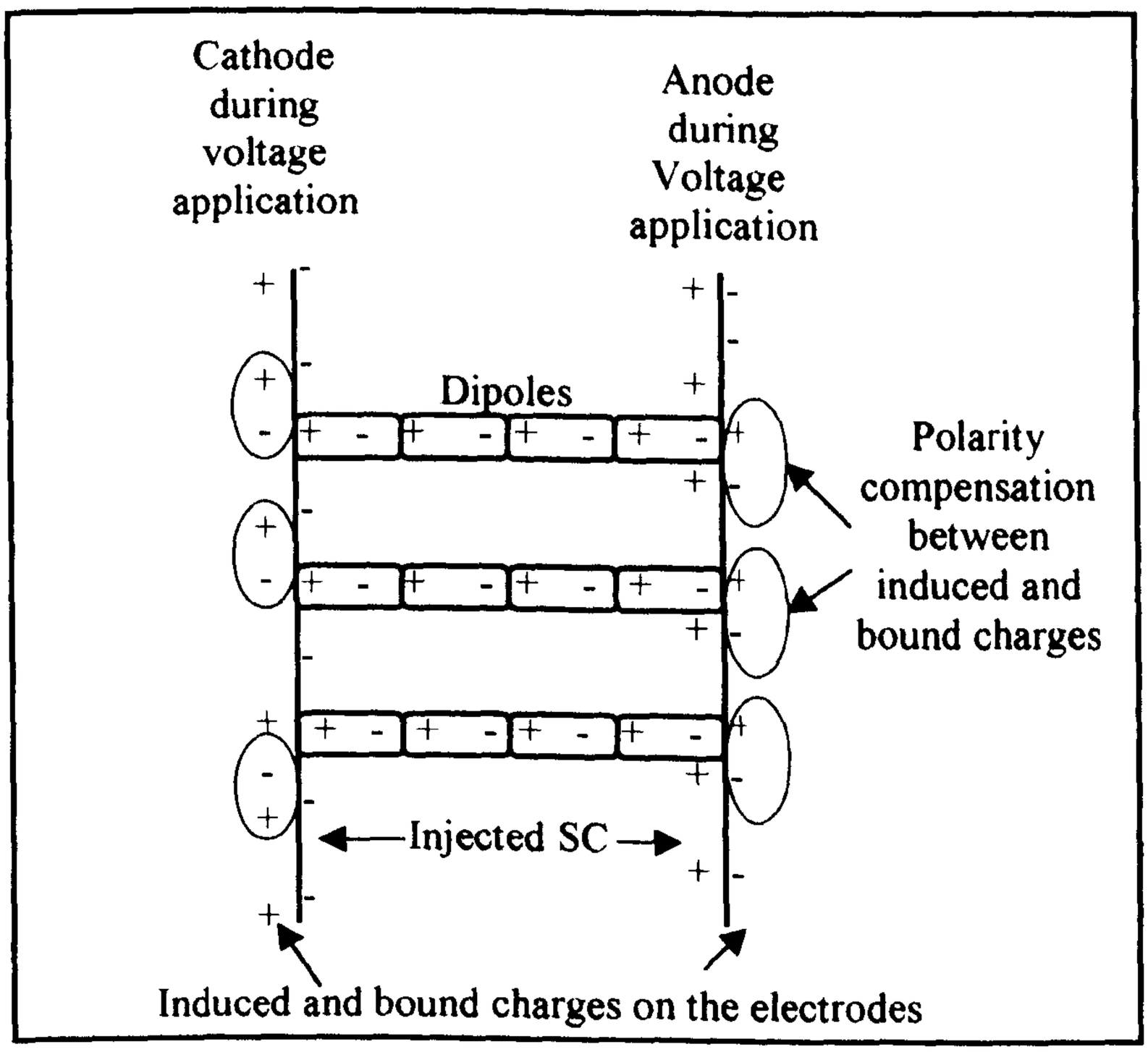

Figure IV-18: Representation of induced charges due to injected charges and bound charges due to dipolar orientation

In most of the cases, the first measurements were taken a few minutes after the removal of the voltage. However, even 5min (300s, 3.3Hz) after the end of the polarization, all the relaxation phenomena have not been completed. It has been observed from dielectric response and external current measurements that some relaxation phenomena occur below $3x10^{-3}$Hz. In particular the dielectric process named A previously, should mainly contribute to the polarization effect observed by PEA measurements. If there were no injected SC, the slow relaxation of the dipoles could be followed by PEA measurements since "bound" induced charges are made free and disappear as the dipoles disorient in the time scale of investigations.

As temperature is increased, the shape of recorded signal after voltage removal changes (figure IV-13). At room temperature the recorded signal is not symmetrical. This tends to be associated with a polarization phenomenon that annuls the effect of the image charge due to the injected charges. With the temperature rise, the relaxation of the dipoles becomes quicker, then around 303K it looks like if the signal due to the SC is dominant in the first few hours then the dipoles that need a longer time to rearrange dominate the signal. However, the principal remark deals with the domination of the signal due the polarization as the temperature surpasses the glass transition. In order to record the signal associated with the injected charge above the glass transition measurements had to be taken on the time scale of seconds and already after 10s the signal was dominated by dipolar effects, see figure IV-14.

Its looks like if one type of dipole remains oriented for several hours or even days whatever the temperature. Below the glass transition, there is a kind of competition between the relaxation of SC and another type of dipole that remains difficult to identify. To explain these phenomena it might be interesting to analyse the compensation effect described for induced SC and bound charges. As soon as the polarization voltage is removed, due to the high field at the electrodes the SC are extracted until the amount of induced charge, i.e. injected SC, and bound charges become equivalent. At that point there is a large attractive field that is created across the bulk compare to the field that made SC to be extracted. This field in the bulk is in the same direction as the applied field (if we consider that homo-charge have been injected). It will therefore maintain the orientation of the bulk polarization, relaxing the cancellation effect due to the bound charge. The removal of the remaining SC requires transport across the bulk of the material and recombination. This can be a very slow process especially below the glass transition. This picture locks the

polarization to the internal field produced by the injected charge that would explain a stabilization in the signal.

In any case, the effect due to SC seems to disappear in a few hours following the removal of the voltage. This could be associated with the depth of injection. In that situation, it shows that charges are injected close to the electrodes and this allows them to be extracted rapidly after the removal of the stress whereas deeper injected charges may remain trapped in the bulk for longer period of time due to the production of a kind of equilibrium with the bound charges.

VI.2- Effect of the polarization time

It has been noticed that as the time of application of the electrical stress is increased (figure IV-10), the amplitude of the signal during voltage application was enhanced. This could be explained by the slow alignment of dipoles that leads to a build up of charges on the electrodes to keep the applied voltage constant. Usually, after a few hours under stress the signal seems to stabilise. The polarization effect becomes dominant as the temperature increases since the alignment of the dipole is made easier as the glass transition is approached.

From experiments in the uniform field configuration, it has been observed that the polarity of the applied stress voltage was not significant and did not lead to noticeable changes. The contribution to the electrode signal from dipole orientation will always be the same whatever the polarity of the voltage. In terms of the SC injection, this means that the injection or extraction of the charge carriers of both polarities during voltage is equivalent. This probably means that charge injection is by tunnelling to local defect states rather than by Schottky mechanism.

When long time polarization (a few days to a few weeks) was carried below the glass transition temperature the amount of SC injected can be seen to increase with the time of voltage application. The rate of increases, however, increases as the polarization time increases beyond 15h, i.e. the signal increases by about 15C.m^{-3} between 15h and 168h, and by about 65 Cm^{-3} between 168h and 504h (figure IV-19). There is also some evidence for bulk ionisation leading up to heterocharge regions next to the injected homocharge layers at the electrode interfaces (figure IV-11). This can be associated with a movement of injected charges across the bulk. This seems to be a really slow process that could be accelerated as the glass transition is reached

since then the dc conduction is facilitated. But, if an heterocharge region is built up this means that charges are accumulating because they remain difficult to extract after crossing the sample (figure IV-9). At low temperature (below RT) a higher field than a few kV might be required to generate the same kind of charge movement.

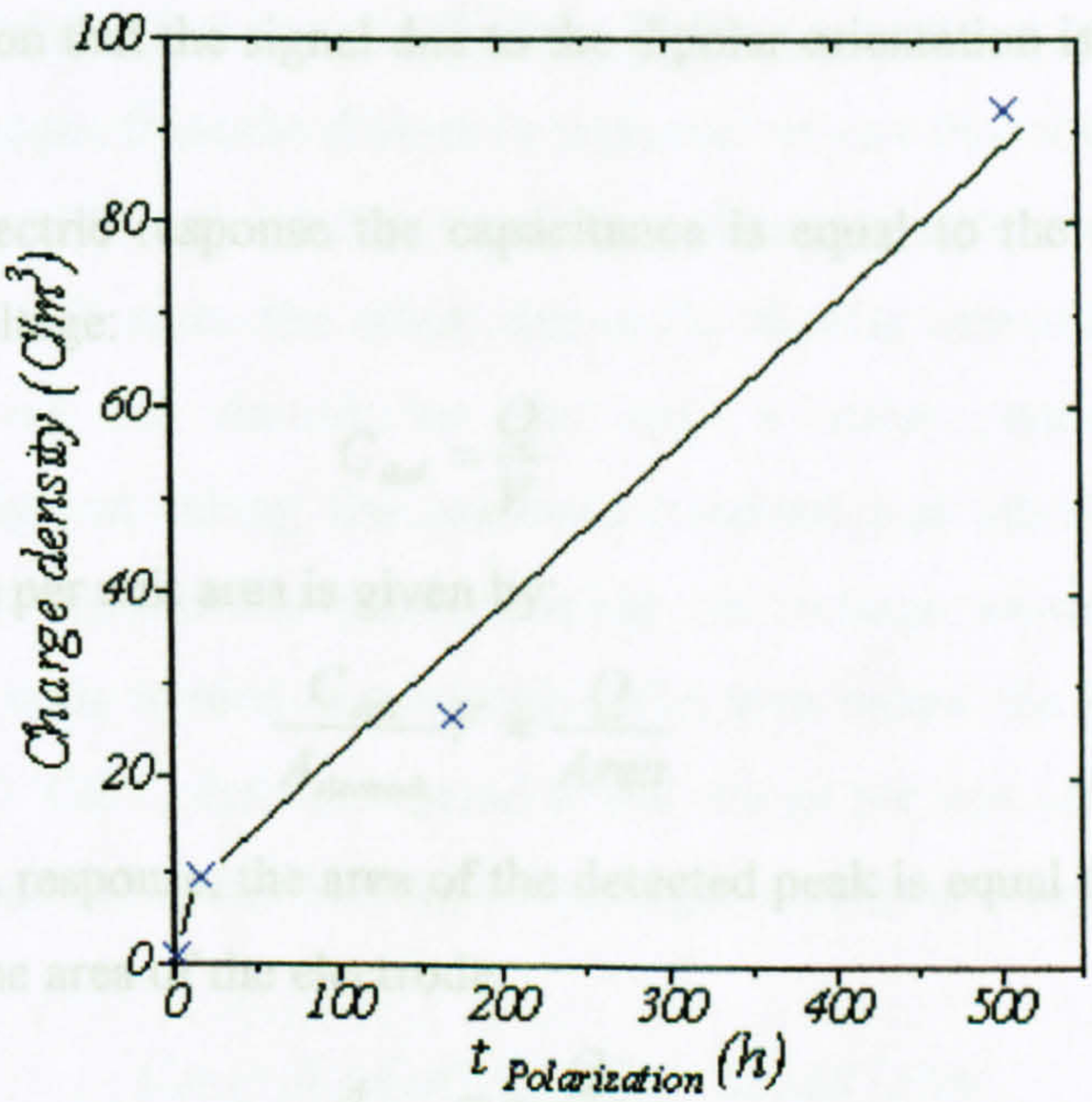

Figure IV-19: Charge density recorded after the end of various period of polarization under +2kV, RT

At 303K both the polarization and SC contribution to the electrode signal after removal of the stress. At this temperature the position of the peak of dielectric process A was estimated to be close to 7.62×10^{-6}Hz from the dielectric spectroscopy. For the PEA measurements the polarization is performed under dc voltage. The polarization time defines the amount of time available for the dipoles to orient in the field and is equivalent to a half-cycle of an ac-voltage. The dipoles associated with process A are in phase with an ac voltage of 7.62×10^{-6}Hz, that corresponds to a half cycle time of about 18h. That means that below 18 hours one half or less of all the dipoles are oriented. This would explain the slow and small increase in the signal during voltage application. The phenomena described above are also valid at other temperatures and are supposed to explain the figure IV-10 that correspond to measurements at the higher temperature T= 308K.

In fact, at the maximum of the loss peak ($f= f_p$) in the dielectric response the real part of the capacitance increases, but the increase is not complete until a frequency $f\cong 0.1 f_p$. This increase corresponds to an increase in the amount of charges built up on the electrode to compensate the alignment of the dipoles. It is then possible to compare the results obtained by the two methods, i.e. dielectric spectroscopy and PEA response, on condition that the signal due to the dipolar orientation is dominant in the PEA response.

From the dielectric response the capacitance is equal to the ratio of induced charge to applied voltage:

$$C_{diel} = \frac{Q}{V} \tag{IV.4}$$

and the charge per unit area is given by:

$$\frac{C_{diel}}{A_{electrode}} V = \frac{Q}{Area} \tag{IV.5}$$

From the PEA response, the area of the detected peak is equal to the ratio of the induced charge to the area of the electrode:

$$A_{peak} = \frac{Q}{A_{electrode}} \tag{IV.6}$$

and the capacitive increment per unit area is:

$$C_{PEA} / A_{electrode} = A_{peak} / V \tag{IV.7}$$

For the dielectric response, it is possible to estimate the increment in capacitance by using the master curve and taking the response at higher temperature where the phenomena is recorded in the measurement frequency-window available. It is important to measure the capacitance increment in order to take into account only the charges that are induced on the electrode for the dipoles of the process A and not all the other shorter time processes.

From the dielectric response the capacitance increment measured for the process A is 2.15×10^{-10}F that gives a capacitance per unit are:

$$C_{diel} = \frac{2.15 x 10^{-10}}{\pi (1.15 x 10^{-2})^2} = 5.17 x 10^{-7} F / m^2$$

The charge increment per unit area from the dielectric measurement per unit area from dielectric measurement is $5.17x10^{-7}X2x10^{3}= 1.03x10^{-3}C/m^{2}$ when the voltage applied V= 2KV.

At 313K the effect due to the dipoles is dominant in the PEA signal. By estimating that the polarization is completed in the time of the experiment and using the calculation of charges from the dielectric response we can do comparative studies. From the PEA response (figure IV-20), the main problem consists in determining the area of the peak at 313K since the effect due to the dipolar orientation is dominant after voltage removal but should last for only a short period of time. An approximation consists in taking the response obtained just after removal of the voltage at 313K. To do so the peak detected on voltage removal after 5h of polarization at 2kV dc is treated as a triangle. The area below the peak is found to correspond to $6.1x10^{-5}C/m^{2}$, that correspond to the charge per unit area. The detection electrode area is estimated to be. The capacitance per unit area when V= 2kV is then estimate to be:

$$C_{PEA}= 6.1X10^{-5}/2x10^{3}= 3.05x10^{-8}F/m^{2}$$

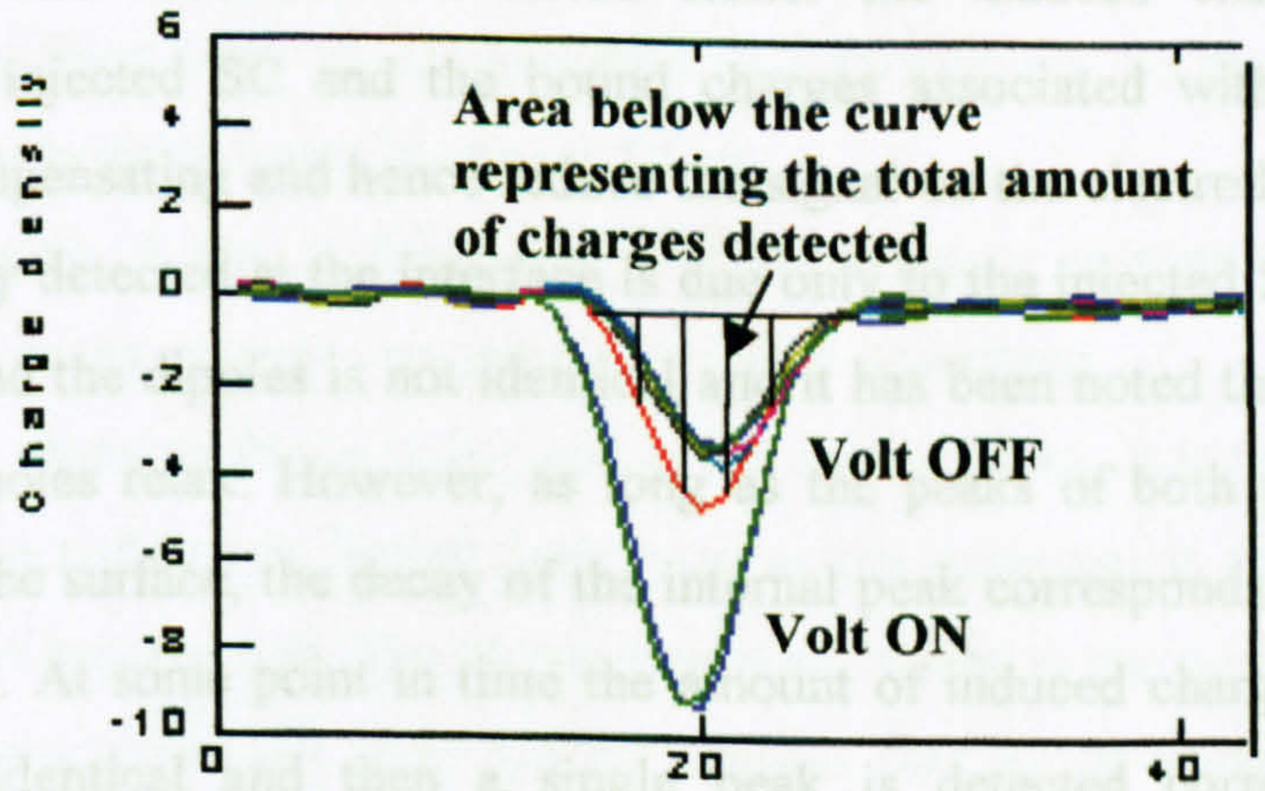

Figure IV-20: PEA signal after 5h +2kV dc (6.9kV/mm) 313K lower electrode side

So the capacitance per unit area (and charge per unit area) estimated from the dielectric response is about 20 times the value estimated from the PEA. The results show that the charge increment per unit area from the dielectric measurements is greater than that estimated from the PEA system. One possible reason is that 5 hours of polarization time may be insufficient to orient all the dipoles corresponding to process A and hence the charge on the electrodes corresponds to a smaller dielectric increment. It is also possible that the polarization peak in the PEA measurement corresponds to the orientation of dipoles from process B rather than process A. The value estimated from the dielectric response assumes a linear response. Actually when 2kV is applied to the sample the polarization might become non-linear and the value found from the linear response is an over-estimated of the situation.

VI.3- Relaxation phenomena

The injection of SC is dependent upon polarization time and temperature and amplitude of applied voltage. It has been observed that even at low field (+7kV/mm) if the time is long enough (figure IV-11) the detected signal increased when the polarization time was increased. As noted earlier the induced charges on the electrodes due to injected SC and the bound charges associated with the dipolar orientation are compensating and hence reduce the signal on the electrode. The signal of opposite polarity detected at the interface is due only to the injected SC. The time decay of the SC and the dipoles is not identical and it has been noted that SC decays faster than the dipoles relax. However, as long as the peaks of both polarities are detected close to the surface, the decay of the internal peak corresponds to the decay of the injected SC. At some point in time the amount of induced charge and bound charge becomes identical and then a single peak is detected corresponding in magnitude to the dipolar polarization.

The decay of the signal has then been analysed following different polarization times.

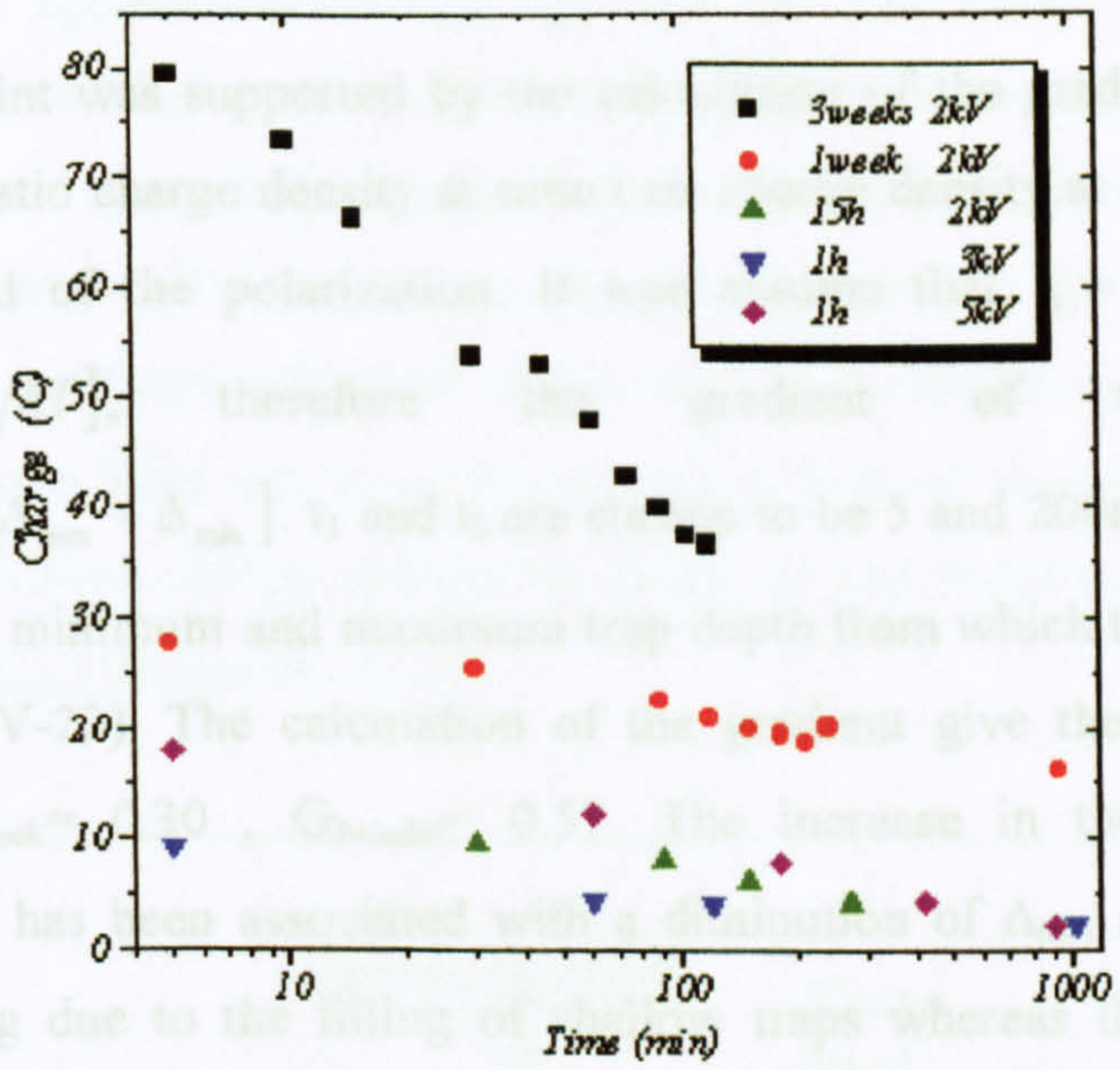

Figure IV-21: Charge decay over time following various periods of polarization at 298K, 2kV dc 15h, 1 and 3 weeks, 1h 3kV and 5kV dc

Concerning the traps three possibilities of filling can be imagined:

- Traps are filled from the lower energetic level to the higher one and as polarization time increases the levels of higher energy closer to the conduction band become filled.

- The traps are filled from top to the bottom energetic levels. As the polarization time increases, progressively lower levels are filled.

- Only one level of trap is filled and as time passes a reorganisation of the charge is necessary as the amount increases in the level concerned.

The first case seems to fit the behaviour of the charge decay. It is then supposed that charges are injected first in deeper traps then as the polarization time increases traps of higher level become full. The higher levels are closer to the conduction band so when the volts are turned off these are the charges that are de-trapped first. The closer the trapped charges are to the conduction level the easier they can be removed. That would explain the time difference in the charge decay observed after different period of polarization and the slowing down of the process after the removal of the voltage since the charges that remain to be de-trapped are in deeper traps and more difficult to move out [14].

This last point was supported by the calculation of the gradient of the curves representing the ratio charge density at time t on charge density at t= 0 over the time following the end of the polarization. It was assume that $t_1 = \nu.\exp[-\Delta_{min}/kT]$, $t_2 = \nu.\exp[-\Delta_{max}/kT]$, therefore the gradient of the slope is $Gradient = [kT]/[\Delta_{max} - \Delta_{min}]$. t_1 and t_2 are chosen to be 5 and 200min that express to correspond to the minimum and maximum trap depth from which the charges are de-trapped (figure IV-22). The calculation of the gradient give the following results G_{15h}= 0.53, G_{1week}= 0.30 , G_{3weeks}= 0.57. The increase in the gradient as the polarization time has been associated with a diminution of Δ_{min} as the polarization time is increasing due to the filling of shallow traps whereas the decrease of the gradient after 3 weeks of polarization might indicate a slowing decrease in the value of Δ_{max} due to a spreading of the trapped charge after all the higher level have been trapped.

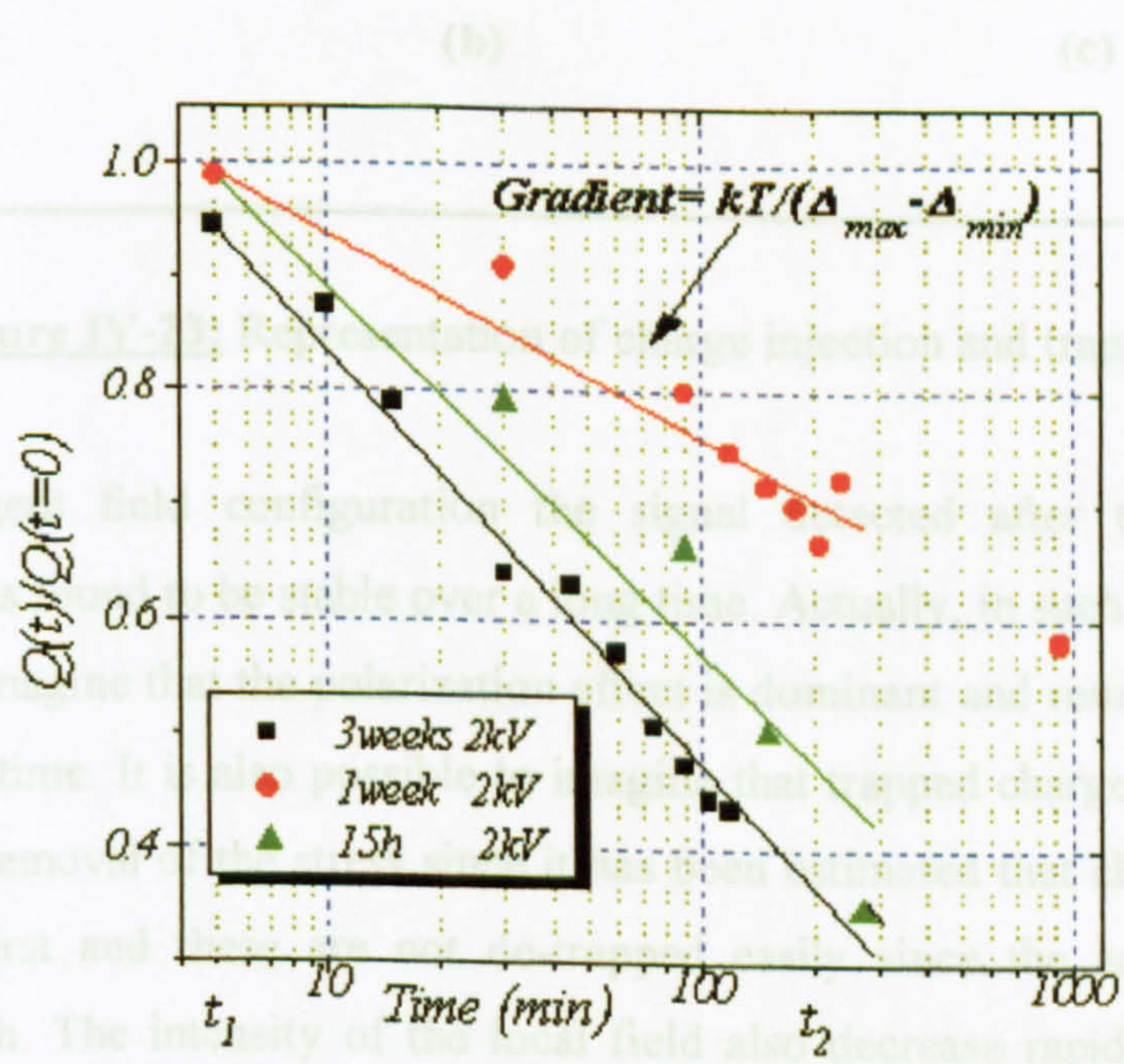

Figure IV-22: Ratio charge at t/ charge at t= 0s over time, following various period of polarization at 298K versus time, 2kV dc 15h, 1 and 3 weeks, 1h 3kVand 5kV dc

Under field application charges are injected and trapped. At the thermal equilibrium, traps are filled until the Fermi Level. When the number of charge carrier is increased, due to the voltage application, the Fermi level is shifted toward the conduction band (figure IV-23.a, b). Charges are expected to fill first deeper traps. Those traps are considered uniformly distributed. As polarization time is increasing the shallow traps are filled and lower traps level is dropped in energy as well as the Fermi level. This allows charge injection to continued and explains the increase in the difference (Δ_{max}-Δ_{min}) (figure IV-23.c).

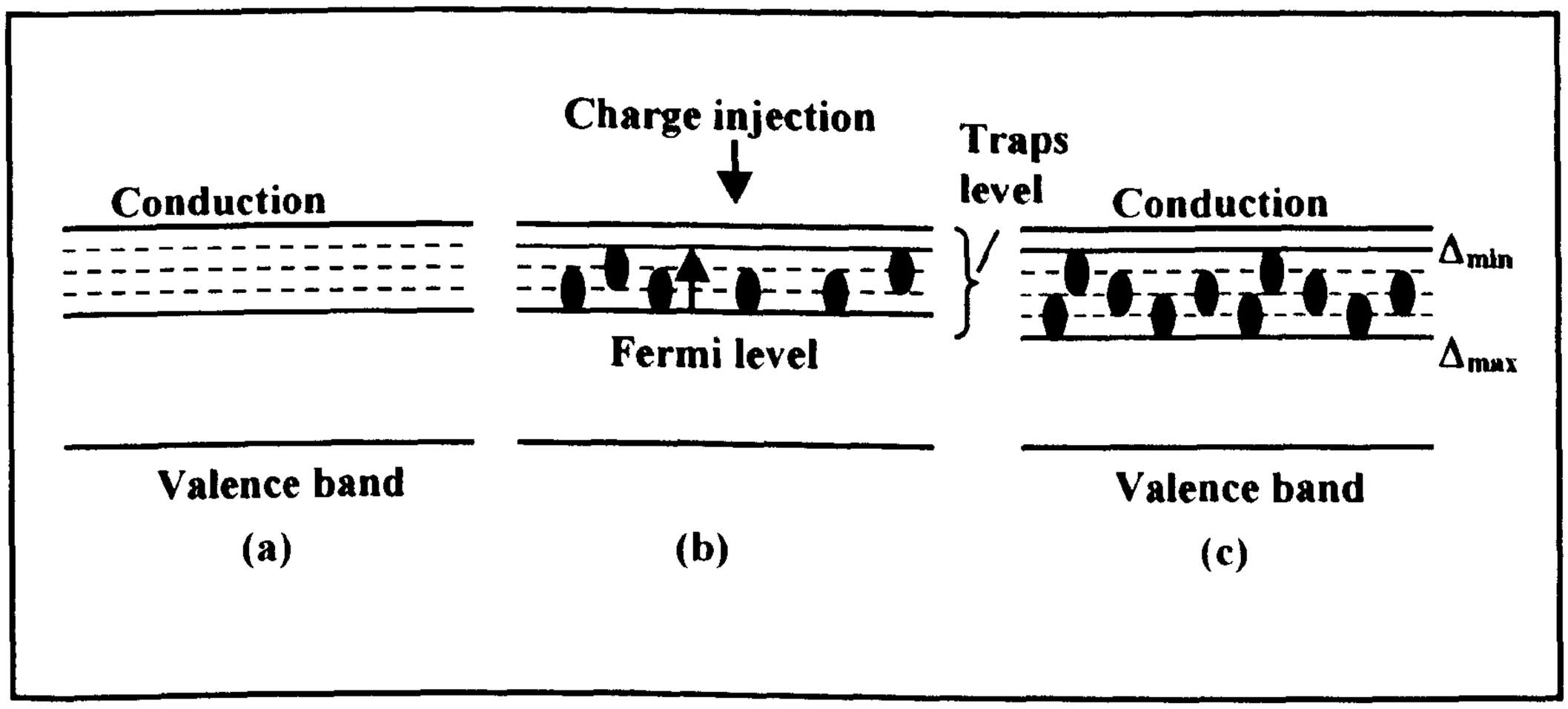

Figure IV-23: Representation of charge injection and trapping

In divergent field configuration the signal detected after the end of the polarization was found to be stable over a long time. Actually, in such configuration it is possible to imagine that the polarization effect is dominant and remains stable for a long period of time. It is also possible to imagine that trapped charges remain a long time after the removal of the stress since it has been estimated that charge are fill the deeper traps first and these are not de-trapped easily since the activation energy required is high. The intensity of the local field also decrease rapidly as we go far from the wires so any field assistance for de-trapping is likely to be weak.

Chapter V

Electroluminescence

The aim of studying the field-induced optical emission from electrical insulation is to investigate the mechanism of energy dissipation when SC is built up by injection or ionisation and evaluate its role in electrical ageing. In this section we are interested by the release of energy that is able to produce light emission. This de-excitation can occur by a number of different processes.

The excitation of the electroluminescence is related to the transport mechanism. It is necessary to detect the electroluminescence, the external current and the spectral components of electroluminescence to perform a complete investigation of the process. Moreover, to understand electroluminescence spectra it is necessary to know the luminescence properties of the material. To do so two sources of excitation will be used in addition to the electric field: one is related to the luminescence excited by the absorption of photons (photoluminescence), the other to the luminescence excited by the radiative recombination of electrical charges (charge recombination induced luminescence). The various spectra recorded will be reported and will be used to interpret the electroluminescence spectrum. Finally, the electroluminescence observed under uniform and divergent fields will be given.

I- Charge transport and electroluminescence

A number of studies have concentrated on the emission of visible photons when the material is submitted to an electric field. The research in this area is not new [1,2]. This kind of radiation is called electroluminescence.

Electroluminescence is caused by the generation of charge carriers within the polymer by the applied electric field. Such carriers can be produced either by injection or by de-trapping. They may be freely mobile or may polarise the neighbouring polymer and move as a polaron. Several mechanisms exist whereby they may excite luminescence, such as impact ionisation, impact excitation or the formation of bound (excitation) pairs with carriers of opposite polarity.

Electroluminescence is found experimentally in a wide variety of materials and appears therefore as a general mechanism. However, it is not easy to ascertain the mechanism that is responsible for the observed emission.

The simplest mechanism of electroluminescence that can be envisaged follows the injection of charge carriers at an electrode contact. After injection, in the absence of an applied field, there is a state of dynamic equilibrium between processes of

thermal production and recombination of electron hole pairs. Some recombination of low-mobility carriers can then be the origin of energy dissipation leading to light emission. In such a situation, the dissipated energy is equal to the potential energies of the two electronic states involved in the process. It has been proposed that the internal energy stored in the surrounding medium polarized by the trapped charges could be responsible for aging and breakdown [3].

Most of the time, electrical ageing leads to changes in the chemical composition in a non-homogeneous manner. Therefore, chemical analyses on a macroscopic scale are unable to observe this type of change. It is believed that the electroluminescence emission from the dielectric can be linked to the structural degradation of the system through the analysis of the energy released by the process. Electroluminescence analysis is a non-destructive method to certain extent, and several comparative measurements can be carried out on samples at different stages of their life.

The interpretation of the results however, necessitates other comparative studies using alternative sources of excitation. An important technique is that of photoluminescence in which luminescence is excited by means of optical (photo-) irradiation. Plasmaluminescence and chemiluminescence are also used in addition to photoluminescence. Low energy photons, energetic species of a non-reactive cold plasma, and chemical energy are all used as comparative excitation sources [4]. Photo-excitation can directly excite various chromophores and the associated luminescence can be compared with the electroluminescence in order to identify the emitting states. Plasma-excitation generates charge recombination in the absence of an electric field and the associated luminescence will indicate if this is the path taken by the electroluminescence. Electroluminescence likewise gives information on chemical generated emission.

I.1- Excitation mechanism

Electroluminescence emission can originate from several different mechanisms. For the electroluminescence the excitation is supplied to the luminescent species by the charge carriers through their potential energy, kinetic energy or both. To be observable in the visible range of the spectrum the luminescence centre must have an excited state higher than the ground state by 2eV.

I.1.1- Impact processes

The most common process reported is based on an *acceleration-collision* scheme [5]. The source of the initial electrons, which are accelerated, is important since few (ideally no) free conduction electrons exist in an insulator at room temperature (RT). Their origin can be explained by injection or a prior injection and trapping. Injected electrons may possess kinetic energy if the field is high enough to keep the electron in the conduction band or if there exist regions, such as microvoids, interfacial defects, in which the scattering length is increased. Carriers with a kinetic energy higher than severals kT are called "Hot electrons". Trapped electrons that are localized in a high field region may be liberated by the action of the field and acquire kinetic energy. Because of the thermal requirement for detrapping, the field effect can be coupled to the effect of the temperature.

This mobile space charge plays an important part in impact processes since it corresponds to the fraction of electrons that can acquire some kinetic energy and are thus able to move in the conduction band.

The charges are accelerated by the field and acquire kinetic energy raising them above the bottom of the conduction band. Then, they can collide with a recombination centre to which their energy is transferred. Depending on the kinetic energy of the mobile charge carrier, two regimes can be distinguished:

- impact ionisation (the centre is ionised)
- impact excitation (the centre is excited)

It is also possible that a recombination centre has been emptied by a tunnelling process or field ionisation. The number of transitions will depend on the field strength. In polymers, however, the field required in the case of Zener (band to band) tunnelling or centre ionisation is usually higher than the dielectric breakdown strength, thus this process is unlikely to be effective.

I.1.1.1- Impact ionisation

A mobile space charge with a kinetic energy higher than 3/2Eg, where E_g is the gap energy, is able to create an electron/hole pair by promotion across the forbidden band (figure V-1) [6, 7]. The acceleration process may be repeated and an "avalanche" initiated. Impact ionisation from deep centres requires less energy. Obviously, this latter process will depend on the energy provided to the system in

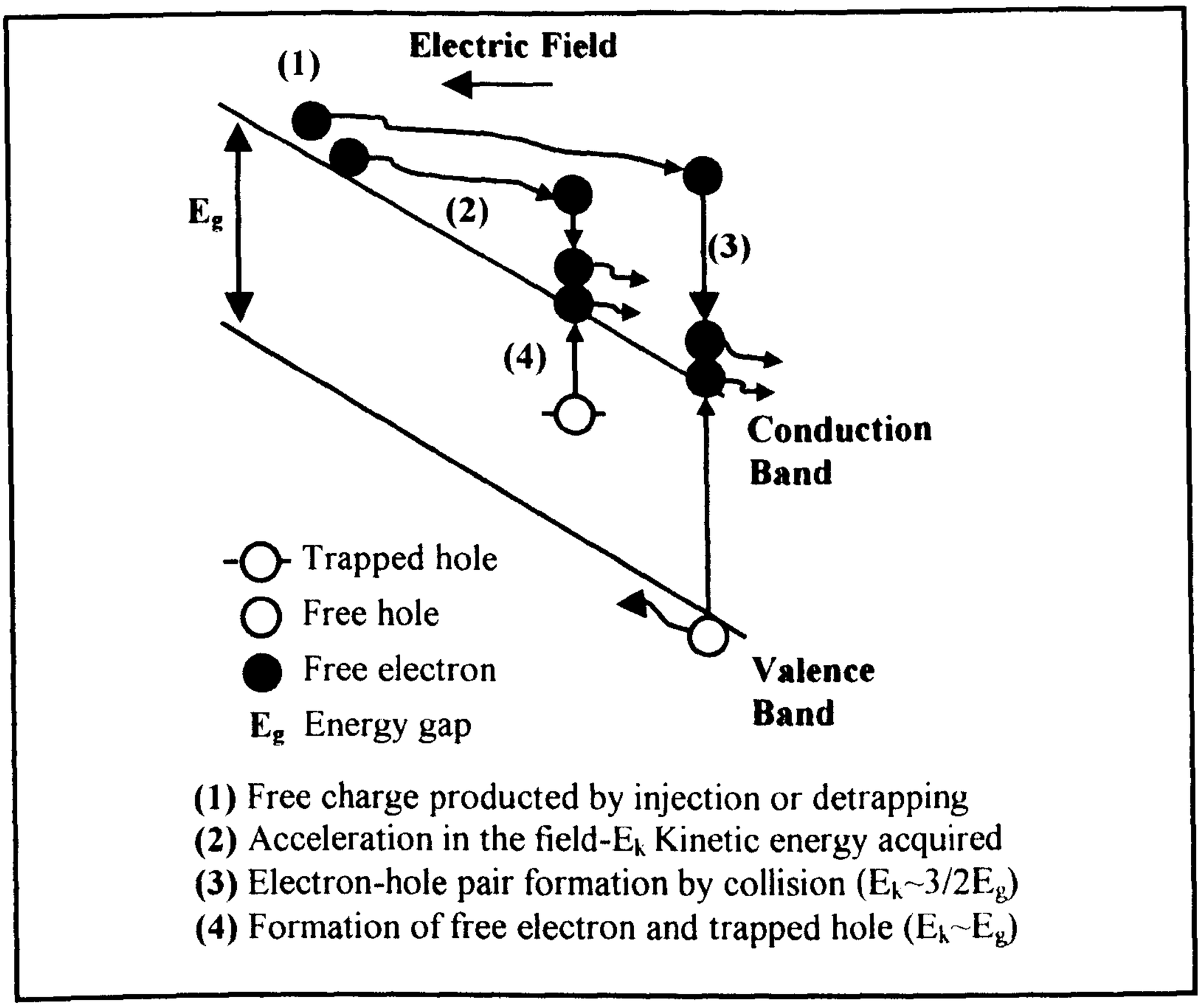

Figure V-1: Impact ionisation mechanism [6]

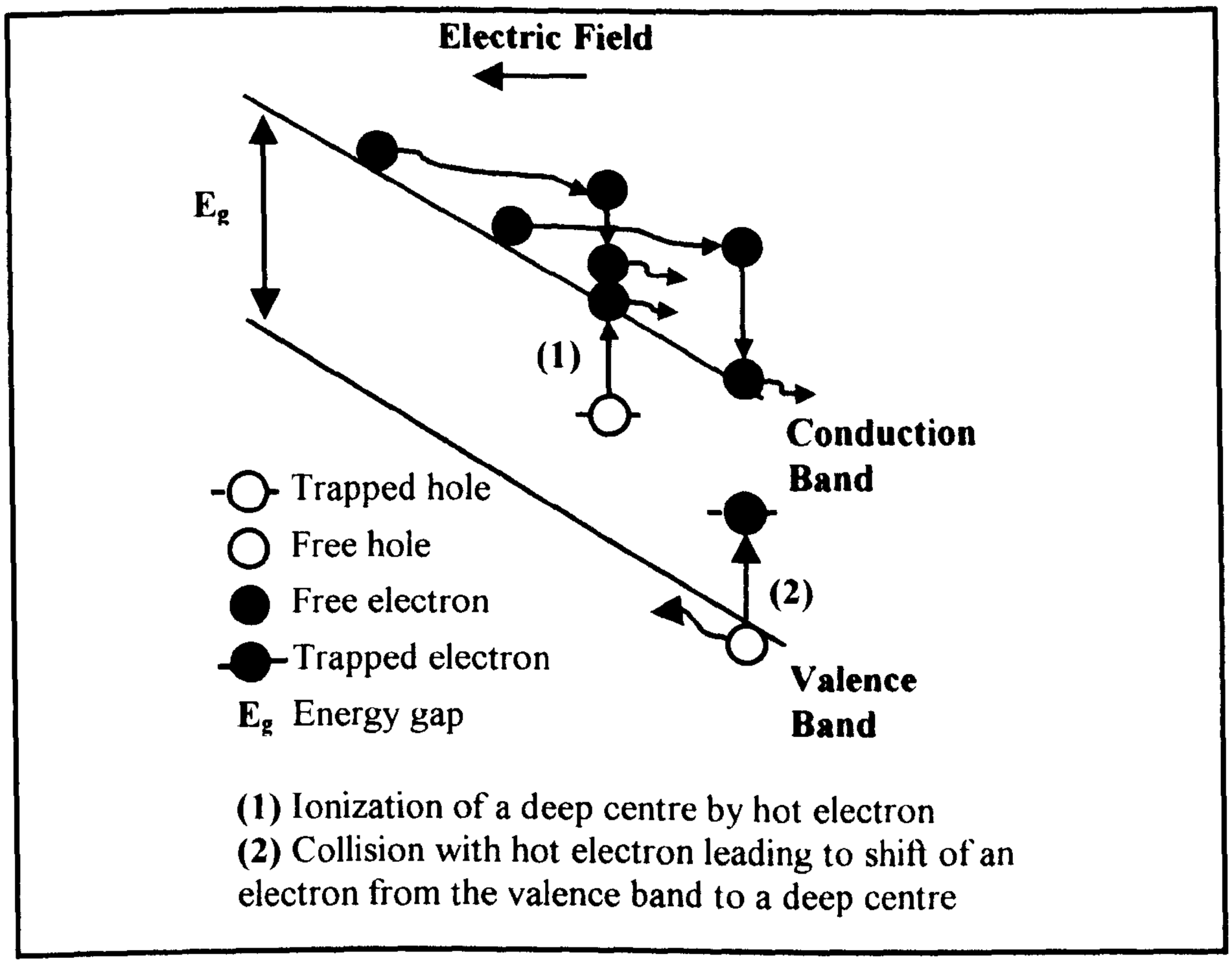

Figure V-2: Impact ionisation, two step-band-process mechanism [6]

addition to the depth of the centre. This process produces free electrons and trapped holes.

There exists also a two-step band process of impact ionisation (figure V-2). In this situation a hot electron ionises a deep level whereas another hot electron raises an electron from the valence band to a deep level. In this way, free electrons and holes are produced by using less energy than by the one-step process previously described.

I.1.1.2- Impact excitation

In the case of impact excitation, excited states are produced by electrons with lower kinetic energy [6, 7]. Electrons are thus excited without becoming free to move in the conduction band because of the strong effect of the electrostatic attraction. In this case exciton states are produced at deep centres or across the forbidden band.
Since polymers are organic solids, impact excitation can generate excited states of the repeat unit of the chain and side group moieties. Such states will have emission spectra related to that of the free molecule by a spectral shift whose magnitude depends on molecular environment. They can be generated as trapped Frenkel excitons or the Wannier type excitons that are both produced in the band gap as represented in figure V-3.

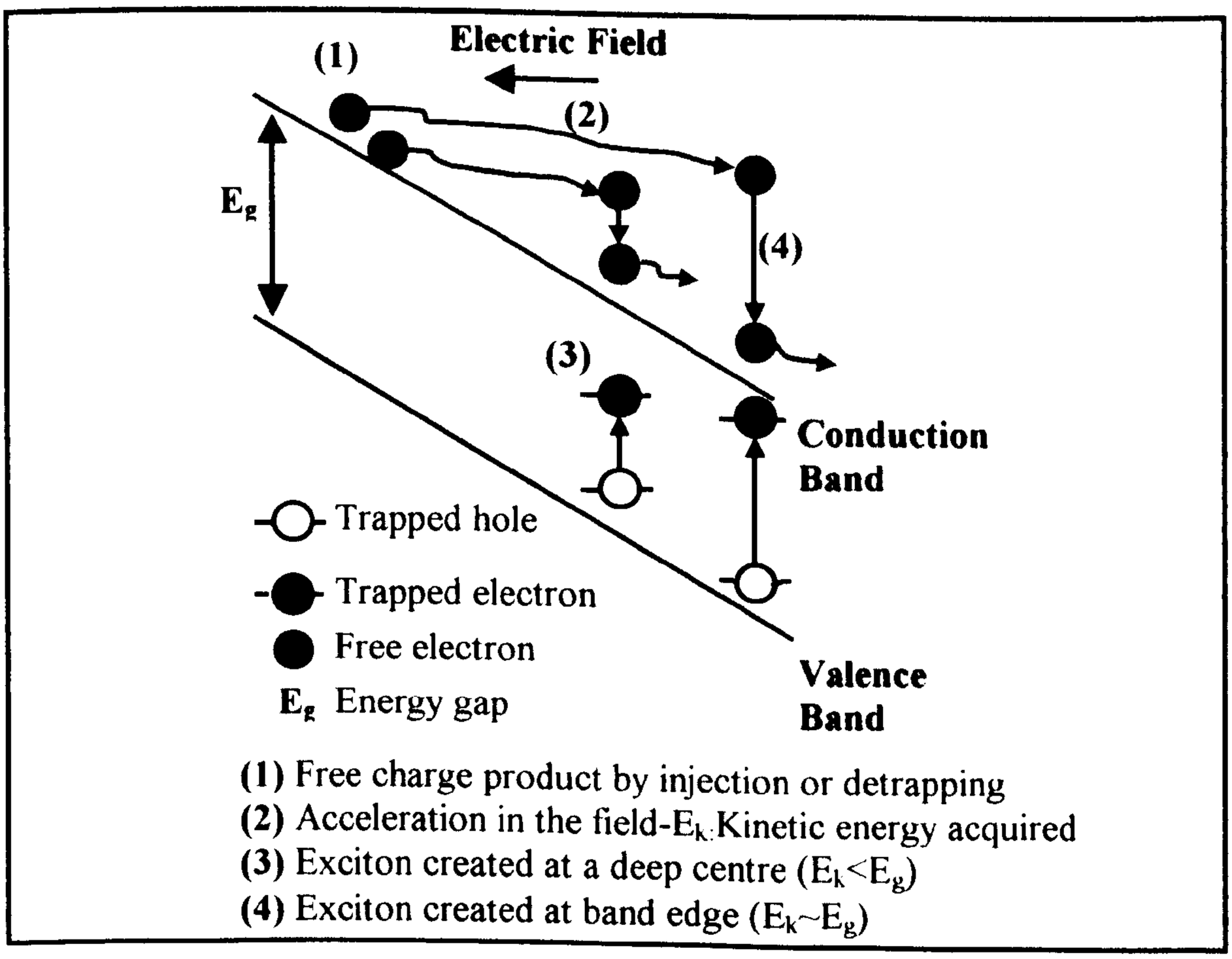

Figure V-3: Impact excitation mechanism [6]

I.1.2- Recombination

There exist several processes of recombination following carrier injection [5, 6, 7]. Not all of them lead to luminescent effects, however, and this can explain in some cases the low amplitude of light emission.

Two kinds of recombination processes can occur and are defined as intra-band processes or inter-band processes (figure V-4).

The energy involved in an intra-band recombination is less than the band gap. This process occurs when trapped charge recombines with a charge carrier of opposite polarity. The field required need not be high. The important point is that the interaction between the trap and mobile charge carrier must be such as to allow their coulombic attraction to dominate, i.e. the capture cross-section must be high.

In the case of dc voltage application charges of opposite polarity can migrate into the material until they reach a critical separation at which they can interact and recombine. Under ac voltage, recombination can appear in the same region of space at the reversal of the voltage polarity.

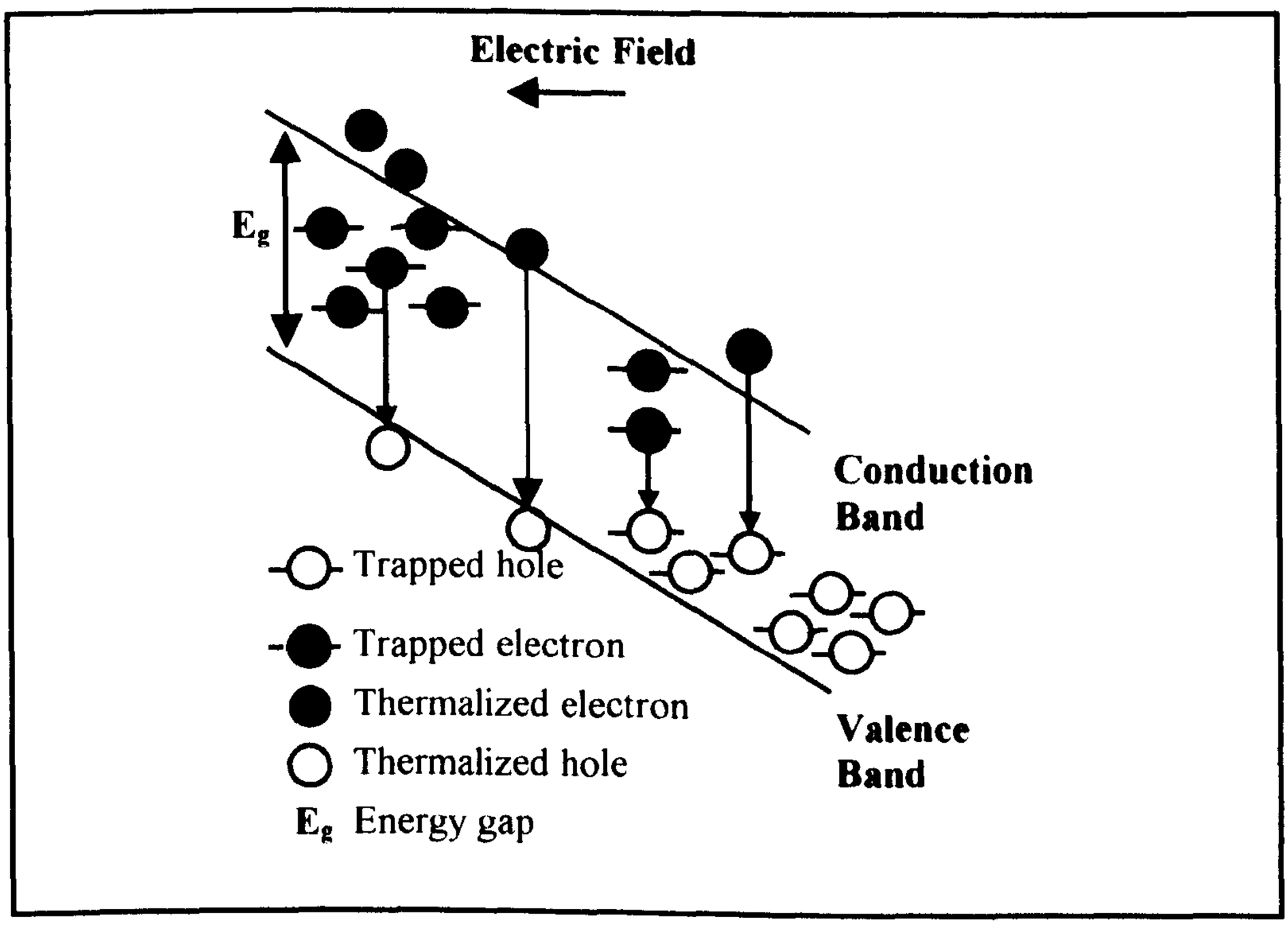

Figure V-4: Recombination mechanism between trapped or thermalized carriers of opposite polarity [6]

Three main types of recombination can be observed:

- Conduction band to valence band transitions (inter-band)
- Conduction or valence band to trap level transitions (intra-band)
- Trap level to trap level transitions (intra-band)

Since any of the excitation processes might be followed by several of the emission processes, it is obvious that in principle a very large number of possibilities exist.

To summarise, the phenomena of luminescence is observed during the relaxation of excited states. We have described the main excitation mechanisms. We will now make a distinction between two groups of relaxation mechanisms. These are first of all the reversible *physical paths* and secondly the irreversible *chemical paths*. In the latter situation, the material is damaged by the creation of free radicals and the breaking of chemical bonds. These phenomena are expected to depend on the nature of the materials and past history, i.e. previous stresses. Further information is given in the following paragraph.

I.2- De-excitation relaxation mechanism

There exist physical processes of relaxation that are reversible. If this is the only process followed, then the *fluorescence* and *phosphorescence* emissions that are recorded can be analysed to determine the excitation rate. If some light is produced by the chemical degradation and can be separately identified, then the dissociation rate would, in theory, be accessible [4].

II.2.1- Physical pathway

As example of physical pathway, we will chose the emission due to photon absorption when the photon energy is below the ionisation energy of the constituents on the material (discarding two photons processes and photochemical reactions).

Fluorescence [8] and phosphorescence are light emission processes that occur following the absorption of incident radiation. The fluorescence emission has a short lifetime typically between 10^{-11} and 10^{-5} sec. It arises from the transition between an excited state with spin quantum number S=0 (i.e. a spin singlet state) and the spin singlet ground state. Such a transition is allowed by the quantum selection rules and is therefore intense. Allowed transitions to rotation and vibration levels of the ground

electronic state cause the fluorescence to be broadened and red-shifted with respect to the exciting wavelength even at cryogenic temperatures. The shortest fluorescence lifetimes correspond to the narrowest emission peaks.

Phosphorescence is characterised by typically an afterglow persisting after the exciting source has been shut-off. Its lifetime is between 10^{-2} and several seconds and it is produced by transitions from an excited spin triplet state (S=1) to a singlet ground state. This process is not allowed by quantum selection rules but spin-orbit coupling makes it possible for it to occur. It is consequently a weak emission, although some species are powerful phosphorescent centres.

The process whereby fluorescence and phosphorescence is excited, is summarised in the Jablonski diagram of figure V-6. On absorption of light a transition occurs raising the molecule from the ground state to an excited state. In the one-electron approximation to the molecular states this can be thought of as the promotion of an electron from the ground sate to an excited state.

Subsequently the molecule will relax to a lower energy level in some cases with emission of light. Absorption spectra recorded on materials are usually similar both in the case of a subsequent fluorescence or phosphorescence emission. In fluorescence spontaneous transitions occur whereas in phosphorescence an intermediate metastable triplet level is involved (figure V-6). The formation of the intermediate state necessitates collaboration of the surrounding medium. Reducing the temperature tends to favour the occurrence of phosphorescence because of the possible quenching of the triplet state by nearby molecules [8]. In fact, the transition between a triplet state and singlet state is a forbidden transition that is why only a weak direct absorption can occur and the inter-system path is fundamental for the generation of the phenomena.

In the presence of a gas molecule such as oxygen the triplet emission can be quenched [8]. That is energy is transferred from a molecular excited state to the oxygen in the environment, and the phosphorescence is extinguished. The oxygen can release energy without light emission and in some case use it for oxidation reactions. It is therefore a particularly important process in commercial resin insulation, which will usually contain antioxidant to prevent its occurrence. To avoid such a side effect in laboratory experiments, it is common to work in an environment of nitrogen that is hardly excited at all by this type of energy transfer.

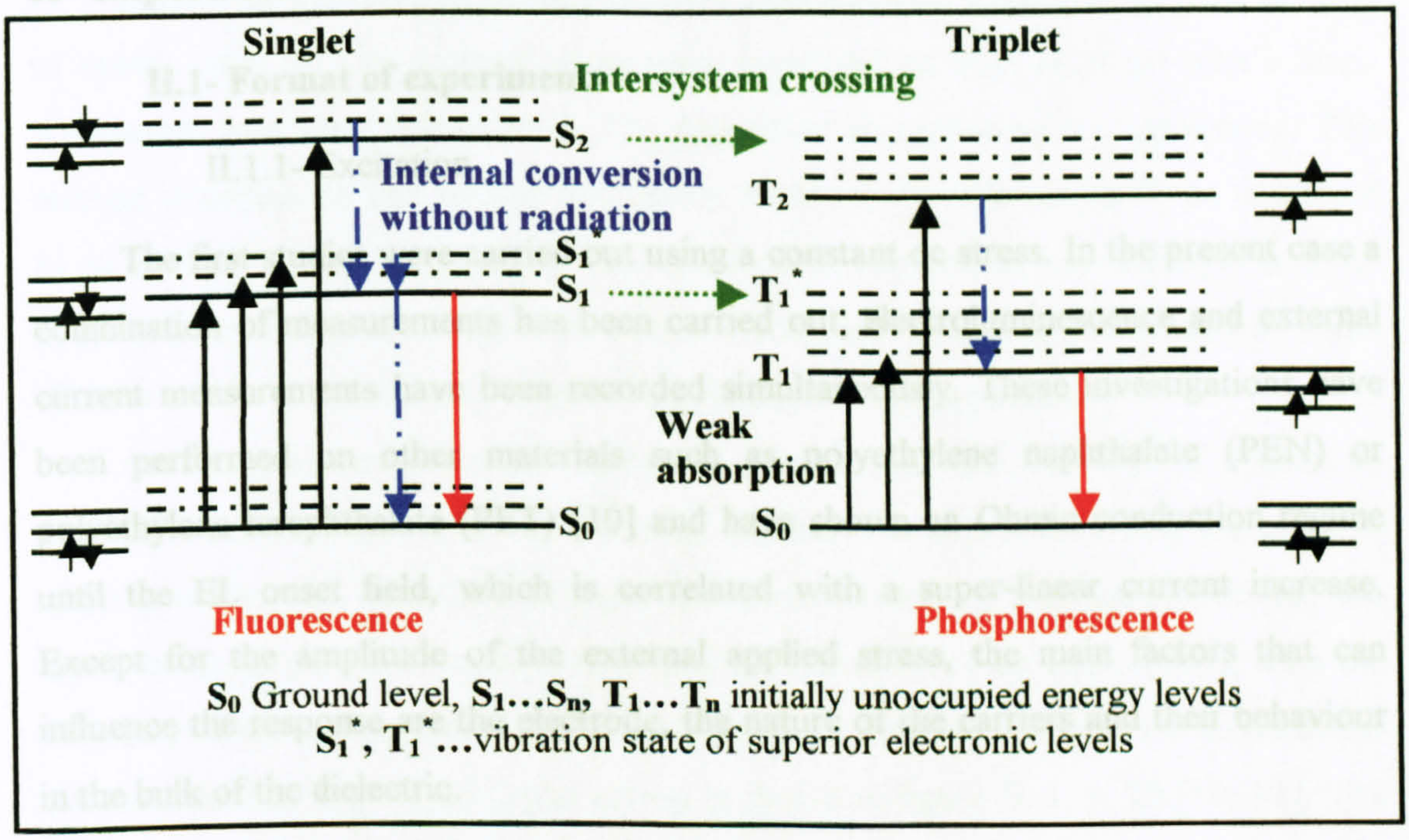

Figure V-6: Jablonski diagram of transition for a small molecule

I.2.2- Chemical pathway

In order to degrade the lattice the energy required needs to be of the order of the covalent bond energy. When a species is brought to a dissociative excited state such as $AB^* \rightarrow A+B$, A and B can give different states of excitation and charging. The relaxation is carried out towards other fundamental state provided by the dissociated species (i.e. A and B) that remain chemically different from the initial. These irreversible processes are called the chemical pathway. Another kind of chemical pathway could be defined during the transfer of energy from an excited carbonyl (triplet) to an oxygen molecule (triplet in the ground state). This can lead two new molecular groups $-(CH)_2-{}^3A^*+{}^3O_2 \rightarrow -(CH)_2-A+{}^1O_2^*$. In this case ${}^1O_2^*$ is produced and chemical changes in the material can be expected since this specie is highly reactive.

II- Experimental

II.1- Format of experiments

II.1.1- Excitation

The first studies were carried out using a constant dc stress. In the present case a combination of measurements has been carried out; electroluminescence and external current measurements have been recorded simultaneously. These investigations have been performed on other materials such as polyethylene naphthalate (PEN) or polyethylene terephthalate (PET) [10] and have shown an Ohmic conduction regime until the EL onset field, which is correlated with a super-linear current increase. Except for the amplitude of the external applied stress, the main factors that can influence the response are the electrode, the nature of the carriers and their behaviour in the bulk of the dielectric.

II.1.2- Relaxation

As the light is a consequence of the recombination of charge or relaxation of excited molecules, the analysis of the luminescence, such as the wavelength, the time of decay, can be a tool to identify the mechanisms that are involved. Spectral analysis was therefore used for that objective. In order to separate the different contributions various excitation sources are used and several types of spectra will be recorded leading to complementary information. For instance, an impact ionisation process, that generates pairs of trapped charges, can be characterised by the analysis of the decay of the luminescence. These have kinetics that are controlled by the recombination mechanism process. Such charge pairs can be generated by deposition of charge at the polymer surface by a cold plasma and will be described as plasmaluminescence analysis. In addition, photoluminescence resulting from photon absorption is expected to give information on the physical path of excitation relaxation by the analysis of the fluorescence and phosphorescence emission.

II.2- Techniques

Except in the case of plasma-induced luminescence experiments, film samples of epoxy resin with or without wires were metalised on both surfaces with a semi-transparent gold layer (figure V-7). The deposition was made by cold sputtering. This method prevents the film sample from being heated since they can easily be deformed by an increase of the temperature. The thickness of the circular metallic layer is about 300Å and the diameter 50mm. The coated electrodes were then surrounded by some silicone rubber to prevent any edge effects during voltage application.

For the measurements the sample is placed between two sets of cylindrical polished electrodes that make the electrical contact. The top one is a ring electrode to make possible the detection of light from the centre of the sample during the experiments. A plastic cover is used to prevent detection of the light coming from the periphery of the sample that is out of control due to the field profile at the edges of the metalised layers. The experimental set-up is shown in figure V-8, 9, 10 [10, 11]. The samples are placed in a chamber where a high vacuum ($<10^{-4}$ Pa) is produced so as to prevent electrical discharges from occurring. If discharges occur the spectra are likely to be obscured by many extra lines and bands [12]. The vacuum is produced in the chamber by a turbo molecular pump.

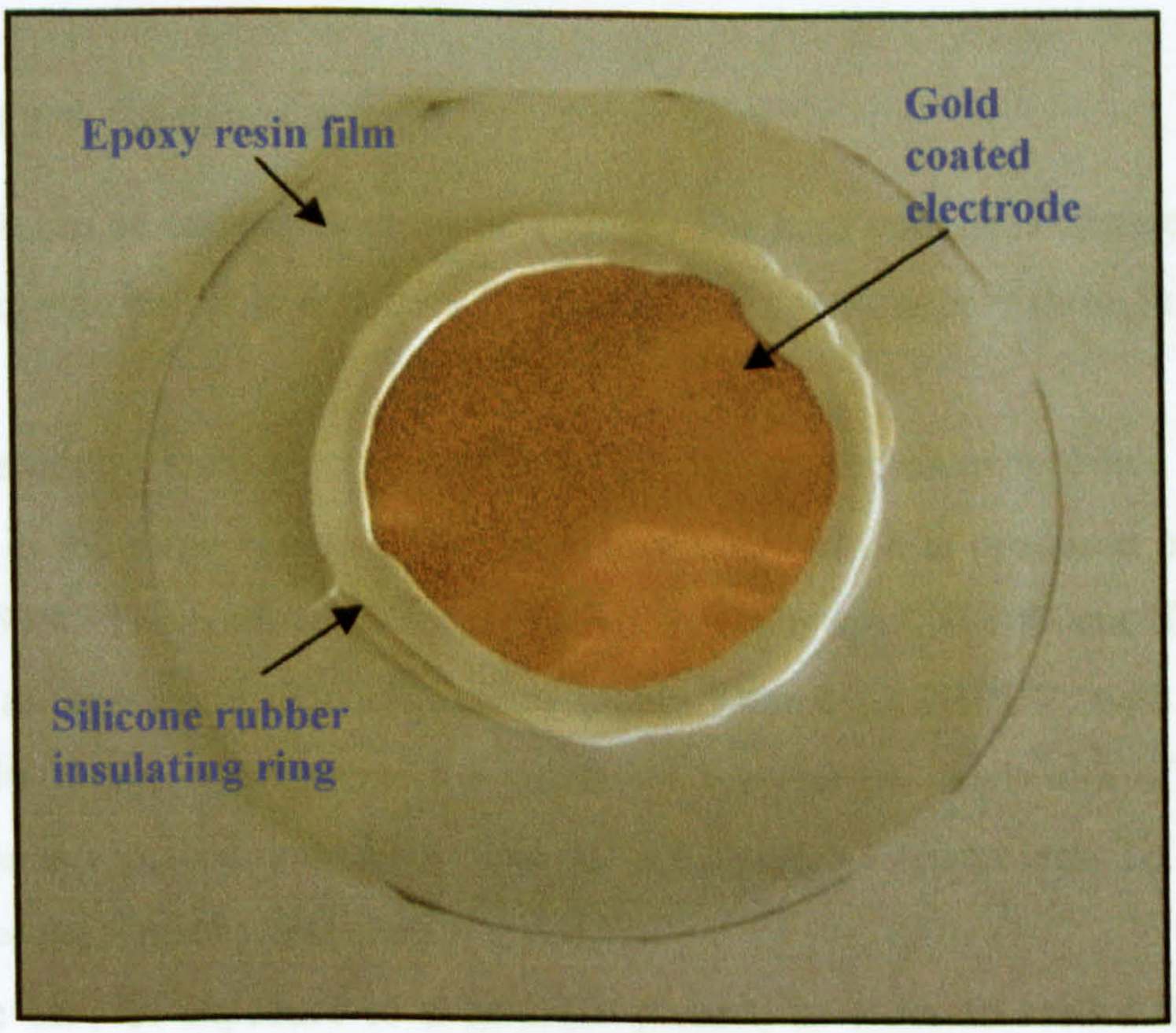

Figure V-7: Film of epoxy with coated gold electrodes and silicone rubber insulating ring

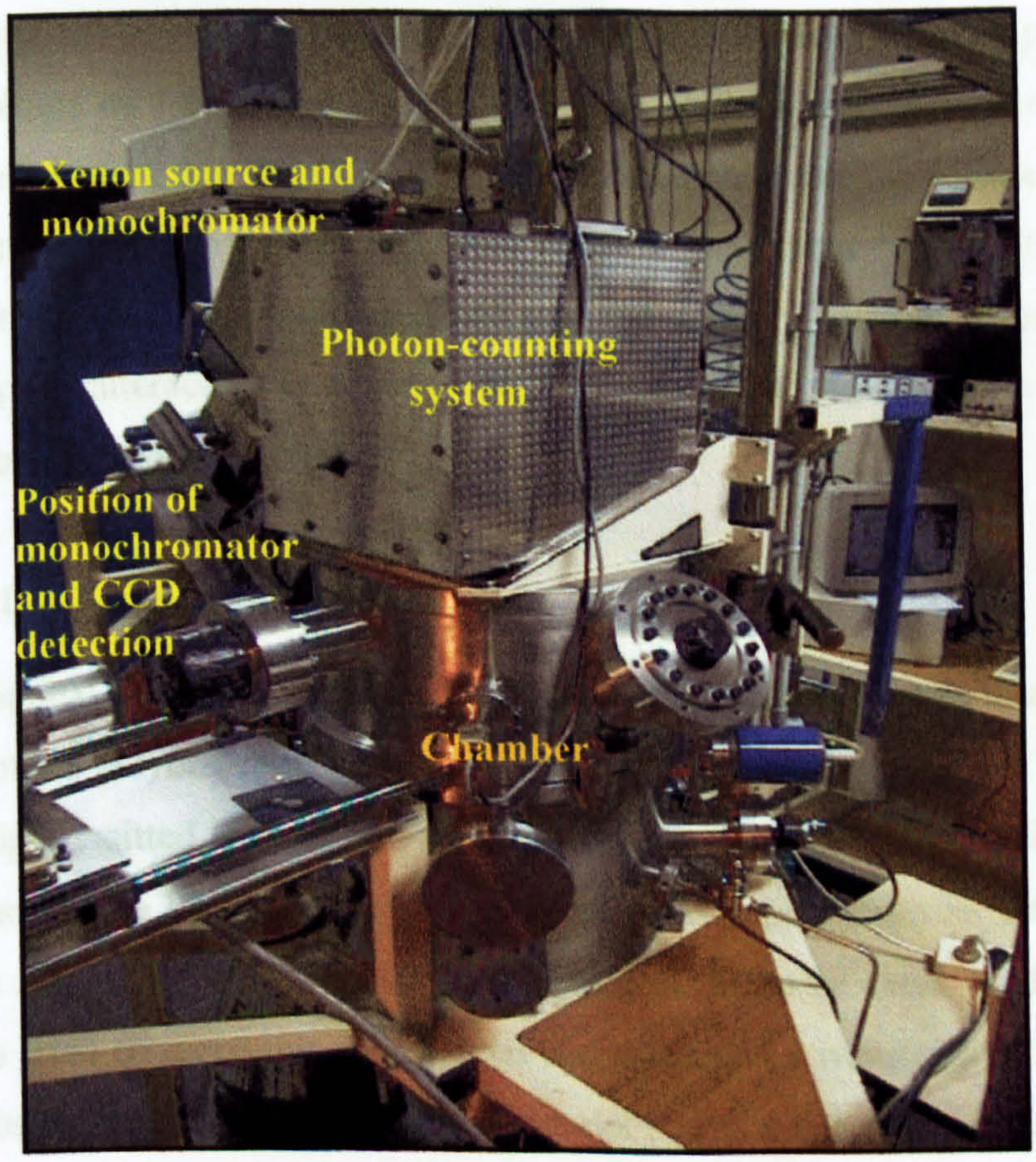

Figure V-8: Picture of the experimental set-up

II.2.1- Excitation systems

The EL can be excited by dc or ac voltage. The high voltage is connected to the top ring electrode and it is delivered by means of a power supply through a limiting resistor.

Comparatives studies can be made by using photoluminescence detection carried out in the same chamber. In this case the excitation is produced by a xenon source of 150W. The continuous spectrum covers the range 200-1000nm. The lamp is coupled to an irradiation monochromator (Jobin-Yvon type H10UV, with a spectral range of 250-750nm) that selects the excitation wavelength bandwidth of 5nm. The output image is focussed onto the sample surface through a quartz lens. To cut off the irradiation beam, a mechanical shutter is used.

In the case of exposure to a cold He plasma, in order to record the plasma-induced luminescence, liquid nitrogen was used to cool the system leading to a temperature of about -185°C. The chamber is first evacuated with the molecular pump

to 1Pa then filled with Helium up to 10^5Pa. The plasma is formed between two plane parallel electrodes separated by a gap of about 5mm and linked to an ac power supply giving a voltage of 1.5kV rms. The sample is in contact with the bottom electrode whereas the top electrode is a plate of quartz in order to create the plasma between the two dielectrics. The high voltage is applied to a gold layer that covered the side of the quartz electrode that is not directed towards the sample. Luminescence due to the plasma-polymer interaction is detected after switch off of the discharge by the same system as for other investigations.

II.2.2- Detection systems

The optical system of detection is organized around three axes that converge at the centre of the polymer film.

The light emitted is measured by a photomultiplier (PM) working in the photon counting mode. The PM photocathode is situated in the perpendicular direction above the sample and is used for integral light detection. In some cases band-path optical filters were used to carry out the analysis around a given wavelength. The averaged PM noise oscillates between 2 and 20 counts per seconds depending on the time it has been in the dark before the experiment. This does not disturb the measurements since it is quite stable. PM pulses are counted in time. It has been verified that the optical components present in the chamber have a flat response in the domain 200nm-900nm.

In order to obtain a spectral resolution another system of detection is required. It is reached by mean of a low dispersive monochromator (Jobin-Yvon CP200) coupled to a liquid nitrogen cooled Charge-Coupled-Device (CCD) camera that allows a long integration time. Long integration is possible since the CCD has a low background noise, that is useful in the case of the EL analysis. The resolution of the luminescence spectral analysis given by the system in use is about 4.5nm in the spectral range 300-800nm.

A semi-transparent mirror is positioned between the PM and the sample to direct the light emitted onto the monochromator and CCD camera when it is required. Quartz lenses are used to focus the active emissive area of the sample and make possible the light detection by the photocathode of the PM, or by the CCD camera.

A Keitley 617 ammeter was used for the charging-discharging current that, in some cases, was also recorded simultaneously with the luminescence.

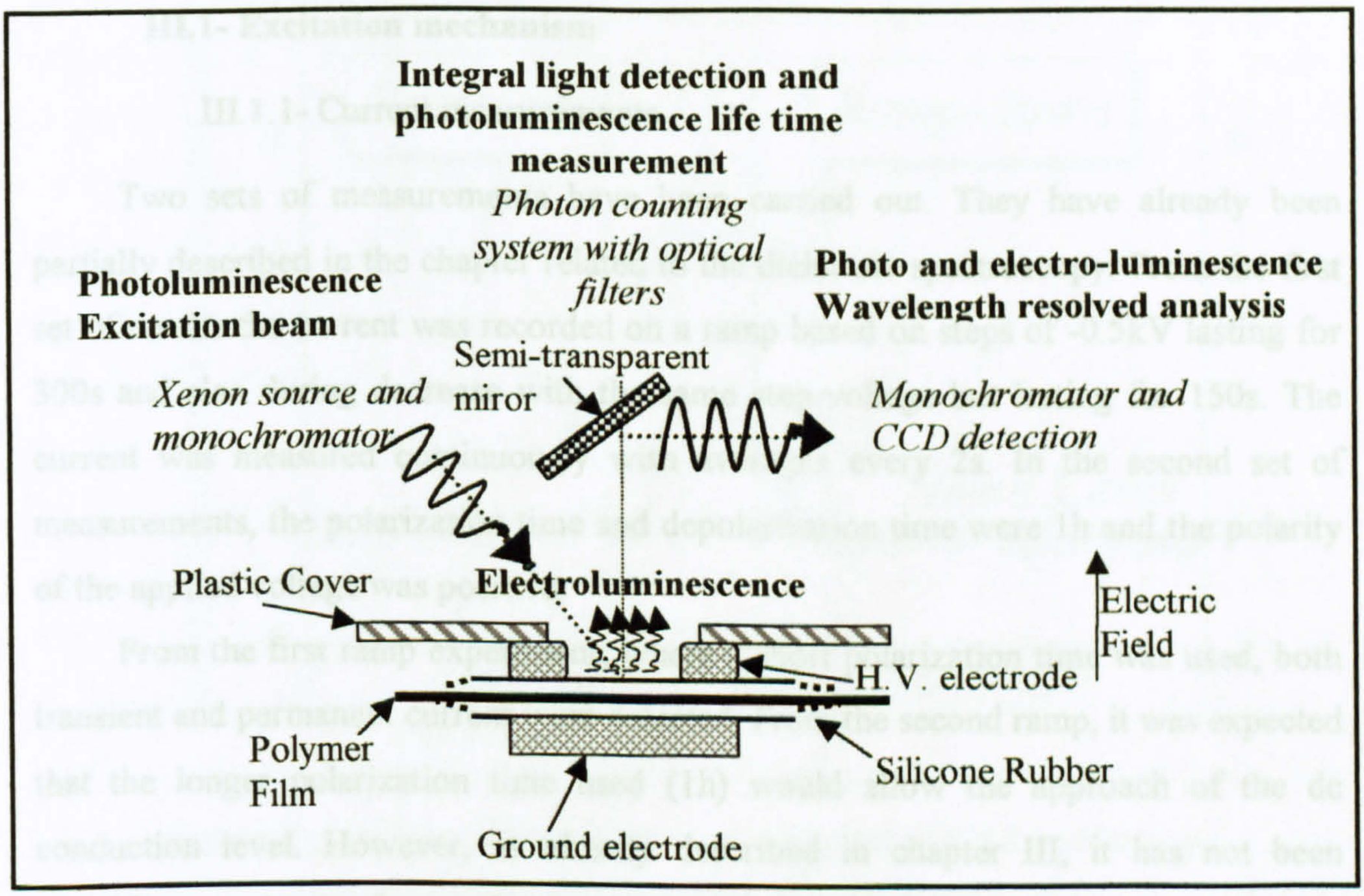

Figure V-9: Experimental set-up [10]

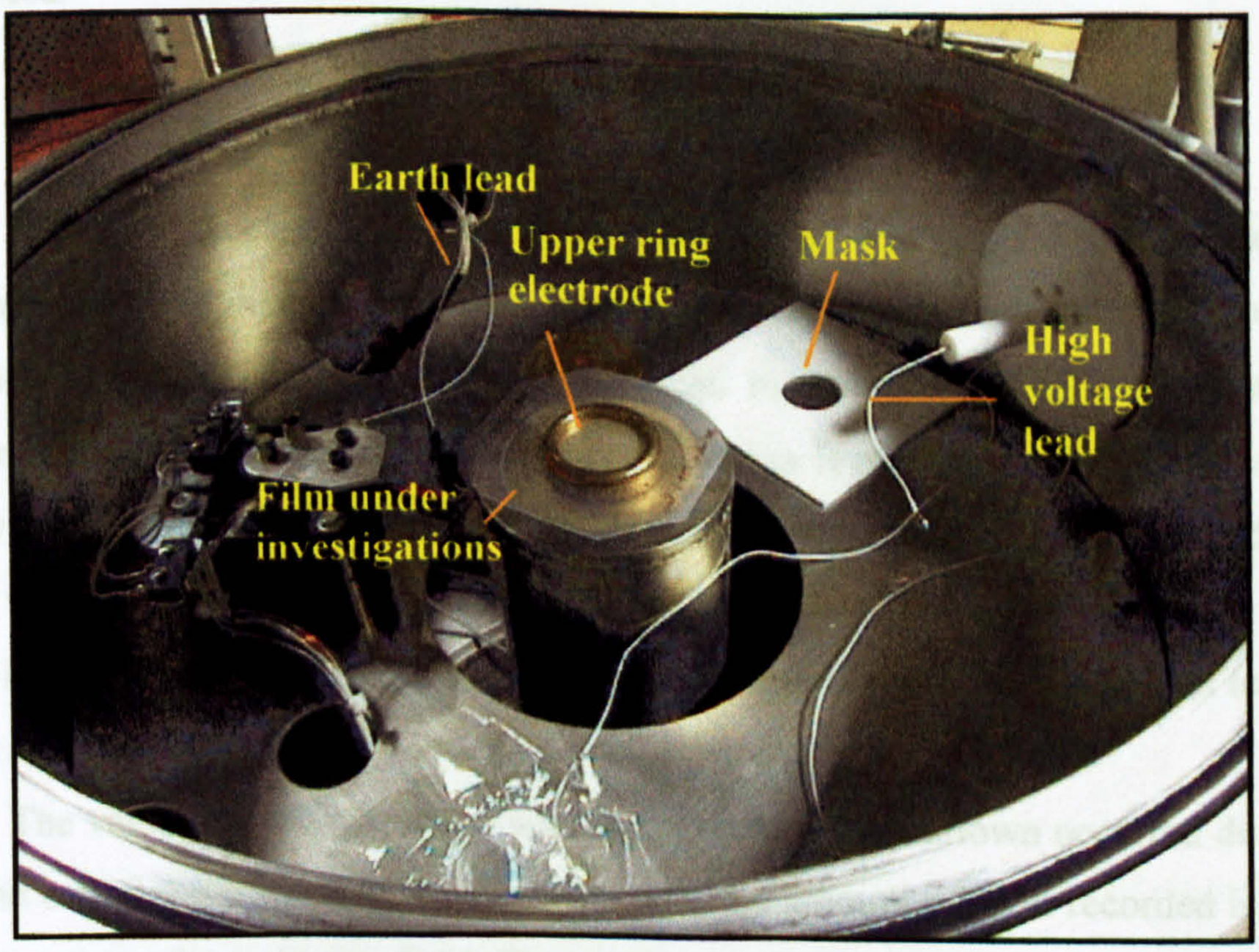

Figure V-10: Inside view of the chamber containing sample

III- Electroluminescence under uniform field configuration

III.1- Excitation mechanism

III.1.1- Current measurements

Two sets of measurements have been carried out. They have already been partially described in the chapter related to the dielectric spectroscopy. From the first set of results the current was recorded on a ramp based on steps of -0.5kV lasting for 300s and also during decrease with the same step-voltage but lasting for 150s. The current was measured continuously with averages every 2s. In the second set of measurements, the polarization time and depolarization time were 1h and the polarity of the applied voltage was positive.

From the first ramp experiment, where a short polarization time was used, both transient and permanent current were detected. From the second ramp, it was expected that the longer polarization time used (1h) would allow the approach of the dc conduction level. However, as already described in chapter III, it has not been possible to estimate the conduction current at low field due to the long transient associated with the polarization. In both cases, the current and the light emitted was recorded.

III.1.2- Electroluminescence measurements

The light recorded by the PM as the voltage was applied was plotted as a function of the applied electric field. Figure V-11 represents the results obtained from the first set of measurements. The noise level is around 2 counts per second. It is noticeable that below +175kV/mm only the noise level is recorded which remains really stable. Above +175kV/mm a continuous increase in the amplitude of detected light was observed. Therefore the threshold for electro-luminescence, E_t, has a value of $\leq$ 175kV/mm. On the ramp down the electroluminescence emission was too small to be recorded below +250kV/mm.

The value of applied voltage was increased until breakdown occurred during the second set of measurements. In this case also, the amount of light recorded is plotted as a function of the electric field. The current is plotted in the same figure (Figure V-12).

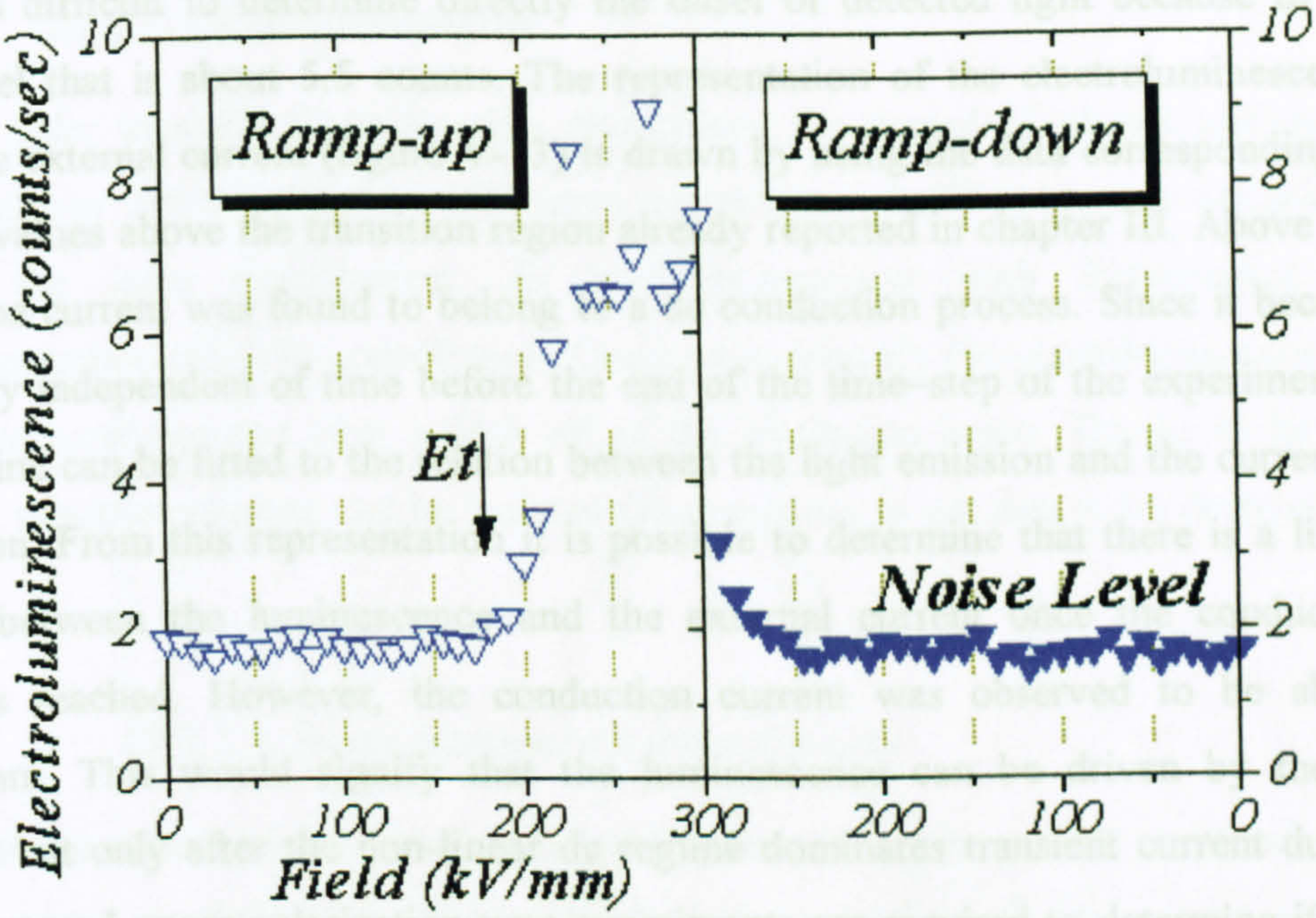

Figure V-11: Electroluminescence as a function of field on ramp-up and ramp-down. Noise level estimated at 2 counts

E_t threshold for electroluminescence

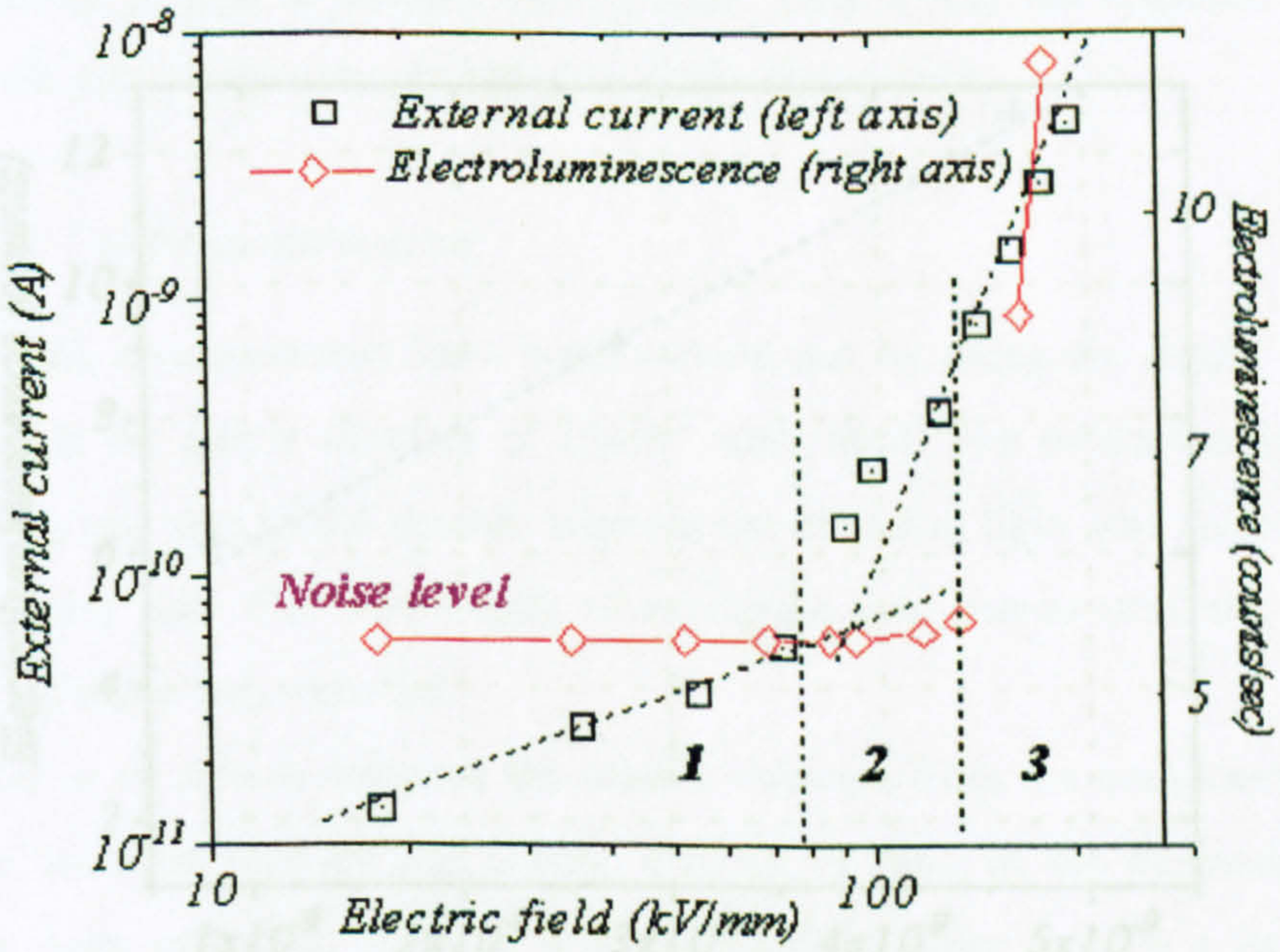

Figure V-12: External current and electroluminescence as a function of electric field.

Noise level estimated at ≅ 5.5 counts,

Current averaged between 2500-3600s of the polarization time.

Region: **1** Transient, **2** Transition region, **3** Conduction

It is difficult to determine directly the onset of detected light because of the noise level that is about 5.5 counts. The representation of the electroluminescence versus the external current (figure V-13) is drawn by using the data corresponding to the field values above the transition region already reported in chapter III. Above this region, the current was found to belong to a dc conduction process. Since it became essentially independent of time before the end of the time–step of the experiment A straight line can be fitted to the relation between the light emission and the current in this region. From this representation it is possible to determine that there is a linear relation between the luminescence and the external current once the conduction region is reached. However, the conduction current was observed to be above 140kV/mm. This would signify that the luminescence can be driven by the dc transport but only after the non-linear dc regime dominates transient current during the time step. Longer polarization time experiments are required to determine if this luminescence onset electric field can be associated with a physical threshold. These are needed to determine whether or not the charging current reaches a dc-level with the same field dependence at fields below the onset level for electroluminescence.

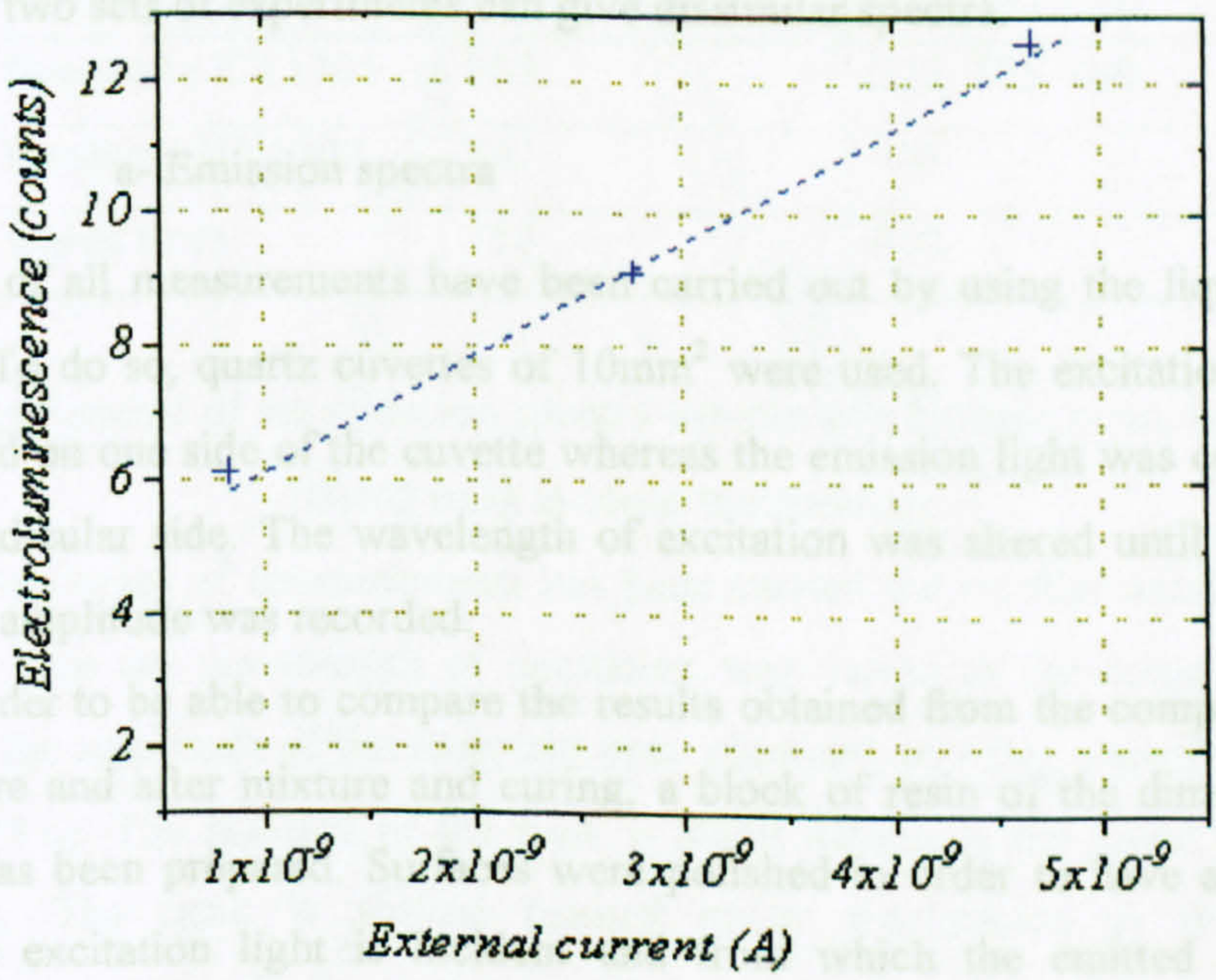

Figure V-13: Electroluminescence versus external current from region 3 Figure V-12

fitting curve: EL= 1.73×10^9 I+ 4.49

III.2- Relaxation

III.2.1- Photoluminescence

In order to study the relaxation phenomena the record of photoluminescence light emission can be effective. At room temperature the fluorescence emission is usually the main contribution. At low temperature, both fluorescence and phosphorescence can give contribution. One way to identify the phosphorescence is to detect the luminescence after switch off of the excitation beam. Thanks to its long lifetime, phosphorescence can be isolated (fluorescence is too fast to be detected that way).

III.2.1.1- Room temperature measurements

Measurements on the base resin and hardener have been first recorded. Then measurements on the cured solid epoxy have been performed and compared with those from its constituents. Since the material is composed of a large variety of chemical species a rather complex spectra can be expected. Besides after mixing, the two initial liquids, i.e. base and hardener, react chemically leading to the consumption of some chemical groups to produce some bonds. That is why the response obtained from these two sets of experiments can give dissimilar spectra.

a- Emission spectra

First of all measurements have been carried out by using the liquid base and hardener. To do so, quartz cuvettes of $10mm^2$ were used. The excitation light beam was applied on one side of the cuvette whereas the emission light was collected from the perpendicular side. The wavelength of excitation was altered until the signal of maximum amplitude was recorded.

In order to be able to compare the results obtained from the components of the resin before and after mixture and curing, a block of resin of the dimension of the cuvettes has been prepared. Surfaces were polished in order to have a flat area on which the excitation light is incident and from which the emitted light can be observed.

Results presented in figure V-14 shows three peaks for the base resin, and a single peak in the case of the hardener or the cured resin. The results are summarised in table III-1.

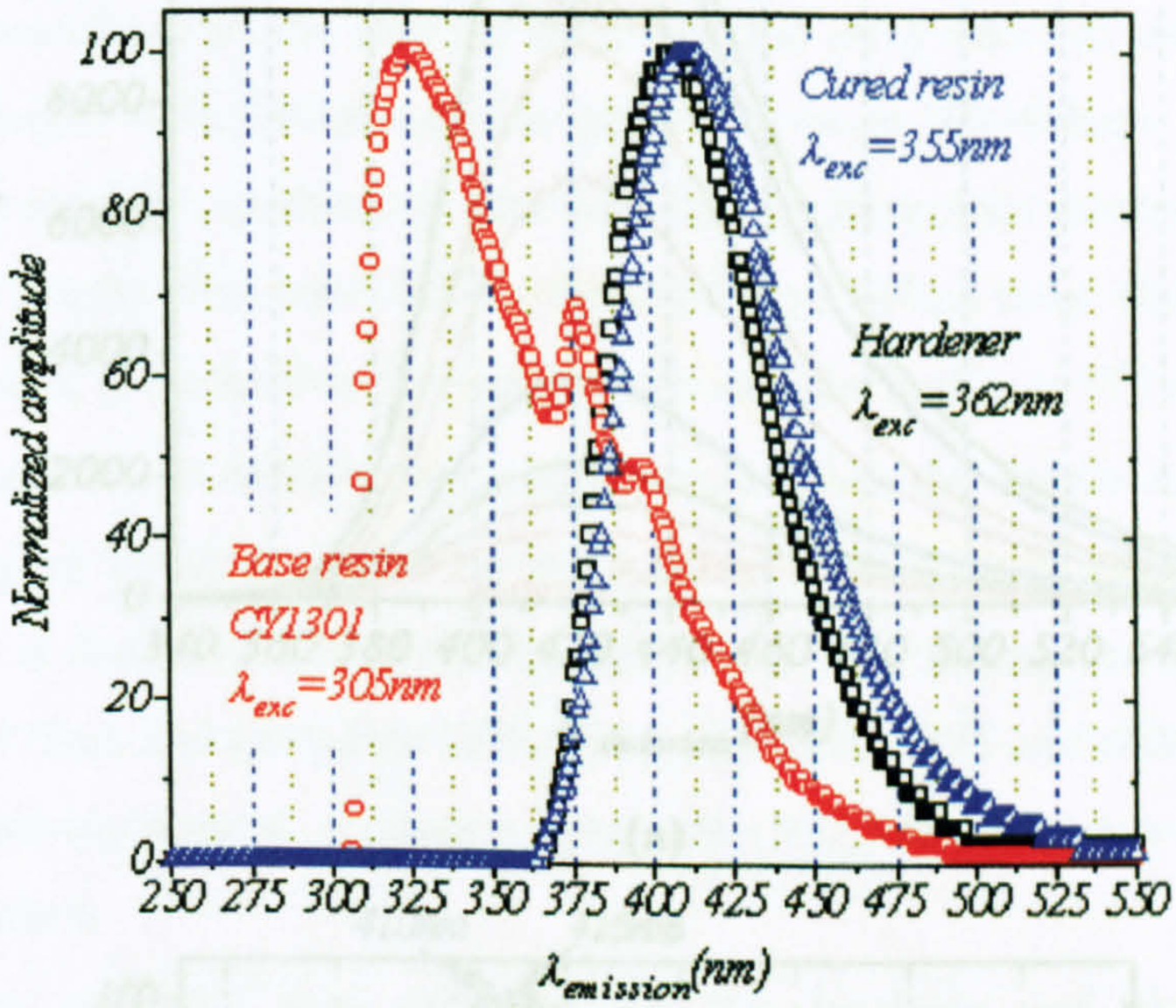

Figure V-14: Normalized emission spectra of liquid base resin, liquid hardener, and block of cured resin at room temperature

Component	$\lambda_{excitation}$ (nm)	$\lambda_{emission}$ (nm)
Base resin CY1301	305	325, 375, 400
Hardener HY1300	362	405
Cured resin	355	410

Table V-1: Résumé of the emission spectra wavelength for base resin, hardener and cured resin at room temperature

Another series of measurements has been carried out on film samples of cured resin. This time the wavelength of excitation was varied in the range 230-370nm. Except for the amplitude of the emission peak recorded no other changes were found (figure V-15.a). The position of the peak is about 420nm in the range of excitation 230-310nm. The peak is shifted toward lower frequencies as the excitation wavelength is increased. Comparison with previous measurements on block resin shows similar results (figure V-15.b). When $\lambda_{excitation}$= 350nm the peak detected from the film sample appears at 416nm whereas it was detected at 410nm from the block sample with $\lambda_{excitation}$=355nm.

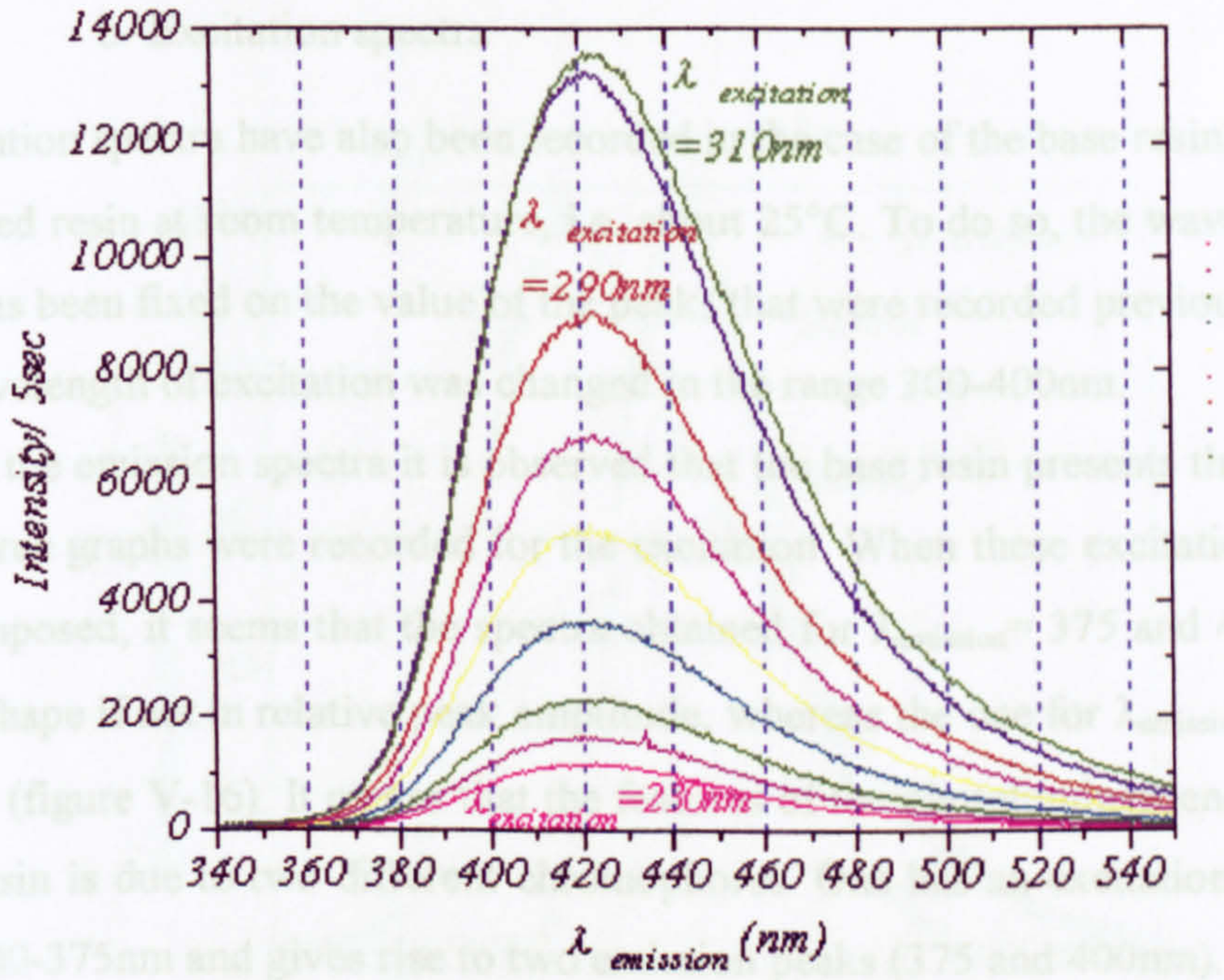

(a)

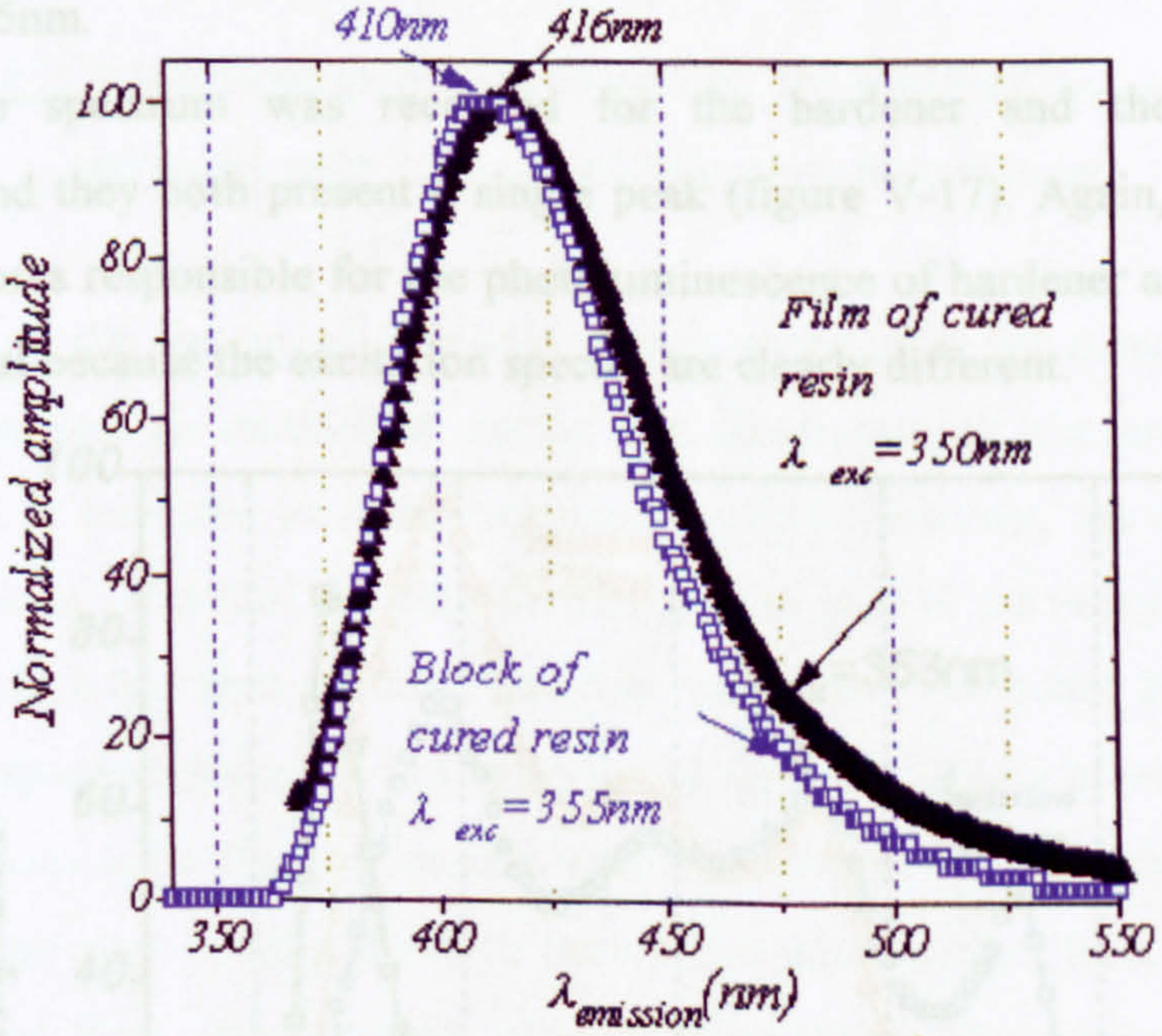

(b)

Figure V-15: Photoluminescence spectra recorded at room temperature

(a) Film sample of cured resin. λ_{exc} range 230-310nm

(b) Comparison sample film λ_{exc}= 350nm and block of cured resin λ_{exc}= 355nm normalized spectra

b- Excitation spectra

Excitation spectra have also been recorded in the case of the base resin, hardener and the cured resin at room temperature, i.e. about 25°C. To do so, the wavelength of emission has been fixed on the value of the peaks that were recorded previously. After this the wavelength of excitation was changed in the range 300-400nm.

From the emission spectra it is observed that the base resin presents three peaks, and thus three graphs were recorded for the excitation. When these excitation spectra are superimposed, it seems that the spectra obtained for $\lambda_{emission}$= 375 and 400nm are similar in shape if not in relative peak amplitude, whereas the one for $\lambda_{emission}$= 325nm is different (figure V-16). It means that the features of the photoluminescence peak of the base resin is due to two different chromophores. One has an excitation spectrum between 300-375nm and gives rise to two emission peaks (375 and 400nm). The other one has a relatively narrow excitation spectrum (300-320nm) and gives rise to the emission at 325nm.

A single spectrum was recorded for the hardener and the cured resin respectively and they both present a single peak (figure V-17). Again, it means that the chromophores responsible for the photoluminescence of hardener and cured resin are not identical because the excitation spectra are clearly different.

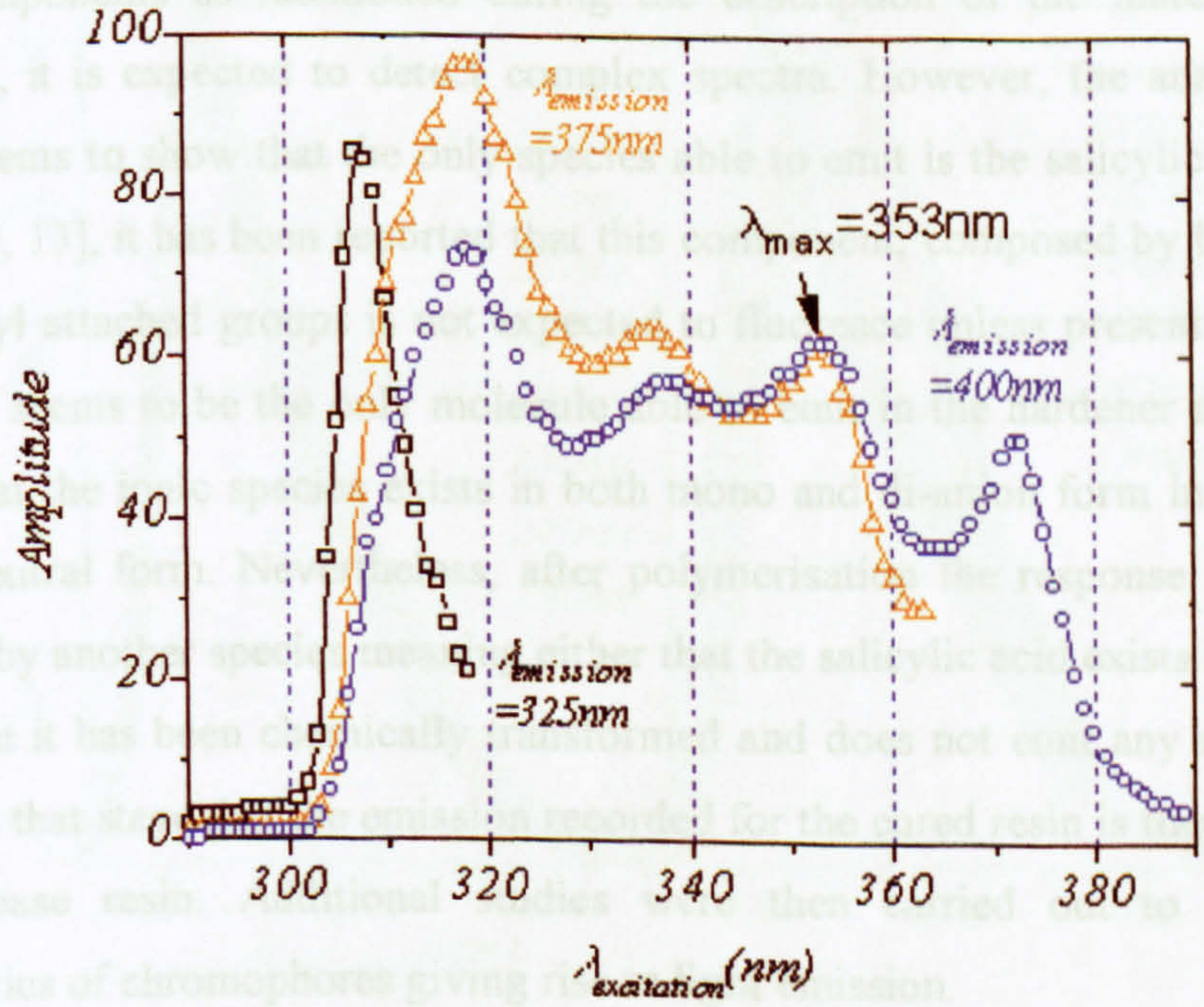

Figure V-16: Excitation spectra for the base resin $\lambda_{emission}$= 325, 375, 400nm, Room temperature

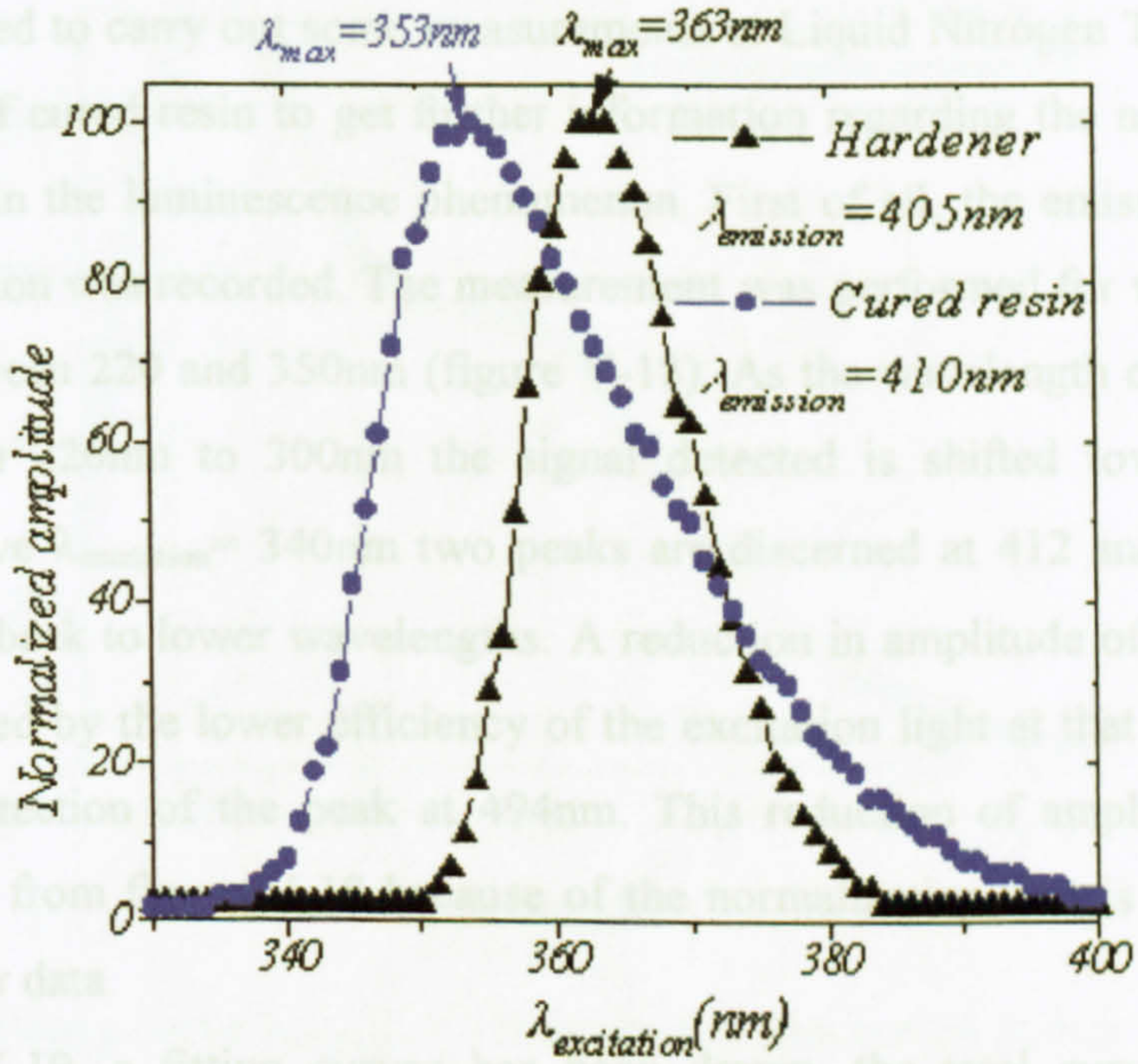

Figure V-17: Normalized excitation spectra for the hardener $\lambda_{emission}$= 405nm and cured resin $\lambda_{emission}$= 410nm room temperature

Because of the variety of chemical groups entering in the composition of the various components as mentioned during the description of the materials in use (chapter II), it is expected to detect complex spectra. However, the analysis of the hardener seems to show that the only species able to emit is the salicylic acid. In the literature [9, 13], it has been reported that this component, composed by benzene ring and carbonyl attached groups is not expected to fluoresce unless present in the ionic form. As it seems to be the only molecule able to emit in the hardener mixture, it is believed that the ionic species exists in both mono and di-anion form in equilibrium with the neutral form. Nevertheless, after polymerisation the response seems to be dominated by another species meaning either that the salicylic acid exists in molecular form or that it has been chemically transformed and does not emit any more. It was conclude at that stage that the emission recorded for the cured resin is therefore linked with the base resin. Additional studies were then carried out to identify the characteristics of chromophores giving rise to light emission.

III.2.1.2- Liquid nitrogen temperature measurements

It was decided to carry out some measurements at Liquid Nitrogen Temperature (LNT) on films of cured resin to get further information regarding the nature of the species involved in the luminescence phenomenon. First of all, the emission spectra during the excitation was recorded. The measurement was performed for wavelengths of excitation between 220 and 350nm (figure V-18). As the wavelength of excitation is increased from 220nm to 300nm the signal detected is shifted toward higher wavelength. Above $\lambda_{excitation}$= 340nm two peaks are discerned at 412 and 494nm as the signal moves back to lower wavelengths. A reduction in amplitude of the peak at 412nm is explained by the lower efficiency of the excitation light at that wavelength leading to the detection of the peak at 494nm. This reduction of amplitude is not observed directly from figure V-18 because of the normalization, but is was clearly detected from row data.

In figure V-19, a fitting curves has been drawn, the total curve obtain at $\lambda_{excitation}$= 350nm is the summation of two peaks that convolves whatever the wavelength of excitation.

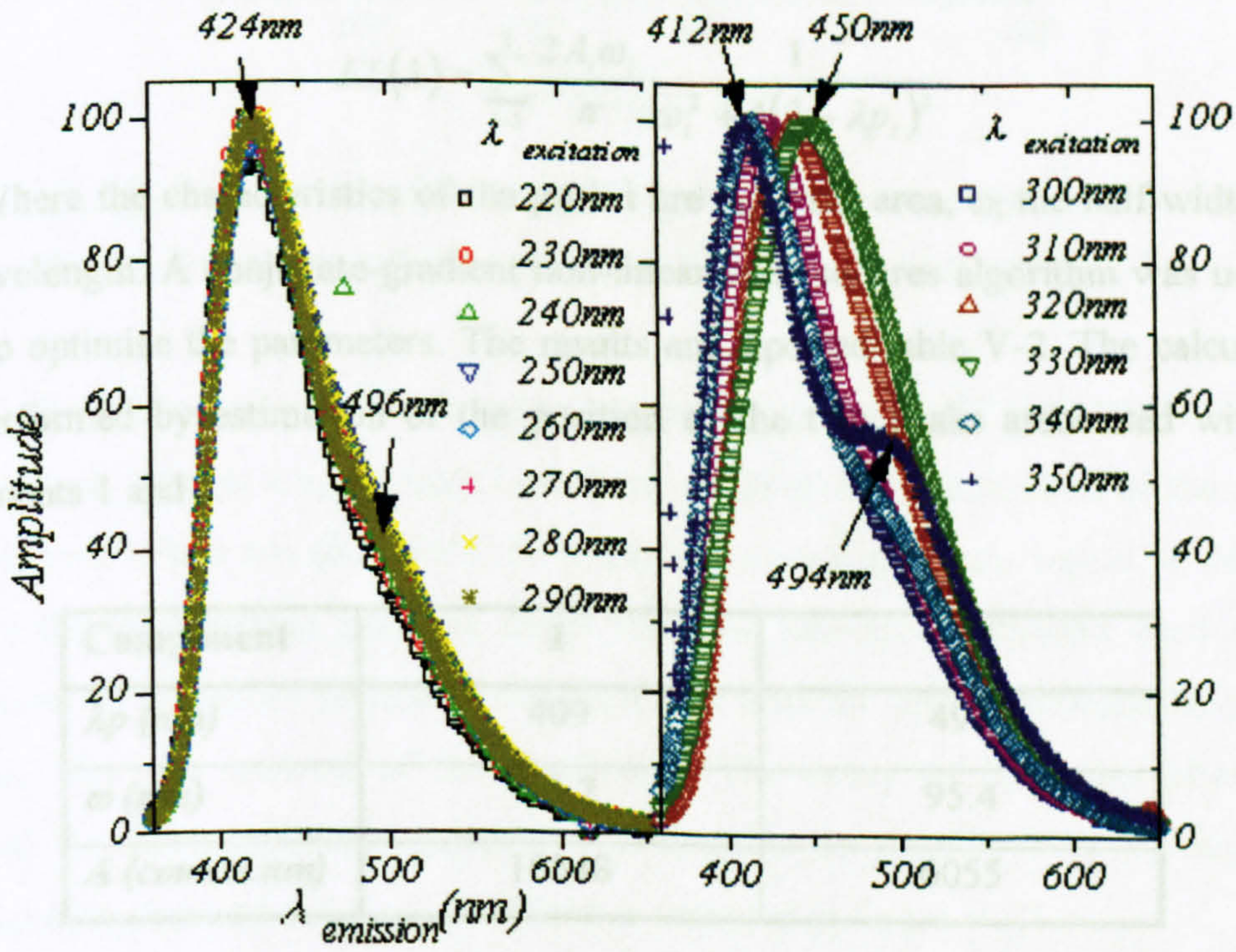

Figure V-18: Normalized emission spectra of cured resin film at Liquid Nitrogen Temperature $\lambda_{excitation}$ from 220 to 350nm

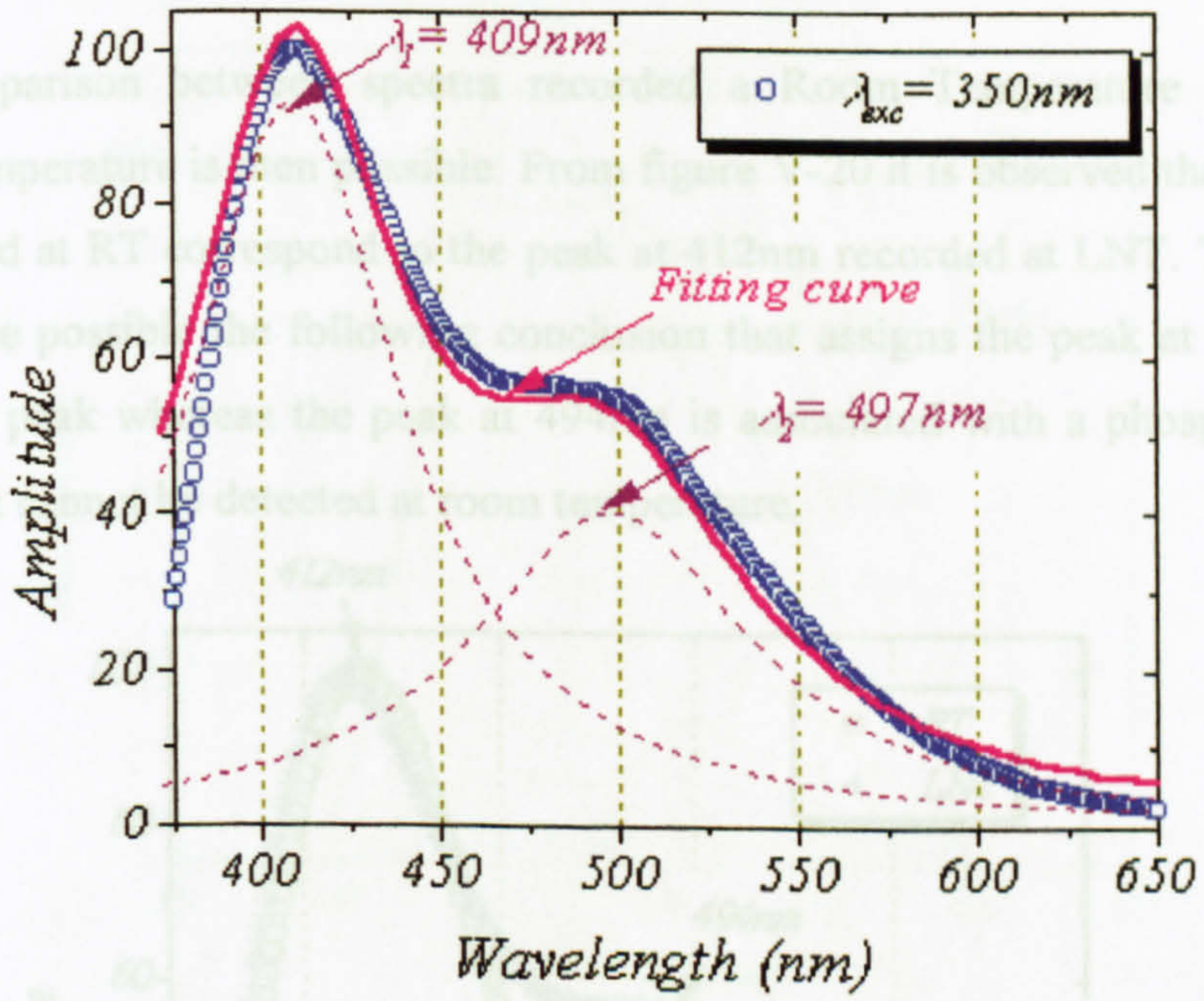

Figure V-19: Fitting curve $\lambda_{excitation}$= 350nm by the summation of two processes

In order to separate the two peaks Lorentzian functions have been used. This method was proposed by Teyssedre et al. [14] and it is described by the following expression:

$$EL(\lambda)=\sum_{i=1}^{2}\frac{2A_i\omega_i}{\pi}\frac{1}{\omega_i^2+4(\lambda-\lambda p_i)^2} \qquad (V.1)$$

Where the characteristics of the peak i are A_i is the area, ω_I the half-width, λp_i the wavelength. A conjugate-gradient non-linear least squares algorithm was used in order to optimise the parameters. The results are reported table V-2. The calculation was performed by estimation of the position of the two peaks associated with the components 1 and 2.

Component	**1**	**2**
λp (nm)	409	497
ω (nm)	71.7	95.4
A (counts.nm)	10548	6055

Table V-2: Details of the calculated components corresponding to the fit of photoluminescence spectrum recorded at $\lambda_{excitation}$= 350nm at LNT

A comparison between spectra recorded a Room Temperature and Liquid Nitrogen Temperature is then possible. From figure V-20 it is observed that the single peak recorded at RT correspond to the peak at 412nm recorded at LNT. This remark tends to make possible the following conclusion that assigns the peak at 412nm to a fluorescence peak whereas the peak at 494nm is associated with a phosphorescence emission that cannot be detected at room temperature.

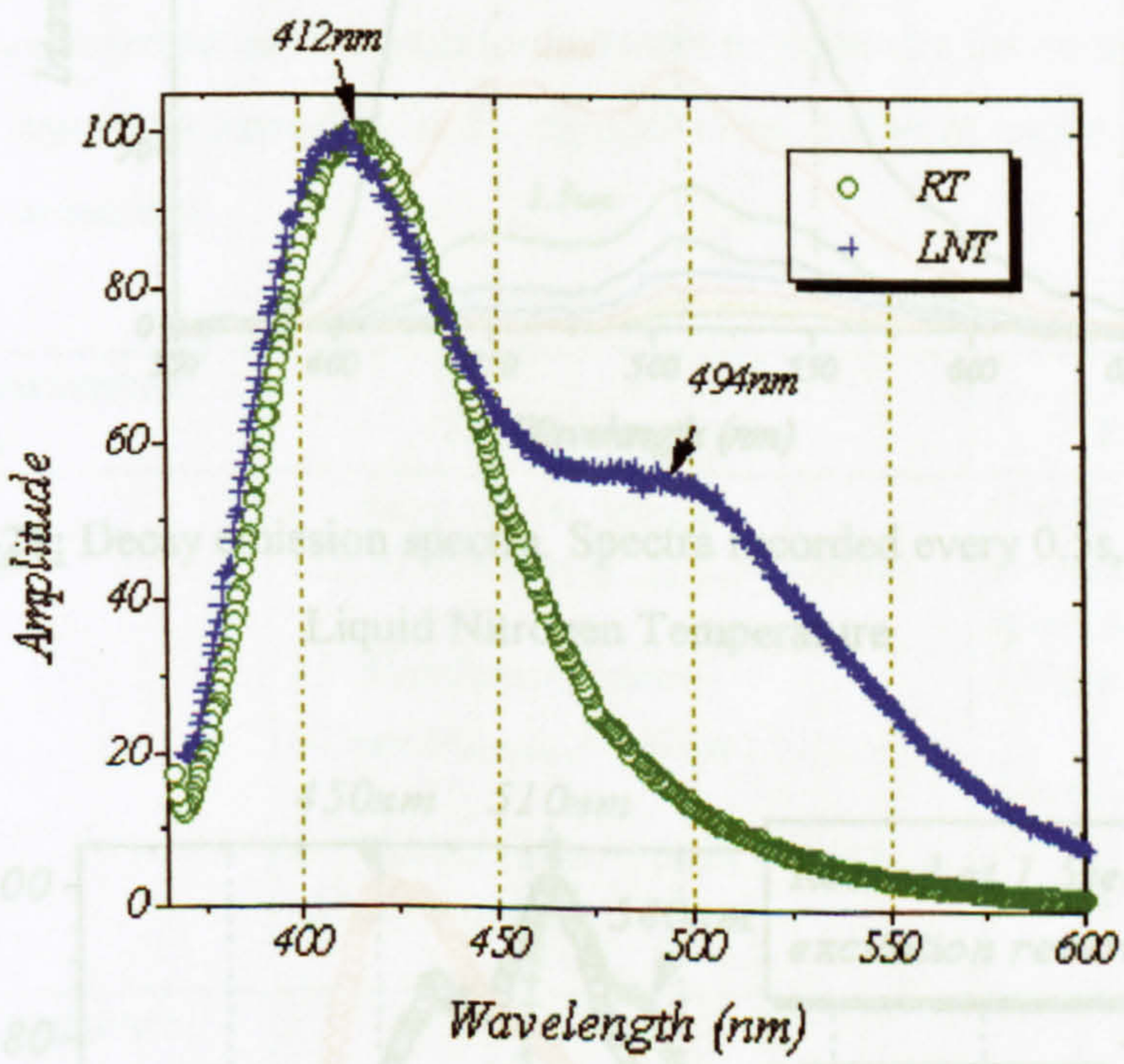

Figure V-20: Comparison of normalized photoluminescence spectra recorded at Room Temperature (RT) and Liquid Nitrogen Temperature (LNT)

Fluorescence and phosphorescence can be detected at LNT but remain difficult to distinguish. That is why, records have been made after the extinction of the source of excitation. In that situation, only the phosphorescence spectrum would be detected because the fluorescence decay is faster than the detection condition used in this experiment. UV-induced photoluminescence that lasts for several seconds have been recorded after the removal of the irradiation. The decay of light was afterwards recorded for three different excitation wavelengths only (280, 320, 360nm). The decay spectra obtained at $\lambda_{excitation}$= 320nm is reported in figure V-21.

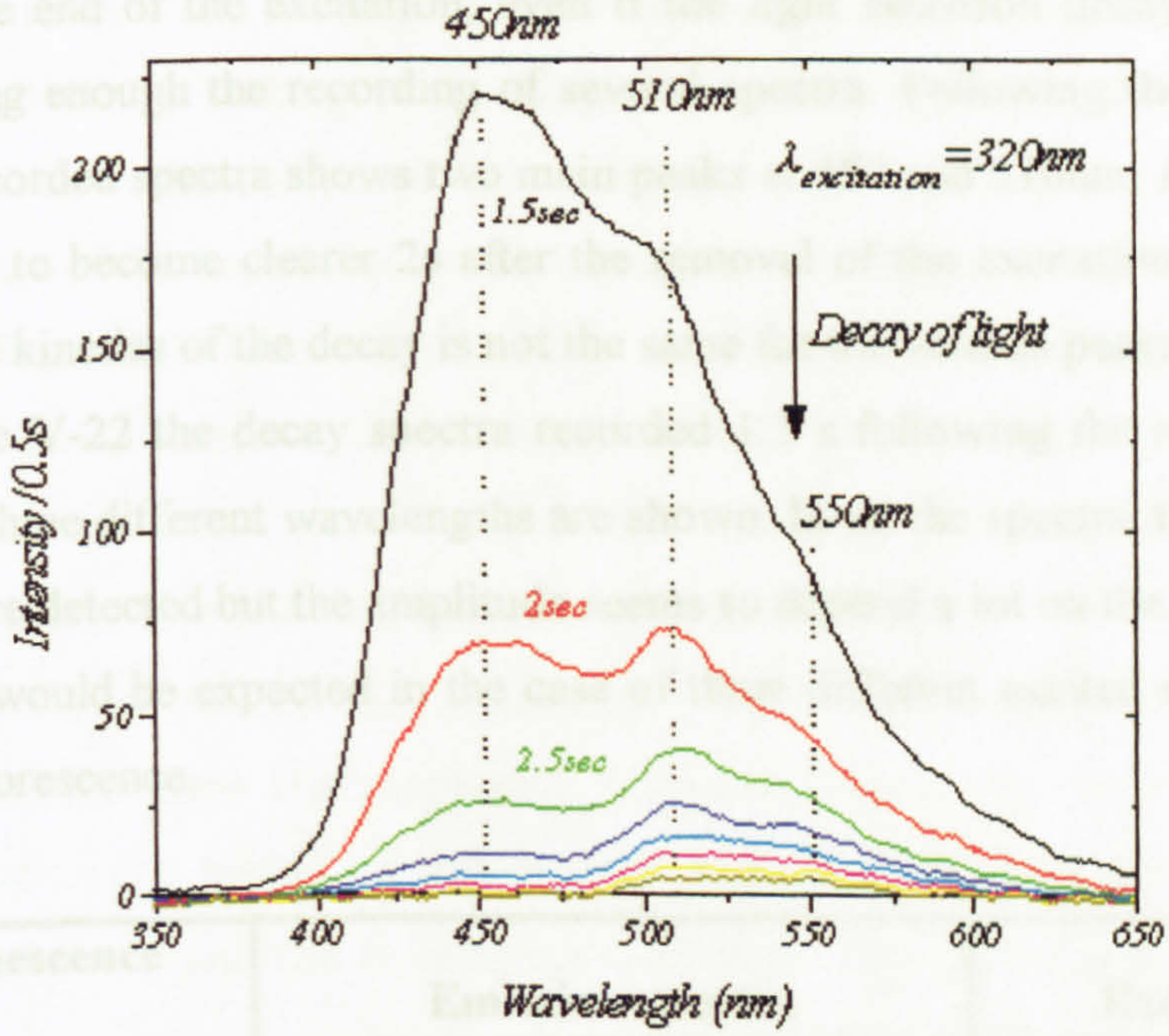

Figure V-21: Decay emission spectra. Spectra recorded every 0.5s, λ_{exc}= 320nm, Liquid Nitrogen Temperature

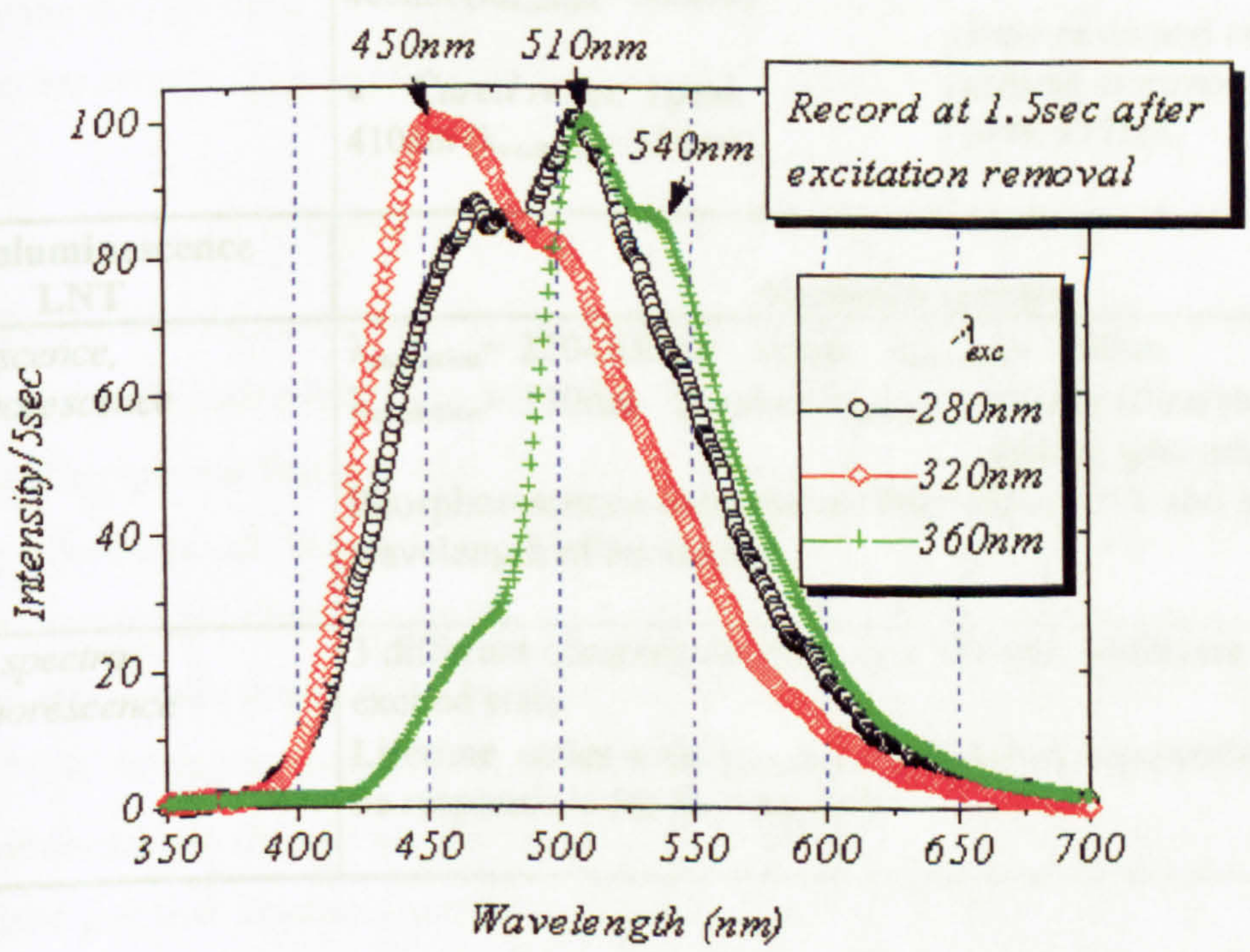

Figure V-22: Comparison of normalized decay spectra 1.5s after removal of the excitation light. λ_{exc}= 280, 320, 380nm, Liquid Nitrogen Temperature (LNT)

After the end of the excitation, even if the light emission decays rapidly, the lifetime is long enough the recording of several spectra. Following the excitation at 320nm the recorded spectra shows two main peaks at 450 and 510nm. A third peak at 550nm seems to become clearer 2s after the removal of the excitation. Moreover, it seems that the kinetics of the decay is not the same for the various peaks.

In figure V-22 the decay spectra recorded 1.5 s following the removal of the excitation at three different wavelengths are shown. In all the spectra, the three peaks of emission are detected but the amplitude seems to depend a lot on the wavelength of excitation as would be expected in the case of three different excited states involved in the phosphorescence.

Photoluminescence RT	**Emission spectra**	**Excitation spectra**
Fluorescence	• *Base resin:* 3peaks 325/375/400nm ($\lambda_{excitation}$= 305nm) • *Hardener:* 1peak 405nm ($\lambda_{excitation}$= 362nm) • *Cured resin:* 1peak 410nm ($\lambda_{excitation}$= 355nm)	*Hardener* and *Cured resin* present different excitation spectra with 1peak (363, 353nm respectively) *Base resin* and *cured resin* present common excitation peak 353nm.
Photoluminescence LNT	**Emission spectra**	
Fluorescence, phosphorescence	$\lambda_{excitation}$= 220-300nm 1peak $\lambda_{emission}$= 424nm $\lambda_{excitation}$> 330nm 2peaks $\lambda_{emission}$= 412nm (fluorescence), 494nm (phosphorescence) Phosphorescence component observed at LNT and high wavelength of excitation	
Decay spectra phosphorescence	3 different components 450, 510, 550nm: 3different type of excited state Lifetime varies with $\lambda_{excitation}$, one of this chromophores may also be responsible for fluorescence	

Table V-3: Summary on photoluminescence emission peaks of the cured resin at RT and LNT

So to summarise this section, photoluminescence features of the cured resin are reported table V-3. By looking at the excitation spectra for both the base resin and cured resin, it is found that there is a common peak at 353nm. In addition, the emission spectra of the base resin at that excitation wavelength is expected to give an emission at 400nm and 375nm with the same amplitude. It is possible to think that the origin of the light emission is the same for the base resin and the cured resin. Note also that in the cured resin only the excitation at 353nm seems to be susceptible to excite state that give rise to a single transition at 412nm.

These emission peaks at $\lambda_{emission\text{-}base\text{-}resin}$= 400nm and $\lambda_{emmision\text{-}cured\text{-}resin}$= 410nm may be due to the same chromophores. The actual shift may be associated with excimer formation that would explain that the excitation spectra are different in both cases. This excimer could lead to complex fluorescence or phosphorescence emission spectra.

III.2.2- Luminescence associated with recombination

Emission of light is often linked to recombination of charge carriers on luminescent centres. The centres may be difficult to identify.

III.2.2.1- Data acquisition and treatment of the information

The principle consists in providing charges of both polarities to the surface of the sample and determining the recombination mechanism from the light decay kinetics. The spectral features after the end of the excitation are also recorded so as to identify the chemical nature of the light emission centre. In the present case the charges are supplied to the system by cold plasma excited by dc voltage stress.

At atmosphere pressure, an Helium discharge radiates photons with energy up to 20eV. This is more energetic than the irradiation beam used in the case of photoluminescence. A cold plasma is not only a high energetic light source but also an ionised gas that irradiates the surface of the material by electrons, ions, radicals and excited neutral particles. Ions that arrive at the surface of the polymer do not penetrate deeply into the bulk. Charge trapping and subsequent recombination then occur in the first atomic layer. The luminescence is excited during recombination process of trapped electric charges.

III.2.2.2- Protocol

The experiments were carried out on sample films of 55μm thickness. The discharge is produced between two plane parallel electrodes. The sample lies on the lower electrodes whereas the second electrode is deposited on a quartz plate. This configuration leads to the formation of the discharge between the two dielectric materials. The plasma gap is about 5mm. Before introducing the He, the system was evacuated to 10^{-5}Pa.

Two treatments were recorded on the same sample to check the reproducibility of the response and that the cold plasma does not damage the surface of the polymer under investigation too much. It was reported that if a short plasma interaction time was used, i.e. in the order of 5s [15], that the surface of the material was only slightly modified.

The light is recorded by the photomultiplier as a function of time after the end of the excitation. Three main regimes can be observed:

- *1-3s* the regime is associated with photoluminescence emission induced by UV irradiation. It is related to phosphorescence since the light is recorded after the end of the excitation and it is performed at LNT.

- *4-20s* this part is usually associated with chemiluminescence emission during which some chemical damage occurs to the surface of sample due to the energy provided by the cold plasma.

- *Above 20s*, this is the plasmaluminescence regime. It is due to carrier recombination and is dominant for a time longer than 1min.

The luminescence decay curve (figure V-23) is fitted as presented by Tesseydre et al [16] by the equation proposed in the case of the analysis of polyolefins.

$$I(t) = A_1 \exp\left(-\frac{t}{\tau_1}\right) + A_2 \exp\left(-\frac{t}{\tau_2}\right) + A_3 t^{-m} \qquad \text{(V.2)}$$

The first two regimes can be fitted by an exponential decay whereas the last one is associated with a power law.

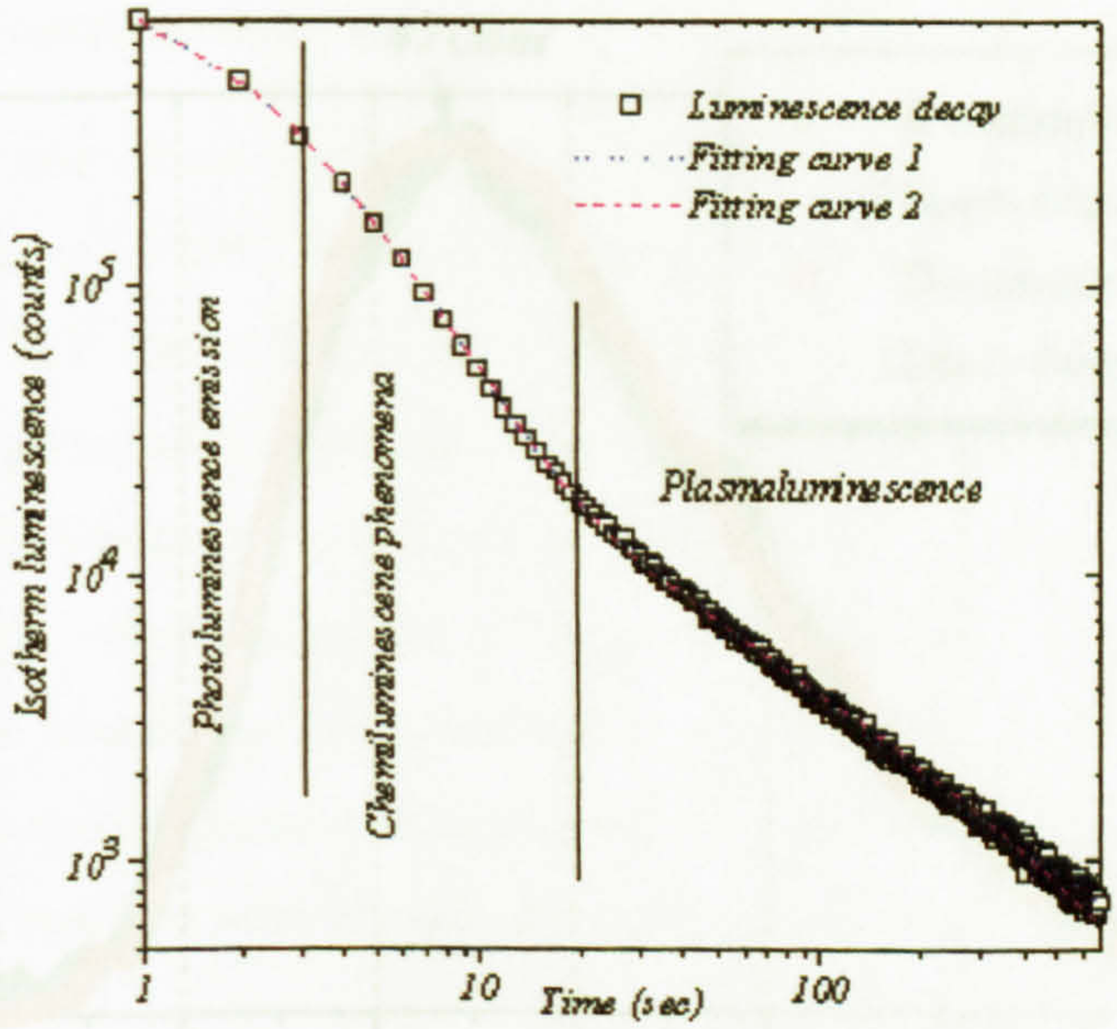

Figure V-23: Amplitude of induced-plasma luminescence as a function of time, -185°C,

fitting equations 1: $3.29x10^5e^{-t/6.64}+9.82x10^5e^{-t/1.44}+1.37x10^5/(1+0.3816t)+208$

fitting equation 2: $1.83x10^5e^{-t/4.79}+9.59x10^5e^{-t/1.73}+1.55x10^5t^{-0.7819}-341$

III.2.2.3- Recombination spectra

As time passes after the end of the excitation, the spectrum evolves. Actually after 20s following the removal of the stress the plasmaluminescence regime is reached. The corresponding spectra have been reported, figure V-24.a, for both consecutives treatments. As observed the response remains the same. If compared with the photoluminescence spectra recorded at low temperature after removal of the excitation (figure V-24.b)) it is noticeable that similar emission at 468-470nm is detected in both cases. On addition a peak at 540nm may also be common. This peak was detected more clearly following an excitation at 360nm (figure V-22). This remark makes one think that the same type of chromophores are involved in both emissive processes that have been identify as phosphorescence emission.

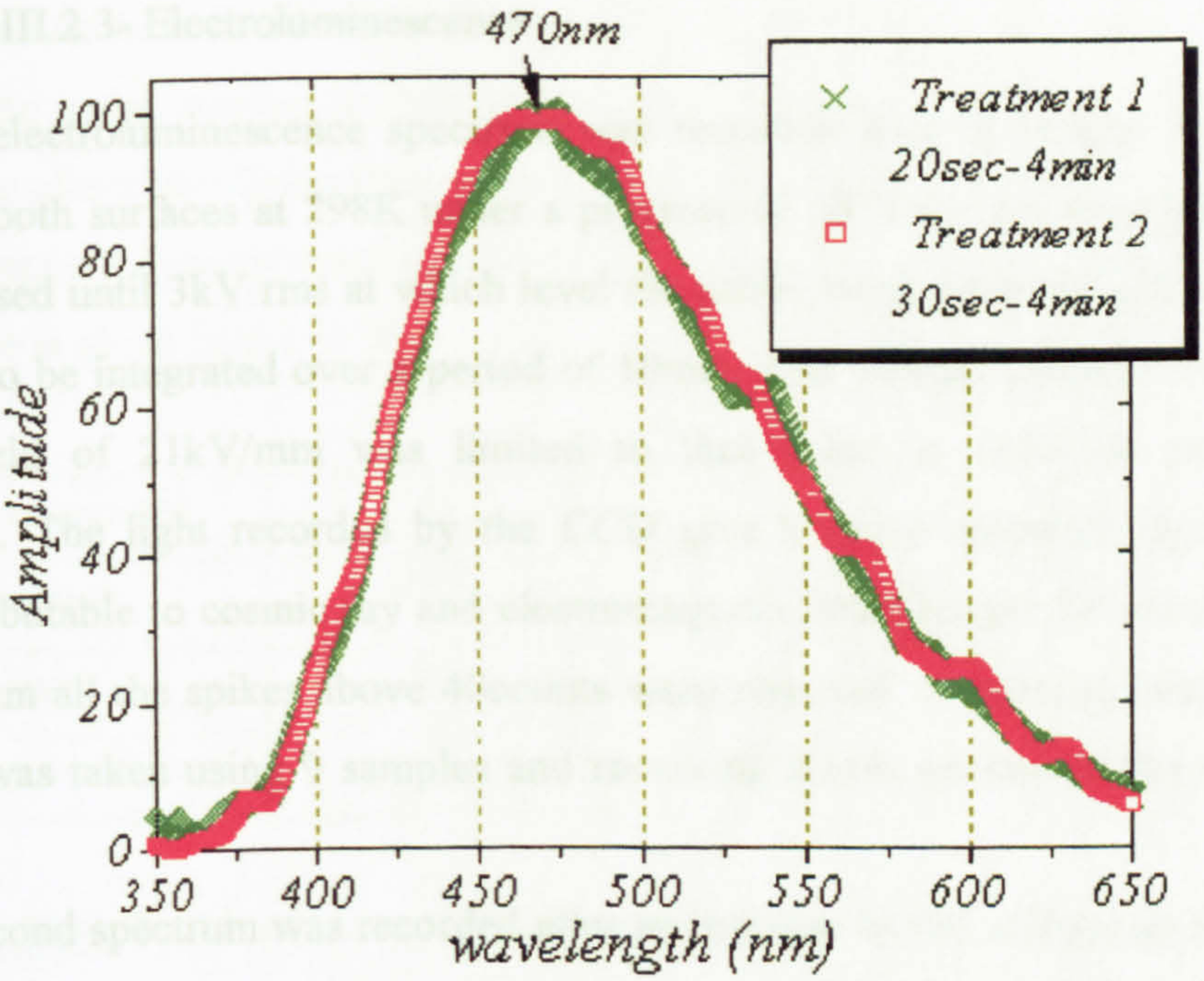

(a) Treatment 1: mean of light detected between 20s and 4min

Treatment 2: mean of light detected between 30s and 4min

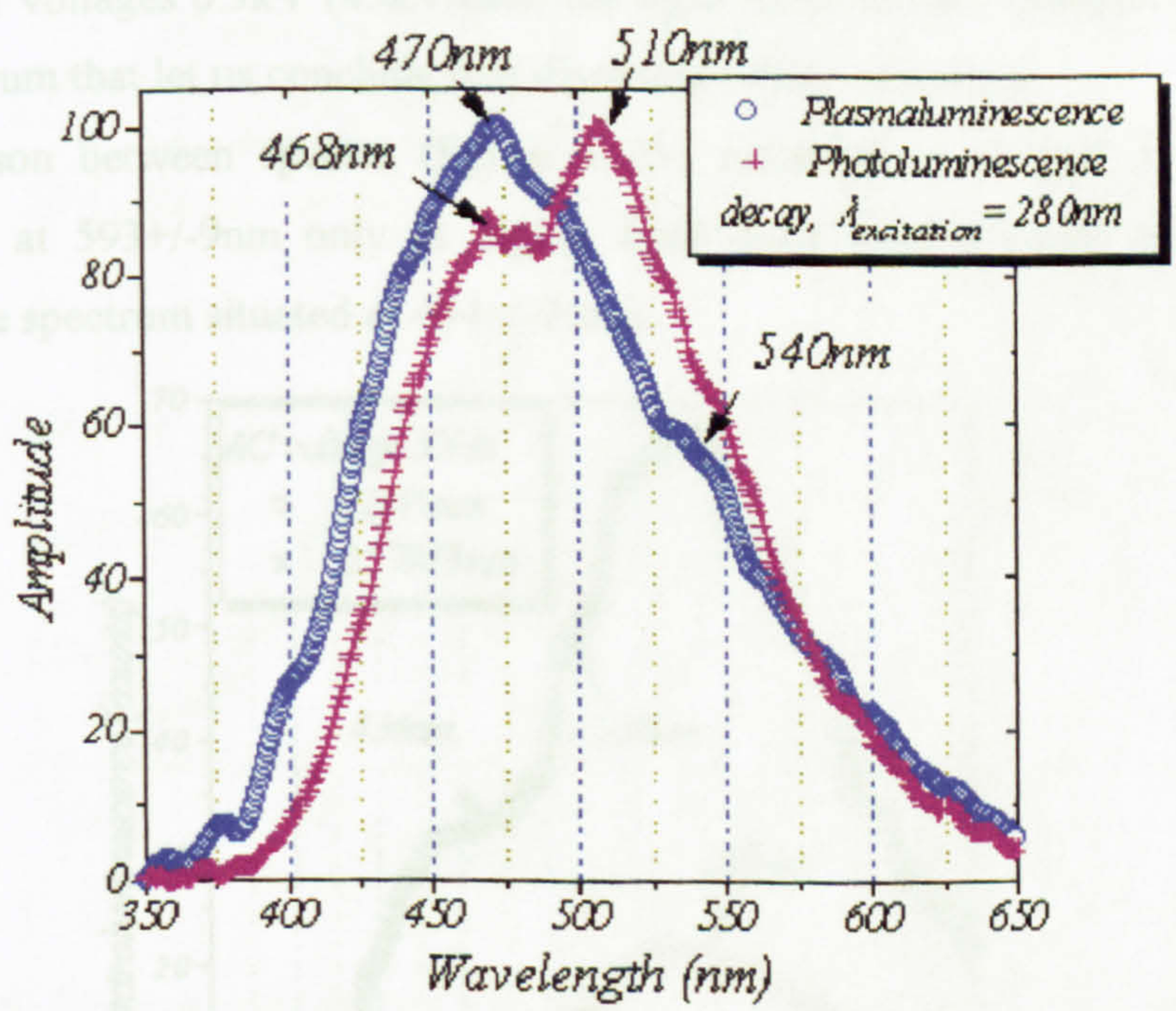

(b)

Figure V-24: **(a)** Normalised induced-plasma luminescence spectra recorded between 20s and 4min after the removal of the stress, -185°C, on treatment 1and 2.

(b) Comparison of plasmaluminescence, decay of photoluminescence recorded at LNT

III.2.3- Electroluminescence

The electroluminescence spectrum was recorded from a 140μm sample gold coated on both surfaces at 298K under a pressure of 10^{-6}Torr. An ac voltage (50Hz) was increased until 3kV rms at which level the rather weak emitted light was judged sufficient to be integrated over a period of 10min. The voltage leading to an applied electric field of 21kV/mm was limited to that value in order to prevent any breakdown. The light recorded by the CCD give a noisy spectrum dominated by spikes attributable to cosmic ray and electromagnetic interference. In order to extract the spectrum all the spikes above 40counts were removed. A moving average of the spectrum was taken using 9 samples and removing points exceeding the average by 10 counts.

A second spectrum was recorded after an increase of the voltage up to 5kV rms (35.7kV/mm). This time the noise above 80counts was removed and the same moving average was carried out to extract the spectrum.

At higher voltages 6.3kV (45kV/mm) the light level became unstable giving an unstable spectrum that let us conclude that discharges were occurring.

Comparison between spectra (figure V-25) recorded at 21 and 35.7kV/mm shows a peak at 593+/-9nm only at higher field does another peak appear as a shoulder on the spectrum situated at 454+/-20nm.

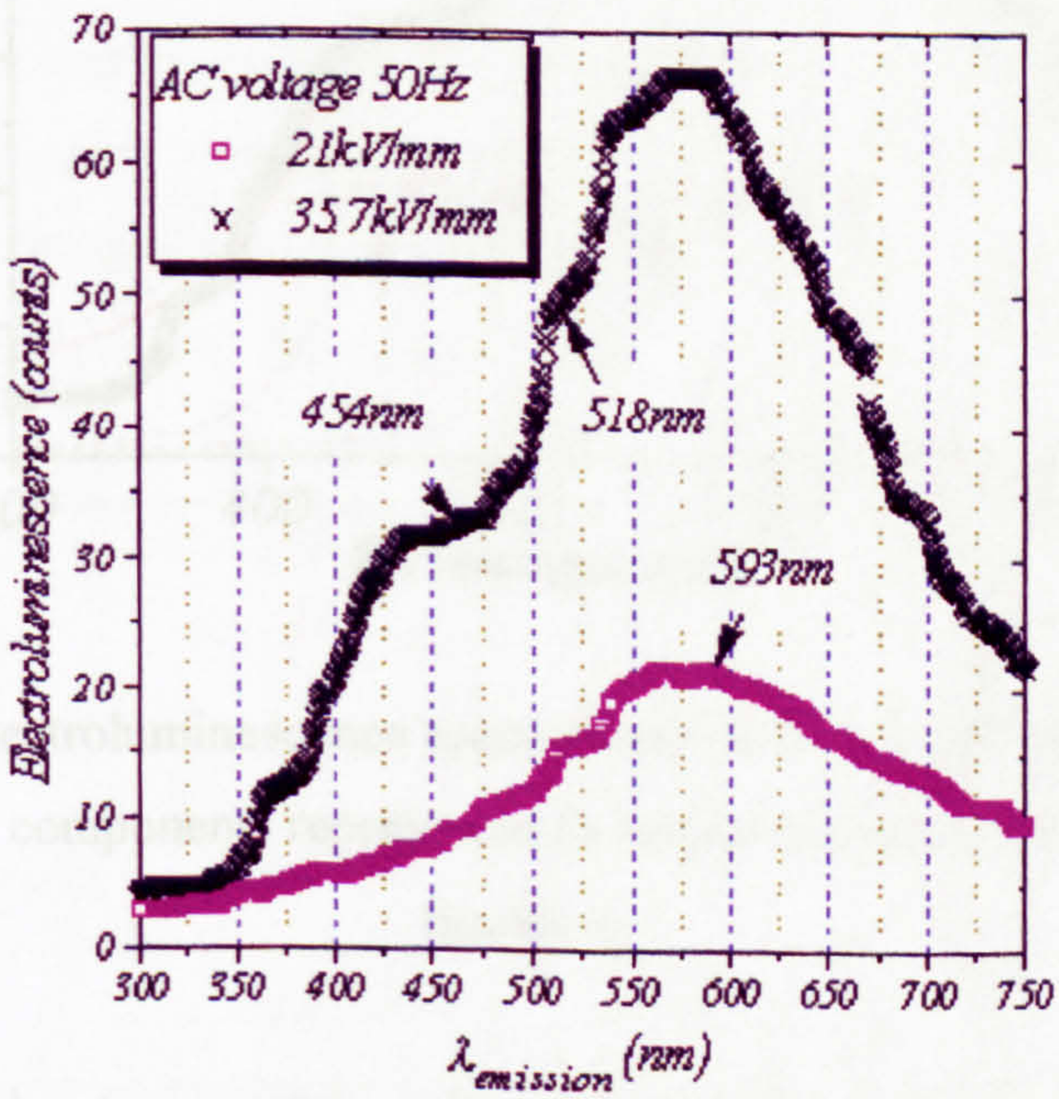

Figure V-25: Electroluminescence spectra, 298K, ac voltage excitation source 21 and 35.7kV/mm

Lorentzian functions have been used to split the total spectrum into 3 functions by using the same method as before that was described by the equation V-1. A conjugate-gradient non-linear least square algorithm was used to find optimum values of the parameters. Finally, results are reported table V-4. The various peaks and total fitting curve is given figure V-26.

Component	1	2	3
λp (nm)	435	541	599
ω (nm)	54	65	207
A (counts.nm)	1165	1544	19445

Table V-4: Details of the calculated components corresponding to the fit of electroluminescence spectrum recorded at 35.7kV/mm

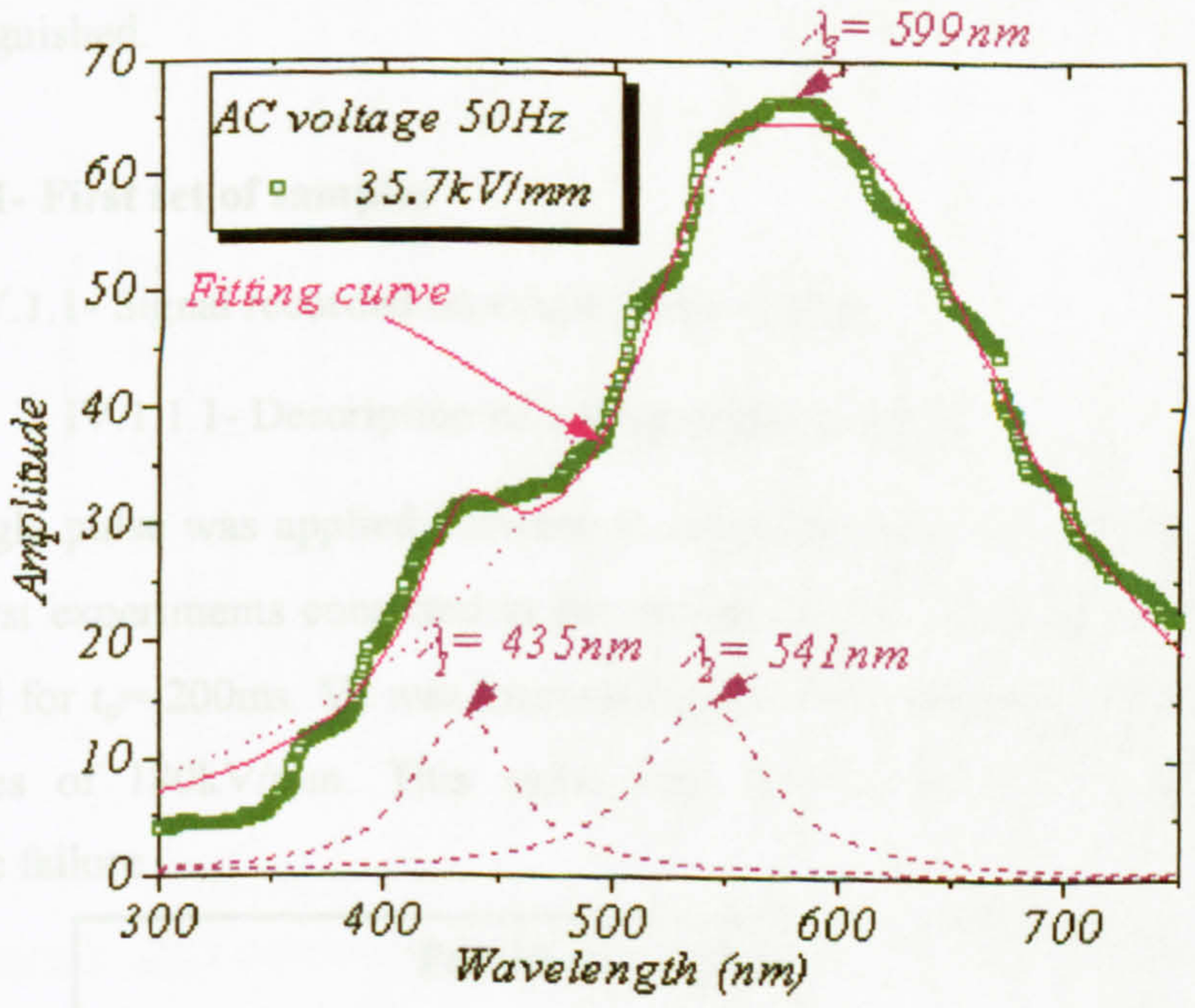

Figure V-26: Electroluminescence spectra recorded at 35.7kK/mm, fitting curve combination of 3 components represented in dashed lines associated to Lorentzian functions

It is possible to compare the results with those obtained for the photoluminescence at LNT. It is found that the peaks at 435 and 541nm appear in the domain of the phosphorescence emission. However, the peak at 599nm might be seen

as another phosphorescent component or a peak due to degradation of the material by a chemical pathway of relaxation.

IV- Electroluminescence under divergent field configuration

Measurements have been carried out on samples with 10µm diameter wires at room temperature, i.e. 25°C. As the wires are used as an electrode, only one side was conditioned with a gold metalization electrode of 300Å and 35mm diameter. A square voltage pulse was first applied from the upper ring electrode in contact with the coated electrode whereas the wires were connected to earth. The light emitted was recorded on the single pulse then pulses of opposite polarities were added. The first measurements consisted in the determination of the influence of each parameter on the light emission such as the polarity, the amplitude, the time of application of both the polarization voltage and pulse. Two sets of samples giving different responses were distinguished.

IV.1- First set of samples

IV.1.1- Signal recorded on single pulse voltage

IV.1.1.1- Description of voltage pulse and light

A single pulse was applied between the top electrode and the wires (figure V-27). The first experiments consisted in the record of the light emitted as the voltage was applied for t_p= 200ms. V_0 was increased up to 3kV, leading to a maximum field at the wires of 180kV/mm. This value was not exceeded in order to prevent catastrophic failure.

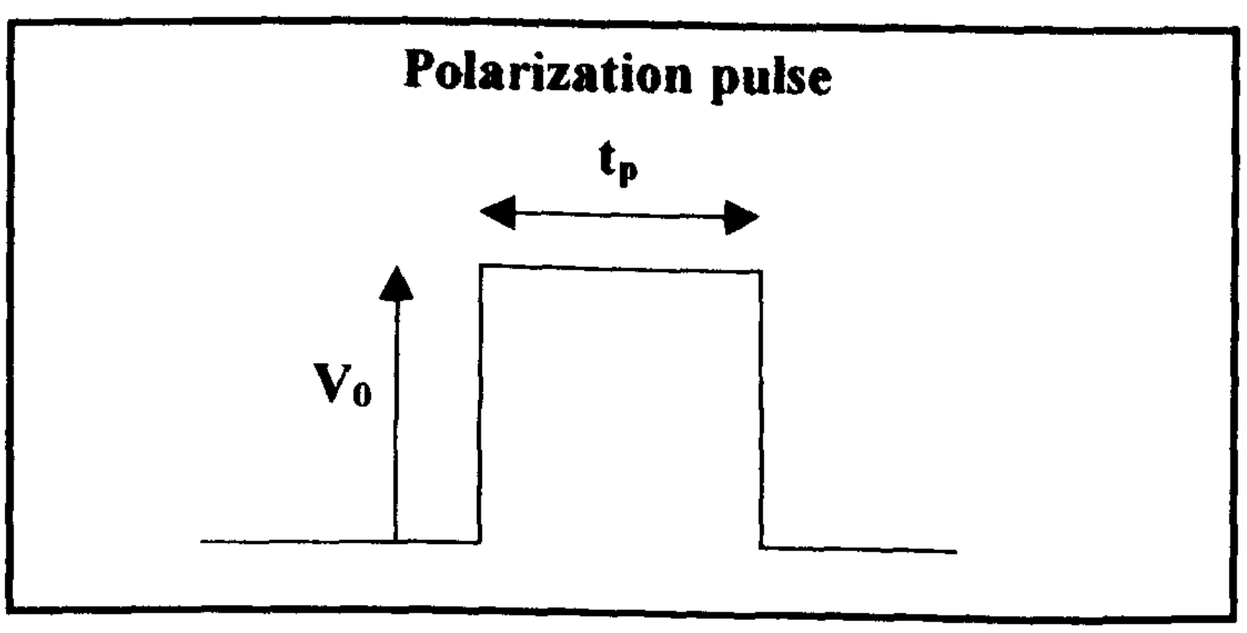

Figure V-27: Shape of the polarization pulse applied.

V_0 Positive or negative polarization voltage, t_p Polarization time.

A peak of luminescence was observed at the beginning of the voltage application and another one was detected at its removal. No luminescence was detected apart from some noise during voltage application (figure V-28). In the absence of any voltage application the photomultiplier detects a signal that corresponds to a noise of 2counts/s, i.e 2.10^{-3}counts/ms. Therefore for a sampling time of 4000ms, 8 counts should be detected on the whole range. However, the luminescence recorded at the beginning and at the end of the polarization can be extracted from the noise level even if it is about 4 counts because of the time correlation between the pulse generator and the signal detector. (It has been verified that the polarization voltage does not generate parasitic signals by electromagnetism interference with the counting unit when switched the voltage on and off.)

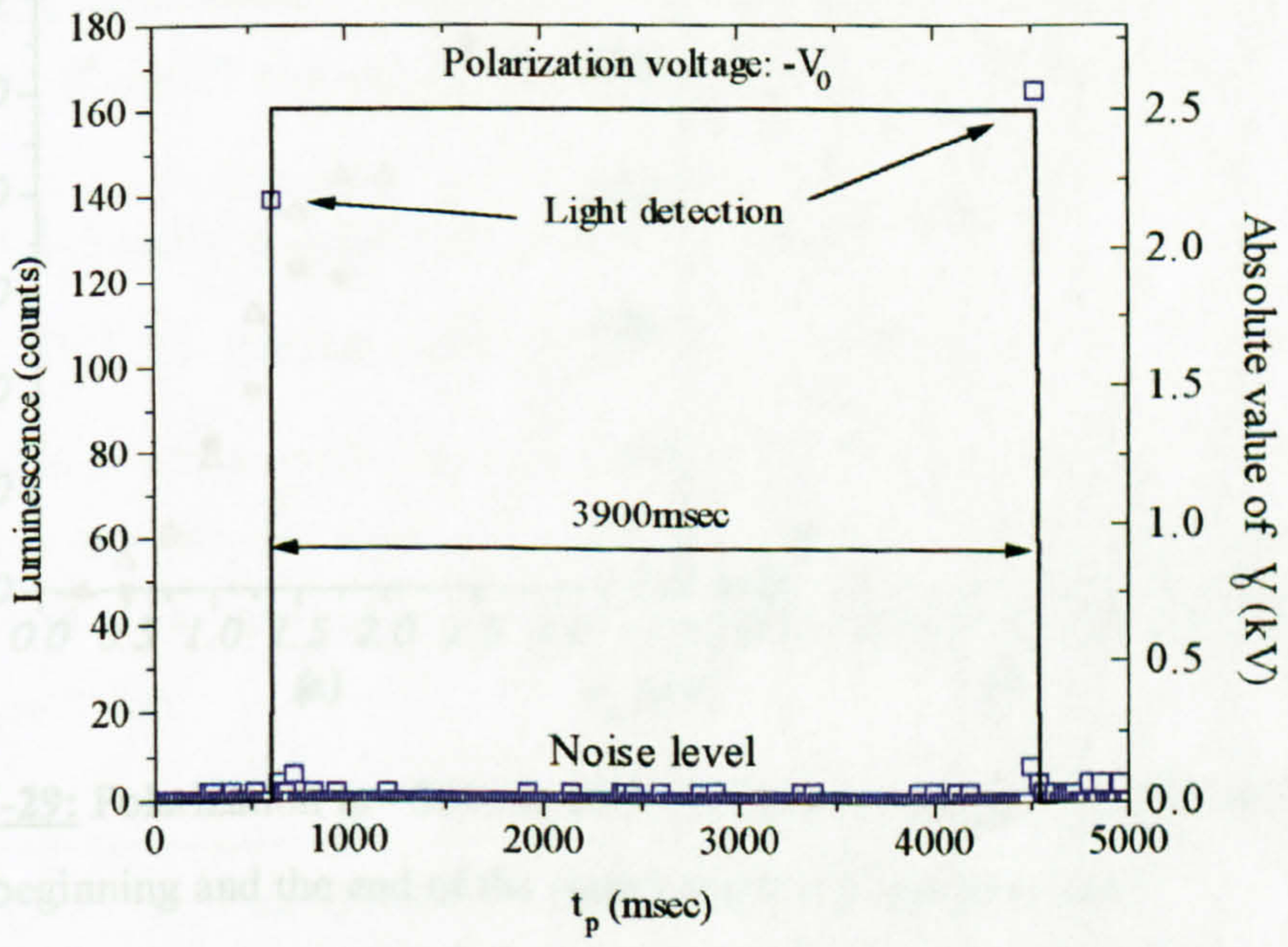

Figure V-28: Luminescence recorded while V_0= –2.5kV, t_p= 3900ms, 25°C

IV.1.1.2- Effect of various parameters

Various parameters have been taken into account. First of all, the voltage applied for 200ms was raised from 0 to 3kV (≈ 180kV/mm) and the amplitude of light recorded on the switch-on and switch-off compared. It has been observed that they have similar amplitude over the whole range investigated. Light starts to be detectable above 0.5kV and the emission amplitude increases with the voltage (figure V-29.a).

However, this value can change a little from sample to sample. This variation was associated with the number of wires and the sample thickness on which the electric field depends.

Secondly, the influence of the polarity of the applied voltage has been studied. The total light emitted during voltage application (volt-on and volt-off peak of emission added) were compared. When either a positive or negative voltage was applied from the upper ring electrode, as shown in figure V-29.b, the same amount of emitted light was recorded whatever the polarity of the voltage.

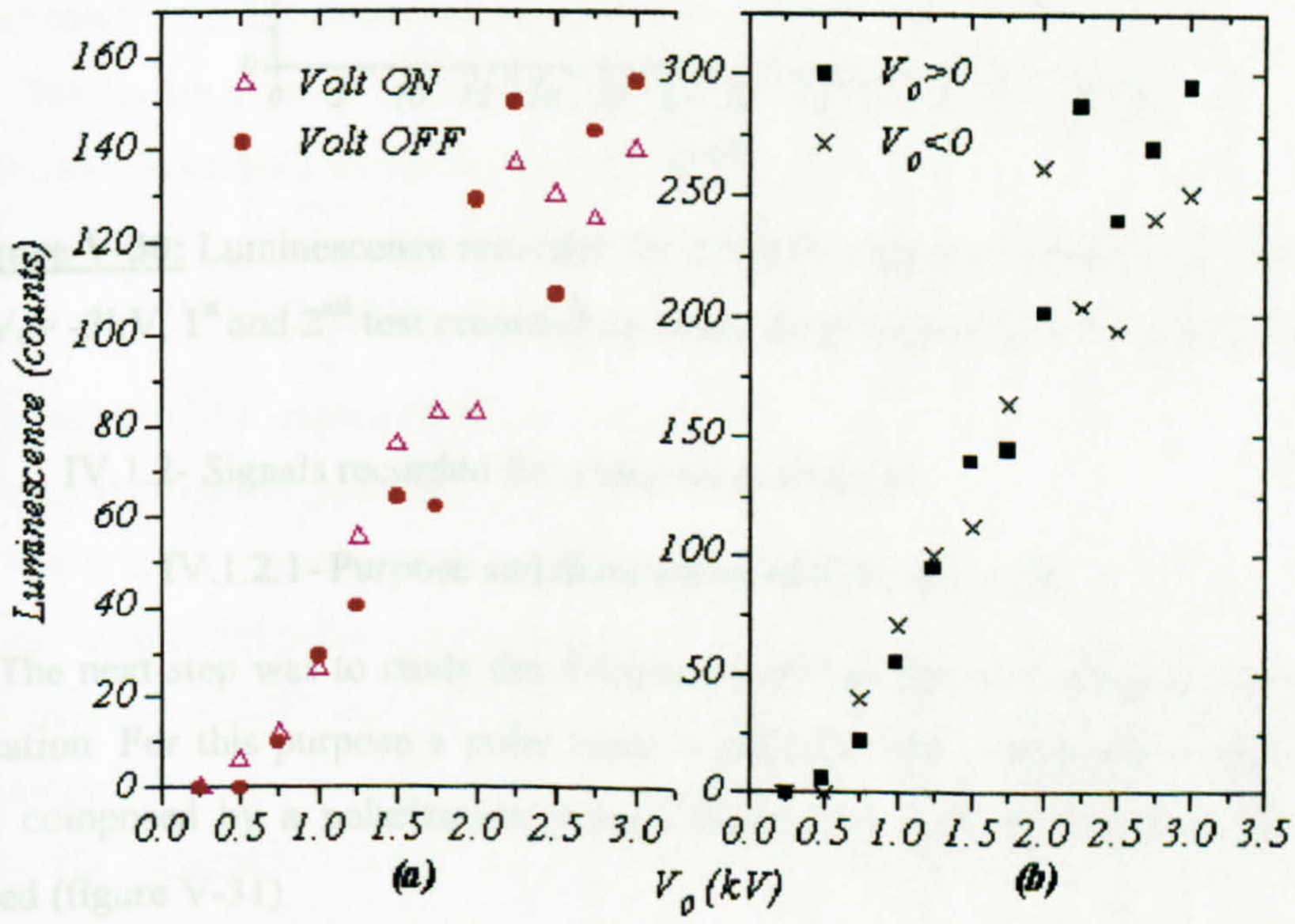

Figure V-29: Polarization tp= 200ms, 25°C, **(a)** Luminescence recorded at the beginning and the end of the polarization voltage application
(b) Total luminescence recorded for positive and negative pulse voltage

Finally, the effect of the polarization time t_p of voltage application was investigated. In these experiments the polarization voltage was kept constant. Tests repeated on different samples are presented in figure V-30. In this case V_0 was fixed to -3kV (-180kV/mm) and t_p was varied from 0.3 to 60s. The measurements seem to be essentially constant with some occasional deviations. It was therefore assumed that above 300ms the system was already saturated by charges and the increase of the polarization time was not relevant. It might however be interesting to work by using shorter periods of polarization.

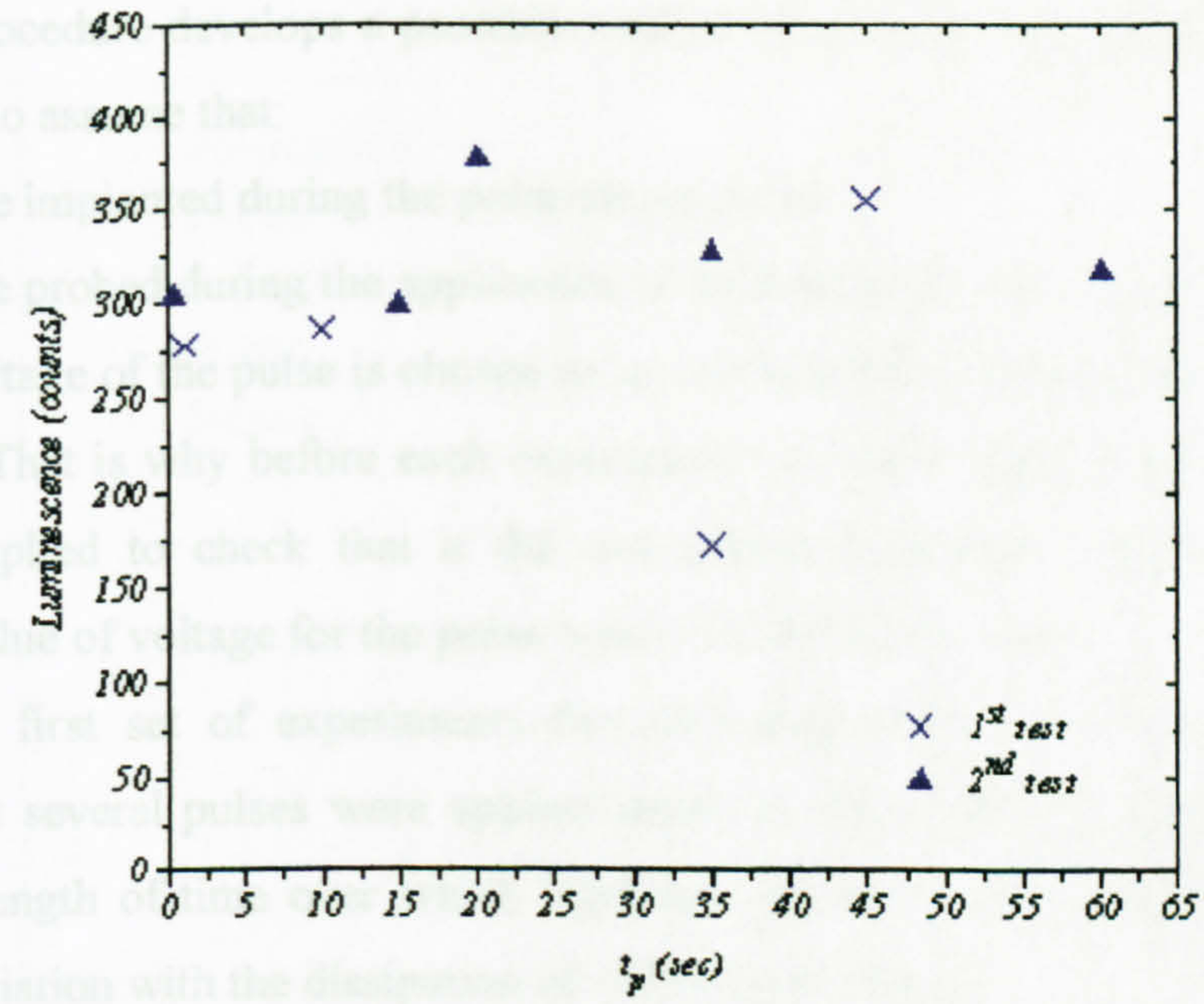

Figure V-30: Luminescence recorded for different values of polarization time t_p. V_0= -3kV, 1st and 2nd test recorded on same sample keeping same conditions

IV.1.2- Signals recorded for a sequence of pulses

IV.1.2.1- Purpose and description of the experiment

The next step was to study the dissipation of the charges following the voltage application. For this purpose a pulse train is added to the experimental protocol. A signal composed by a polarization pulse followed by a pulse train has thus been selected (figure V-31).

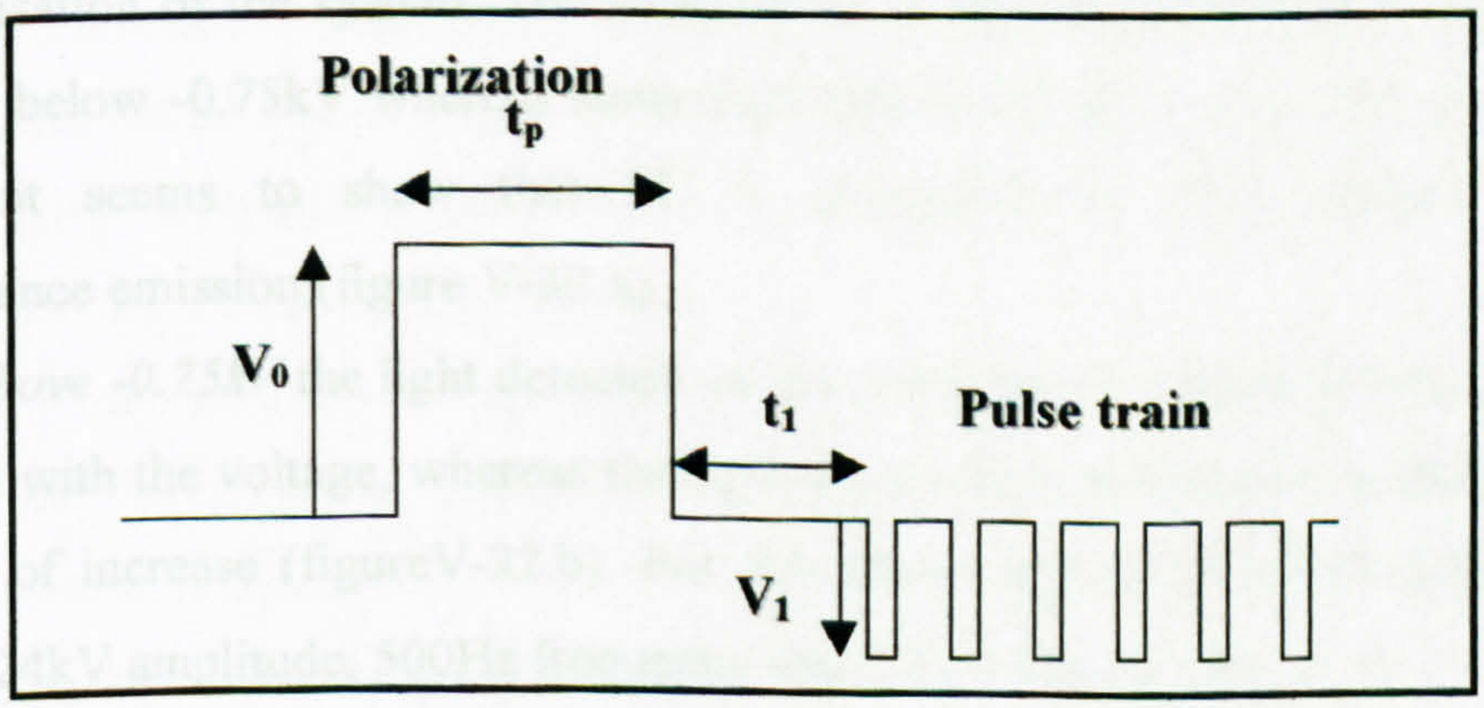

Figure V-31: Shape of the polarization pulse applied with pulse train. V_0 polarization voltage, t_p Polarization time, V_1 pulse voltage, t_1 time between polarization and first train-pulse

This procedure develops a possible method of space charge probing in which it is necessary to assume that:

- SC are implanted during the polarization pulse

- SC are probed during the application of subsequent pulses of opposite polarity

The voltage of the pulse is chosen so as not to produce some light when applied on its own. That is why before each experiment on a new sample the pulse voltage only was applied to check that it did not induce detectable light emission. The maximum value of voltage for the pulse was +/-0.5kV in all cases.

In this first set of experiments the minimum value of t_1 was 1s. In each measurement several pulses were applied until no more light was detected on each pulse. The length of time over which light was detected was called the dissipation time in association with the dissipation of the injected charges.

IV.1.2.2- Effect of various parameters

In most of the experiments the polarization voltage was negative and thus the pulse train voltage was positive.

The first few measurements consisted in recording the light on the polarization pulse and on the first pulse as the amplitude of the polarization was raised.

- *Between -0.25kV and -0.75kV* the light recorded on the polarization and on the first four pulses of the train is reported in figure V-32.a. The pulse train characteristics were 0.5Hz frequency, 0.1s duration and amplitude +0.5kV with t_1= 1s.The amount of light recorded on each pulse was small but was clearly identified due to the time synchronisation of the system. The polarization lasting for 200ms does not generate any light below -0.75kV whereas some light was detected on the train pulses. This experiment seems to show that SC is implanted at "low voltage" without luminescence emission (figure V-32.a).

- *Above -0.75kV* the light detected on the polarization voltage lasting for 300ms increased with the voltage, whereas the light on the first pulse remains small without any sign of increase (figureV-32.b). For this measurement the pulse characteristics were +0.24kV amplitude, 500Hz frequency and 0.1s duration with t_1= 1s.

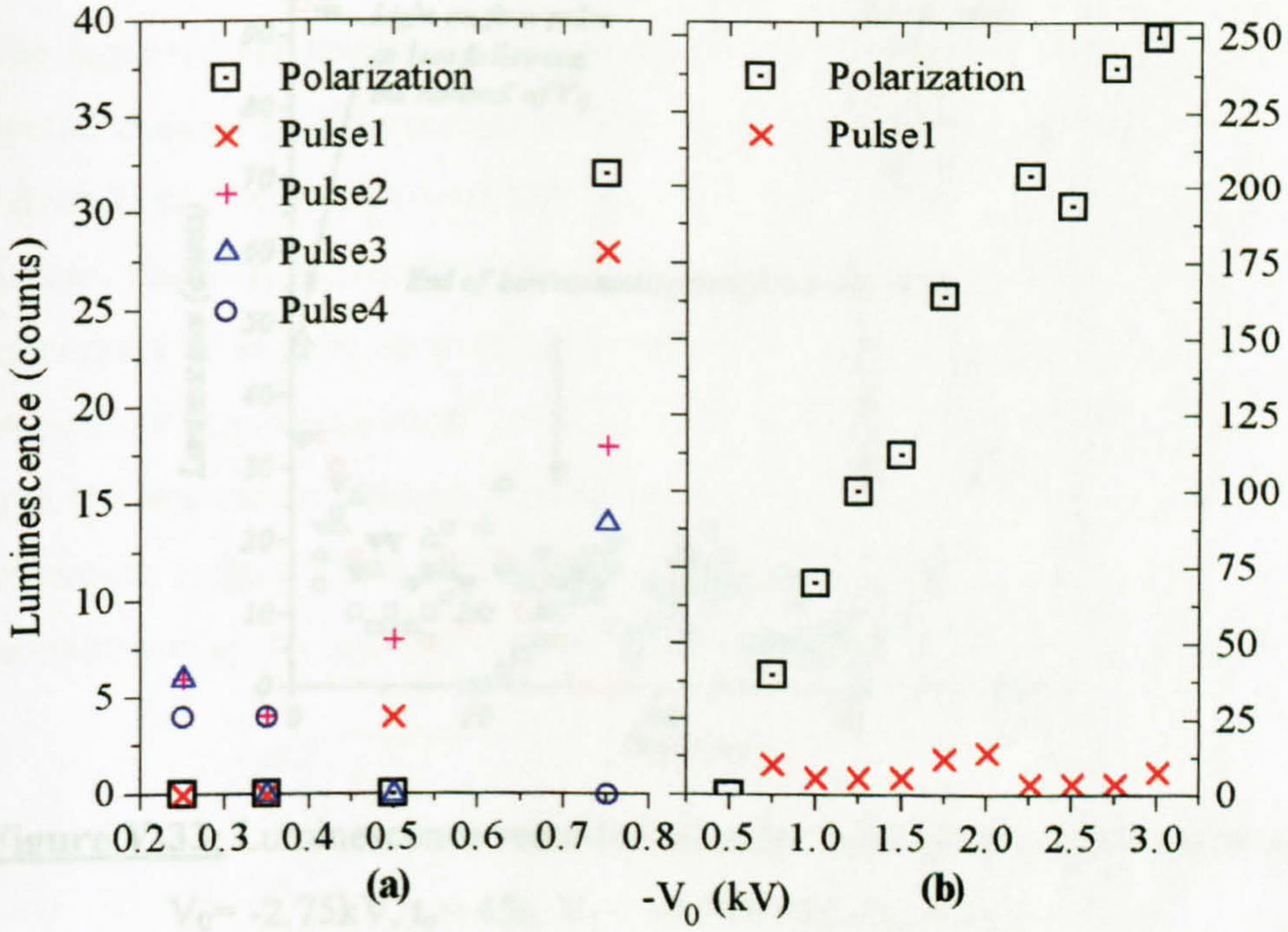

Figure V-32: Luminescence recorded on the polarization and train pulses characteristics t_1= 1s, 0.1s **(a)** t_p=200ms, V_1 0.5Hz **(b)** t_p=300ms, V_1 500Hz

The next investigation consisted in studying the length of time between the end of the polarization and the last pulse giving some measurable light. Three values of polarization were selected V_0 (-2, -2.5, -2.75kV).

First of all V_0 and tp were fixed to –2.75kV and 45s respectively, and the same light measurement on pulse train repeated on the same sample after a minimum grounding period of 10min. The pulse characteristics were V_1= +0.5kV, 0.5Hz, 0.1s duration. Large fluctuations have been recorded in the number of pulses on which some light was detected, i.e. the length of time before no more light become detectable. These values were spread between 29 and 75s (figure V-33). However it is observed that the amount of light decreases rapidly on pulses after the removal of the polarization and the first one at 1s always gives the highest amplitude of light.

Then t_p has been changed keeping V_0 constant. The same measurements were performed after minimum period of rest of 10min. Once again large fluctuations in the time over which light is recorded on the pulse train has been observed. The t_p values used for the results presented in figure V-34 were 200ms, 20, 45 and 60s.

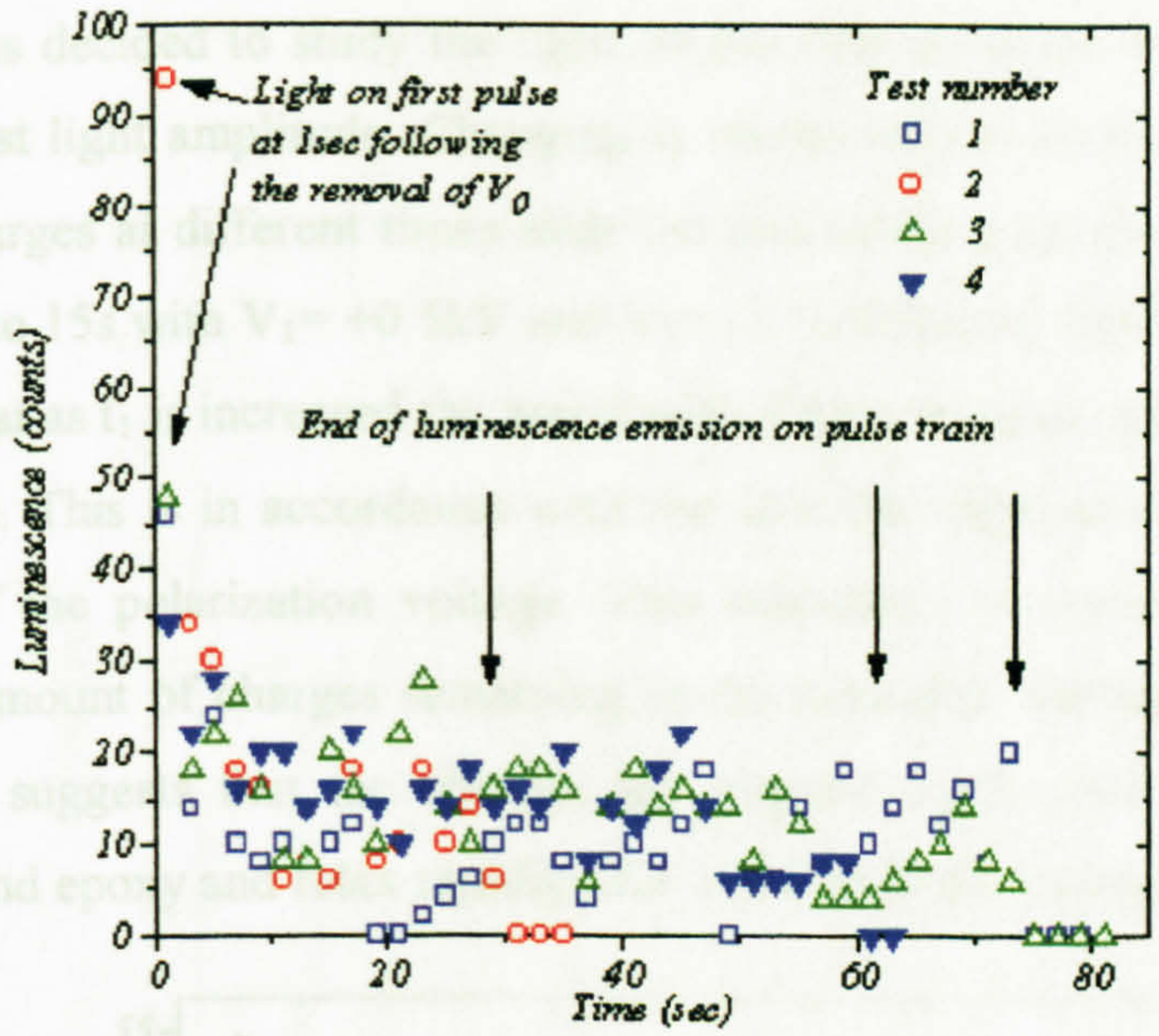

Figure V-33: Luminescence recorded on pulse train following polarization

V_0= -2.75kV, t_p= 45s, V_1= +0.5kV, 0.5Hz, 0.1s, t_1= 1s

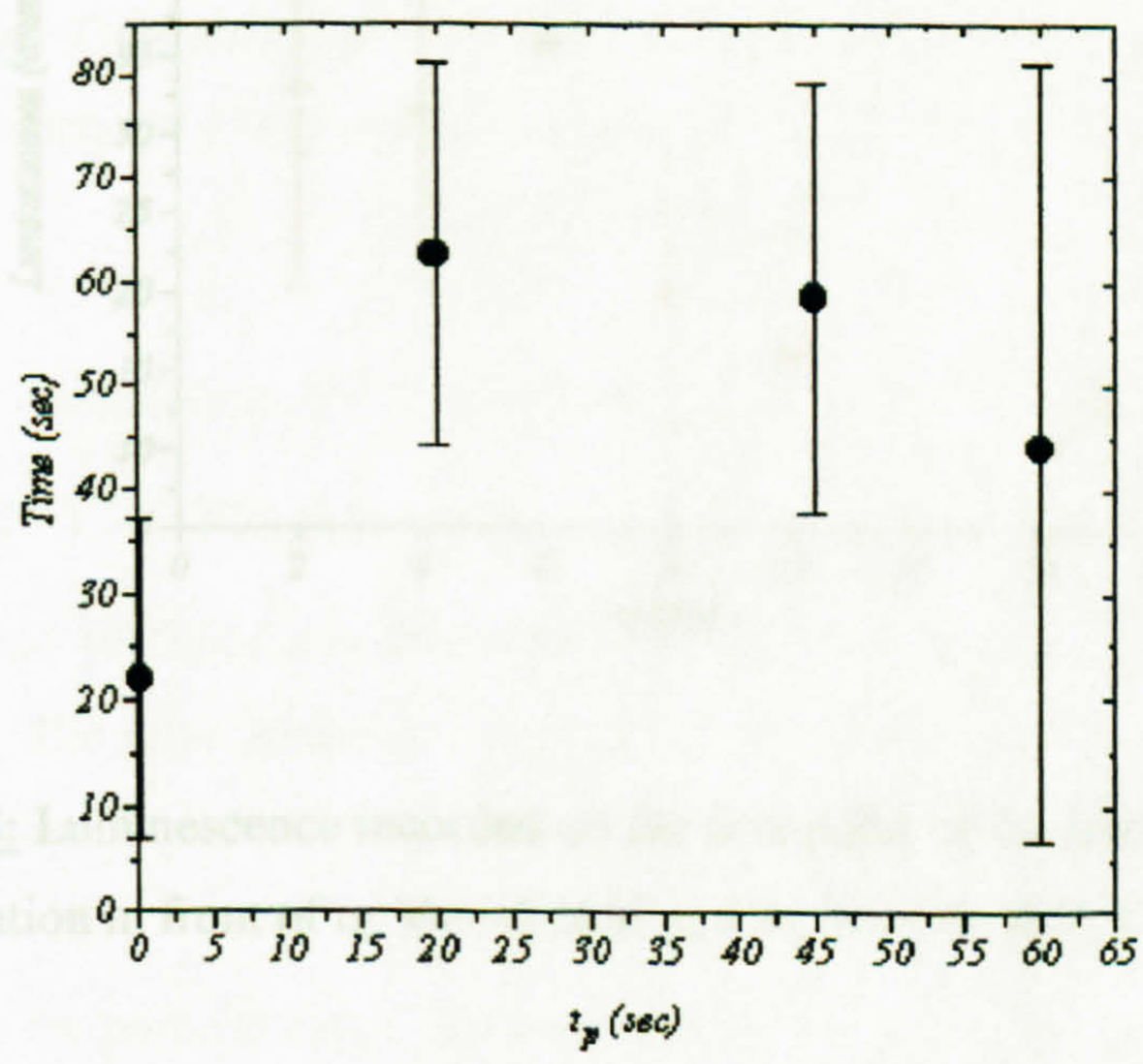

Figure V-34: Time during which light is detected on pulse as a function of t_p.

V_0= -2.75kV, V_1= +0.5kV, 0.5Hz, 0.1s, t_1= 1s

The time during which light is detected on the pulse train does not increase continuously with the polarization time. It seems to show that already above 200ms the system is saturated with injected charges under the voltage amplitude we are working with. Moreover, the fluctuations in relaxation time seem to indicate that the relaxation of the charges can occur by different mechanisms that might not produce light emission.

It was thus decided to study the light on the first pulse since it is the one that gives the highest light amplitude. Changing t_1 allows one to probe the behaviour of the injected charges at different times after the end of the polarization. Time t_1 was varied from 1s to 15s with V_1= +0.5kV and V_0= -2.5kV lasting for 5s. From figure V-35 it appears that as t_1 is increased the amplitude of luminescence detected on the first pulse decreases. This is in accordance with the fact that injected charges relax after the removal of the polarization voltage. This relaxation is non-radiative. As t_1 is increased the amount of charges remaining in the materials decreases. Actually this rapid decrease suggests that the charges are trapped really close to the interface between wire and epoxy and relax rapidly after the end of the stressing period [17].

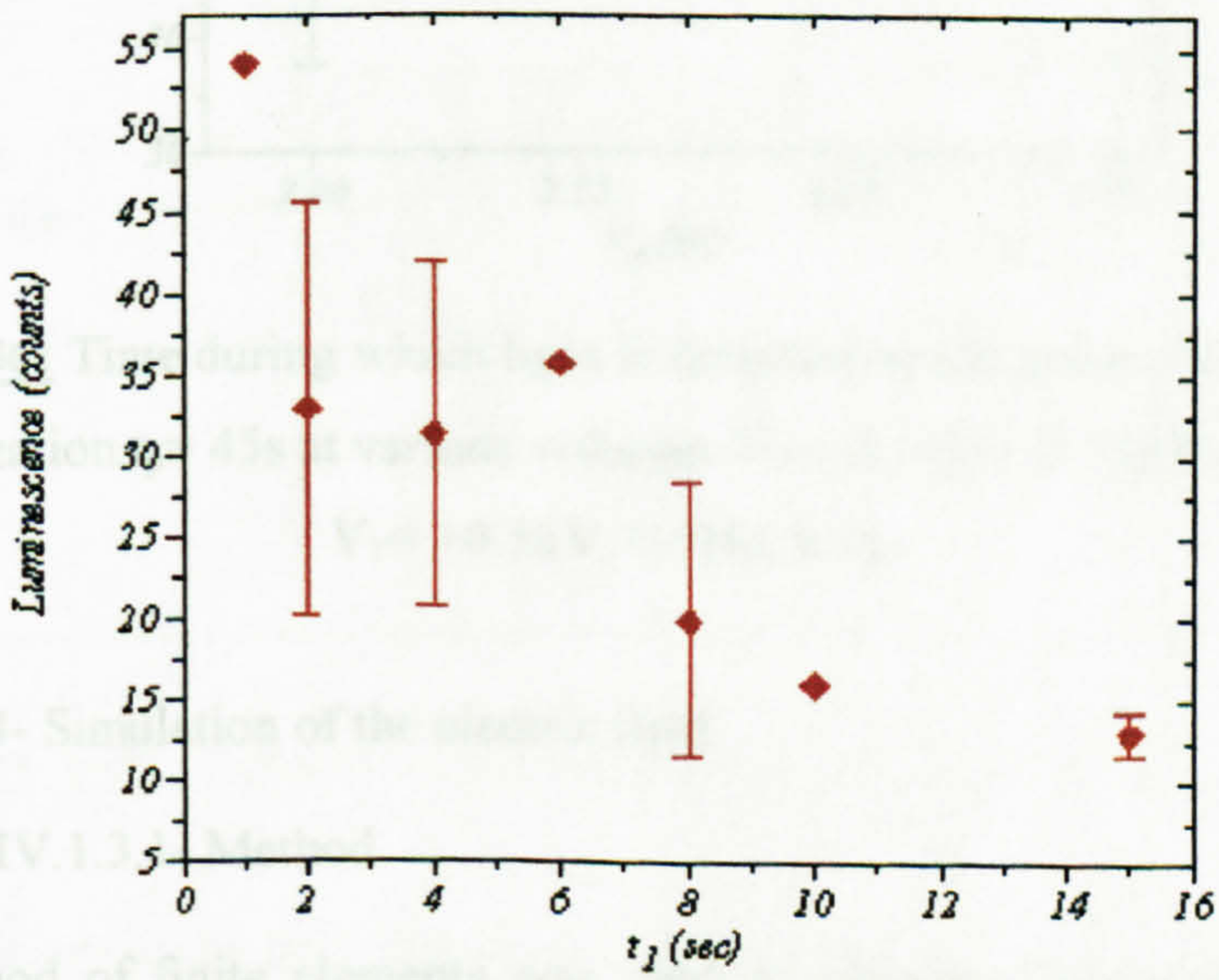

Figure V-35: Luminescence recorded on the first pulse of the train following the polarization in front of t_1. V_0= -2.5kV, t_p= 5s, V_1= +0.5kV, 0.5Hz, 0.1s

Finally, the amplitude of the voltage V_0 has been studied with the same set of samples. The time during which the light was detectable on each pulse train was recorded as a function of the polarization voltage amplitude. Each experiment was repeated several times so as to check the reproducibility of the answer. Three values of V_0 have been used (-2, -2.5, -2.75kV) lasting for t_p= 45s. From figure V-36 it seems that the amplitude of polarization has no significant effect on the time during which light is detected on pulse train.

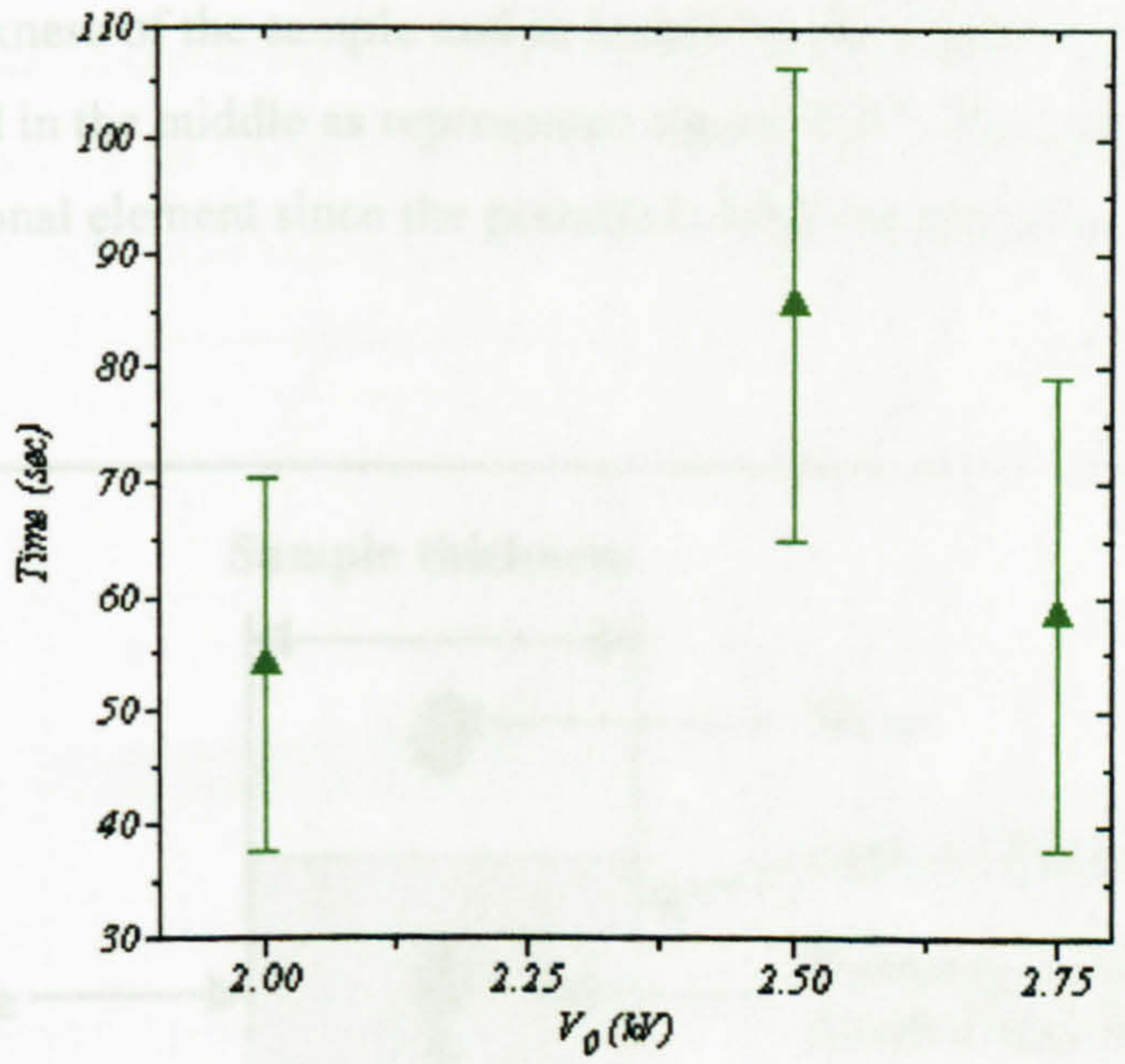

Figure V-36: Time during which light is detected by the pulse train following polarization t_p= 45s at various voltages V_0= -2, -2.5, -2.75kV, t_1= 1s, V_1= +0.5kV, 0.5Hz, 0.1s,

IV.1.3- Simulation of the electric field

IV.1.3.1- Method

The method of finite elements was used to calculate the electric field in the present system. The same technique used by Naz-Paris [20] was used. It is described by Gauss' equation:

$$div(\varepsilon E) + \rho = 0 \qquad (V.3)$$

where ε is the permittivity, E the electric field and ρ the charge density. The aim of the finite element method consists in finding a system of linear equations. In this way the electric field is determined from a number N of functions φ giving the equation:

$$E = \sum_{i=1}^{N} E_i \varphi_i \qquad (V.4)$$

where each φ_i function varies on one define finite element. E_i is calculated in each cases by the introduction of V.4 into V.3 so as to determine E.

The system is reduced to a smaller volume that represents the material by using its symmetries. In the present case this volume is reduced to a rectangle limited in width by the thickness of the sample and in length by the distance between wires. The wire is positioned in the middle as represented figure V-37. The system is also limited to a two dimensional element since the potential along the direction of the wires is the same.

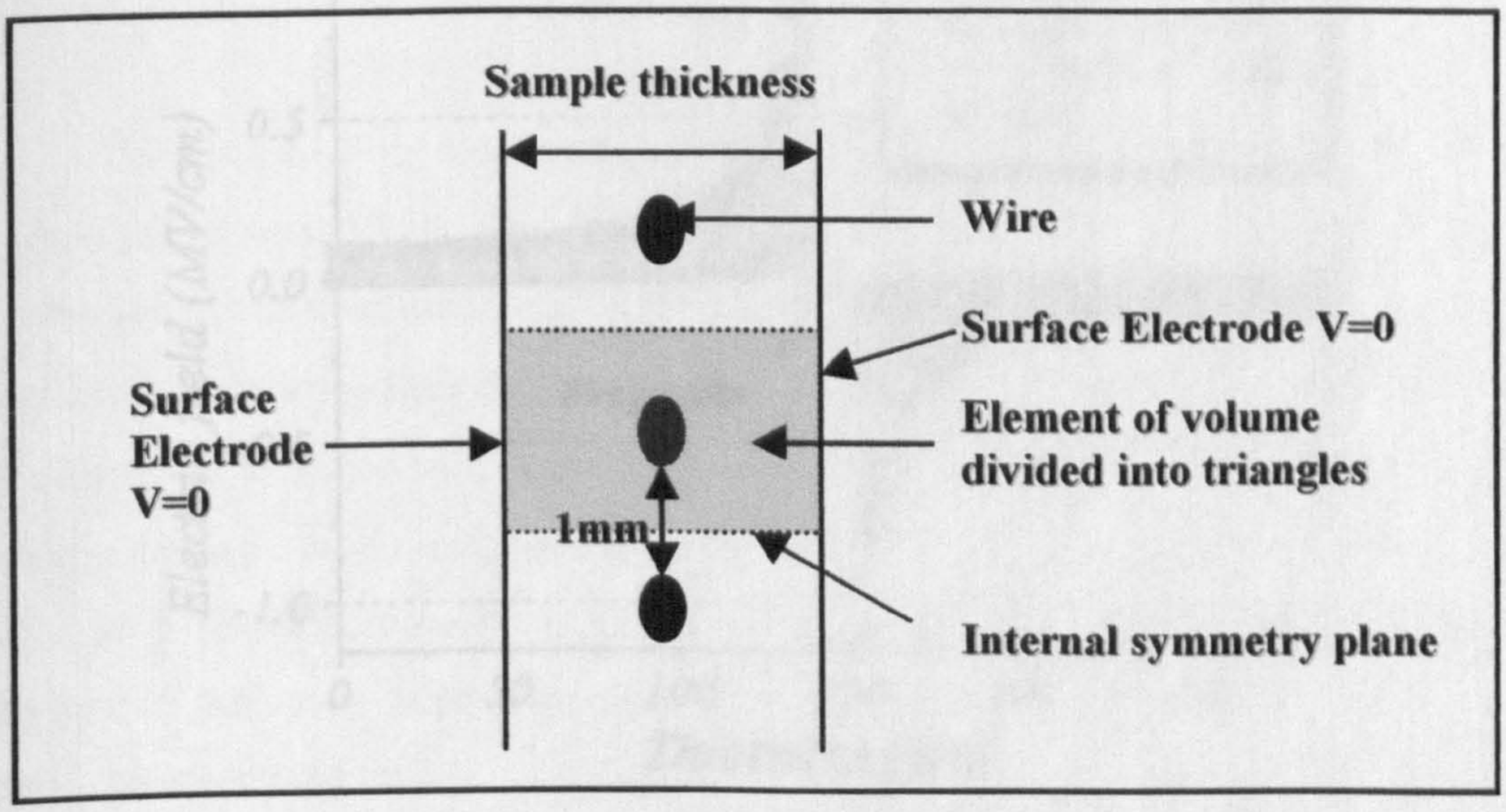

Figure V-37: Domain on which the field calculation is carried out

The conditions at the limit are chosen as follows:

- Potentials that are given to the electrodes are defined by Dirichlet conditions: V=0 on the plane electrodes whereas the potential V is applied on the wires.

- Limits that correspond to the internal symmetrical plane are described by Neumann conditions where the normal component of the field is cancelled due to symmetry.

$$\frac{\partial V}{\partial n} = 0 \qquad \text{(V.5)}$$

The system is divided into small triangles in our case. Their numbers define the precision of the calculation. In the present case it is the value of the field between the wire and the surface along the shortest line that will be calculated and represented. In all the calculations it is considered that the wires are 5μm radius separated by a 1mm gap. They are located in the middle of the 290μm thick samples.

IV.1.3.2- Application

The first step consists in doing the calculation for the system while a potential is applied to the wires whereas the surface electrodes are connected to the ground. It will be called $E_{electrostatic}$. In this case it is considered that there is no space charge in the bulk. Figure V-38 represents $E_{electrostatic}$ for values of voltage between 250V and 3kV.

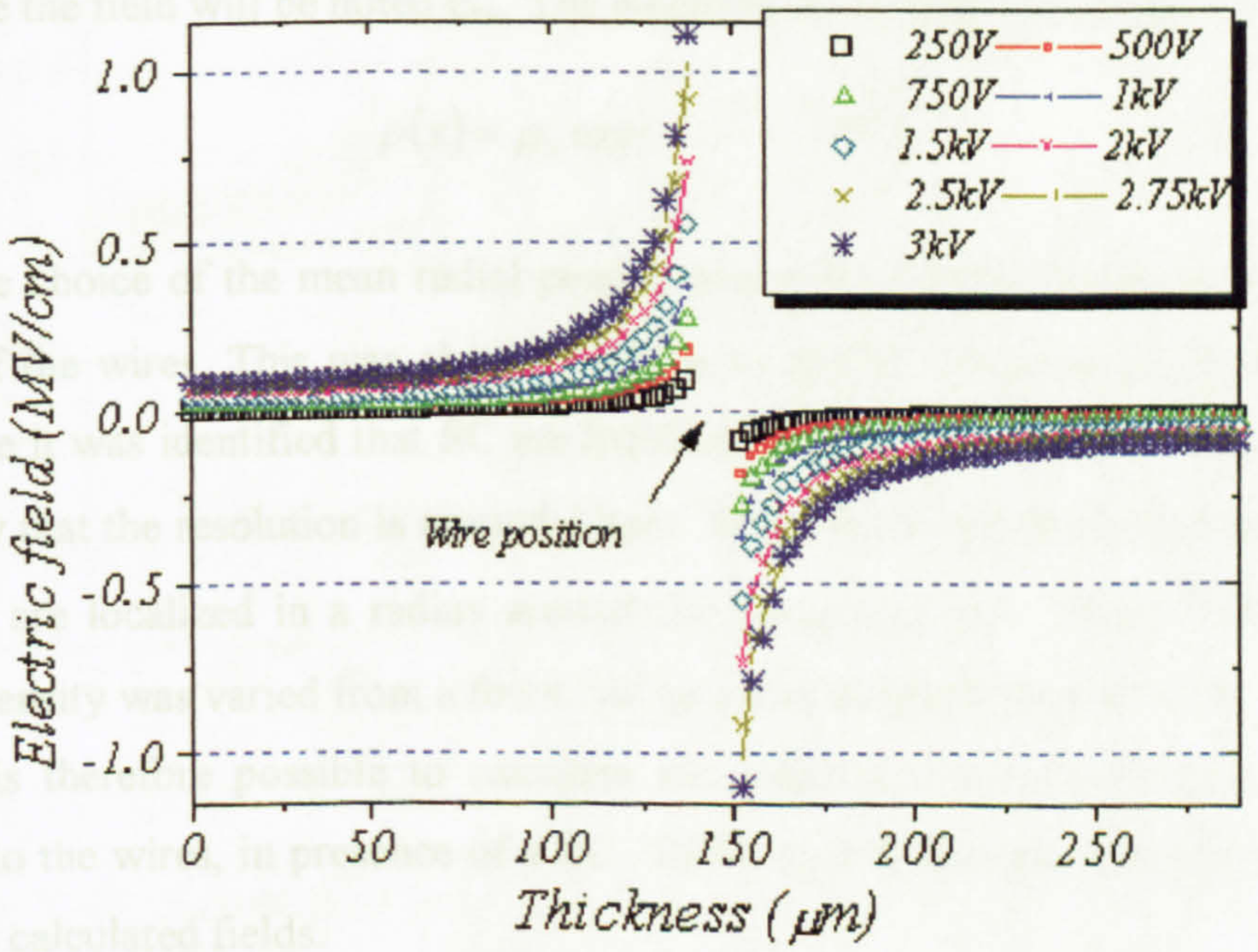

Figure V-38: Electrostatic field calculated in absence of SC.

Voltage applied on the wire, V= 0V on surface electrodes

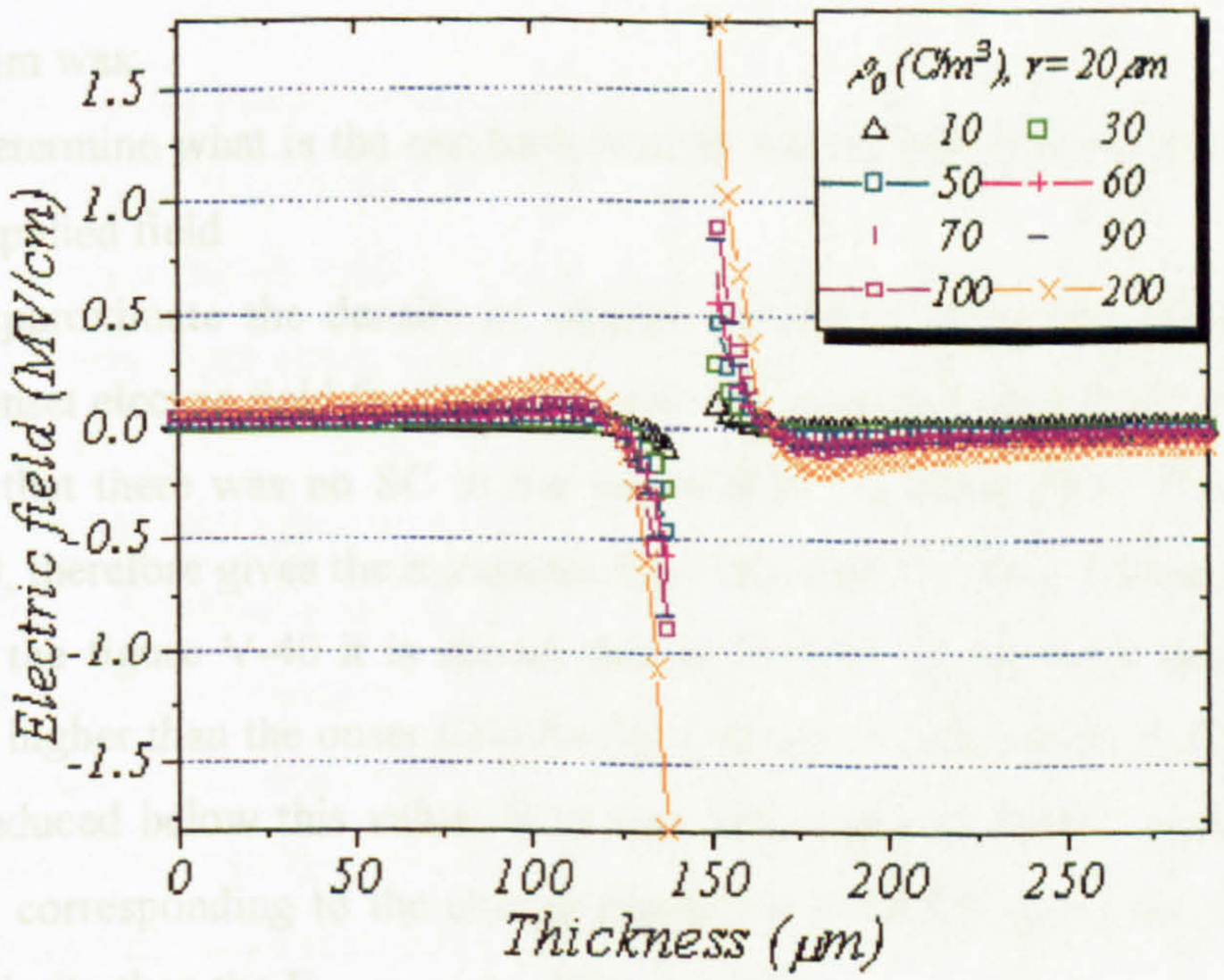

Figure V-39: E_{sc} Gaussian distribution of SC $\rho(x) = \rho_0 \exp\left[-\left(\frac{x - x_{wire}}{r}\right)^2\right]$

The second calculation has been performed by setting V= 0V on both the wires and the surface electrodes. Therefore the contribution of the SC is calculated by choosing a Gaussian profile, with a radial width, r, and a maximum charge density ρ_0. This time the field will be noted E_{sc}. The equation describing the charge density is:

$$\rho(x) = \rho_0 \exp\left[-\left(\frac{x - x_{wire}}{r}\right)^2\right] \quad \text{(V.6)}$$

The choice of the mean radial penetration was taken as 20µm radius from the centre of the wires. This was chosen relative to the SC detection by PEA. By PEA technique it was identified that SC are localized close to the surface of the wires but we know that the resolution is around 10µm. That means that the net charges that are detected are localized in a radius around the wires that is ≥ 10µm. The maximum charge density was varied from a few C/m^3 to a few hundred (figure V-39)

It is therefore possible to calculate the value of the field while a voltage is applied to the wires, in presence of a SC. To do so it is necessary to add both of the previous calculated fields.

$$E = E_{electrostatic} + E_{sc} \quad \text{(V.7)}$$

The aim was:

- to determine what is the resultant field by taking into account the effect of the SC on the applied field

- to approximate the density of charge necessary to reduce the electric field below the onset electric field for light emission that was recorded at V= 0.5KV. It was considered that there was no SC in the material at the onset field. The calculation, figure V-40, therefore gives the minimum field required for space-charge injection.

From the figure V-40 it is shown that at $50C/m^3$, E has been reduced but the field is still higher than the onset field for light emission whereas at $100C/m^3$ the field has been reduced below this value. It is also interesting to notice from figure V-39 that the E_{sc} corresponding to the charge density of $100C/m^3$ gives the field value of opposite polarity than the $E_{electrostatic}$ in absence of SC.

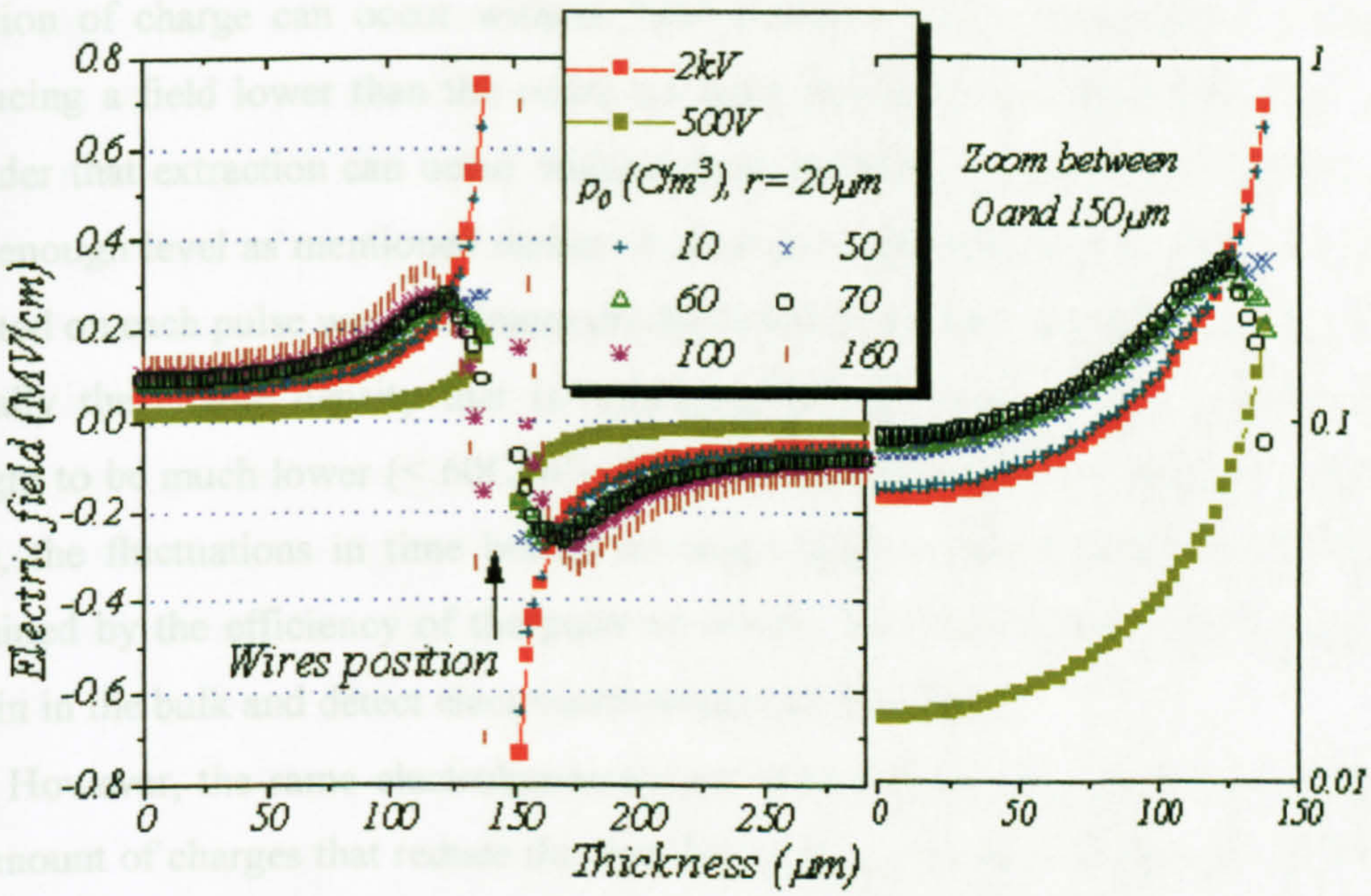

Figure V-40: E created by an applied voltage of 2kV by taking into account E_{sc}, Charge density varying from 10 to 160C/m^3, Gaussian distribution radius 20µm

The detection of light on the onset and removal of the voltage application seems to fit this calculation. It is thought that charges are rapidly injected from the electrode and act in lowering the electric field below the onset field of emission E_{onset}. During voltage application some charges can be injected until the value of E_{sc} counterbalance $E_{electrostactic}$. In the present case, the charge density necessary is about 100C/m^3. Therefore when the voltage is switched off the trapped charges tend to go back to the electrode. Since the field is the same as the initial applied field but in the opposite direction the amount of charges extracted leading to light emission is expected to be of the same order as the one detected at switch on. Then the field is decreased below the onset field of emission, as the SC is de-trapped. Some SC is expected to be de-trapped without light emission and some others may remain in the bulk for a longer period of time.

By using a pulse of opposite direction after polarization, it was observed that injection of charge can occur without light emission if the polarization voltage is producing a field lower than the onset for light emission. It is therefore possible to consider that extraction can occur without light emission if the field did not reach a high enough level as mentioned earlier. It was also observed that the light amplitude detected on each pulse was maximum on the first one and decreased rapidly on others. Actually the charge density that is remaining after the end of the polarization is thought to be much lower ($< 60C/m^3$). This amount is de-trapped mainly on the first pulse, the fluctuations in time before no more light is detected on pulses may be explained by the efficiency of the pulse to de-trap the small amount of charges that remain in the bulk and detect electroluminescence from them.

However, the same electroluminescence detection system may be saturated by the amount of charges that reduce the field below E_{onset} on short timescales (< 200ms) for all the voltages used in this set of experiment. Since, the extraction of charges on voltage removal is produced by a equivalent field amplitude to the injection field the amount of charges remaining to be de-trapped by the pulses is small. Therefore it should be probed much faster after the end of the polarization because then less charge will have been removed.

IV.2- Second set of samples

From the previous set of measurements it seems that injection, trapping and de-trapping phenomena are very quick. For instance it has been observed that the polarization time above 200ms did not produce significant changes in the light detected neither on the pulse nor on the pulse train. Besides, the application of the pulse train with t_{1min}= 1s was thought to be too large compared to the relaxation time of the charges that is suspected to be of the order of a few ms. It was therefore decided to change the parameters and study the effect of short time polarization and a short time of separation between the end of the polarization and the starting point of the pulse train. The conditions available were t_p< 100ms, V_0= +/-5kV, t_1< 100ms.

Unfortunately the response given by the second lot of samples was different from the first one. Even by using the same conditions of investigation as for the

previous set the light emission was different. For instance as shown in figure V-41 it can be seen that the total amount of light detected remains really small (< 70counts) over the range of voltage going from +0.2 to +2.75kV. The application of the stress was varied from 50 to 300ms and no differences were recorded. Even the application of a pulse train of opposite polarity did not give sufficient light emission amplitude to be taken into account. It was thought that the difference comes from the sample rather than the experimental set-up. The main difference could be due to the position of the wires. These experiments have not been carried out further since it is important to identify first the origin of the distortion in the response.

Interestingly, however, the voltage above which EL becomes detectable remain at +0.5kV as before, see figure V-32. It is voltage dependence, which is changed. That could be due to a smaller trap density in the samples coming from the processing step.

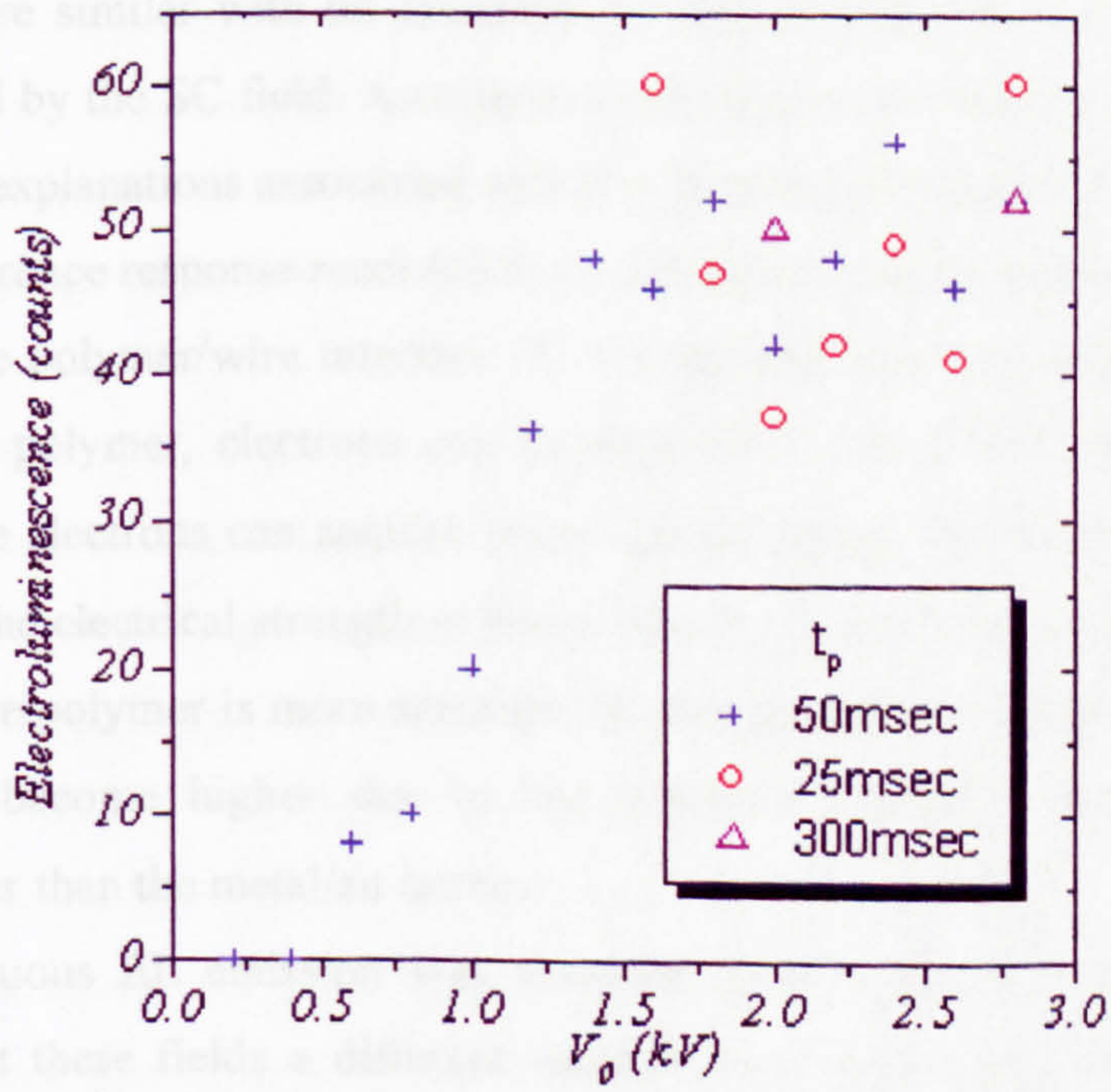

Figure V-41: Luminescence recorded under different polarization voltage V_0 lasting for t_p= 50, 25 and 300ms

V- Discussion

V.1- Excitation mechanism

In the divergent field configuration EL was observed on the application and removal of the voltage. The light detected increased with field once a specific onset value had been exceeded. However, there is no continuous light detected during dc polarization. This transient EL can be explained by an excitation of luminescence centres by inelastic scattering of the injected carriers up to the point where a sufficient amount of charges have been trapped to counterbalance the injecting field. When the polarization voltage is turned off the same EL excitation occurs because the field at the wires has the same magnitude as the applied field but of the opposite polarity. In other words, the amplitude of the luminescence recorded at the voltage application and removal are similar with no emission inbetween. This fits a transient injection process limited by the SC field. A computer calculation was also performed and used to support the explanations associated with the light emission phenomena.

The difference response recorded from the second set of samples could be due to a change in the polymer/wire interface. If, for instance an air gap exists between the metal and the polymer, electrons can be injected at lower field into the polymer. Actually, those electrons can acquire some kinetic energy while they are injected in the air where the electrical strength is lower than in the polymer. On the other hand if the contact wire/polymer is more accurate the energy required to inject charges in the material will become higher due to the potential barrier metal/polymer that is therefore higher than the metal/air barrier.

A continuous EL emission was recorded in uniform dc applied field above 160kV/mm. At these fields a different mechanism of excitation can occur. For PE based materials this phenomena was observed and explained by the generation of charge packet that result in recombination between positive and negative charge carriers [12, 18]. The transport phenomenon that is observed at lower fields therefore seems to be at the origin of the light emission. As reported for other materials the high-field conduction process can drive the excitation of EL by impact ionisation rather than an impact excitation process [19]. Here, impact ionisation includes the

generation of charge pairs. As the conductivity has been reported to be exponentially dependent, a trap-to-trap mechanism for the mobile carriers can be imagined. It is not possible to give more details on the relationship between the current and the EL except that the change from transient to conduction current was not detected at the same electric field as the onset of EL. It is important to note that the conduction current is difficult to measure since the polarization current is mixed with the transient current due to the dipolar polarization effect when the voltage is applied for short period of time. Even the experiments carried out by using 1h stress were not giving access to that level unless the voltage was dramatically increased. A correlation between the onset of the luminescence and the current was established. It appears that the onset of light emission is about 160kV/mm. The increase in the current that was found to be started at lower field could be explained by the fact that the processes leading to light emission are really driven by the current, but it is necessary to have an amount of charge minimum corresponding to a certain value of current before which any light emission processes can be initiated. The absence of continuous luminescence in the divergent field configuration can be explained by the fact that the maximum electric field reached in that configuration was below the limit for which continuous light was detected in the uniform field configuration. It was not possible to go higher in voltage since breakdown was suspected to occur rapidly under a higher stress.

In the divergent configuration, the probe-pulse shows that even below the onset field for transient luminescence some light could be emitted. This means that the applied voltage had produced SC but these charges were able to produce light when a pulse of opposite polarity was applied Actually, this luminescence occurs when the sum of the polarization voltage and the probe voltage is large enough to exceed the EL onset field found in a single pulse experiment. As the quantity of charges available to produce light decays very quickly with time (~ 10.5s), the light detected only last for a short period. Therefore, it seems that the charges have a non-radiative form of neutralisation and luminescence occurs only when the local field exceeds a level large enough for a rapid injection or extraction of charge. It is associated with charges possessing a high kinetic energy that are able to initiate EL by inelastic scattering. Under lower fields extraction can be performed without light emission. This is in accordance with the observation of the onset fields and the field dependence of the

luminescence that is the same for the polarization and depolarization transients in both positive and negative polarity. The actual transient of light seems to be associated with an excitation phenomenon by inelastic scattering as long as the field is high enough, i.e. as long as the injected SC does not decrease the value of the field below the injecting field threshold.

V.2- Excitation relaxation studies by spectral analysis

The analysis of the components and cured resin by photoluminescence shows that the response of the various components is widely influenced by the environment. In polymeric structures it is therefore rarely possibly to associate a wavelength directly with a chemical group since the emission depends on the complex structure.

From the base resin, by using excitation and emission spectra, it looks as if two chromophores are involved, one of them being at the origin of two emissions peaks. This was supported by the fact that two emission peaks were associated with similar excitation spectra. The species that give rise to the light are difficult to identify since the base resin is a mixture of several components but is likely to be associated with benzene rings provided by the DGEBA. By determining the available chromophores in the resin and studying UV-absorption table of simple un-conjugated chromophores (table V-5) and substituted benzene rings from the literature [21], it is observed that none of the species can account for an absorption corresponding to $\lambda_{excitation} \sim 350nm$.

	Chromophores	**Transition**
Cured resin	-C-C-; -C-H; -C-O-	σ-σ^*
	-C=C- in Phenyl rings	π-π^*
	-Ö-	n non bonding orbitals
Hardener	-Ñ<	
	-CÖH=Ö	
	HO-Ph-COOH	

Table V-5: Available transition of simple un-conjugated chromophores in the cured resin and hardener

However, impurities or molecular interaction in the ground state (A-A) or between species in the ground state and the excited state (A + A*) forming excited excimer are found to be at the origin of the luminescence emission. They relax by giving $\lambda_{emission} \neq \lambda_{emission(A^*)}$. This type of intermolecular interactions is likely to happen in polymer network such as epoxy resin. Similar results as ours (cf. table V-3) have been reported in table V-6 [21].

$\lambda_{excitation}$ (nm)	$\lambda_{emission}$ (nm)	**Chromophore**
350	424	*Fluorescence:* Attributed to an impurity in amine
275, 350	460	*Phosphorescence:* Monomer/dimer and triplet excimer

Table V-6: Bisphenol A-based epoxy resin fluorescence and phosphorescence properties [21]

The hardener gives a single peak of emission that was associated with the salicylic acid. Its contribution seems to disappear in the cured resin. This could be explained by a change in the chemical form, which might turn the emissive group inactive. After polymerisation of the resin, a single peak of emission was detected at RT. This does not mean that only one emissive chromophore remains after the polymerisation but it is more likely to be due to the shift of the excitation to higher wavelength of emission, i.e. lower transition energy. This peak was shown to be clearly different from the response of the hardener however a deeper analysis tends to show that there is a common origin with the base resin. A common excitation wavelength was identified, and the actual shift in the emission peak was associated with the formation of an excimer.

At lower temperatures the phosphorescence emission is expected to be detected. During the excitation light, another peak at high wavelength appears compared to that observed at RT. This new peak was associated with phosphorescence emission. After the removal of the excitation light, the decay of the phosphorescence emission was clearly observed revealing three peaks that are decaying with different rates.

Three regimes of light emission have been recorded in the plasma-induced luminescence spectra over time. The spectra obtained at the longest times were the plasmaluminescence emission, and it was found to be similar to the phosphorescence. The same phenomenon was reported for polypropylene [15]. If the possibility of energy transfer is ruled out, the emitting site could also be the recombination centre, i.e. charges could be trapped by aromatics, which disturb the environment leading to complex charge transfer. It is therefore possible to conclude that the molecular states involved in light emission upon charge recombination are the lowest lying triplet levels of the material chromophores. Actually, impact ionisation by hot electrons can produce thermalized carriers that can be trapped at different distances from the cation (from a few to tens of angstroms). These shallow or deep-trapped charges can recombine with the cation by thermal de-trapping or tunnelling recombination depending on the difference in energy between the trapping state and the excited state of the recombination centre. Charges in shallow traps are expected to be trapped and extracted into the conduction band then recombine with fluorescence or phosphorescence emission. Charges in the deepest traps are likely to tunnel in the forbidden gap to a triplet state leading to phosphorescence.

A decrease in magnitude of EL and current has been observed as the field was lowered; a steady state current was not reached at low field. Also the amount of light detected on simultaneous ramp in voltage show a decrease. This seems to be in accordance with a progressive charging of the material using an injection limited current and homopolar SC. As the electroluminescence spectrum was recorded it seemed to show an extra peak as the applied voltage is increased; it might then be possible to estimate that this effect is linked with a progressive charging of the material. Unfortunately, the resolution of the spectra was not good enough and it is not possible to go further into interpretation from this set of results. It is therefore not possible to conclude on the presence of a threshold above which Electroluminescence emission would be detected. From the spectra recorded it was however feasible to associate the emission peaks with phosphorescence components and recombination in the range 400-550nm whereas the peak detected at about 600nm was thought to be due to degradation of the polymer following a chemical pathway of relaxation.

Chapter VI

Conclusions

The aim of this work was to study the effect of the application of high electric fields on an epoxy resin film. As polymeric structure usually plays an important role in the material response, it was consistent to begin with the characterization of the material from a chemical point of view in addition to the determination of physical properties such as T_g. That was the objective of chapter II where the reactions of polymerisation were presented followed by the protocol of sample preparation.

Dielectric spectroscopy was used at first to determine the dielectric properties of the polymer. The primary effect due to voltage application was detected by a change in the dielectric response. These studies were conducted in chapter III.

The second part of the study consisted of an analysis of the processes involved in charge injection and extraction. To do so, the detection of space charge by PEA method and electroluminescence detection have been found to be useful tools to study the phenomena without damaging the material physically. Results obtained by these two techniques were reported and analysed in chapters IV and V respectively.

In this chapter we will discuss the main points that have been identified to be related to the effect of the application of an electric field. At the same time the complementarities of the techniques used will be reported as a means of verification of some properties by different ways and in order to gain additional information.

I- Overview of main results

I.1- Dielectric spectroscopy response

Apart from the identification of the various processes of relaxation over the frequency range, the main point reported in this study as a consequence of voltage application was linked with the change in the shape and magnitude of the loss peak associated with "process B". This process was found not to be directly associated with the glass temperature unlike "process A". Both processes seem to depend on the temperature and are difficult to distinguish but they are definitively different because of their different dependencies of peak frequency on temperature.

As the decrease in the amplitude of the loss peak associated with process B was observed after a period of stress under both uniform and divergent field configurations whether the film was post-cured or not, this decrease was considered to be due to the voltage application and associated with an irreversible process.

From these studies some explanations can be given. Two types of mechanism can be induced by the application of external electrical stress:

- First of all electrochemical reactions can occur as a result of external electric field application. In such a case, the creation of new dipolar species could be expected. But in this particular instance and because of the disappearance of the loss peak associated with process B it is more likely that a dipolar group has been consumed in a chemical reaction. In such a condition it is expected that extra bonding is created reducing the degree of freedom of the molecules. If this were the case, the glass transition temperature would be expected to increase. As the dielectric response associated with the glass transition, i.e. process A, was not affected by thermo-electric stress, the observed change cannot be associated with additional cross-linking. It has been thought that relaxing dipoles that depend on their environment belong to a local hierarchy of dipoles that are embedded one within an other and therefore their response is self-dependent on the other processes. A fragmentation of this hierarchy is expected if some dipoles get involved in some cross-linking. This fragmentation would reduce the number of responding elements in the system leading to the disappearance of certain processes such as process B without affecting other processes. This explanation is further supported by the fact that process B is not affected by either post-curing, which affects T_g or by long time storage in the laboratory of non post-cured samples which does not affect T_g. This process appears exclusively disturbed by electrical stress.

- Secondly, the application of voltage for long periods of time can lead to charge injection even if originally the voltage produces lower fields than normally required for injection. In this case, it is possible to imagine a process in which ionic species migrate toward the electrodes producing heterocharge accumulation as observed after long time polarization by PEA measurements. Therefore, the field created at the electrodes might be enhanced enough to allowed homo-charge injection. Such a process probably leads to material changes as a response to the injection current and local field modifications. To check the effect of this kind of electrical variation the Ohmic current while the material is submitted to voltage cycling could be measured.

These two mechanisms lead to non-reversible processes through bonding reactions or SC injection under low field producing local changes. As will be reported in the next section, injection followed by charge de-trapping was found to stabilize at one stage. This equilibrium might well be at the origin of changes in the dielectric response. In such a case the process B might be affected because of a stabilization in the dipolar orientation until the equilibrium is modified by charge extraction for instance. These relaxation phenomena are unlikely to happen without the application of a high enough external electric field that might in that case inject other charges or cause bond breaking. In both cases, the material does not recover its initial properties.

I.2- Space charge detection

From SC measurements it has been observed that homo-charge is injected from the electrodes whatever the polarity of the applied voltage. The values of the voltage for injection can be rather small, corresponding to levels that are used in practice, if the polarization time is long enough (from a few hours to a several weeks). The accumulation of charge was always observed to occur close to the electrodes and is accompanied by dipolar polarization. This can lead to a complex signal that corresponds to the addition of induced charges on the electrodes and bound charges respectively due to injected net charge and dipolar orientation.

However, the amount of injected charge can be estimated by the analysis of the peak' associated with the net internal SC close to the surface' that is detected after the removal of the polarization voltage. The analysis of the decay tends to show that the deeper traps are being filled first during voltage application. Therefore after the end of the polarization, those that are trapped closer to the surface may be de-trapped using less energy because of the field distortion created by the SC itself. Then the field created by the SC is lowered and the deeper trapped charges are extracted with increasing difficulty. Finally, it was observed that induced charge and bound charge should become equal at some point. Since they are of opposite polarity the net charge on the electrodes is zero, and electric field now exists only in the bulk of the sample where it attracts the injected charges (homocharges) towards one another. From this particular point an equilibrium is created preventing the extraction of more charges or the relaxation of dipoles; this was confirmed by the observation of a stable recorded signal for a long period of time after the end of the polarization, i.e. from several

hours to days. Eventually this equilibrium can be displaced by the application of an external electrical stress.

Finally long time polarization shows that the lower level of traps is dropped in energy. This phenomenon is expected to occur after all the trap levels from the deeper to the shallow have been filled.

I.3- Luminescence emission

From electroluminescence measurements two types of information have been extracted. First of all from the spectral analysis of the base resin some information about the excited species produced by various sources of excitation have been identified. A relation between the various set of results has been established as follows. From photoluminescence experiments it was found that the main response detected by an excitation of wavelength 350nm gives rise to UV-visible emission for the cured resin. This can be produced either by impurities or molecular interactions. These interactions can be formed from associated ground state dimers (A-A) that are excited ($A\text{-}A^*$) or from the interaction between a molecule in an excited singlet state and a similar molecule in the ground state ($A+A^* \rightarrow A\text{-}A^*$) that relax giving an emission peak usually at a higher wavelength than a single excited molecule. The phosphorescence has been associated with the relaxation of excited dimers from their triplet state or the association of one monomer in the ground state and one in the triplet excited state. Similar observations were found by literature surveys for molecules that are likely to originate intermolecular interactions, which is the case in the present polymeric network system.

The response produced by salicylic acid in the hardener is not effective after polymerisation; the signal being dominated by chromophores provided by the base resin or impurities. In the present case, the study was completed by the analysis of charge recombination induced *luminescence and* electroluminescence spectra. A comparison between the plasma induced luminescence and phosphorescence emission shows similar features. It is therefore possible to rule out the possibility of a transfer of energy by assuming that the emitting centre is also the recombination centre. In other words charges are likely to be trapped on aromatic rings, leading to complex charge transfer in the polymeric structure before relaxation. Charge recombination might contribute to the electroluminescence emission mechanism (especially for the

emission at about 450nm). However, the electroluminescence emission at higher wavelengths (i.e. $\lambda > 500$nm) might be due to other phosphorescence components.

Secondly, the analysis of the light emission while a polarization voltage, in divergent field configuration, is applied seems to confirm the conclusion that space charge is injected at fields above approximately 10kV/mm drawn from PEA measurement results. In addition, the use of a probe voltage pulse of opposite polarity in order to detect injected charges, by means of a luminescent SC de-trapping process, leads to a complementary image of the trapping de-trapping mechanisms involved. The results can be described as follows:

- The light emission was detected only on the voltage application and removal, though the polarization was applied for 200ms. This phenomenon was explained by a charge injection that generates light only above an onset electric field. It was proved also that charges could be injected at lower fields without emission of light. However, as charge is injected the interfacial electric field is reduced. The reduction is high enough to decrease the field below the onset for light emission; therefore no light is recorded during voltage application even if extra SC can be injected. The reduction of electric field was successfully simulated by computer calculation.

- At the removal of the voltage the field created by the SC is of opposite polarity and same amplitude as the field created during voltage application. The charges that are located in shallow traps can be ejected with emission of light until the field has been reduced below the onset value. At that stage charges are more difficult to extract due to the reduction of the field. The probe voltage pulse, which was selected so as not to produce light emission by itself, is used to de-trap the remaining SC. It was observed that the biggest amplitude of light was recorded on the first probe. This is explained by the fact that only a small amount of charge remained in the sample after the polarization voltage was switched off. It was also shown that if the probe was used after an interval of time of 15s the amount of light detected was reduced by about 75% compare to the signal detected with a probe voltage at 1s after the removal of the polarization voltage. This can be explained by an extraction of charge without light emission in the order of seconds and even milliseconds after voltage removal. For this reason, the same kind of measurements carried out using a much shorter time interval between polarization and probe pulses.

However, some variation in the response from one set of samples to another was clearly found. This difference has been associated with a difference in the electrode/polymer contact, which is extremely important for all processes of charge injection and extraction. Actually, if an air gap exists between the wire and the resin an acceleration of the electrons in the air, where the electrical strength is lower than in the polymer, is expected to help the injection phenomena and the emission of light. Since the energy acquired by the accelerated charge in the air is much higher it can excite the luminescent centre easier. On the other hand, a better contact increases the level of the field required to inject charges from the electrode into the polymer, therefore no light emission would be detected below a higher onset field compared to the previous case. It is also possible that in order to observe light the voltage to be applied is so high that breakdown occurs before a sufficient amount of light that could be analysed has been detected.

From uniform field experiments, the light emission was found to be linked with a change in the current-voltage characteristics. This tells us that the processes involved in the production of light are driven by the high field charge transport process. The high field current was fitted by a power law but could also be fitted by an exponential that is associated with a charge hopping process. However, the onset field for light emission was higher than that for the high field conduction current. This shows that the regime must be properly initiated before luminescence can be excited.

II- Complementarities of the investigation techniques

The main common feature in all these experiments was the detection of the external current that allows the identification of different regimes. Actually, the dc conduction process was not reached during short polarization times (t_p< 3500s) especially if the applied voltage was low (V< 7kV). In first instance, the conduction process is dominated by dipolar orientation that gives rise to a building up of charge on the electrodes.

By using the discharging current, where no conduction processes are involved, it was found that the process B relaxation time-domain, identified by dielectric spectroscopy, corresponds to the time domain of the decaying current recorded. The measurements confirm the dependence on the molecular environment in addition to the past electrical treatments. As this measurement was coupled with light emission

detection, it is expected that a change associated with process B would be accompanied by changes in the amplitude of detected current and in the amplitude of detected light emission. It is even possible that the onset field for light emission may be lowered if ageing reduces the contribution of process B to the charging current. As luminescence experiments coupled with current detection were carried out first of all on non thermo-electrically stressed samples such a change could not be confirmed and should be part of further work.

SC detection by PEA and electroluminescence experiments are also complementary. It was through the analysis using both techniques that it was possible to explain why there was just a pulse of light on voltage application and removal. It was also possible to explain the rapid decay of the signal associated with SC by PEA and the dipolar polarization stability

Such complementary techniques of investigations are rather informative on their own but their coupling seems to be successful to find a deeper interpretation of the results or as tool to confirm previous measurements by using different probing methods.

III- Further work to be carried out

In order to go further into an investigation of the effect of electrical stress on an epoxy resin some other measurements should be performed. These points have mostly already been mentioned but they will be reported in this section.

As external current measurements seems to give access to information that directly link the dielectric response, the mechanism of SC injection and luminescence production it would be interesting to perform more measurements. It would be especially informative to carried out the measurements for long time polarization such as to reach the conduction current level that can be subtracted from the total current detected so as to obtain the value of the polarization current in order to aid better comprehension of the PEA response signal.

Luminescence coupled with current measurements should also be performed after a period of thermo-electric ageing so as to compare with the changes that are detected in process B from the dielectric response. In this way it may be possible to relate changes in luminescence directly with changes in process B.

For the spectral analysis the record of the electroluminescence spectra should be repeated in order to complete the comparative *studies. This work should* be performed using thicker film (100 to 300μm) in order to be able to applied higher voltages and reach higher fields whilst reducing the risk of breakdown. It has been observed that the emission is quite low in amplitude when the field is just above the onset of detection and an increase in the applied voltage that is accompanied by an increase in the light emission is causing catastrophic failure in ultra thin films (50μm). A compromise must therefore be established.

Finally, an imaging record to determine the location of light emission should bring some information on the nature of the emissive centre. These experiments should be preferably performed under divergent field configuration since the emission is favoured by the high field application and should be easier to locate since it is expected to occur around the wire.

It is hoped that the work presented in this thesis, together with the proposals for further work, will lead to a much improved understanding of thermo-electric ageing and the long-term effects of high voltages on epoxy resin systems.

References

Chapter I - Electrical processes in polymeric insulation

[1] J.C. Anderson, K.D. Leaver, R.D. Rawlings, J.M. Alexander, *Materials Science*, chapter 12, Third Edition, London Chapman & Hall, ISBN 0442306261, 1985

[2] J.R. Fried, *Polymer Sciences and Technology*, London: Prentice-Hall International Editions ISBN 013685561x, 1995

[3] J. Muccigrosso, P.J. Phillips, *"The Morphology of Cross-linked PE"*, IEEE trans. E.I., Vol. EI-13, pp. 172-178, 1978

[4] H. Barker, *High-Voltage Technology* edited by L.L. Alston, pp. 229-253, Oxford University Press 1968

[5] V.A. Brzhezitsy, O.S. Il'enko, A.V. Mamihev, B.D. Russel, S.A. Sokolovsky, *"Partial Empirical Model of the Multifactor Aging of High Voltage Insulation"*, Annual Report CEIDP, 94CH3456-1, pp. 367-372, 1994

[6] C. Mayoux, *"Aging of Polymeric Materials in Power Cables"*, IEEE Trans. Diel. E.I., Vol. 4, pp. 665-673, 1997

[7] J.P. Parpal, J.P. Crine, C Dang, *"Electrical Aging of Extruded Dielectric Cables, A Physical model"*, IEEE Trans. E.I., Vol. 4, pp. 197-209, 1997

[8] G.C Montanari, G. Mazzanti, L.A. Dissado, D.K. Das Gupta, *"Space Charge as a Trigger for electrial Ageing of Polymeric Insulation"*, Space charge in Solid Dielectrics edited by J.C. Fothergill and L.A Dissado, ISBN 095335380 X, pp. 259-272, 1998

[9] M. Ieda, *"Electrical Conduction and Carrier Traps in Polymeric Materials"*, IEEE Trans. E.I., Vol. EI-19, pp.162-178, 1984

[10] K. Kojima, Y. Takai, M. Ieda, *"Electronic Conduction in Polyethylene Naphthalate at High Electric Fields"*, J. Appl. Phys., Vol. 59, pp. 2655-2659, 1986

[11] L.A. Dissado, J.C. Fothergill, *Electrical Degradation and Breakdown in Polymers*, Ed. G.C. Stevens (P. Peregrinus for IEE, 1992, U.K), ISBN 0 86341196 7

[12] G. Damamme, C Le Gressus, A.S. De Reggi, *"Space Charge Characterisation for the 21th Century"*, IEEE Trans. Diel. E.I., Vol. 4, pp. 558-584, 1997

[13] D.K. Das-Gupta, K. Doughty, *"Dielectric and Conduction Processes in Polyetherether Ketone (PEEK)"*, Trans. E.I., Vol. EI-22, pp. 1-7, 1987

[14] A.R. Blythe, *Electrical Properties of Polymers*, Cambridge University Press, ISBN 0521219027, 1979

[15] D.A. Seanor, *Electrical Properties of Polymers*, Academic Press, INC. London LTD., ISBN 0-12-633690-6, 1982

[16] N.F. Mott, E.A. Davis, *Electronic Processes in Non-Crystalline Materials*, 2nd ed., Oxford: Clarendon Press, ISBN 0198512880, 1979

[17] H.B. Zeller, W. R. Schneider, *"Electrofracture Mechanics of Dielectric Aging"*, J. Appl. Phys., Vol. 56, pp. 455-459, 1984

[18] N.H, Ahmed, N.N. Srivinas, *"Review of Space Charge Measurements in Dielectrics"*, IEEE trans. Diel. E.I., Vol. 4, pp. 644-656, 1997

[19] J.M. Braun, J. Densley, K. Younsi, H.J Wintle, *"TSDC Measurements on Miniature and Full-Size Polymeric Cables"*, *Space charge in Solid Dielectrics* edited by J.C. Fothergill and L.A Dissado, ISBN 095335380 X, pp. 315-325, 1998

[20] T. Hino, *"Thermally Stimulated Measurements in Solid Dielectrics"*, IEEE Trans. E.I., Vol. EI-21, pp. 1007-1010, 1986

[21] I. Glowacki, J. Ulansski, B. Kozankiewicz, *"Charge carrier detrapping in PVK films as seen by thermoluminescence after excitation at 15K"*, *Space charge in Solid Dielectrics* edited by J.C. Fothergill and L.A Dissado, ISBN 095335380 X, pp. 251-258, 1998

[22] A. Cherifi, M. Abou Dakka, A. Toureille, *"The Validation of the Thermal Step Method"*, IEEE Trans. E.I., Vol. 27, pp. 1152-1158, 1992

[23] A. Toureille, J.P. Reboul, P. Merle, *"Détermination des densités de charge d'espace dans les isolants solides par la méthode de l'onde thermique"*, J. Phys. III, Vol. 1, pp. 111-123, 1991

[24] T Takada, T, Sakai, *"Measurement of Electric Fields at a Dielectric/Electrode Interface Using an Acoustic Transducer Technique"*, IEEE Trans. E.I., Vol. EI-18, pp. 619-628, 1983

[25] T.Takada, T. Maeno, H Kushibe, "An Electric Stress-Pulse Technique for the Measurement of Charges in a Plastic Plate Irradiated by an Electric Beam", IEEE trans. E.I., Vol. EI-22, pp.497-501, 1987

[26] J. Lewiner, *"Evolution Techniques for the Study of the Electrical Properties of Insulating Materials"*, IEEE Trans. E.I., Vol. EI-21, pp. 351-360, 1986

[27] G.M Sessler, J.E. West, R. Gerhard-Multhaupt, H. V. Seggern, *"Nondestructive Laser Method for Measuring Charge Profiles in Irradiated Polymer Films"*, IEEE Trans. Nucl. Sci., Vol. NS-29, pp. 1644-1649, 1982

[28] M. Ieda, N.M. Nagao, M. Hikita, *"High-field Conduction and Breakdown in Insulating Polymers"*, IEEE Trans. Diel. E.I., Vol. 1, pp. 934-945, 1994

[29] K. Kitagawa, G. Sawa, M. Ieda, *"Observation of Dielectric Breakdown Sites in Polyethylene thin Film"*, Japan. J. Applied Phys., Vol. 19, pp. 389-390, 1980

[30] K. Kitagawa, G. Sawa, M. Ieda, *"Self-healing Breakdown at Spherulite Boundaries of Polyethylene Thin Films"*, Japan. J. Applied Phys., Vol. 20, pp. 87-94, 1981

[31] T. Tanaka, T. Okamoto, K. Nakanishi, T. Miyamoto, *"Review: Aging and Related Phenomena in Modern Electric Power Systems"*, IEEE trans. E.I., Vol. 28, pp. 826-844, 1993

[32] T. Hibma, H.R. Zeller, *"Direct Measurement of Space Charge Injection from a Needle Electrode into Dielectric"*, J. Appl. Phys., Vol. 59. 1986

[33] J.P. Parpal, J.P. Crine, C. Dang, *"Electrical Aging of Extruded Dielectric cables A Physical Model"*, IEEE Trans. E.I., Vol. 4, pp. 197-209, 1997

[34] G. Bahder, T. Garrity, M. Sosnowski, R. Eaton, C. Katz, *"Physical Model of Electric Aging and Breakdown of Extruded Polymeric Insulated Power Cables"*, IEEE Trans. Power Appar. Syst., Vol. PAS-101, pp. 1379-1390, 1982

[35] T.J. Lewis, J.P. Llewellyn, M.J. Van Der Sluijs, J. Freestone, R.N. Hampton, *"A New Model for Electrical Ageing and Breakdown in Dielectrics"*, DMMA Conference publication No. 430, pp. 220-224, IEE 1996

[36] B.S. Bernstein, E.L. Brancato *"Ageing of Equipment in the Electric Utilities"*, IEEE Trans. E.I., Vol. 28, pp. 866-875, 1993

[37] T. Mizutani, *"Space Charge Measurement Techniques and Space Charge in Polyethylene"*, Trans. Diel. E.I., Vol. 1, pp. 923-933, 1994

[38] L.A. Dissado, G. Mazzanti, G.C. Montanari, *"The Role of Trapped Space Charges in the Electrical Aging in Insulating Materials"*, Trans. Diel. E.I., Vol. 4, pp. 496-506, 1997

[39] J.P. Crine, *"A Molecular Model to Evaluate the Impact of Aging on Space Charges in Polymer Dielectrics"*, Trans. Diel. E.I., Vol. 4, pp. 487-495, 1997

[40] G.C. Stone, M. Kurtz, R.G. Van Heeswijk, *"The Statistical Analysis of a High Voltage Endurance Test on an Epoxy"*, IEEE Trans. E.I., Vol. EI-14, pp. 315-326, 1979

[41] J.V. Champion, S.J. Dodd, *"The effect of Voltage and Material Age on the Electrical Tree Growth and Breakdown Characteristics of Epoxy Resins"*, J. Phys. D: Appl. Phys., Vol. 28, pp. 398-407, 1995

[42] J.V. Champion, S.J. Dodd, G.C. Stevens, *"An Examination of the Effect of Mechanical Stress on Electrical Breakdown in Synthetic Resin Insulators"*, J. Phys. D: Appl. Phys., Vol. 27, pp. 142-147, 1994

[43] J.V. Champion, S.J. Dodd, *"An Assessment of the Effect of Externally Applied Mechanical Stress and Water absorption on the Electrical Tree Growth Behaviour in Glassy Epoxy Resins"*, J. Phys. D: Appl. Phys., Vol. 32, pp. 305-316, 1999

[44] J.V. Champion, S.J. Dodd, G.C. Stevens, *"Quantitative Measurement of Light Emission During the Early Stages of Electrical Breakdown in Epoxy and Unsaturated Polyester Resins"*, J. Phys. D: Appl. Phys., Vol. 26, pp.819-828, 1993

[45] O. Naz, J. Lewiner, T. Ditchi, C. Alquié, *"Study of Charge Injection in Insulators Submitted to Diverging Fields"*, IEEE Trans. Diel. E.I., Vol. 5, pp. 2-8, 1998

[46] L.A. Dissado, O. Paris, T. Ditchi, C. Alquié, J. Lewiner, *"Space Charge Injection and Extraction in High Divergent Fields"*, Annual Report CEIDP, IEEE 99CH36319, Vol. 1, pp. 23-26, 1999

[47] O. Naz-Paris, Thèse de Doctorat, Université Paris VI, *"Etude d'Isolants Soumis à des Champs Divergents par une Mesure Directe des Distributions de Charges Injectées"*, January 2000

[48] J.V. Champion, S.J. Dodd, G.C. Stevens, *"Long-term Light Emission Measurement and Imaging during the Early Stages of Electrical Breakdown in Epoxy Resin"*, J. Phys. D: Appl. Phys., Vol. 27, pp. 604-610, 1994

[49] T.Tanaka, A. Greenwood, *"Effect of Charge Injection and Extraction on Tree Initiation in Polyethylene"*, IEEE Trans. Power Appar. Syst., Vol. PAS-97, pp. 1749-1759, 1978

[50] S.S. Bamji, A.T. Bulunski, R.J. Densley, *"Evidence of Near-Ultraviolet Emission during Electrical-Tree Initiation in Polyethylene"*, J. Appl. Phys., Vol. 61, pp. 694-699, 1987

[51] J.M. Alison, J.V. Champion, S.J. Dodd, G.C. Stevens, *"Dynamic Bipolar Charge Recombination Model for Electroluminescence in Polymer Based Insulation during Electrical Tree Initiation"*, J. Phys. D: Appli. Phys., Vol. 28, pp. 1693-1701, 1995

[52] Y. Li, J. Unsworth, *"Effect of Physical Aging on Dielectric, Thermal and Mechanical Properties of Cast-Epoxy Insulators"*, IEEE Trans. Diel. E.I., Vol. 1, pp. 9-17, February 1994

[53] J.V. Champion, S.J. Dodd, *"The Effect of Absorbed Water on Electrical Treeing in Epoxy Resins"*, DMMA Conference publication No. 430, pp. 206-210, IEE 1996

Chapter II - Material description and sample preparation

[1] J.C. Anderson, K.D. Leaver, R.D. Rawlings, J.M. Alexander, *Materials Science*, Third Edition, Chapman & Hall, ISBN 0442306261, 1985

[2] Ciba-Geigy, *"Low-Viscosity Unfilled Epoxy Casting and Impregnating System Instruction"*, sheet No.C.110c, 1990

[3] Private Communication

[4] M.P. Stevens, *Polymer Chemistry: an Introduction*, Reading, Mass.; London: Addison-Wesley, ISBN 0201073137, 1975

[5] H.R. Simonds, J.M. Church, *A Concise guide to Plastics*, second edition, Reinhold Publishing Corporation, New York, Chapman & Hall, LTD., London, 1963

[6] H. Lee, K. Neville, *Handbook of Epoxy Resins*, Mc Graw-Hill Book Company

[7] G. Challa, *Polymer Chemistry: an Introduction*, New York; London, Ellis Horwood, ISBN 0134896912, 1993

[8] H Saechtling, *International Plastics Handbook*, New York Macmillan, ISBN 0-02-949620-5, 1983

[9] W.R. Moore, *An Introduction to Polymer Chemistry*, University of London Press LTD, 1963

[10] J.R. Fried, *Polymer Science and Technology*, London Prentice Hall International Editions, ISBN 013685561x, 1995

[11] F. Knapp, *"Les Résines Epoxydes"*, Revue Brown Boveri, Société Anonyme Brown, Boveri & Cie (Baden), Tome 52, No. 8, pp.575-589, 1965

[12] H. R. Simonds, editor, *Source Book of the New Plastics*, Vol. 2, Reinhold Publishing Corporation, New York, Chapman & Hall, LTD., London, 1961

[13] Instructions Specific Heat Kit 219-0136, Perkin Elmer Corporation, 1968

[14] M.J Richardson, N.G. Savill, *"Derivation of Accurate Glass Transition Temperatures by Scanning Calorimetry"*, Polymer, Vol. 16, pp. 753-757, 1975

[15] M.J. Richardson, *"Precision Differential Calorimetry and the Heat of Fusion of Polyethylene"*, J. Polymer Sci., Part C, pp. 251-259, 1972

Chapter III - Dielectric spectroscopy

[1] A.K. Jonscher, *"The Universal Dielectric Response and its Physical Significance"*, IEEE Trans. EI, Vol. 27, pp. 407-423, 1992

[2] A.K. Jonscher, *"Review Article: Dielectric Relaxation in Solids"*, J. Phys. D: Appl. Phys., Vol. 32, pp. R57-R70, 1999

[3] D.K. Das-Gupta, P.C.N. Scarpa, *"Modelling of Dielectic Relaxation Spectra of Polymers in the Condensed Phase"*, DEIS feature article, Vol.15, pp. 23-37

[4] A. R. Kannurpatti, C.N. Bowman, *"Structural Evolution of Dimethacrylate Networks Studied by Dielectric Spectroscopy"*, Macromolecules, Vol. 31, pp. 3311-3316, 1998

[5] J.P. Runt, J.J. Fitzgerald, *Dielectric Spectroscopy of Polymeric Materials*, American Chemical Society, ISBN 0841233357, 1997

[6] A.J. Harrop, *Dielectrics*, London Butteworths, ISBN 0408703873, 1972

[7] C.N.R. Rao, K.J. Rao, *Phase Transitions in Solids*, London McGraw-Hill International Book Company, ISBN 0070511853, year 1978

[8] M.E. Baird, *"Determination of Dielectric Behavior at Low Frequencies from Measurements of Anomalous Charging and Discharging Currents"*, Rev. Modern Phys., Vol. 1, pp. 219-227, 1968

[9] B.V. Hamon, *"An Approximate Method for Deducing Dielectric Loss Factor from Direct-Current Measurements"*, Proc IEE, Vol. 99, pp. 151-155, 1952

[10] 1255 H.F. Frequency Response Analyser, *Operating Manuel*, Solatron Instruments, Issue 2a, Part No. 12550006 1987

[11] A.K. Jonscher, *Universal Relaxation law*, London: Chelsea Dielectrics Press, ISBN 0950871125, 1995

[12] J. Pugh, *"Dielectric Spectrometer - User Guide"*, Private issue provided with the system of measurements

[13] Y. Feldman, A. Andrianov, E. Polygalov, I. Ermolina, G. Romannychev, Y. Zuev, *"Time Domain Dielectric Spectroscopy: an Advanced Measuring System"*, Rev. Sci. Instrum., Vol. 67, pp. 3208-3216, 1996

[14] M. Meunier, N. Quirke, D. Binesti, G. Martic, J.M. Fourmigué, *"Identification of Space Charge in Cable Insulation: a New Approach Using Molecular Simulation"* Annual report CEIDP 97CH36046, pp. 68-71, 1997

[15] M. Meunier, N. Quirke, A. Aslanides, *"Characterisation of Charge Carrier Traps in Polymeric Insulators"*, Annual report CEIDP, 2000, to be published

Chapter IV - Space charge profile using PEA measurements

[1] O. Naz, J. Lewiner, T. Ditchi, C. Alquié, *"Study of Charge Injection in Insulators Submitted to Diverging Fields"*, IEEE Trans. Diel. EI, Vol. 5, pp. 2-8, 1998

[2] G.M. Sessler, *"Charge Distribution and Transport in Polymers"*, IEEE Trans. Diel. EI, Vol. 4, pp. 614-628, 1997

[3] J. Alison, *"A High Field Pulsed Electro-Acoustic Apparatus for Space Charge and External Circuit Current Measurement Within Solid Insulators"*, Meas. Sci. Technol., Vol. 9, pp. 1737-1750, 1998

[4] Y.Li, M. Yasuda, T. Takada, *"Pulsed Electroacoustic Method for Measurement of Charge Accumulation in Solid Dielectrics"*, IEEE Trans. Diel. E.I., Vol.1, pp. 188-195, 1994

[5] T. Maeno, T. Futami, H. Kushibe, T. Takada, C.M. Cooke, *"Measurement of Spatial Charge Distribution in Thick Dielectrics Using the Pulse Electroacoustic Method"*, IEEE Trans. E.I, Vol. 23, pp. 433-439, 1988

[6] T. Maeno, K. Fukunaga, *"High-Resolution PEA Charge Distribution Measurement System"*, IEEE Trans. Diel. EI, Vol. 3, pp. 754-757, 1996

[7] T. Takada, Y. Tanaka, N. Adachi, X. Qin, *"Comparison Between the PEA Method and the PWP Method for Space Charge Measurement in Solid Dielectrics"*, Vol.5, pp. 944-951, 1998

[8] T. Takada, *"Acoustic and Optical Methods for Measuring Electric Charge Distributions in Dielectrics"*, Annual Report CEIDP, 99CH36319, pp. 1-14, 1999

[9] A.S. De Reggi, B. Dickens, T. Ditchi, C. Alquié, J. Lewiner, I.K. Lloyd, *"Determination of the Polarisation-Depth Distribution in Poled Ceramic Ferroelectrics Using Thermal and Pressure Pulse Technique"*, J. Appl. Phys., Vol. 2, pp. 854-863, 1992

[10] T. Maeno, *"Calibration of the Pulse Electroacoustic Method for Measuring Space Charge Density"*, T. IEE Japan, Vol. 119-A, pp. 1114-1119, 1999

[11] T. Maeno, K. Fukunaga, T. Takada, *"High Resolution PEA Charge Distribution Measurement System"*, Annual report CEIDP, 94CH3456-1, pp. 200-205, 1994

[12] J.M. Alison, *"Thin Film, High Voltage AC/DC Pulsed Electro-Acoustic Apparatus"*, 2nd biannual report, May 1999 Ercos contract no: GRL/93904

[13] J.M. Alison, L. Askew, R.M. Hill, *"Experimental Determination of the Dynamics of Space Charge Development in Insulators"*, annual report, October 1994-september 1995

[14] L.A. Dissado, O. Paris, T. Ditchi, C. Alquié, J. Lewiner, *"Space Charge Injection and Extraction in High Divergent Fields"*, annual report CEIDP, 99CH36319, pp. 23-26, 1999

Chapter V - Electroluminescence

[1] W.W. Piper, F.E. Williams, *"Theory of Electroluminescence"*, Phys. Rev., Vol. 8, pp. 1809-1813, 1955

[2] W.A. Hartman, H.L. Armstrong, *"Electroluminescence in Organic Polymers"*, J. Appl. Phys., Vol. 38, pp.2393-2395, 1967

[3] L. Sanche, *"Nanoscopic Aspect of Electronic Aging in Dielectrics"*, IEEE Trans. Diel. E.I., Vol. 4, pp. 507-543

[4] C. Laurent, *"Optical Pre-Breakdown Warning in Insulating Polymers"*, Annual Report Conference on Electrical Insulation and Dielectric Phenomena (CEIDP), Västerås, Sweden, 98CH36132, pp. 1-12, 1998

[5] F.I. Henry, *Electroluminescence and Related Effects*, New York and London, Academic Press, 1963

[6] C. Laurent, F. Massines, C. Mayoux, *"Optical Emission due to Space Charge Effects in the Electrically Stressed Polymers"*, IEEE Trans. Diel. E.I., Vol. 4, pp. 585-603, 1997

[7] L. Cissé, *"Contribution à l'Etude des Mécansimes d'Electroluminescence dans les Isolants Polymères"*, thèse de Doctorat, Université Paul-Sabatier, 1998

[8] E. Hirschlaff, *Fluorescence and Phosphorescence*, London: Methuen, 1938

[9] E.J. Bowen, *Luminescence in Chemistry*, D. Van Nostrand Company LTD, London, ISBN 0442009615, 1968

[10] D. Mary, M. Albertini, C. Laurent, *"Understanding Optical Emissions from Electrically Stressed Insulating Polymers: Electroluminescence in Poly(ethylene terephtalate) and Poly(ethylene 2,6-naphthalate) Films"*, J. Phys.D: Appl. Phys., Vol. 30, pp 171-184, 1997

[11] G. Teyssedre, D. Mary, C. Laurent, C. Mayoux, *"Optical Emission due to Space Charge Recombination in Insulating Polymers: an Insight into Electrical Ageing"*, Space Charge in Solid Dielectrics, ISBN 095335380X, pp. 285-302, 1997

[12] J.L. Augé, C. Laurent, G.C. Montanari, D. Fabiani, *"Detection of DC threshold of Polyethylene Materials Through Space Charge and Electroluminescence Measurements"*, Annual report CEIDP, 99CH36319, pp. 564-567, 1999

[13] R. Martin, G.A. Clarke, *"Fluorescence of Benzoic Acid in Aqueous Acidic Media"*, J. Phys. Chem., Vol. 82, pp. 81-86, 1978

[14] G. Teyssedre, D. Mary, J.L. Augé, C. Laurent, *"Dependence of Electroluminescenceintensity and Spectral Distribution on Ageing Time in Polyethylene Naphthalate as Modelled by Space Charge Modified Internal Field"*, J. Phys. D: Appl. Phys., Vol. 32, pp. 2296-2305, 1999

[15] F. Massines, P. Tiemblo, G. Teyssedre, C. Laurent, *"On the Nature of the Luminescence Emitted by a Propylene film after Interaction with a Cold Plasma at Low Temperature"*, J. Appl. Phys., Vol. 81, pp. 937-943, 1997

[16] G. Teyssedre, L. Cissé, C. Laurent, F. Massines, *"Spectral Analysis of Optical Emission Due to Isothermal Charge Recombination in Polyolefins"*, IEEE Trans. Diel. E.I., Vol.5, pp. 527-535, 1998

[17] L.A. Dissado, O. Paris, T. Ditchi, C. Alquié, J. Lewiner, *"Space Charge Injection and Extraction in High Divergent Fields"*, Annual report CEIDP, 99CH36319, pp. 23-26, 1999

[18] L.A. Dissado, private communication

[19] G. Teyssedre, D. Mary, C. Laurent, *"Analysis of the luminescence Decay Following Excitation of Polyethylene Naphtalate Films by an Electric Field"*, J. Phys. D: Appl. Phys., Vol. 31, pp. 267-275, 1998

[20] O. Naz-Paris, Thèse de Doctorat, Université Paris VI, *"Etude d'Isolants Soumis à des Champs Divergents par une Mesure Directe des Distributions de Charges Injectées"*, January 2000

[21] D.H. Williams, I Fleming, *Spectroscopy Methods in Organic Chemistry*, McGraw-Hill, London, 5th ed. ISBN 0077091477, 1995

Appendices

Appendix I

The following values have been measured by the manufacturer Ciba-Geigy [1].

Properties	Values	Comments
Electric strength	12-14MV/m	Measured by step-by-step method [2] 3mm, 20°C
Relative permittivitty	3.7-3.9	Measured at 1kHz
Loss tangent	0.007-0.009	Measured at 1kHz
Water absorption	15-25mg	Cured resin 24h at 23°C
	40-50mg	Cured resin 1/2h at 100°C

NB : It is commonly estimated that the samples are saturated with water when used in the different experiments if not stored in desiccators at any time.

[1] Ciba-Geigy, *"Low-viscosity Unfilled Epoxy Casting and Impregnating System Instruction"* sheet No.C.110c, 1990

[2] International Standard, *Methods of Test for Electrical Strength of Solid Insulating Materials,* IEC 243-1, 1988

Appendix II

Experimental protocol performed to measure the glass transition temperature T_g by Differential Scanning Calorimetry (DSC) method.

Measurement carried out by steps:

(a) Sample

3min 0°C
Heat from 0°C to 100°C at 20°C/min
Hold 6min 100°C
Cool from 100°C to 0°C at 20°C/min
Hold 6min 0°C
Heat from 0°C to 100°C at 20°C/min
Hold 3min 100°C

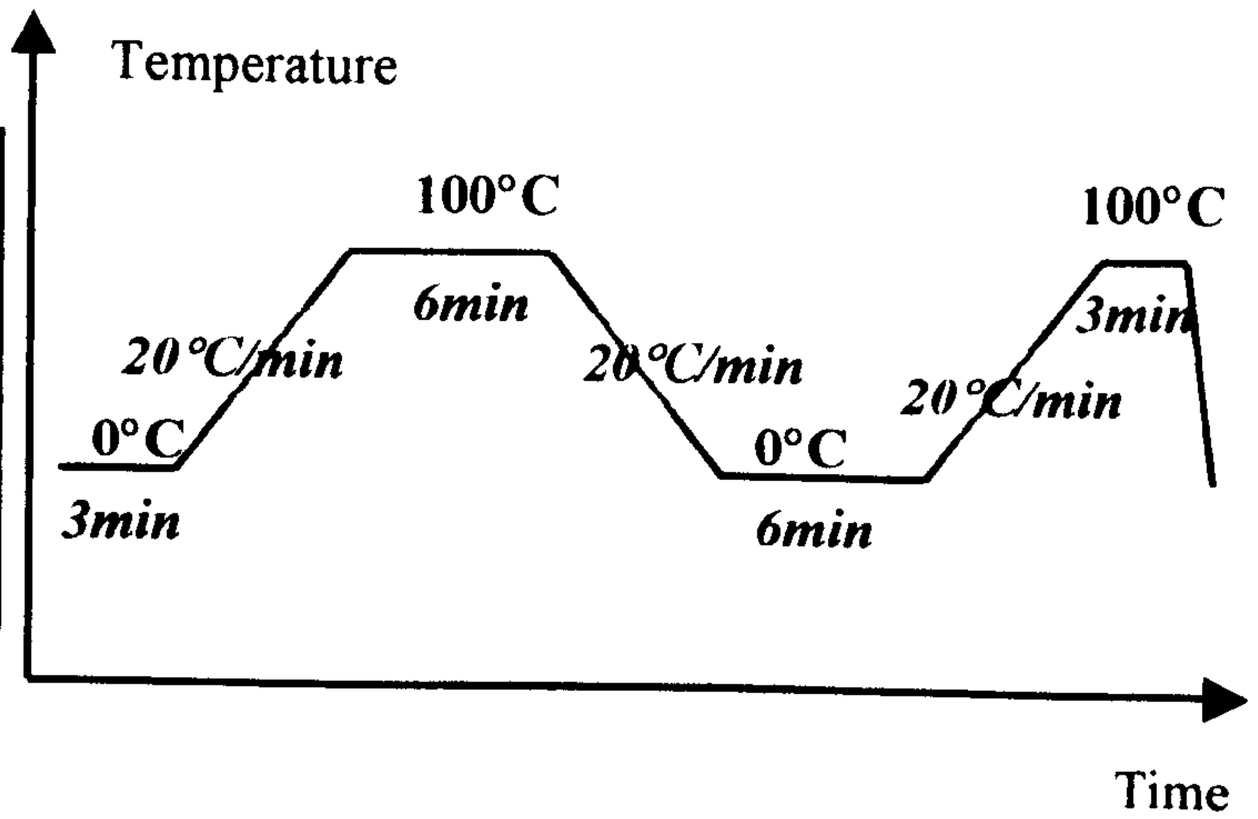

(b) Empty pan

3min 0°C
Heat from 0°C to 100°C at 20°C/min
Hold 3min 100°C

(c) Sapphire standard

3min 0°C
Heat from 0°C to 100°C at 20°C/min
Hold 3min 100°C

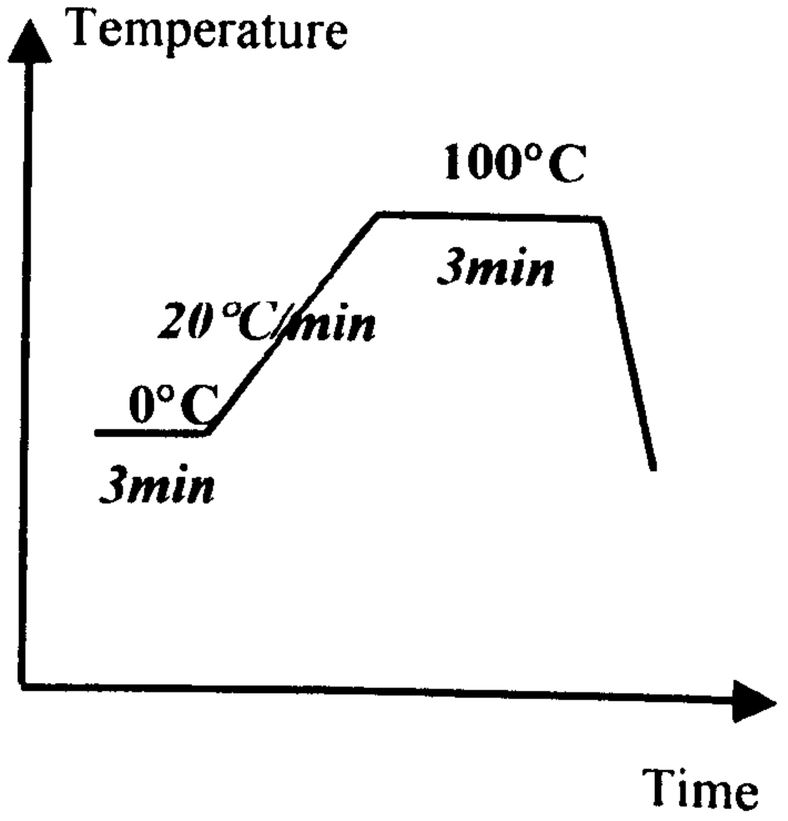

Publications

Publications

K. Fukunaga, V. Griseri, *"Space Charge and Exernal Current Measurements of a Filler-Free Epoxy Resin"*, Trans. IEE of Japan, Vol. 120-A, No. 5, May, 2000

V. Griseri, K. Fukunaga, C. Laurent, D. Mary, L.A. Dissado, J.C. Fothergill, *"Charge Injection, Electroluminescence, and Ageing of an Epoxy Resin in High Divergent Fields"*, Dielectric Materials, Measurements and Applications Conference publication No. 473, pp. 88-93, IEE 2000

K. Fukunaga, T. Maeno, V. Griseri, *"Space Charge Observation of a Filler-Free Epoxy Resin"*, Annual Report Conference on Electrical Insulation and Dielectric Phenomena, IEEE 00CH37132, Vol. 1, pp. 125-127, 2000

Letter

Space charge and external current measurements of a filler-free epoxy resin

Kaori Fukunaga, member (Communications Research Laboratory)
and Virginie Griseri, non-member (University of Leicester)

Space charge behaviour in epoxy resin has been investigated for several years. For example, epoxy resin of a printed circuit board has also been investigated in order to analyse ion migration phenomena by measuring space charges.

In this paper, a type of filler-free epoxy resin was used to know the fundamental space charge phenomena in epoxy resin. Based on the space charge measurement by the pulsed electroacoustic (PEA) method and external current measurement, it is concluded that space charge formation in the filler-free epoxy resin under dc electric field was strongly influenced by the temperature.

keywords: space charge, pulsed electroacoustic method, epoxy resin, external current

Space charge behaviour in epoxy resin has been investigated for several years. According to the space charge profiles measured at various temperatures and humidities, ionic impurities were generated after water absorption at high temperature[1]. These ions were able to move under dc electric field and accumulated near the electrodes. Epoxy resin from a printed circuit board has also been investigated in order to analyse ion migration phenomena by measuring space charges[2]. Although the influence of the temperature was studied on printed circuit boards, all the conditions were below their glass transition temperatures.

On the other hand, there is much interesting work on tree growth behaviour in filler-free epoxy resins that has a glass transition temperature of about 50 °C [3, 4]. The high reproducibility of the electrical trees in addition to other electrical properties, such as partial discharge characteristics, proved that their specimens were extremely useful in obtaining information about the ageing of the resin. We therefore used a type of the same filler-free resins (CY1301) to investigate the temperature dependence of space charge behaviour of epoxy resin. The thickness of the sample was 270 μm, and the space charge profiles were measured by the PEA method [5, 6] at 20 °C and 40 °C under the electric field of 15 kV/mm for 150 hrs and after the electrodes were short circuited.

Surface charges on both electrodes were observed under the electric field as shown in Fig. 1. The solid line shows the space charge and the broken line shows the electric field. This distribution appeared at both temperatures of 20 °C and 40 °C . After 150 hours voltage application, the space charge and electric field profiles did not change significantly.

Figure 2 shows the remaining charge profile at 20 °C immediately after the electrodes were short-circuited (< 5 sec). Negative charges appeared near the cathode, and positive charges appeared near the anode. Since the surface charges changed their polarities after the short-circuit, they were considered to be induced by the injected internal charges.

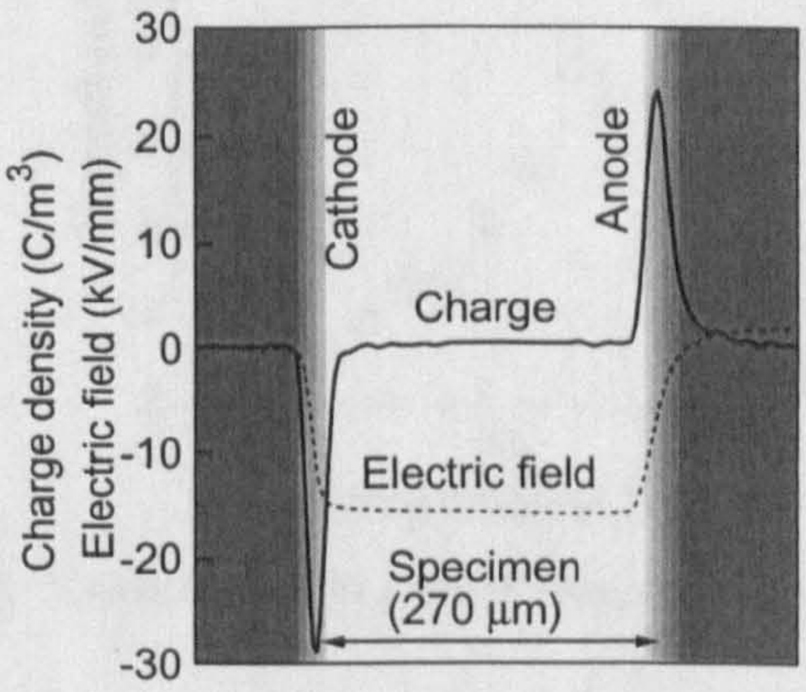

Fig. 1 Space charge and electric field profiles under dc electric field of 15 kV/mm.

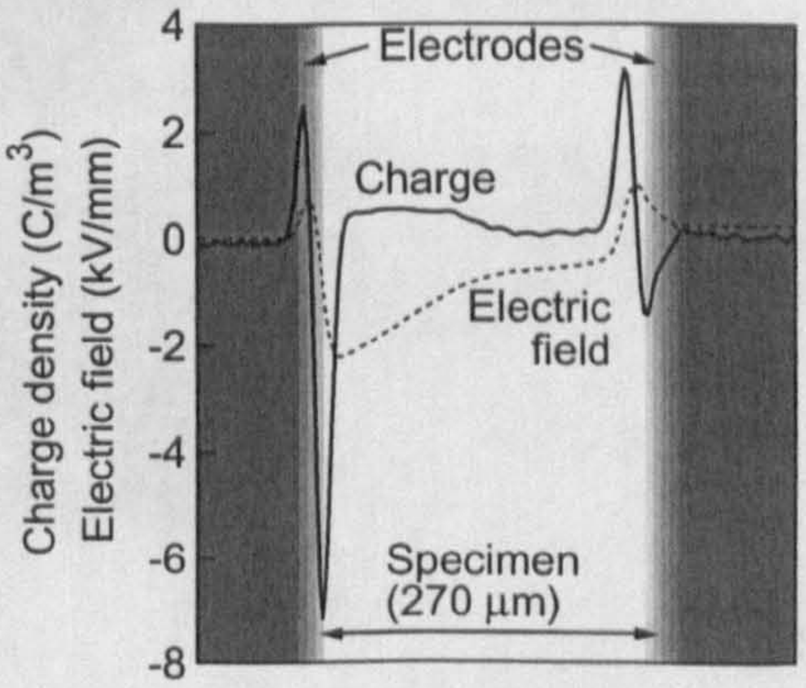

Fig. 2 Space charge and electric field profiles after the electrodes were short circuited (at 20 °C)

In the case of 40 ˚C , on the other hand, internal space charge was not observed and only surface charge remains on the both electrodes immediately after the electrodes were short-circuited (< 5 sec). Similar phenomena was found by Dr. J. M. Alison with the same specimen by applying an electric field of 25 kV/mm. It was explained that the slow polarisation existed in epoxy resin, resulting in the remaining charge distribution due to the slow depolarisation.

Here, charges are expected to be injected also at 40 ˚C . In order to know the reason why the injected charge could not been observed at 40 ˚C , the external circuit current was measured by changing the temperature. As shown in Fig. 4, the current at 40 ˚C is about 3 times larger than that at 20 ˚C .

The increase of the current suggests that injected charge were not able to accumulate near the surface and move through.

Although further investigation is required, it is clear that the space charge phenomena is strongly influenced by the temperature, and it could be related to the glass transition temperature of the resin.

The authors would like to express their thanks to Dr. J. V. Champion and Dr. S. J. Dodd, London Guildhall University, Dr. John M. Alison, King's College London and Dr. John Fothergill, University of Leicester for their helpful advice and valuable comments on this work. We also thank Mr. T. Forryan for his help on preparation of specimens.

(Manuscript was received on 10 February, 2000)

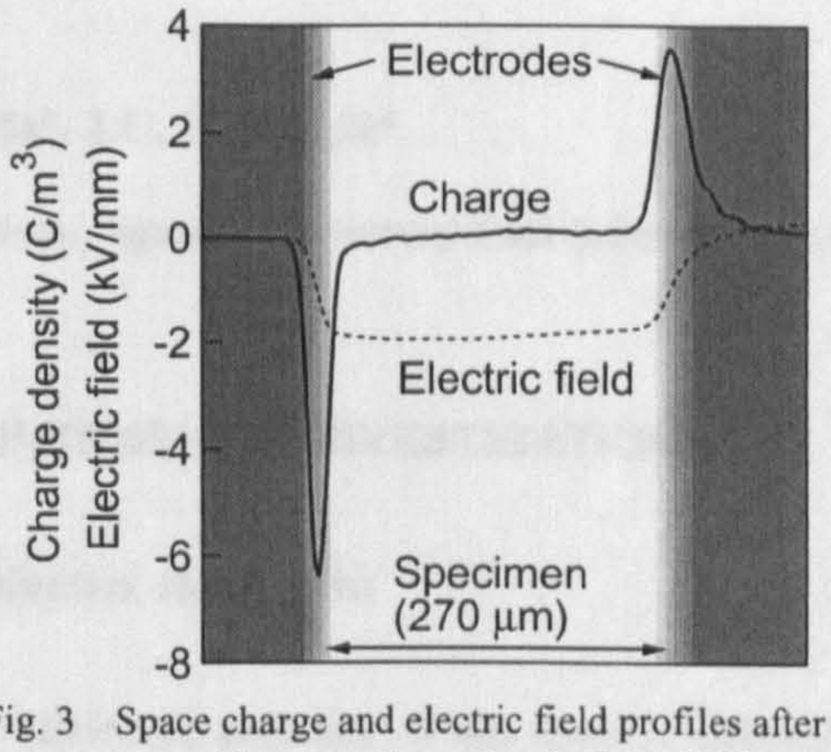

Fig. 3 Space charge and electric field profiles after the electrodes were short circuited (at 40 ˚C)

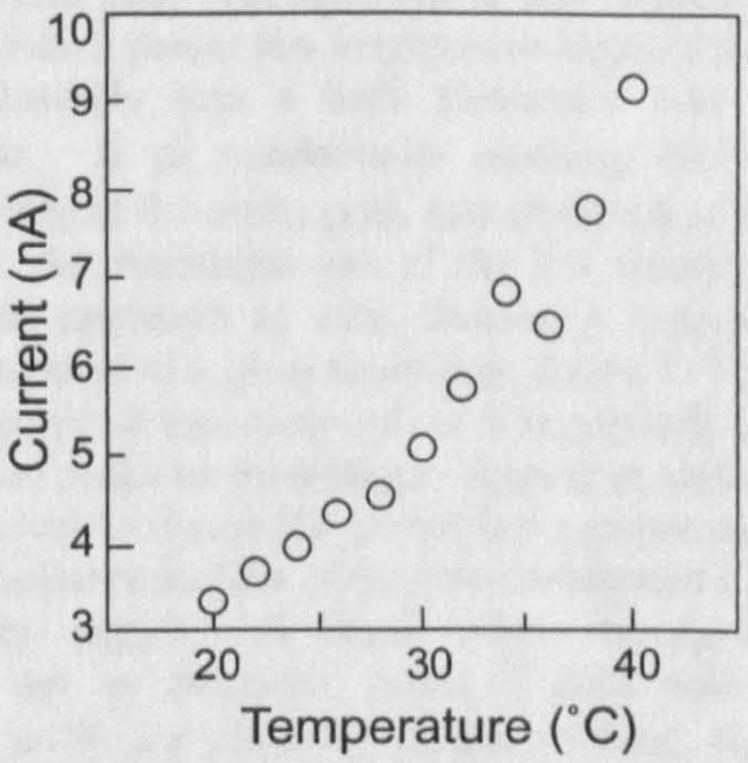

Fig. 4 External current measured be changing the temperature.

References

(1) T. Iizuka, Y. Takai, K. Fukunaga and T. Maeno, "Measurement of space charge distribution in epoxy resin after water absorption treatment", IEEE Conference on Electrical Insulation and Dielectric Phenomena, Minneapolis, No. 2A-2, pp. 41-44 (1997)

(2) K. Fukunaga: IEEE Electrical Insulation Magazine, Review Paper, "Industrial Applications of Space Charge Measurement in Japan", Vol. 15, No. 5, pp. 6-18 (1999)

(3) J. V. Champion, S. J. Dodd and J. M. Alison, "The correlation between the partial discharge behaviour and the spatial and temporal development of electrical trees grown in an epoxy resin.", J. Phys. D: Appl. Phys. Vol 29, pp. 2689-2695 (1996)

(4) J. V. Champion and S. J. Dodd, " An assessment of the effect of externally applied mechanical stress and water absorption on the electrical tree growth behaviour in glassy epoxy resins.", J. Phys. D: Appl. Phys. Vol 32 , pp. 305-316 (1999)

Kaori Fukunaga (member) received her Ph.D. in electrical engineering from Tokyo Denki University in 1993. She joined Communications Research Laboratory in 1995, and had been visiting the University of Leicester in 1999, UK. Her major is dielectrics and electrical insulation. She is a member of IEEE and IEE of Japan.

Virginie Griseri (non-member) received her M. Sc. in polymer chemistry from University of Paul Sabatier, France in 1996, and she is a PhD student of the University of Leicester, UK. Her major is polymer dielectrics.

CHARGE INJECTION, ELECTROLUMINESCENCE, AND AGEING OF AN EPOXY RESIN IN HIGH DIVERGENT FIELDS

V. Griseri*, K. Fukunaga[+], C. Laurent,[#] D. Mary[#], L.A. Dissado*, J.C. Fothergill*

*University of Leicester, UK, + Communications Research Laboratory, Japan, # University Paul Sabatier, France

INTRODUCTION

Most experimental studies of electrical ageing have concentrated on semi-crystalline polymers such as those used in cable insulation and capacitors (see for example [1]). Theoretical models [2-4] for electrical ageing have been developed on the basis of these studies. The consensus is that ageing involves the formation of low-density regions, though the mechanisms responsible are disputed. For example, bond scission by high-energy electrons [2,5], and mechanical deformation have both been suggested. Both of these mechanisms are related to charge injection and the subsequent formation of high local fields. The semi-crystalline polymers studied so far have similar chemistries and almost identical morphologies. They tend, therefore, to show many similarities in, for example, the size of the energy barriers for the ageing reaction, critical ageing levels, and field dependence of ageing [4]. These similarities make it difficult to discriminate between mechanisms. Epoxy resins, however, are network polymers with a different molecular chemistry to that of the semi-crystalline polymers and are thus ideal to evaluate the proposed ageing mechanisms. We have therefore studied an epoxy resin (CY1301) under both uniform field and high divergent field conditions. Uniform field conditions were used to gain baseline characteristics for the properties of the unaged epoxy resin, and also for the effects of electrical ageing in low fields. Studies in high divergent fields were made using an electrode arrangement adapted from that of [6]. A number of wires set approximately *0.5mm* apart were embedded, parallel to the flat faces, in thin (~290 μm) flat samples. The radius of the wires ranged from 5 μm (gold plated tungsten) to 25 μm (tungsten). Relatively small voltages applied to the wires (≤5 kV DC) therefore produced local fields up to 170 kV/mm depending upon the wire radius chosen. These field levels are high enough to inject space-charge [6] without leading to instantaneous failure. This geometry, therefore, may both inject charge and simulate local stress enhancements arising from charge accumulation. The number of wires is large (~30) so that the volume affected is big enough to allow changes on ageing to be detectable.

EXPERIMENTAL INVESTIGATIONS

Dielectric Response

The dielectric response of the epoxy exhibited a glass transition just below 40 °C [7]. At this temperature and above a loss peak was observed at low frequencies that merged into a power law response at higher frequencies and eventually into a high frequency loss peak at ~3 10^5Hz. A dc conductivity masking the low frequency side of the alpha peak was observed at T≥70 °C, figure 1. An Arrhenius plot of the low frequency peak show the approach to zero frequency typical of the alpha response of a glass transition, figure 2. The power law response is less clear-cut as it is partially obscured by the two peaks surrounding it. Ageing in uniform field progressively reduced the power law component, figure 3a. A similar reduction of the loss component C" in this frequency region was found when the ageing was carried out in divergent fields (7 days with –2 kV applied to 50 μm diameter tungsten wires), figure 3b. Here the dielectric measurement was carried out both between the two plane electrodes and between the wires and a plane electrode. The results differed only by a multiplicative factor arising from the different geometries.

Current-Voltage Measurements

Uniform Applied Fields. These measurements were performed on samples 55 μm thick using a step ramp technique. The dwell time was *300s* on the ascending ramp and *150s* on the descending ramp. The current was averaged after the first *50s* of the dwell time and was measured simultaneously with the electroluminescence (EL). The ascending ramp shows a linear I-E dependence up to 140 kV/mm, and thereafter a strongly field dependent current up to 300 kV/mm. In the experiment the sample was cycled to progressively higher applied fields. It was noted that the current in the ohmic region varied from cycle to cycle whereas that in the high field region was effectively unchanged. Figure 4 shows the current obtained on the final cycle. The high field current could be described empirically by an E^4 law, but it also fits an exponential dependence appropriate to charge hopping between neutral traps, i.e. $I \propto \left[\exp(aeE/kT) - \exp(-aeE/kT)\right]$, see figure 4. The

estimated value of a is 0.52 nm, which is acceptable for this kind of mechanism. The descending ramp shows a reverse current that changed sign below 220 kV/mm, indicating the presence of a zero-field plane in the dielectric at and below these applied fields as a consequence of the strong charging occurring on the ramp-up.

Space Charge Measurements

In Uniform Applied Fields. The pulsed electroacoustic (PEA) technique was used to measure the space charge generated in the epoxy under uniform fields applied by brass electrodes. The form of the space charge distribution observed depended upon the duration of the period of electric stress and the temperature. Under short term stressing (1-6h) at room temperature (~25°C) a field of ≥18 kV/mm was required before charge injection could be identified via the formation of homocharges near the electrodes, figure 5. Homo space-charge was also, however, produced by prolonged stressing (1day to 2 weeks) at lower fields, e.g. 7kV/mm. A similar behaviour was obtained at 35 °C, figure 6. At temperatures of 40 °C and above any space charge produced by prolonged stressing at low fields was obscured by the polarisation charges on the electrodes.

In Divergent Applied Fields. These samples were first measured at room temperature with 0.67 kV applied between the plane electrodes with the wires floating, figure 7a. No signal was observed from parts of the samples that contained no wires but a weak peak (approx. -0.5 C/m^3) was obtained around the region of the wires. A sample was then stressed by applying 1.5 kV to the wires for 1 week at 33 °C. The voltage was removed and the sample measured at 33 °C. A positive signal was observed across most of the sample rising to a peak of ~0.75 C/m^3 close to the wires, figure 7b. The signal persisted for at least 90 min at 33 °C. This result is consistent with the injection of positive charge from the wires that are retained in deep traps [8]. The contribution of a polarisation gradient [9] to the effective charge would be expected to give a similar signal but it should decay rapidly as the polarisation relaxed.

Electroluminescence Measurements

In Uniform Applied Fields. These were measured simultaneously with the charging and discharging currents. Continuous EL was observed to occur above –150 kV/mm dc when ramping up. When the voltage was ramped down EL ceased at –250 kV/mm dc, figure 8.

In Divergent Applied Fields. In the first instance a square voltage pulse of duration of 100 ms to 60 s was applied to the sample. Electroluminescence was observed at the beginning and end of the pulse if an onset voltage is exceeded, figure 9. The onset voltage ~400-500V corresponds to a field of 22-27 kV/mm if the wires are assumed to lie exactly in a plane midway through the sample. Continuous electroluminescence was not observed in these experiments even at the highest fields reached of 160 kV/mm. No appreciable polarity effect was found. A second set of experiments was carried out in which a train of positive probe pulses was applied following a negative polarisation pulse. The probe voltage level was chosen so that it did not excite any luminescence by itself. The delay time between the polarisation pulse and the 1st probe was varied with a minimum of 1 s. The repetition frequency of the probe pulses was also varied, but this parameter was not influential and most of the results were obtained by using a frequency of 1Hz. The luminescence intensity detected decreased throughout the sequence of probe pulses following on from the initial polarisation pulse. In these experiments the probe pulses detected luminescence up to several seconds after polarisation. A large scatter about a typical mean value of 60 s was observed with extremes of 35 s and 80 s. The period over which luminescence is detected ('decay' time) can be taken to be the time required for the space charge to reduce to a level below which it is incapable of exciting luminescence centres to a detectable extent. This interpretation is valid as long as the probe pulses themselves do not affect the amount of space charge existing at the time of their application. In order to check that this is indeed the case the delay time between the polarisation pulse and the 1st probe pulse was varied over the range 1 s to 16 s. The EL measured by the 1st probe pulse decreased (approximately exponentially with time) but the time for the EL to decay (i.e. decay time) was not altered appreciably. This indicates that the probe pulses did indeed act as true probes for the space charge field. No appreciable effect on the 'decay' time was observed when the polarisation pulse was varied in magnitude (from 2 to 2.8 kV) and duration (from 100ms to 60 s). This indicates that the process of charge injection and accumulation in the vicinity of the wires is saturated in a time less than 100 ms, and that the field dependence of charge injection is not very strong at these levels (108 to 150 kV/mm). This is in agreement with other workers [8]. It was also noted that EL was observed on the first two probe pulses even when the voltage of the polarisation pulse was set below the EL threshold of 500 V. This observation demonstrates that charge injection can occur without detectable EL, but its presence can be revealed when the probe pulse increases the local field. The need to increase the local field through the opposite polarity pulse implies that a true threshold field is required in order to generate EL in this case.

DISCUSSION

The PEA technique has shown that short-time space charge injection occurs in uniform applied fields above

18 kV/mm and in divergent fields of at least 52 kV/mm (at the wire) over a period of time. This latter measurement could be attributed to a positive polarisation gradient around the wires, however, the dielectric response shows that any polarisation should have relaxed within a few seconds, whereas the positive PEA signal has not decayed even 90 minutes after voltage removal. The signal therefore appears to be due to injected positive charge. This is confirmed by the transient EL data in divergent fields, for which the onset threshold field of 22-27 kV/mm correlates well with that found for injection in the PEA experiments.

These experiments also show that the common assumption that uniform field injection occurs at low fields because of local stress enhancing features on the electrode surfaces is not applicable in this case unless the injecting features are smaller in size than the 5 μm wire radius, e.g. crystalline boundary edges. Because of the presence of space charge at low fields we would expect to find a non-ohmic I-E dependence above 18 kV/mm in uniform fields. This is not the case. When the high-temperature low-field (3.5 V/mm) conductivity determined from the dielectric response is extrapolated to T=24 °C (activation energy = 1.6 eV) it yields a value ($2.2\ 10^{-16}$ S/m) close to that found for fields up to 140kV/mm (i.e. ~ $5.2\ 10^{-17}$ S/m). This implies that space charge injection does not modify the conductivity very much in the experiments performed at uniform fields up to ~140 kV/mm. The high activation energy for the linear conductivity indicates that charge transport is dominated by hopping between neutral deep traps. Hence, in the thin samples, injected charge may be trapped close to the electrodes to form a virtual electrode during the dwell time at a given voltage. The dielectric thickness would then be reduced slightly giving an actual electric field that would be slightly higher than the applied field but still uniform.

A possible explanation of the transient EL observed in divergent fields lies with the excitation of luminescence centres by inelastic scattering of the injected carriers up to the point where a sufficient amount of charges have been trapped in the vicinity of the wire to counterbalance the injecting field. On depolarisation the field at wires has the same magnitude as the applied injecting field but in the opposite direction. Consequently the same EL excitation occurs on extraction and with essentially the same magnitude. The absence of continuous dc EL is in accordance with a transient injection process limited by the space charge field. An alternative mechanism based on discharges in sub-micro sized mesovoids cannot be ruled out, however, without a spectral analysis of the EL emission. Conversely, a continuous EL emission is found for uniform applied fields above 160 kV/mm. At these fields, different continuously operating excitation mechanisms can be invoked e.g. charge packet generation leading to a recombination front between positive and negative charge carriers [10]. It is noteworthy that the EL onset-corresponds to the change from the ohmic to the non-linear regimes in the current measurements. This correlation has previously been reported for different polymeric materials submitted to a dc field [5]. It indicates that the high-field conduction process drives the excitation of EL. Our observation of an exponential field-dependence of the conductivity indicates a trap-to trap hopping mechanism for the mobile carriers that enables the charge packet to advance in the form of an ionisation front [11]. Further work is, however, needed to determine the details of the relationship between current and EL in epoxy resins.

The maximum applied field achieved so far in the divergent field geometry only just reaches the onset value for continuous EL in uniform applied fields and does not generate continuous EL. Transient electroluminescence is, however, observed on polarisation and depolarisation at fields above an onset value. The results of the probe-pulse experiments indicate that even below the onset field for transient luminescence, the applied voltage generates space charge. At these fields the PEA experiments show that some space charge can be generated given sufficient time. These charges can produce luminescence when a sufficiently large pulse of opposite polarity is applied. It is noticeable that luminescence occurs when the sum of the polarisation voltage and the probe voltage is sufficient to exceed the EL onset field found in the single pulse experiments. The quantity of charges available to produce luminescence decays rapidly with time (time constant ~ 10.5 s). It therefore appears that the charges have a non-radiative form of neutralisation, with luminescence only occurring when the local field exceeds a level sufficient for rapid charge injection or extraction. These results associate the luminescence with charges possessing a high kinetic energy, i.e. those charges that initiate EL via inelastic scattering. In lower fields extraction or non-radiative recombination can proceed without luminescence. This would be consistent with the observation that the onset fields and field dependence of electroluminescence are the same for the polarisation and depolarisation transients in both positive and negative polarity.

The evidence for ageing under the influence of electric fields high enough to inject space charge comes from two directions. In the first instance there is reduction of the intermediate power law response in the dielectric response. The epoxy used was cured at room temperature and thus had a T_g about 10 °C lower than if it had been post-cured at high temperature. However, the change cannot be assigned to a global increase of T_g by additional cross-linking, as the alpha-response is not affected. Power law dielectric responses have been associated with a hierarchy of relaxing dipoles embedded within one another in a self-similar form (e.g. see [12]). Fragmentation of such a hierarchy such as to reduce the number of embeddings, will reduce the frequency range of the power law dependence. The removal of this response on ageing would thus be attributable to a fragmentation of the self-similar sys-

tem; probably by additional cross-linking which would break connections in the hierarchy of relaxations. The second instance of ageing relates to charge injection on long time exposure to fields below the short-time onset threshold. It is not clear what is happening here, except that the factors influencing charge injection are being altered over a period of time. Possibly ionically dissociated species migrate slowly to the electrode in the electric field and produce heterocharge that eventually builds up sufficiently to induce homocharge injection. A process like this can also be expected to cause material changes over a long period of stressing in consequence of injection currents and local field modification. The changes in the ohmic current that are observed during voltage cycling may provide further evidence that changes are introduced by exposure to high fields. A systematic investigation is, however, required in order to verify this effect.

CONCLUSIONS

- Charge injection in both uniform and divergent fields has been observed. The onset field for injection in both cases is essentially the same and equal to the onset field for transient electroluminescence.
- Charge injection at these fields has been shown to reduce the response of certain set of re-orientable dipoles in the epoxy resin.
- Long term stressing at lower fields can lead to charge injection even at fields below the onset threshold for short-term injection and electroluminescence.
- A high field conduction process involving trap-to trap hopping is associated with continuous EL.

ACKNOWLEDGMENTS

The authors would like to thank Dr. J. Alison (King's College London), Prof. J. Champion and Dr. S. Dodd (London Guildhall University) for their useful discussions and practical assistance.

REFERENCES

1. J-L Parpal, J.P.Crine, C.Dang, 1997, IEEE Trans. Diel.&EI-4, 197-209
2. J.P.Crine, 1997,IEEE Trans. Diel. & EI- 4, 487-495
3. T.J.Lewis, J.P.Llewellyn, M.van der Sluijs, R.N.Hampton, 1996, IEE Conf. Pub. 430, 220-224
4. L.A.Dissado, G.Mazzanti, G.C.Montanari, 1997, IEEE Trans Diel.& EI-4, 496-506
5. D.Mary, C.Albertini, C.Laurent, J.Phys.D., 1997, Appl.Phys., 30, 171-184
6. O.Naz, J.Lewiner, T.Ditchi, C.Alquie, 1998, IEEE Trans. Diel. & EI-5, 2-8
7. J.V.Champion, S.J.Dodd, J.Alison, and L.Askew, 1998, Proc.IEEE 6th Int.Conf.Cond. & Breakdown in Solid Dielectrics, 321- 324
8. L.A.Dissado, O.Paris, T.Ditchi, C.Alquie, and J.Lewiner, 1999, Ann. Rep.CEIDP, 23-26.
9 A.De Reggi , B.Dickens, T.Ditchi, C.Alquie, J.Lewiner, I.K.Lloyd, J.Appl.Phys.,1992, 71, 854-863.
10. J.L.Augé, C.Laurent, G.C. Montanari, D.Fabiani, 1999, Ann. Rep. CEIDP, 564-567
11. K.Kaneko, T.Mizutani, Y.Suzuoki,, 1999, IEEE Trans. Diel. & EI, 6, 152-158.
12. R.M.Hill, L.A.Dissado, R.R.Nigmatullin, 1991, J.Phys.Cond.Mat., 3, 9773-9790

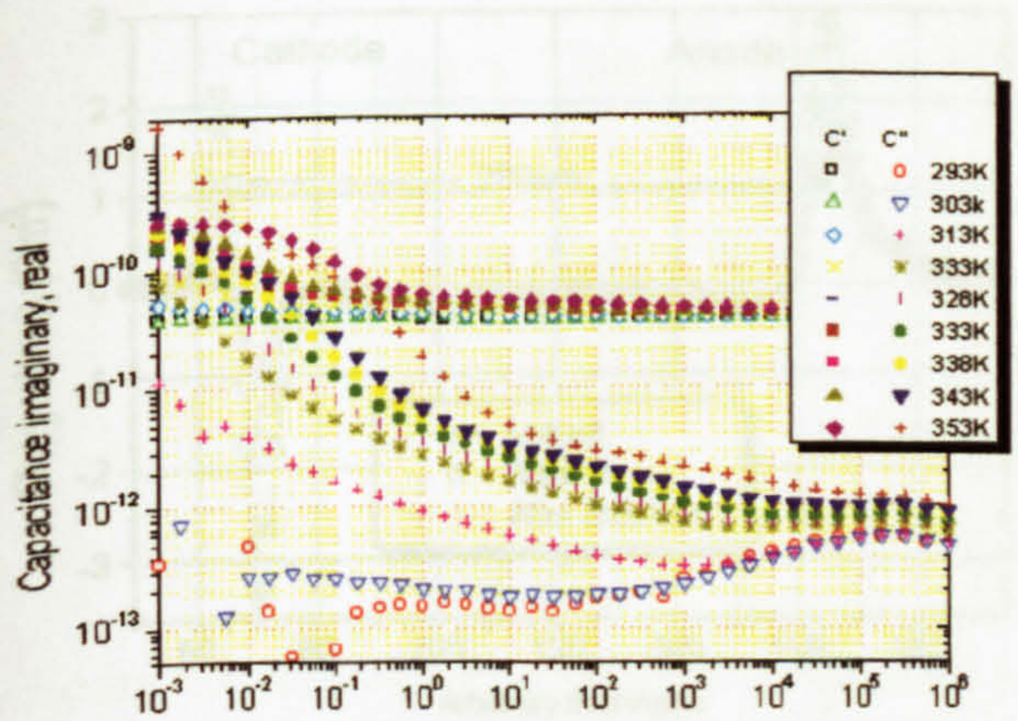

Figure 1. Dielectric response measured for a range of temperatures.

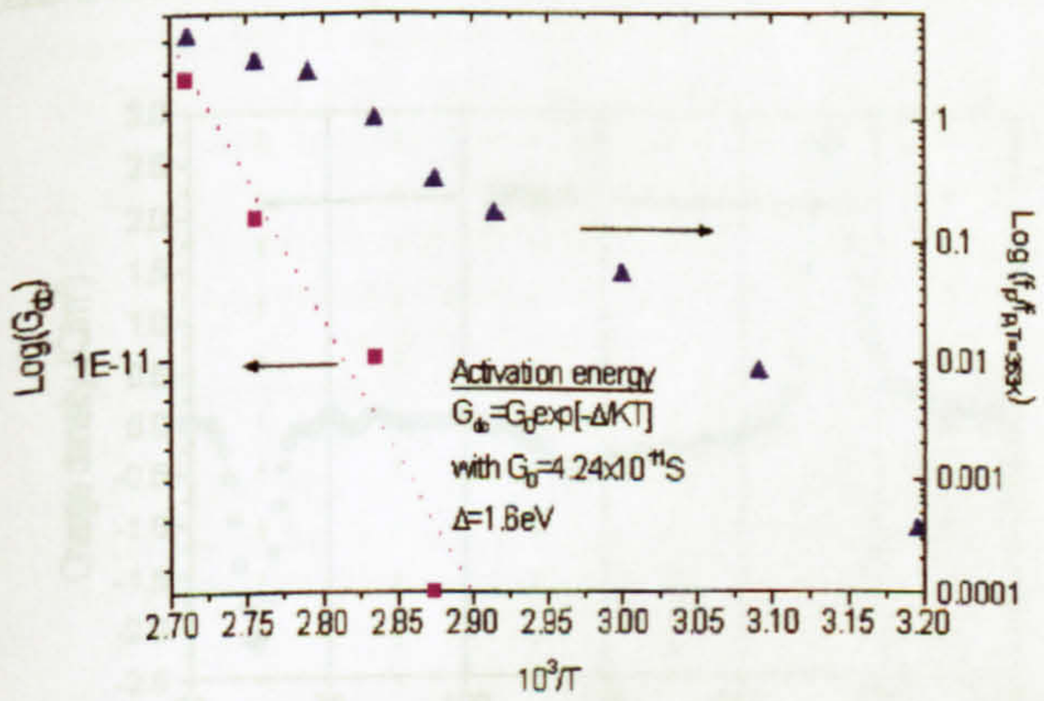

Figure 2. Arrhenius plots of the relative position of the alpha dielectric response ▲ (Right Hand Scale) and the conductance ■ (Left Hand Scale)

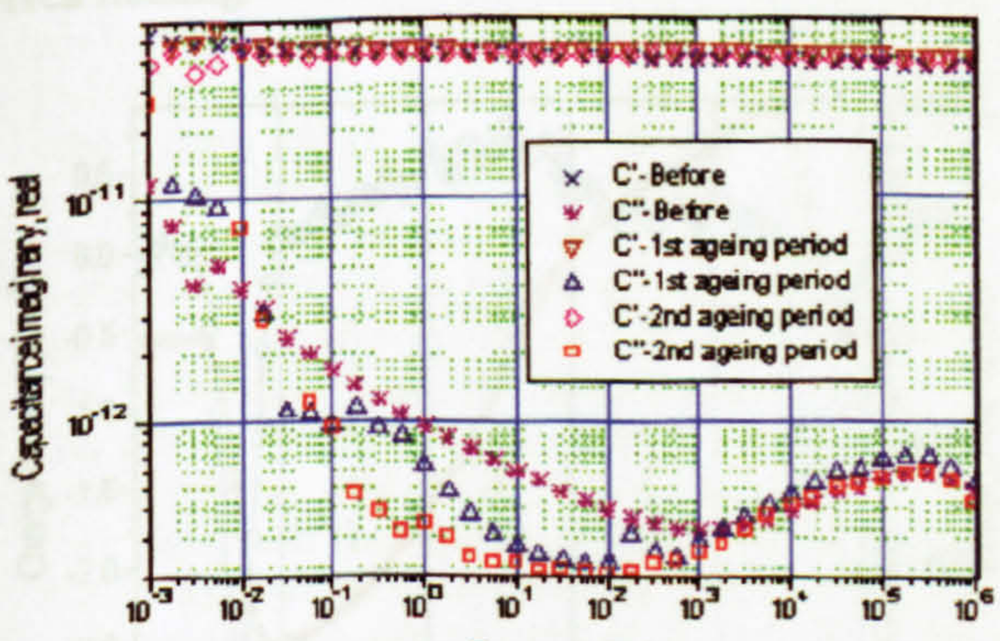

Figure 3(a) Dielectric response of epoxy resin at 40 °C before and after ageing in a uniform field (72h/34.5kV/mm at 35 °C + 47h/51.7kV/mm at 40°C; second curve for additional 47h/51.7kV/mm at 40°C)

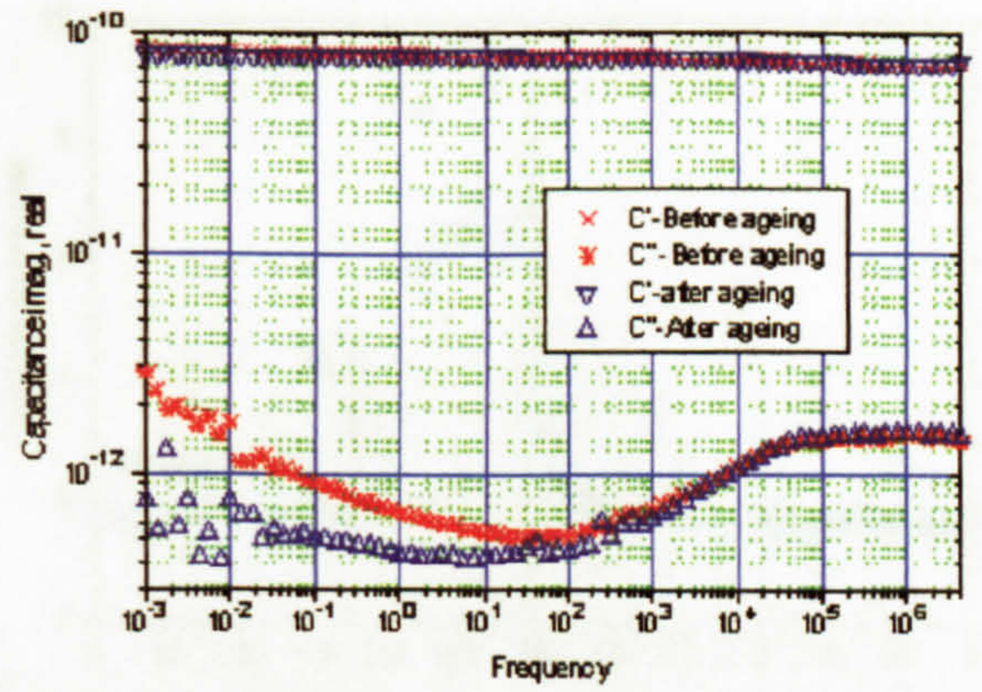

Figure 3(b) As Fig. 3(a) but in a divergent field at 20°C.

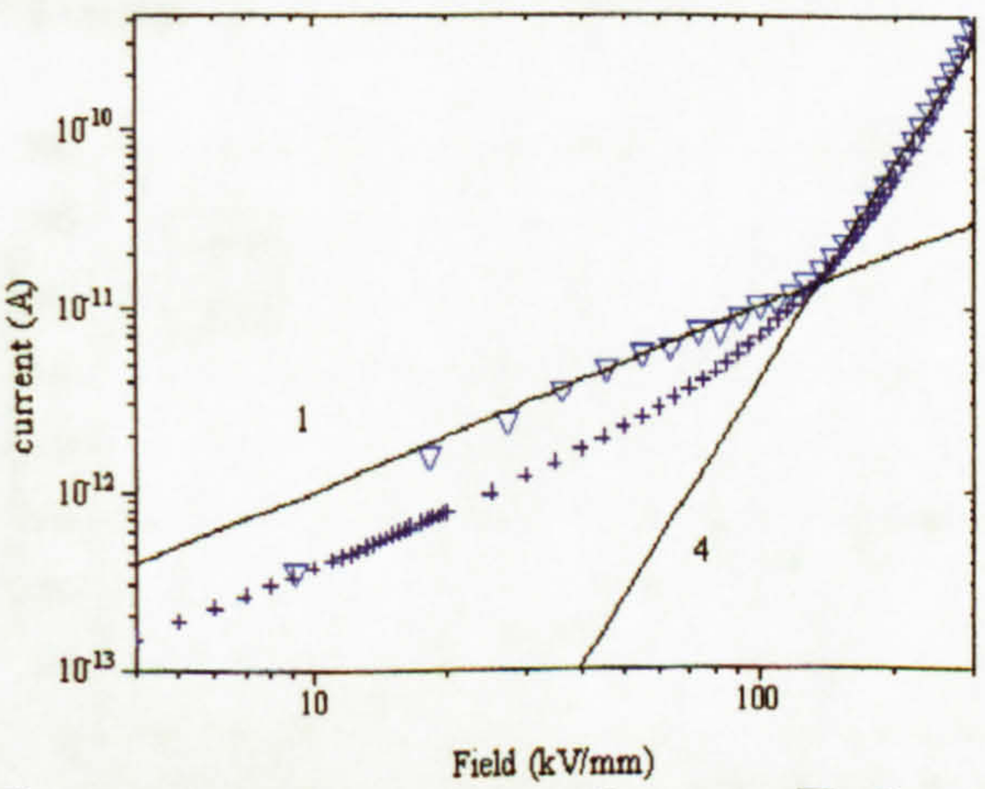

Figure 4. I-E plot for the ascending ramp □. Continuous line, power law fit, crosses (+) exponential fit

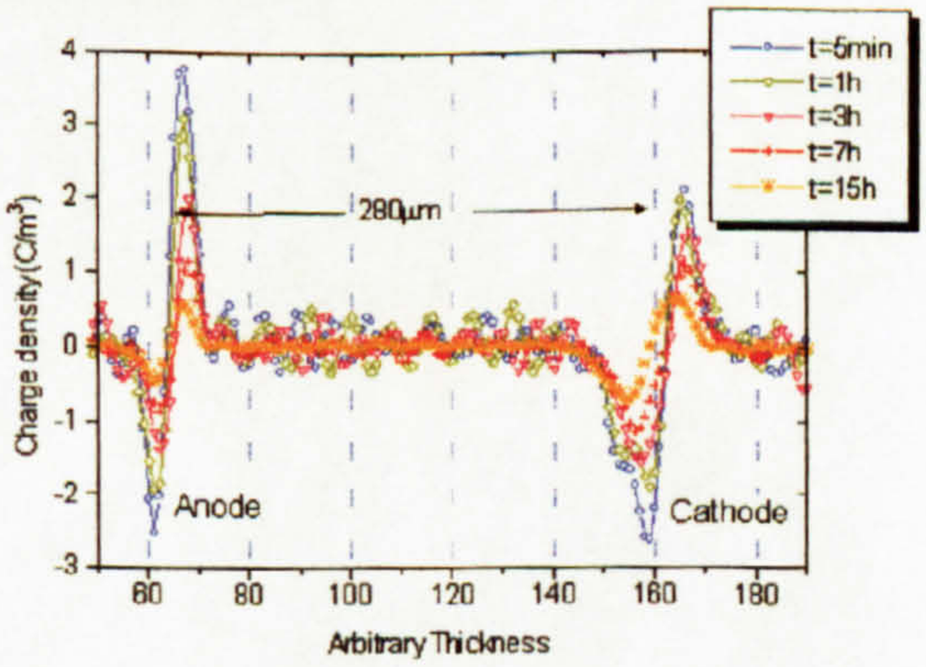

Figure 5. Space charge distribution measured following voltage removal after 1h under a uniform applied field of 18kV/mm at room temperature. Horizontal scale is time in ns and converts to distance on multiplying by acoustic velocity. The times at which measurements are made after voltage-removal are shown inset.

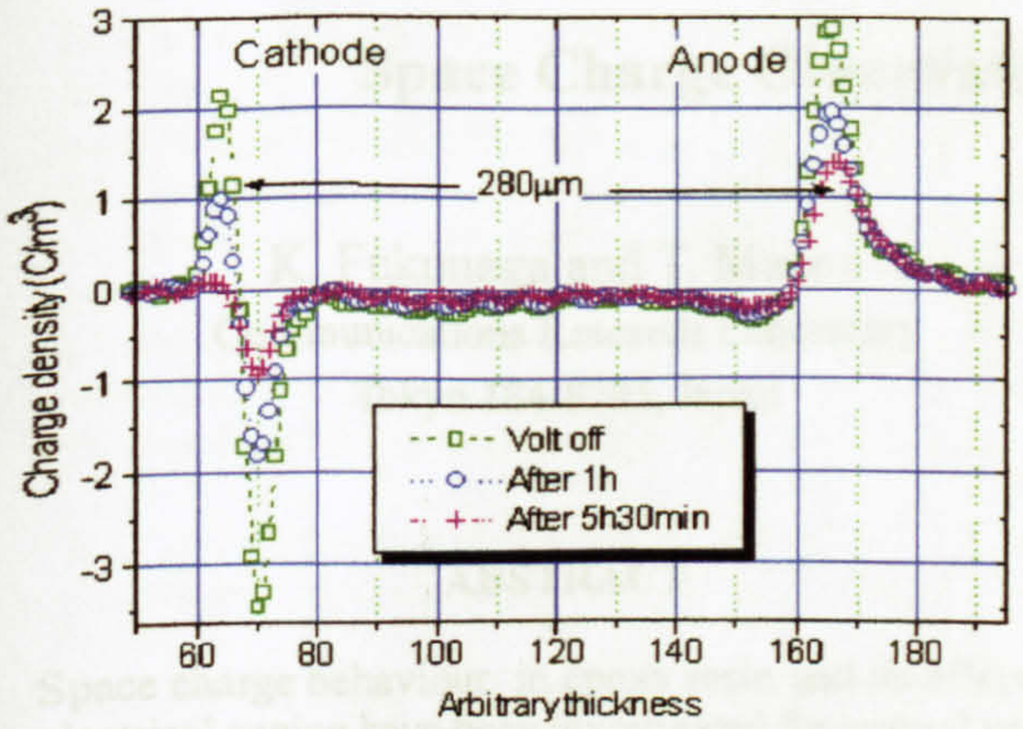

Figure 6. Space charge distribution observed on voltage removal after a polarisation time of 42h under a uniform applied field of 7kV/mm at 35°C. Horizontal scale is time in ns and converts to distance by multiplying by the acoustic velocity.

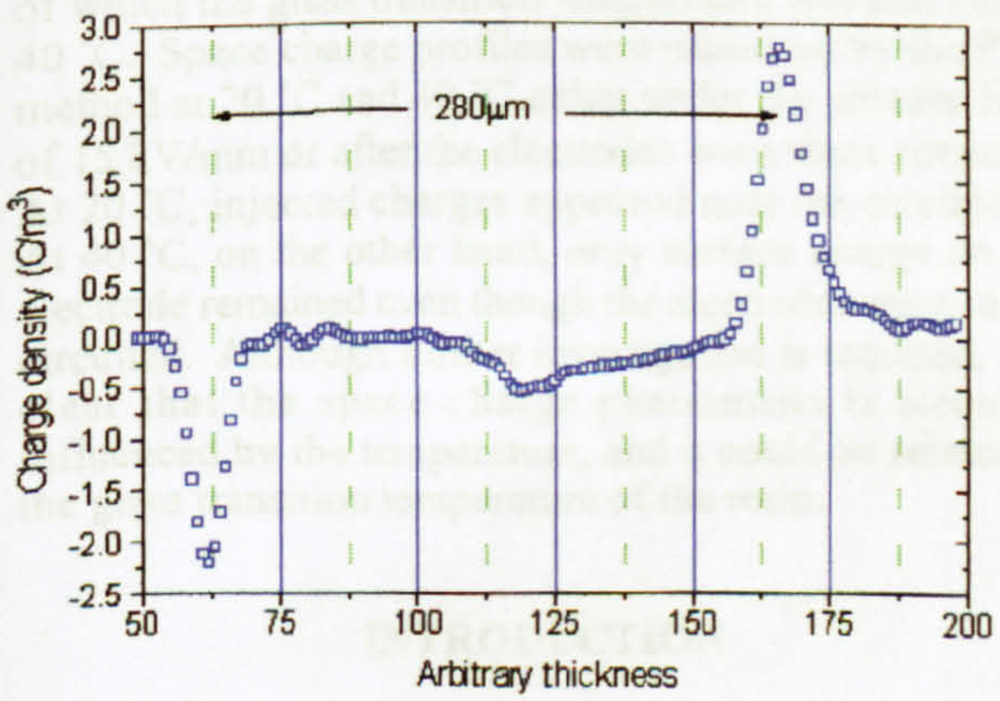

Figure 7(a) Space charge distribution obtained by applying 0.67kV between the plane electrodes with the wires floating.

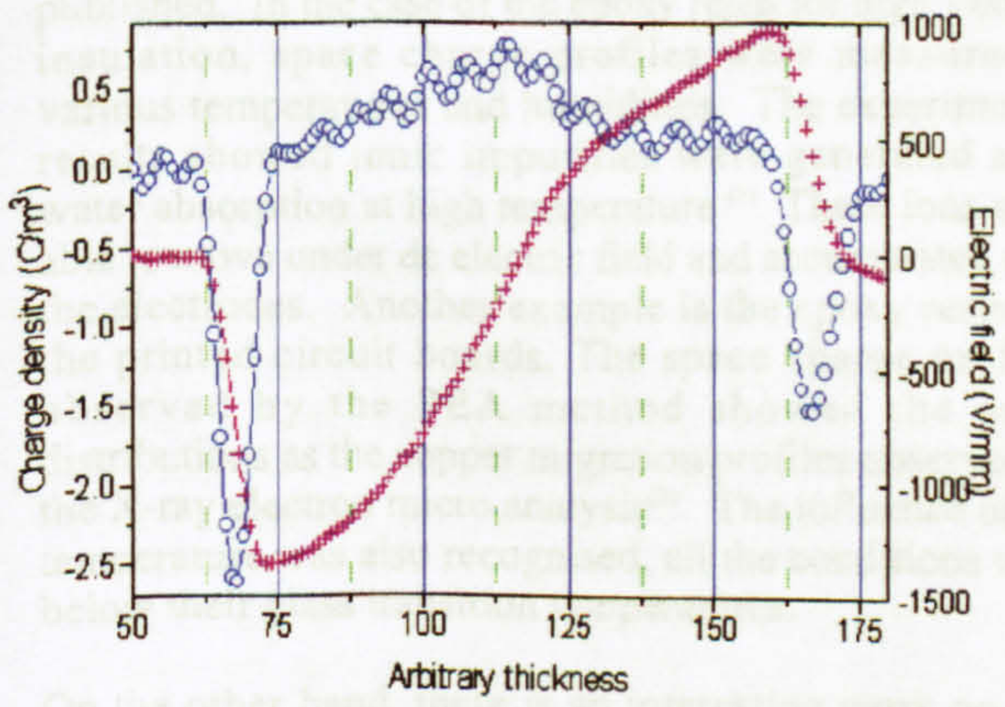

Figure 7(b).Space charge distribution measured at 33°C following 2 weeks with 1.5kV applied to the 25µm diameter gold plated tungsten wires at 33 °C. Left hand scale gives the charge density and the right hand scale the derived field.

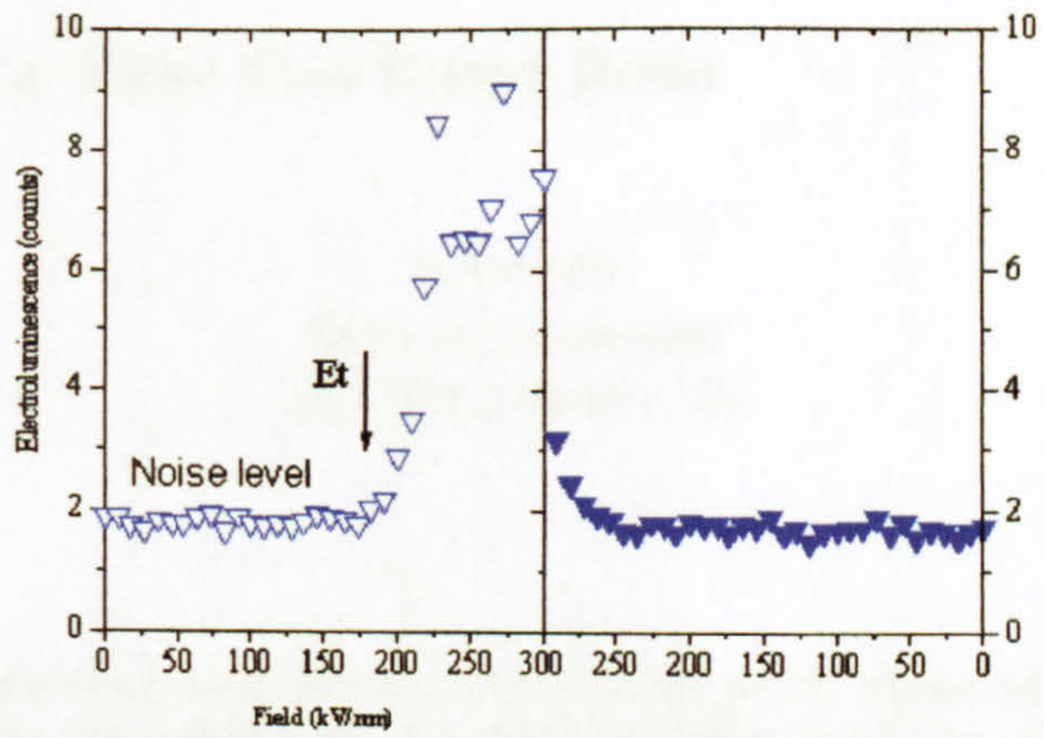

Figure 8. Electroluminescence counts as a function of field during ramp-up □ and ramp-down ▼. Noise level = 2 counts.

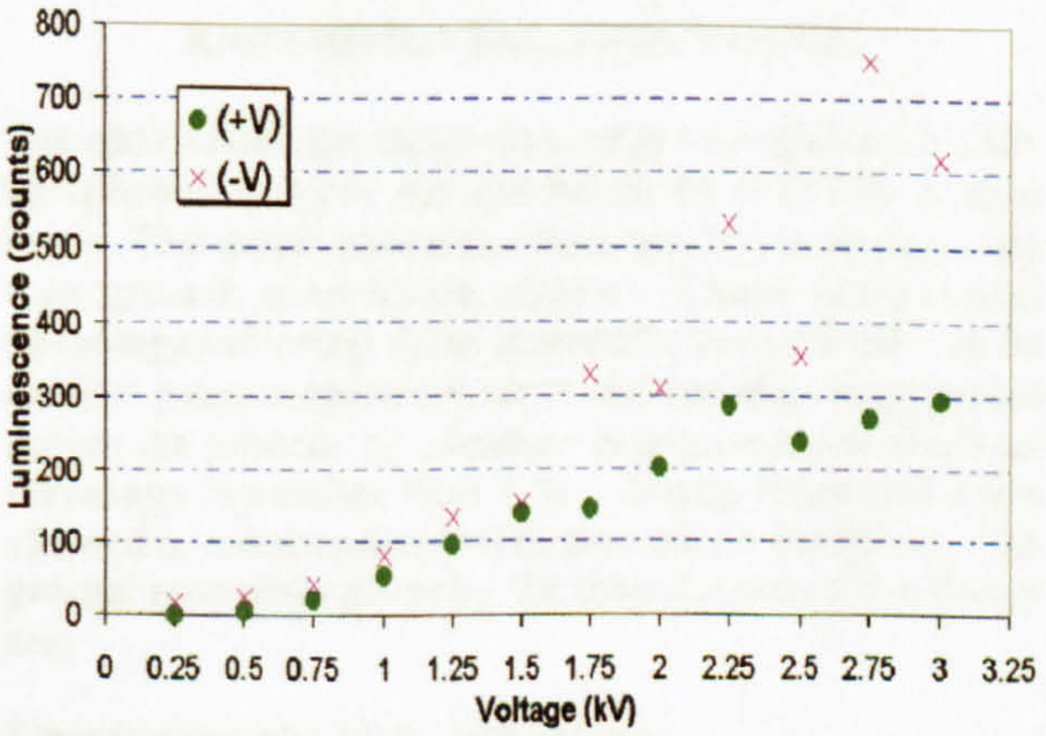

Figure 9. Electroluminescence counts. Positive pulses (•), and negative pulses (6).

Space Charge Observation of a Filler Free Epoxy Resin

K. Fukunaga and T. Maeno
Communications Research Laboratory
Tokyo 184-8795, Japan

V. Griseri
University of Leicester
LE1 7RH, Leicester, UK

ABSTRACT

Space charge behaviour in epoxy resin and its effect on electrical ageing have been investigated for several years. For example, copper ion migration in an epoxy resin of a printed circuit board was observed by using the pulsed electroacoustic (PEA) space charge measurement system. In this work, a type of filler-free resins (CY1301) was used as a specimen in order to investigate the temperature dependence of space charge behaviour in an epoxy resin of which the glass transition temperature was just below 40 °C. Space charge profiles were measured by the PEA method at 20 °C and 40 °C either under the electric field of 15 kV/mm or after the electrodes were short circuited. At 20 °C, injected charges appeared near the electrodes. At 40 °C, on the other hand, only surface charge on the electrode remained even though the electrodes were short-circuited. Although further investigation is required, it is clear that the space charge phenomena is strongly influenced by the temperature, and it could be related to the glass transition temperature of the resin.

INTRODUCTION

Space charge behaviour in polymer insulations are mainly studied on polyethylene based materials. The epoxy resin is also one of the most important insulating materials, some experimental works have been published. In the case of the epoxy resin for high voltage insulation, space charge profiles were measured at various temperatures and humidities. The experimental results showed ionic impurities were generated after water absorption at high temperature [1]. These ions were able to move under dc electric field and accumulated near the electrodes. Another example is the epoxy resin for the printed circuit boards. The space charge profiles observed by the PEA method showed the same distributions as the copper migration profiles observed by the X-ray electron micro analysis[2]. The influence of the temperature was also recognised, all the conditions were below their glass transition temperatures.

On the other hand, there is an interesting work on tree growth behaviour in filler free epoxy resins [3, 4]. The previous works proved that the tree growth is influenced by the temperature and must be related to the glass transition temperature. Thus, the same resin was used as the specimen, and its space charge behaviour was observed at around the glass transition temperature.

EXPERIMENTAL PROCEDURE

The epoxy resin specimen was made of Araldite CY1301 (Bisphenol-A type) and the hardener HY1300 (amine type). This combination has been used to investigate the tree growth mentioned above. There are several advantages of using these materials; the mixture can be cured at room temperature, no volatile product is generated during the process, no pressure is required, and the final shrinkage is smaller than 1 %. Using filler-free resin allowed to reduce unknown factors due to the fillers. The general properties given by the manufacturer Ciba-Geigy are;

Electric strength: 12 0 - 140 kV/mm
Permitivity: 3.7 - 3.9 at 1 kHz
Dielectric loss tangent: 0.007 - 0.009.

Figure 1 shows the mould used in this work which was originally designed by J. Champion from London Guildhall University. The size of each Alminium plates is 78 mm (L) x 77 mm (W) x 10 mm (H). The inside surface must be polished carefully to obtain the mirror

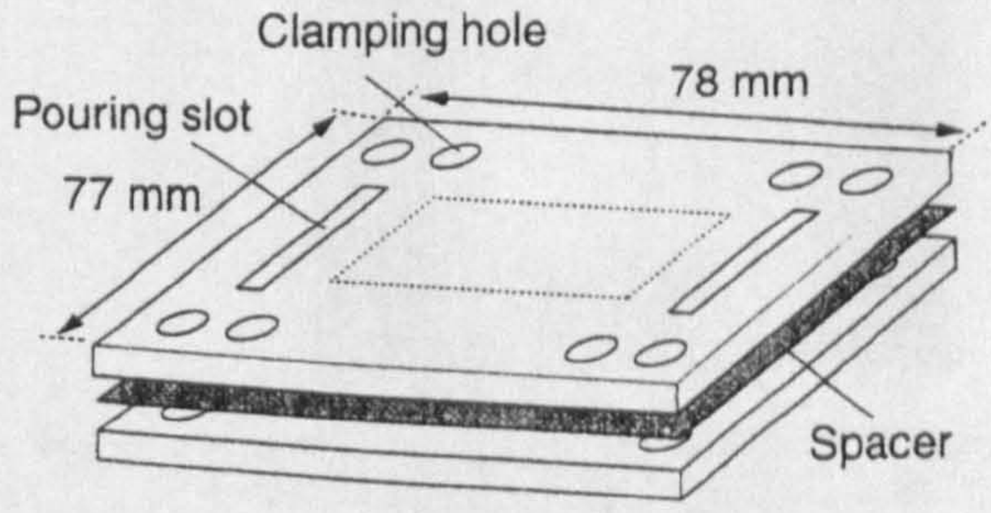

Fig. 1 The mould for curing a specimen.

finish. For holes of both plates are used to close the mould with screws. Two 7 mm wide slots of the top plate were used to pour the materials and allow them to flow through. The initial treatment of the mould surface is important to make a practically flat, reproducible specimen without a void, a crack, contamination, etc. The surface of the mould cleaned by aceton was coated with a silicone grease, and was heated in a oven at 150 °C for 10 hrs. Then it was polished with a piece of chanois leather cloth.

It is also necessary to spread some silicone oil on the surface as a remover of the cured specimen from the mould.

The The thickness of the specimen is determined by the thickness of the spacer made with a PET film. In this work, the thickness was 270 mm.

The ratio of the resin and the hardener was 100:33. They were put into the vacuum oven at 35 °C to remove gaseous components. They are mixed at 35 °C by using a magnetic stirrer, and the mixture was put into the vacuum oven at 35 °C for about 15 min. to avoid any defects remaining. The mixture was poured into the mould, and kept flat for three days at room temperature. A 50 mm square specimen was obtained by cutting a cured resin after removing from the mould.

The space charge behaviour were measured by the PEA method [5, 6] at 20 °C and 40 °C. The charge profiles were measured either under the electric field of 15 kV/mm or after the electrodes were short circuited.

TEMPERATURE DEPENDENCE OF SPACE CHARGE PROFILES

Surface charges on both electrodes were observed under the electric field as shown in Fig. 2. The solid line shows the space charge and the broken line shows the electric field. This distribution appeared at both temperatures of 20 °C and 40 °C . After 150 hours voltage application, the space charge and electric field profiles did not change significantly.

Figure 3 shows the remaining charge profile at 20 °C immediately after the electrodes were short-circuited (< 5 sec). Negative charges appeared near the cathode, and positive charges appeared near the anode. Since the surface charges changed their polarities after the short-circuit, they were considered to be induced by the injected internal charges.

In the case of 40 °C , on the other hand, internal space charge was not observed and only surface charge remains

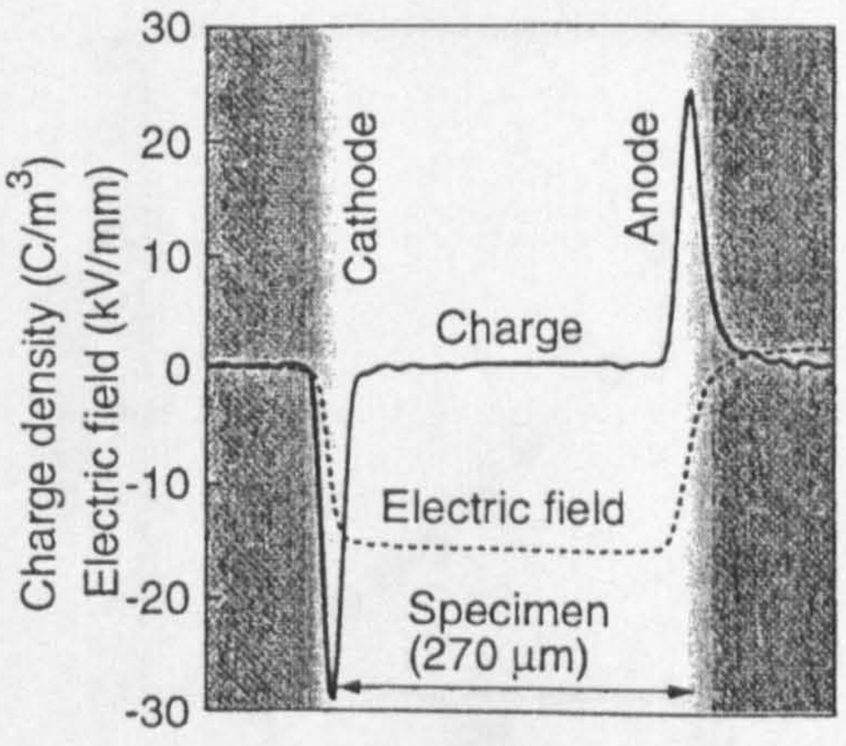

Fig. 2 Space charge and electric field profiles under dc electric field of 15 kV/mm.

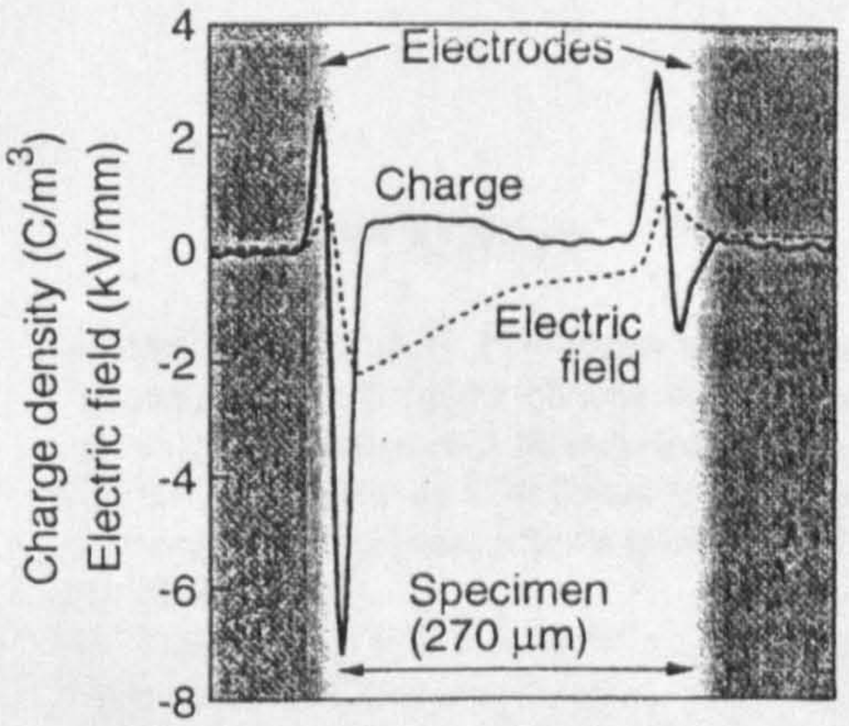

Fig. 3 Space charge and electric field profiles after the electrodes were short circuited (at 20 °C)

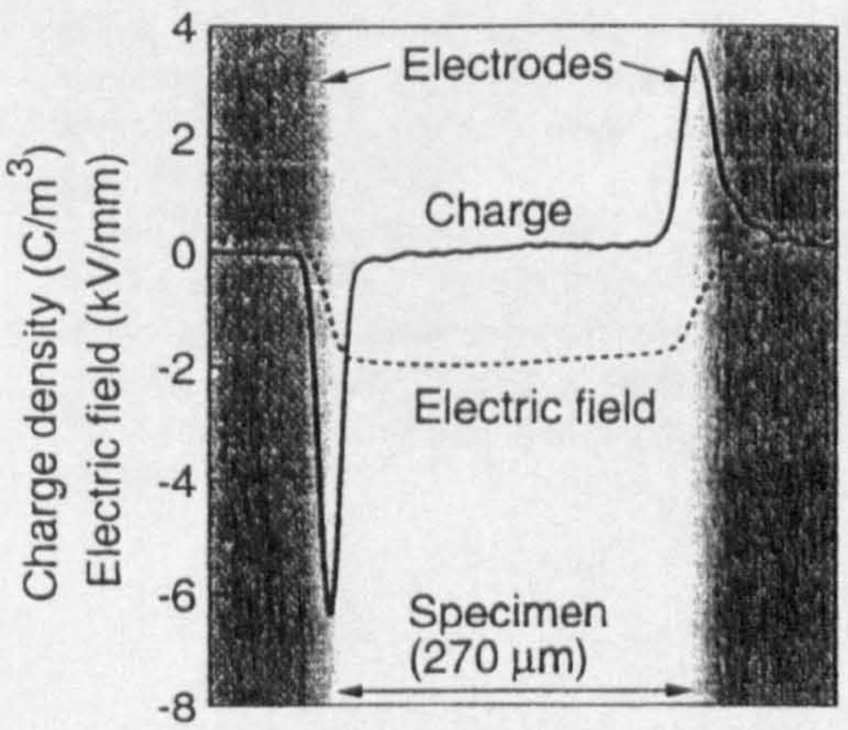

Fig. 4 Space charge and electric field profiles after the electrodes were short circuited (at 40 °C)

on the both electrodes immediately after the electrodes were short-circuited (< 5 sec) as shown in Fig. 4. Similar phenomena was found by Dr. J. M. Alison with the same specimen by applying an electric field of 25 kV/mm. It was explained that the slow polarisation existed in epoxy resin, resulting in the remaining charge distribution due to the slow depolarisation.

Here, charges are expected to be injected also at 40 °C . In order to know the reason why the injected charge could not been observed at 40 °C , the external circuit current was measured by changing the temperature. As shown in Fig. 5, the current at 40 °C was about 3 times larger than that at 20 °C, and the increasing ratio of the current to the temperature changed at about 30 °C. The increase of the current suggests that injected charge were not able to accumulate near the surface and move through.

Although further investigation is required, it is clear that the space charge phenomena is strongly influenced by the temperature, and it could be related to the glass transition temperature of the resin. Concerning that the glass transition temperature of the specimen was just below 40 °C, and the space charge profile significantly changes at about the same temperature, the space charge phenomena could be related to the glass transition temperature.

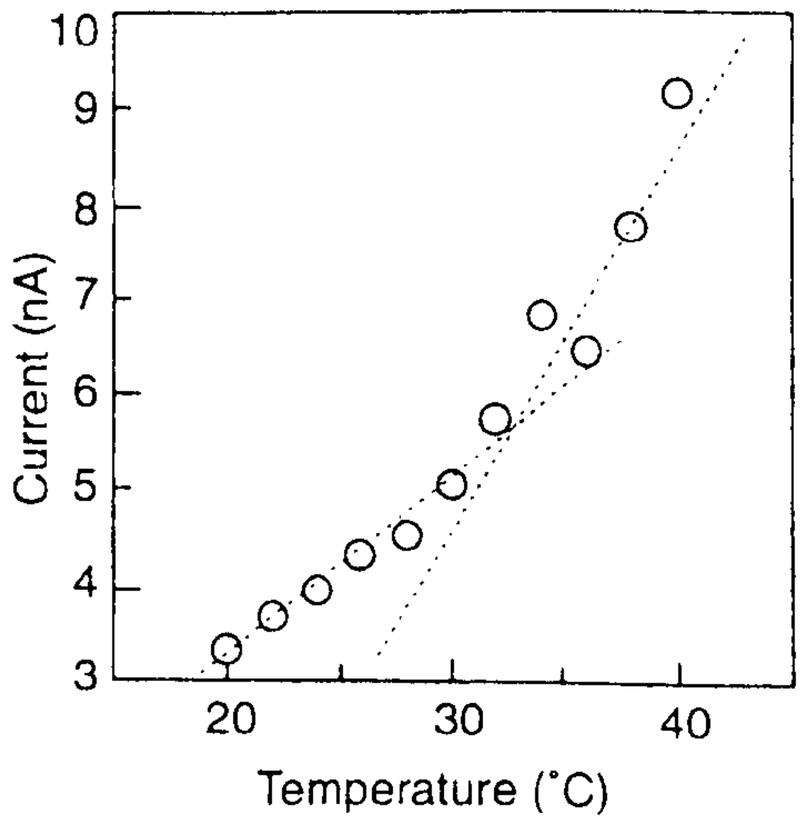

Fig. 5 External current vs temperature.

CONCLUSIONS

Space charge behaviour of a filler free epoxy resin was measured by using the PEA method. Injected charge were observed below the glass transition temparature of the specimen, and long time polarisation appeared above the glass transition temperature. It is expected that the relationship between the space charge phenomena and glass transition temperature is important to investigate the charge injection and conduction properties of epoxy resin.

ACKNOWLEDGEMENTS

The authors would like to express their thanks to Dr. J. V. Champion and Dr. S. J. Dodd, London Guildhall University, Dr. John M. Alison, King's College London and Dr. John Fothergill, University of Leicester for their helpful advice and valuable comments on this work. We also thank Mr. T. Forryan for his help on preparation of specimens.

REFERENCES

(1) T. Iizuka, Y. Takai, K. Fukunaga and T. Maeno, "Measurement of space charge distribution in epoxy resin after water absorption treatment", IEEE Conference on Electrical Insulation and Dielectric Phenomena, Minneapolis, No. 2A-2, pp. 41-44 (1997)

(2) K. Fukunaga: IEEE Electrical Insulation Magazine, Review Paper, "Industrial Applications of Space Charge Measurement in Japan", Vol. 15, No. 5, pp. 6-18 (1999)

(3) J. V. Champion, S. J. Dodd and J. M. Alison, "The correlation between the partial discharge behaviour and the spatial and temporal development of electrical trees grown in an epoxy resin.", J. Phys. D: Appl. Phys. Vol 29, pp. 2689-2695 (1996)

(4) J. V. Champion and S. J. Dodd, " An assessment of the effect of externally applied mechanical stress and water absorption on the electrical tree growth behaviour in glassy epoxy resins.", J. Phys. D: Appl. Phys. Vol 32 , pp. 305-316 (1999)